The Gutzwiller Variational Theory and Related Methods for Correlated Electron Systems

Habilitationsschrift

zur Erlangung der Lehrbefugnis für Theoretische Physik
im Fachbereich Physik der
Philipps-Universität Marburg

vorgelegt von

Dr. Jörg Bünemann

Marburg 2009

Contents

Chapter 1

Introduction

The mutual interaction of electrons has profound consequences for the physical properties of many solids. Transition metals and transition metal compounds, in particular, exhibit a variety of phenomena, which are caused, or at least significantly influenced, by the Coulomb interaction. Such phenomena include, e.g., all forms of magnetic order, metal-insulator transitions, colossal magneto-resistance, or high-temperature superconductivity.

The standard tool in solid-state physics for the investigation of metals is the Local-Density Approximation (LDA) to Density-Functional Theory. For the investigation of transition metals and their compounds, however, this method often turns out to be insufficient. It is generally believed that the shortcomings of the LDA for these materials are due to an inadequate treatment of the local (atomic) Coulomb interaction. Thus, phenomena in transition metals require the treatment by means of more reliable many-particle theories.

Unfortunately, for the investigation of real three-dimensional electronic systems, many-particle theory does not provide a viable alternative to effective single-particle theories such as the LDA. While perturbation theories at small or large interaction strength could be applied, they are usually not adequate for transition metals or their compounds, where the Coulomb interaction is neither small nor large compared to the electron band width. Numerically exact methods, e.g., exact diagonalisation and quantum Monte-Carlo algorithms, are not suitable either, due to the limited number of lattice sites that can be treated within such approaches.

In the past two decades, significant progress in the investigation of realistic correlated electron models has been made by means of approximations which are based on the limit of infinite spatial dimensions. The exact evaluation of Hubbard models in that limit leads to the 'Dynamical-Mean-Field-Theory' (DMFT), which has been applied to quite a number of systems in the past decade. A solution of the DMFT equations for multi-band Hubbard models, which describe transition metals and their compounds, is numerically quite challenging. Up to now, this method has only been able to provide a gross picture of the quasi-particle band structures in multi-band systems, e.g., the momentum-integrated density of states.

An important alternative to the DMFT is the Gutzwiller variational theory, which is based on a diagrammatic expansion that also becomes exact in the limit of infinite spatial dimensions. In recent years, we have formulated the analytical aspects of this theory and have developed a numerical code, which makes a numerical treatment of a large number of multi-band models for real materials possible. In comparison to the DMFT, the numerical effort to carry out Gutzwiller calculations for multi-band models is significantly smaller. It thus yields results which resolve the quasi-particle band structure more accurately.

It is the purpose of this work to give a thorough introduction to all relevant aspects of the Gutzwiller theory and to related methods. Our presentation is structured as follows:

In chapter 2, we begin with an introduction into the general class of multi-band Hubbard

models, which are believed to yield a suitable description of transitions metals and their compounds. To investigate a specific material by means of the Gutzwiller theory, one has to employ ab-initio methods which allow a Hubbard model to be derived from the full electronic Hamiltonian. We discuss the two most important ab-initio methods, the Hartree- Fock theory and the Density-Functional Theory, in chapter 3.

In chapter 4, we introduce the general class of Gutzwiller wave functions, which are used for our investigation of multi-band Hubbard models. In addition, we give a brief historical review of the theory as it has developed since Gutzwiller introduced his variational method for a single-band Hubbard model in his seminal work in 1963.

We discuss the evaluation of Gutzwiller wave functions in the limit of infinite spatial dimensions in detail in chapter 5. Alternative ways to derive the same energy functional are introduced in chapter 6. The Gutzwiller approximation scheme, which is based on Gutzwiller's combinatorial counting arguments, and the slave-boson mean-field theory both allow the investigation of particular Hubbard models with only density-density-type interaction terms. Up to now, both methods could not be applied successfully to general multi-band models. We introduce a new slave-boson scheme that allows the treatment of general Hubbard models and reproduces the results of the Gutzwiller theory derived in chapter 5.

The Gutzwiller wave function constitutes an approximation for the true many-particle ground state of a multi-band Hubbard model. For certain properties, this already yields valuable insights into the physics of such models, e.g., the appearance of spin-ordered ground states. More interesting than the properties of the ground state, however, are those of the elementary excitations because they are probed by the majority of experiments relevant to solid-state physics. In chapter 7, we explain how single-particle excitations in a Fermi liquid can be calculated within the Gutzwiller theory. For the calculation of two-particle excitations, the time-dependent Gutzwiller theory can be employed. We give a derivation of this theory for general multi-band models in chapter 8.

Chapters 9 and 10 contain applications of the Gutzwiller theory. In chapter 9, we consider the physics of two-band model systems. We discuss the emergence of ferromagnetism, orbital order, and metal-insulator transitions in such models. In chapter 10, we address the physics of two materials. First, we present our results for the quasi-particle bands and the magnetic properties of fcc nickel. Next, we investigate the Fermi-surface topology of Na_xCoO_2.

Chapter 2

Systems and Models

In the first section of this chapter, we briefly remind the reader of the general electronic many-particle problem that we face in solid-state theory. Due to the two-particle Coulomb interaction between electrons, it is not possible to solve the full electronic problem, even numerically. Many properties of solids, however, are already well described by much simpler model Hamiltonians. For transition metals and their compounds, these are the 'multi-band Hubbard models'. They will be we derived in sections 2.2 and 2.3. Finally, in section 2.4, we introduce some related models, which we investigate later in this work.

2.1 The Electronic Many-Particle Problem

The starting point of non-relativistic solid-state theory is the many-particle Hamiltonian [1]

$$\begin{aligned} \hat{H}_{\mathrm{SS}}^{1.\mathrm{Q}} &= \sum_{i}^{N_{\mathrm{N}}} \frac{\hat{\boldsymbol{P}}_i^2}{2M_i} + \frac{e^2}{2} \sum_{i\neq j=1}^{N_{\mathrm{N}}} \frac{Z_i Z_j}{|\hat{\boldsymbol{R}}_i - \hat{\boldsymbol{R}}_j|} + \sum_{n}^{N_{\mathrm{e}}} \frac{\hat{\boldsymbol{p}}_n^2}{2m} \\ &\quad + \frac{e^2}{2} \sum_{n\neq m=1}^{N_{\mathrm{e}}} \frac{1}{|\hat{\boldsymbol{r}}_n - \hat{\boldsymbol{r}}_m|} - e^2 \sum_{n}^{N_{\mathrm{e}}} \sum_{i}^{N_{\mathrm{N}}} \frac{Z_i}{|\hat{\boldsymbol{R}}_i - \hat{\boldsymbol{r}}_n|} \,, \end{aligned} \tag{2.1}$$

which describes a system with

i) N_{N} nuclei with charge eZ_i, mass M_i, and momentum and position operators $\hat{\boldsymbol{R}}_i$, $\hat{\boldsymbol{P}}_i$,

ii) $N_{\mathrm{e}} = \sum_i Z_i$ electrons of charge e, mass m, and momentum and position operators $\hat{\boldsymbol{r}}_n$, $\hat{\boldsymbol{p}}_n$.

Note that vectors are denoted by bold variables (e.g., $\boldsymbol{r}$) throughout this work. The operator $\hat{H}_{\mathrm{SS}}^{1.\mathrm{Q}}$ is given in first quantisation in (2.1). In order to obtain the correct quantum mechanical problem, the corresponding many-particle wave functions for electrons and nuclei must obey the (anti)symmetry conditions for identical particles; see, e.g., reference [2]. Technically this can be achieved most easily by employing the method of second quantisation [3]. Before we introduce this formalism, the very general Hamiltonian (2.1) is simplified for the purpose of this work, which is solely the investigation of the *electronic* properties of solids.

We take for granted the experimental finding that the nuclei form a regular crystal lattice at zero temperature. Quantum mechanically, this is obviously a somewhat dubious statement since Heisenberg's uncertainty principle also applies to the nuclei. More precisely, it means that to leading order in the expansion parameter $c_{\mathrm{eb}} \equiv (m/M_i)^{1/4}$, electronic dynamics is decoupled from the nucleal dynamics. This is the essence of the 'adiabatic' or 'Born-Oppenheimer'

approximation [4, 5]. In this approximation, the nuclei appear in the effective electronic Hamiltonian

$$\hat{\bar{H}}_{\mathrm{el}}^{1.\mathrm{Q}} = \sum_{n}^{N_\mathrm{e}} \left(\frac{\hat{\boldsymbol{p}}_n^2}{2m} + V(\hat{\boldsymbol{r}}_n) \right) + \frac{e^2}{2} \sum_{n \neq m=1}^{N_e} \frac{1}{|\hat{\boldsymbol{r}}_n - \hat{\boldsymbol{r}}_m|} = \hat{\bar{H}}_0^{1.\mathrm{Q}} + \hat{\bar{H}}_\mathrm{I}^{1.\mathrm{Q}} \tag{2.2a}$$

as a static potential

$$V(\boldsymbol{r}) \equiv e^2 \sum_{i}^{N_\mathrm{N}} \frac{Z_i}{|\boldsymbol{R}_i - \boldsymbol{r}|} \tag{2.2b}$$

with vectors $\boldsymbol{R}_i$ that define the periodic lattice. The effective Hamiltonian of the nuclei in the adiabatic approximation leads to phonons. In this work, we are solely interested in the electronic properties of solids. Hence, we are not going into more details on the phonon degrees of freedom and, consequently, we also neglect the electron-phonon coupling, which, energetically, is an effect of order c_eb^3.

Apart from the spatial degrees of freedom, electrons carry a spin 1/2, i.e., the actual electronic problem is given by the Hamiltonian

$$\hat{H}_{\mathrm{el}}^{1.\mathrm{Q}} = \hat{\bar{H}}_{\mathrm{el}}^{1.\mathrm{Q}} \otimes \hat{1} \,, \tag{2.2c}$$

where $\hat{1}$ is the unit matrix in spin-space.

We introduce a basis of single-particle states $|\sigma\rangle$, where the label σ combines the spatial and the spin degrees of freedom. Hence, the corresponding wave function is given by $\phi_\sigma(\boldsymbol{r})\chi_\sigma$ with a spatial wave function $\phi_\sigma(\boldsymbol{r}) = \langle \boldsymbol{r}|\sigma\rangle$ and a two-dimensional spinor $\chi_\sigma = \langle \chi|\sigma\rangle$. With this basis, the Hamiltonian (2.2c) in second quantisation has the form

$$\begin{aligned} \hat{H}_{\mathrm{el}} &= \sum_{\sigma_1,\sigma_2} \varepsilon_{\sigma_1,\sigma_2} \hat{c}_{\sigma_1}^\dagger \hat{c}_{\sigma_2} + \frac{1}{2} \sum_{\sigma_1,\sigma_2,\sigma_3,\sigma_4} U_{\sigma_1,\sigma_2,\sigma_3,\sigma_4} \hat{c}_{\sigma_1}^\dagger \hat{c}_{\sigma_2}^\dagger \hat{c}_{\sigma_3} \hat{c}_{\sigma_4} && (2.3a) \\ &\equiv \hat{H}_0 + \hat{H}_\mathrm{I} \,, && (2.3b) \end{aligned}$$

where, setting $\hbar = 1$ in this work,

$$\begin{aligned} \varepsilon_{\sigma_1,\sigma_2} &\equiv \delta_{\chi_{\sigma_1},\chi_{\sigma_2}} \int d^3\boldsymbol{r}\; \phi_{\sigma_1}^*(\boldsymbol{r}) \left(-\frac{\Delta_{\boldsymbol{r}}}{2m} + V(\boldsymbol{r}) \right) \phi_{\sigma_2}(\boldsymbol{r}) \,, && (2.3c) \\ U_{\sigma_1,\sigma_2,\sigma_3,\sigma_4} &\equiv \delta_{\chi_{\sigma_1},\chi_{\sigma_4}} \delta_{\chi_{\sigma_2},\chi_{\sigma_3}} e^2 \int d^3\boldsymbol{r} \int d^3\boldsymbol{r}' \frac{\phi_{\sigma_1}^*(\boldsymbol{r}) \phi_{\sigma_2}^*(\boldsymbol{r}') \phi_{\sigma_3}(\boldsymbol{r}') \phi_{\sigma_4}(\boldsymbol{r})}{|\boldsymbol{r} - \boldsymbol{r}'|} \,. && (2.3d) \end{aligned}$$

When we work with a basis of position eigenstates $|\boldsymbol{r}\rangle$ and the corresponding field operators $\hat{\psi}_s^{(\dagger)}(\boldsymbol{r})$, the Hamiltonian (2.3a) can be written in the form

$$\begin{aligned} \hat{H}_{\mathrm{el}} &= \sum_{s} \int d^3\boldsymbol{r}\; \hat{\psi}_s^\dagger(\boldsymbol{r}) \left(-\frac{\Delta_{\boldsymbol{r}}}{2m} + V(\boldsymbol{r}) \right) \hat{\psi}_s(\boldsymbol{r}) && (2.3e) \\ &\quad + \frac{1}{2} \sum_{s,s'} \int d^3\boldsymbol{r} \int d^3\boldsymbol{r}'\; \hat{\psi}_s^\dagger(\boldsymbol{r}) \hat{\psi}_{s'}^\dagger(\boldsymbol{r}') \frac{e^2}{|\boldsymbol{r} - \boldsymbol{r}'|} \hat{\psi}_{s'}(\boldsymbol{r}') \hat{\psi}_s(\boldsymbol{r}) \,, \end{aligned}$$

where s, s' are spin indices.

Despite the fact that the Hamiltonian (2.3) only contains electronic degrees of freedom, it still represents a difficult many-particle problem, which, in general, is unsolvable. Strategies to deal with it approximately fall into two categories:

i) *Model-system approaches*: In order to explain experiments, which probe certain electronic properties, we will usually be interested into excitations within a certain energy range. For example, the excitation of electrons in inner shells of transition metals requires energies of up to 10^4 eV. Therefore, it should be possible to describe their influence on electrons near the Fermi level of a metal by a proper adjustment of the one-particle potential (2.2b). In this way, the full electronic Hamiltonian may be replaced by some 'model system' of which one hopes that it describes the particular electronic properties of interest correctly. An important class of models in many-particle theory, the 'multi-band Hubbard models', will be introduced in the following section.

ii) *Ab-initio approaches*: In order to work with the full Hamiltonian (2.2c), one has to accept that the available approximations are significantly cruder than many of those, which have been developed for the treatment of model systems. The two most important of such 'ab-initio' approaches are the 'Hartree-Fock theory and the 'Local-Density Approximation' to the 'Density-Functional Theory'. We will give an introduction to both approaches in chapter 3. Often, ab-initio methods are used to derive the explicit form of a model Hamiltonian for the investigation of a specific material. Practical ways to derive multi-band Hubbard models from ab-initio data will be discussed in chapter 10 and appendix G.

2.2 Hubbard Models

The basis of single-particle wave functions $\phi_\sigma(\boldsymbol{r})$ that is used in the second quantisation can be chosen arbitrarily. In order to derive multi-band Hubbard models, we need to introduce a basis of states that are localised around the sites $\boldsymbol{R}_i$ of our lattice. As a first step, we assume that the 'atomic' one-particle problem is solved, i.e., we start from the eigenstates $\eta_{i,\alpha}(\boldsymbol{r})$ of the Schrödinger equation

$$\left(-\frac{\Delta_{\boldsymbol{r}}}{2m} + e^2\frac{Z_i}{|\boldsymbol{R}_i - \boldsymbol{r}|}\right)\eta_{i,\alpha}(\boldsymbol{r}) = \varepsilon_{i,\alpha}\eta_{i,\alpha}(\boldsymbol{r}) \;, \tag{2.4}$$

with corresponding eigenvalues $\varepsilon_{i,\alpha}$. As an abbreviation, we introduce the index $\gamma \equiv (i,\alpha)$, which combines the lattice site index i and the orbital quantum number α. The orbital states $\eta_\gamma(\boldsymbol{r})$, are localised around their respective lattice site $\boldsymbol{R}_i$. They are, however, not necessarily orthogonal. In general, one finds

$$\langle \eta_\gamma | \eta_{\gamma'} \rangle = \int d^3\boldsymbol{r}\; \eta^*_\gamma(\boldsymbol{r})\eta_{\gamma'}(\boldsymbol{r}) \equiv \delta_{\gamma,\gamma'} + S_{\gamma,\gamma'} \;, \tag{2.5}$$

where $S_{\gamma,\gamma'}$ are the elements of a finite 'overlap'-matrix $\tilde{S}$. Following reference [6], we introduce

$$\tilde{M} = (\tilde{1} + \tilde{S})^{-1/2} \approx \tilde{1} - \frac{1}{2}\tilde{S} + \frac{3}{8}\tilde{S}^2 - \cdots \;, \tag{2.6}$$

which is a well defined matrix since $\tilde{S}$ is Hermitian. The matrix $\tilde{M}$ yields a transformation to a new basis of states

$$|\bar{\eta}_\gamma\rangle = \sum_{\gamma'} M_{\gamma',\gamma}\,|\eta_{\gamma'}\rangle \;, \tag{2.7}$$

which are, by construction, orthogonal

$$\langle \bar{\eta}_\gamma | \bar{\eta}_{\gamma'} \rangle = \sum_{\tilde{\gamma},\tilde{\gamma}'} M_{\gamma,\tilde{\gamma}} \underbrace{\langle \eta_{\tilde{\gamma}} | \eta_{\tilde{\gamma}'} \rangle}_{[\tilde{M}^{-1}\tilde{M}^{-1}]_{\tilde{\gamma},\tilde{\gamma}'}} M_{\tilde{\gamma}',\gamma'} = \delta_{\gamma,\gamma'} \;. \tag{2.8}$$

The new states $\bar{\eta}_{i,\beta}(\boldsymbol{r}) = \langle \boldsymbol{r}|\bar{\eta}_{i,\beta}\rangle$ still carry a site index i, although, from (2.7) it is clear that they have an admixture of states $\eta_{i',\alpha}(\boldsymbol{r})$ at different sites $i' \neq i$. As long as the states $\eta_{i,\alpha}(\boldsymbol{r})$ are well localised in comparison to the distances to neighbouring sites, the elements $\tilde{S}_{(i,\alpha),(i',\alpha')}$ of the overlap-matrix are small. Consequently, the states $\bar{\eta}_{i,\alpha}(\boldsymbol{r})$ are also well localised around the site i since the main contribution in (2.7) stems from states at the same site.

Now, with a proper basis of localised states at hand, we diagonalise the local Hamilton matrix

$$H^{0;i}_{\beta,\beta'} \equiv \langle \bar{\eta}_{i,\beta}|\hat{\bar{H}}^{1.\mathrm{Q}}_0|\bar{\eta}_{i,\beta'}\rangle \tag{2.9}$$

for each site i via some unitary transformation $T^i_{b,\beta}$,

$$\sum_{\beta,\beta'} T^i_{b,\beta} H^{0;i}_{\beta,\beta'} \left(T^i_{b',\beta'}\right)^* = \delta_{b,b'}\varepsilon_{i,b} \; . \tag{2.10}$$

The resulting eigenstates

$$\phi_{i,b}(\boldsymbol{r}) = \sum_{\beta} T^i_{b,\beta}\bar{\eta}_{i,\beta}(\boldsymbol{r}) \tag{2.11}$$

of $H^{0;i}_{\beta,\beta'}$ now have the proper site symmetry, i.e., they are classified by representations of the point-symmetry group of each site i.

With the orbital basis (2.11), the one-particle Hamiltonian $\hat{H}_0$ in second quantisation has the 'tight-binding' form

$$\hat{H}_0 = \sum_{i,j}\sum_{\sigma,\sigma'} t^{\sigma,\sigma'}_{i,j}\,\hat{c}^\dagger_{i,\sigma}\hat{c}_{j,\sigma'} \; , \tag{2.12}$$

where the indices $\sigma = (b, s)$ combine the orbital index b and the spin index s. The 'hopping' parameters $t^{\sigma,\sigma'}_{i,j}$ are defined analogous to $\varepsilon_{\sigma_1,\sigma_2}$ in (2.3c). Here, the local parameters $t^{\sigma,\sigma'}_{i,i}$ are diagonal by construction,

$$t^{\sigma,\sigma'}_{i,i} = \delta_{\sigma,\sigma'}\varepsilon_{i,\sigma} \; , \tag{2.13}$$

where $\varepsilon_{i,\sigma} = \varepsilon_{i,b}$ with b as the orbital part of the combined index σ. The interaction part of the Hamiltonian in second quantisation reads

$$\hat{H}_\mathrm{I} = \frac{1}{2}\sum_{\substack{\sigma_1,\sigma_2,\sigma_3,\sigma_4\\ i_1,i_2,i_3,i_4}} U^{\sigma_1,\sigma_2,\sigma_3,\sigma_4}_{i_1,i_2,i_3,i_4}\hat{c}^\dagger_{i_1,\sigma_1}\hat{c}^\dagger_{i_2,\sigma_2}\hat{c}_{i_3,\sigma_3}\hat{c}_{i_4,\sigma_4} \; , \tag{2.14}$$

with respect to the local basis (2.11). Here, the Coulomb parameters $U^{(\dots)}_{(\dots)}$ are defined in the same way as those in equation (2.3d).

So far, we have made no approximations and we still work with the full electronic Hamiltonian. Due to the locality of the local basis (2.11), the biggest of the Coulomb parameters in (2.14) are certainly those with the same lattice site indices $i_1, \dots, i_4$. The approximation that leads us to multi-band Hubbard models is to neglect all terms in (2.14) with more than one lattice site involved. Hubbard models, thus, have the general form

$$\hat{H}_\mathrm{H} = \sum_{i,j}\sum_{\sigma,\sigma'} t^{\sigma,\sigma'}_{i,j}\,\hat{c}^\dagger_{i,\sigma}\hat{c}_{j,\sigma'} + \frac{1}{2}\sum_i \sum_{\sigma_1,\sigma_2,\sigma_3,\sigma_4} U^{\sigma_1,\sigma_2,\sigma_3,\sigma_4}_i \hat{c}^\dagger_{i,\sigma_1}\hat{c}^\dagger_{i,\sigma_2}\hat{c}_{i,\sigma_3}\hat{c}_{i,\sigma_4} \; . \tag{2.15}$$

The Hamiltonian (2.15) still contains an infinite number of orbitals. We diagonalise the single-particle term,

$$\hat{H}_0 = \sum_{\boldsymbol{k},\sigma,\sigma'} \varepsilon^0_{\boldsymbol{k};\sigma,\sigma'}\hat{c}^\dagger_{\boldsymbol{k},\sigma}\hat{c}_{\boldsymbol{k},\sigma'} = \sum_{\boldsymbol{k},\gamma} E^0_{\boldsymbol{k},\gamma}\hat{h}^\dagger_{\boldsymbol{k},\gamma}\hat{h}_{\boldsymbol{k},\gamma} \; , \tag{2.16}$$

with

$$\varepsilon^0_{\boldsymbol{k};\sigma,\sigma'} \equiv \frac{1}{L}\sum_{i,j} t^{\sigma,\sigma'}_{i,j} e^{\mathrm{i}\boldsymbol{k}(\boldsymbol{R}_i-\boldsymbol{R}_j)} , \tag{2.17a}$$

$$\hat{c}^{(\dagger)}_{\boldsymbol{k},\sigma} \equiv \frac{1}{\sqrt{L}}\sum_{i} e^{\mp\mathrm{i}\boldsymbol{k}\boldsymbol{R}_i}\hat{c}^{(\dagger)}_{i,\sigma} , \tag{2.17b}$$

by means of a unitary transformation

$$\hat{h}^\dagger_{\boldsymbol{k},\gamma} = \sum_\sigma u_{\gamma,\sigma}(\boldsymbol{k})\hat{c}^\dagger_{\boldsymbol{k},\sigma} . \tag{2.18}$$

This leads to band states $|\boldsymbol{k},\gamma\rangle$, which, in the ground state of $\hat{H}_0$, are occupied below the Fermi energy, $E^0_{\boldsymbol{k},\gamma} < E_\mathrm{F}$. Obviously, all orbitals $\phi_{i,b}(\boldsymbol{r})$ that are energetically far below or above the Fermi energy are either fully occupied or unoccupied and, hence, they do not influence the physics of the system also for finite Coulomb interactions. Therefore, in Hubbard models one usually includes only a limited number of orbitals, which are energetically near the Fermi energy of $\hat{H}_0$. In the following sections, we discuss the two simplest examples for this procedure, the Hubbard models with one and two orbitals per lattice site.

The local approximation for the Coulomb interaction, which led to the Hubbard Hamiltonian (2.15), is difficult to justify within the derivation we used in this section. Although some of the purely local interaction parameters are certainly amongst the biggest, the non-local terms will usually not be smaller by orders of magnitude and their number is much larger than that of the local terms. Therefore, from our derivation here, it seems unlikely that the Hubbard model captures the physics of the full electronic Hamiltonian correctly, at least quantitatively. As we will see in the following section, however, ab-initio methods like the Hartree-Fock or the Density-Functional Theory describe the electronic many-particle system by an effective single-particle Hamiltonian. Such a Hamiltonian captures already, to some extent, non-local contributions from the Coulomb interaction. Practical ways to derive an effective Hubbard model Hamiltonian for a material from ab-initio calculations will be discussed in chapter 10 and appendix G.

2.3 Examples

As the simplest examples we introduce the Hubbard models with one and two orbitals per lattice site in this section.

2.3.1 One-Band Hubbard Model

When there is only one orbital per site and the Coulomb interaction parameter

$$U = U_i^{\uparrow,\downarrow,\downarrow,\uparrow} \tag{2.19}$$

is site independent, the Hubbard model (2.15) has the form [7–9]

$$\hat{H}_\mathrm{1B} = \sum_{i,j}\sum_s t_{i,j}\hat{c}^\dagger_{i,s}\hat{c}_{j,s} + U\sum_i \hat{n}_{i,\uparrow}\hat{n}_{i,\downarrow} , \tag{2.20}$$

where

$$\hat{n}_{i,s} = \hat{c}^\dagger_{i,s}\hat{c}_{i,s} \tag{2.21}$$

counts the number of electrons on site i with spin $s =\uparrow,\downarrow$. Due to its simplicity, the Hubbard

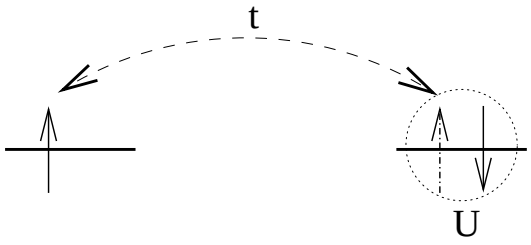

Figure 2.1: A qualitative illustration of the two-site model (2.22).

model with one orbital or, as it is often denoted, the 'one-band' Hubbard model, is generally regarded as the 'standard model' in correlated electron theory. It is the subject of innumerable analytical and numerical works because, in general, it cannot be solved exactly. For an overview on the Hubbard model in one dimension, see, e.g., reference [10]. The opposite limit of large spatial dimensions can be tackled within the 'Dynamical-Mean-Field-Theory'; for an overview on this approach see, e.g., references [11, 12].

The simplest one-orbital Hubbard model consists of only two lattice sites, see figure 2.1. It has the form

$$\hat{H}_{\mathrm{ts}} = t \sum_{s} \left(\hat{c}^{\dagger}_{1s} \hat{c}_{2s} + \hat{c}^{\dagger}_{2s} \hat{c}_{1s} \right) + U \sum_{i=1}^{2} \hat{n}_{i,\uparrow} \hat{n}_{i,\downarrow} \; . \tag{2.22}$$

In the subsequent chapters, we will use this 'toy model' several times in order to compare the different theoretical methods that are used in this work; see sections 3.1.3, 4.2.2, 5.4.2 and appendix G.2. The exact eigenstates and energies of the two-site Hubbard model are derived in appendix B.

2.3.2 Two-Band Hubbard Model

For simplicity, and later use, we consider a model with two degenerate e_{g} orbitals φ_u and φ_v per site on a cubic lattice. Here, we focus on the Coulomb part of the Hubbard Hamiltonian (2.15). The tight-binding parameters in the corresponding single-particle Hamiltonian $\hat{H}_0$ will be specified in section 9.1 where we investigate the physical properties of the two-band Hubbard model.

The local atomic Hamiltonian of a d-shell in a cubic environment is studied in appendix C. We can derive the local Hamiltonian for two e_{g} orbitals from the general Hamiltonian (C.3) by keeping only those terms that contain e_{g} orbitals. This leads to

$$\begin{aligned} \hat{H}^{\mathrm{2b}}_{\mathrm{I}} \;=\; & U \sum_{e} \hat{n}_{e,\uparrow} \hat{n}_{e,\downarrow} + U' \sum_{s,s'} \hat{n}_{1,s} \hat{n}_{2,s'} - J \sum_{s} \hat{n}_{1,s} \hat{n}_{2,s} \\ & + J \sum_{s} \hat{c}^{\dagger}_{1,s} \hat{c}^{\dagger}_{2,\bar{s}} \hat{c}_{1,\bar{s}} \hat{c}_{2,s} + J \Big(\hat{c}^{\dagger}_{1,\uparrow} \hat{c}^{\dagger}_{1,\downarrow} \hat{c}_{2,\downarrow} \hat{c}_{2,\uparrow} + \hat{c}^{\dagger}_{2,\uparrow} \hat{c}^{\dagger}_{2,\downarrow} \hat{c}_{1,\downarrow} \hat{c}_{1,\uparrow} \Big) \; . \end{aligned} \tag{2.23}$$

Here, $e = 1, 2$ labels the e_{g} orbitals, $s = \uparrow, \downarrow$ is the spin index and we use the convention $\bar{\uparrow} \equiv \downarrow$, $\bar{\downarrow} \equiv \uparrow$. The Coulomb parameters U, U' and the exchange parameter J are related to the Racah parameters A, B, C, see equations (C.7), through

$$U = A + 4B + 5C \; , \tag{2.24a}$$

$$U' = A - 4B + 3C \; , \tag{2.24b}$$

$$J = 4B + C \; . \tag{2.24c}$$

Only two of the three parameters (2.24) are independent, and we have $U = U' + 2J$, compare equation (C.5a).

#	Atomic eigenstate $\|\Gamma\rangle$	Symmetry	energy E_Γ
1	$\|\uparrow,\uparrow\rangle$	${}^3A_2$	$U'-J$
2	$(\|\uparrow,\downarrow\rangle+\|\downarrow,\uparrow\rangle)/\sqrt{2}$	${}^3A_2$	$U'-J$
3	$\|\downarrow,\downarrow\rangle$	${}^3A_2$	$U'-J$
4	$(\|\uparrow,\downarrow\rangle-\|\downarrow,\uparrow\rangle)/\sqrt{2}$	${}^1E$	$U'+J$
5	$(\|\uparrow\downarrow,0\rangle-\|0,\uparrow\downarrow\rangle)/\sqrt{2}$	${}^1E$	$U-J_\mathrm{C}$
6	$(\|\uparrow\downarrow,0\rangle+\|0,\uparrow\downarrow\rangle)/\sqrt{2}$	${}^1A_1$	$U+J_\mathrm{C}$

Table 2.1: Two-particle eigenstates with symmetry specifications and energies.

There are four spin-orbital states $\sigma=(e,s)$ per atom, leading to a $2^4=16$-dimensional atomic Hilbert space. All eigenstates $|\Gamma\rangle$ of $\hat{H}_\mathrm{I}^\mathrm{2b}$ with particle numbers $N\neq 2$ are simple Slater determinants of spin-orbital states $|\sigma\rangle$ and their energies are

$$\begin{array}{ll} E_\Gamma=0 & (N=0,1)\,, \\ E_\Gamma=U+2U'-J & (N=3)\,, \\ E_\Gamma=2U+4U'-2J & (N=4)\,. \end{array} \tag{2.25}$$

The two-particle eigenstates are slightly more complicated because some of them are linear combinations of Slater determinants. We introduce the basis

$$\left|s,s'\right\rangle \equiv \hat{c}^\dagger_{1,s}\hat{c}^\dagger_{2,s'}\left|0\right\rangle\,, \tag{2.26a}$$

$$|\uparrow\downarrow,0\rangle \equiv \hat{c}^\dagger_{1,\uparrow}\hat{c}^\dagger_{1,\downarrow}\left|0\right\rangle\,, \tag{2.26b}$$

$$|0,\uparrow\downarrow\rangle \equiv \hat{c}^\dagger_{2,\uparrow}\hat{c}^\dagger_{2,\downarrow}\left|0\right\rangle \tag{2.26c}$$

of two-particle states, which are used to set up the eigenstates of $\hat{H}_\mathrm{I}^\mathrm{2b}$, see table 2.3.2. The states of lowest energy are the three triplet states with spin $S=1$, which belong to the representation A_2 of the cubic point-symmetry group. Finding a high-spin ground state is a simple consequence of Hund's first rule. Higher in energy are the two degenerate singlet states of symmetry E and the non-degenerate singlet state of symmetry A_1.

2.4 Related Models

2.4.1 Non-Local Coulomb Interactions

In Hubbard models, as derived in section 2.2, only the local terms of the Coulomb interaction are captured. An obvious generalisation of these models arises when we add non-local terms between certain sites, e.g., nearest neighbours,

$$\begin{aligned} \hat{H}_\mathrm{I,nn} \equiv \frac{1}{2}\sum_{\sigma_1,\sigma_2,\sigma_3,\sigma_4}\sum_{\langle i,j\rangle}\Big[& U^{\sigma_1,\sigma_2,\sigma_3,\sigma_4}_{i,j,j,i}\hat{c}^\dagger_{i,\sigma_1}\hat{c}^\dagger_{j,\sigma_2}\hat{c}_{j,\sigma_3}\hat{c}_{i,\sigma_4} + U^{\sigma_1,\sigma_2,\sigma_3,\sigma_4}_{i,j,i,j}\hat{c}^\dagger_{i,\sigma_1}\hat{c}^\dagger_{j,\sigma_2}\hat{c}_{i,\sigma_3}\hat{c}_{j,\sigma_4} \\ & + U^{\sigma_1,\sigma_2,\sigma_3,\sigma_4}_{i,i,j,j}\hat{c}^\dagger_{i,\sigma_1}\hat{c}^\dagger_{i,\sigma_2}\hat{c}_{j,\sigma_3}\hat{c}_{j,\sigma_4} \\ & + \left(U^{\sigma_1,\sigma_2,\sigma_3,\sigma_4}_{i,j,j,j}\hat{c}^\dagger_{i,\sigma_1}\hat{c}^\dagger_{j,\sigma_2}\hat{c}_{j,\sigma_3}\hat{c}_{j,\sigma_4} + U^{\sigma_1,\sigma_2,\sigma_3,\sigma_4}_{j,i,j,j}\hat{c}^\dagger_{j,\sigma_1}\hat{c}^\dagger_{i,\sigma_2}\hat{c}_{j,\sigma_3}\hat{c}_{j,\sigma_4} + \mathrm{h.c.}\right)\Big]\,. \end{aligned} \tag{2.27}$$

Here, $\langle i,j\rangle$ denotes a restriction of the sum to those neighbouring sites for which the Coulomb interaction is assumed to be finite. If the orbitals are very localised, the first term in (2.27) is dominant since these direct Coulomb interactions ($\sim U^{\sigma_1,\sigma_2,\sigma_3,\sigma_4}_{i,j,j,i}$) stay finite even if the overlap of orbitals on different sites vanishes.

For the one-band Hubbard model, the Coulomb interaction Hamiltonian (2.27) simplifies to

$$\begin{aligned}\hat{H}^{\mathrm{1b}}_{\mathrm{I,nn}} &= \sum_{<i,j>}\Bigg[\sum_{s,s'}(V-J\delta_{s,s'})\hat{n}_{i,s}\hat{n}_{j,s'}+2J\hat{c}^{\dagger}_{i,\uparrow}\hat{c}_{i,\downarrow}\hat{c}^{\dagger}_{j,\uparrow}\hat{c}_{j,\downarrow}+J_{\mathrm{c}}\hat{c}^{\dagger}_{i,\uparrow}\hat{c}^{\dagger}_{i,\downarrow}\hat{c}_{j,\downarrow}\hat{c}_{j,\uparrow} \\ &\quad +\sum_{s}\left(T\hat{c}^{\dagger}_{i,s}\hat{c}_{j,s}\hat{n}_{i,\bar{s}}+\mathrm{h.c.}\right)\Bigg]\ . \end{aligned} \tag{2.28}$$

The implications of non-local terms in the single-band Hubbard model are studied, for example, in references [13–18].

2.4.2 t-J Model

The t-J model has been studied extensively within the Gutzwiller theory. It derives perturbatively from the single-band Hubbard model in the large-U limit. For $U=\infty$ and band fillings $n\leq 1/2$, there are no doubly-occupied sites in the single-band Hubbard model. Therefore, one can investigate the effective Hamiltonian

$$\hat{H}^{\mathrm{eff}}_{1}\equiv\sum_{i,j}\sum_{s}t_{i,j}(1-\hat{n}_{i,\bar{s}})\hat{c}^{\dagger}_{i,s}(1-\hat{n}_{j,\bar{s}})\hat{c}_{j,s}\ , \tag{2.29}$$

instead of $\hat{H}_{\mathrm{1B}}$ since, in the subspace without double occupancy, both Hamiltonians are equivalent. Mathematically, this means that

$$\hat{P}_0\hat{H}_{\mathrm{1B}}\hat{P}_0=\hat{P}_0\hat{H}^{\mathrm{eff}}_{1}\hat{P}_0\ , \tag{2.30}$$

where

$$\hat{P}_0\equiv\prod_{i}(1-\hat{n}_{i,\uparrow}\hat{n}_{i,\downarrow}) \tag{2.31}$$

is the projector onto the space without doubly-occupied sites.

To find the ground state (or excited states) of (2.29), is already quite challenging and, in general, impossible; see, e.g., reference [19] on exact results for a $U=\infty$ Hubbard model with a single hole. Apart from the special case of half band filling [20–24], standard perturbation theory cannot be employed to investigate the leading corrections in powers of $t_{i,j}/U$ for the single-band Hubbard model since it requires a diagonalisation of (2.29).

It is possible to derive an effective Hamiltonian beyond (2.29), which is correct up to a certain order in $t_{i,j}/U$. Such an effective Hamiltonian may then be investigated by approximate numerical or analytical techniques. The derivation of effective Hamiltonians for large U goes back to a work by Harris and Lange [25]. More recent results on large U expansions for the Hubbard model can be found in references [26–29].

We write the single-band Hubbard model as

$$\hat{H}_{\mathrm{1b}}=H_{0\|}+H_{0\perp}+H_{\mathrm{I}}\ , \tag{2.32}$$

where the operators

$$\hat{H}_{0\|}\equiv\sum_{i,j}\sum_{s}t_{i,j}(1-\hat{n}_{i,\bar{s}})\hat{c}^{\dagger}_{i,s}(1-\hat{n}_{j,\bar{s}})\hat{c}_{j,s}+t_{i,j}\hat{n}_{i,\bar{s}}\hat{c}^{\dagger}_{i,s}\hat{n}_{j,\bar{s}}\hat{c}_{j,s}\ , \tag{2.33a}$$

$$\hat{H}_{0\perp}\equiv\sum_{i,j}\sum_{s}t_{i,j}(1-\hat{n}_{i,\bar{s}})\hat{c}^{\dagger}_{i,s}\hat{n}_{j,\bar{s}}\hat{c}_{j,s}+t_{i,j}\hat{n}_{i,\bar{s}}\hat{c}^{\dagger}_{i,s}(1-\hat{n}_{j,\bar{s}})\hat{c}_{j,s}\ . \tag{2.33b}$$

either preserve the number of doubly occupied sites ($\hat{H}_{0\|}$), or, change this number by one ($\hat{H}_{0\perp}$). For large U, the operator $\hat{H}_{0\perp}$ induces high-energy excitations, which, to leading order in $t_{i,j}/U$, one can eliminate by the unitary transformation

$$\hat{H}'_{1\mathrm{b}} \equiv e^{\mathrm{i}\hat{S}} \hat{H}_{1\mathrm{b}} e^{-\mathrm{i}\hat{S}} \tag{2.34}$$

with

$$\hat{S} \equiv \mathrm{i} \sum_{i,j} \sum_{s} \frac{t_{i,j}}{U} \left((1 - \hat{n}_{i,\bar{s}}) \hat{c}^{\dagger}_{i,s} \hat{n}_{j,\bar{s}} \hat{c}_{j,s} - \mathrm{h.c.} \right) . \tag{2.35}$$

An expansion of $e^{-\mathrm{i}\hat{S}}$ to leading order in $t_{i,j}/U$ yields

$$\hat{H}'_{1\mathrm{b}} = \hat{H}_{\mathrm{I}} + \hat{H}'_1 + \hat{H}'_2 + \mathcal{O}\left(\frac{t^3_{i,j}}{U^2} \right) , \tag{2.36}$$

where

$$\hat{H}'_1 = \hat{H}_0 + \mathrm{i}[\hat{S}, \hat{H}_{\mathrm{I}}] = \hat{H}_{0\|} \sim t_{i,j} , \tag{2.37a}$$

$$\hat{H}'_2 = \mathrm{i}[\hat{S}, \hat{H}_0] + \frac{i^2}{2} [\hat{S}, [\hat{S}, \hat{H}_{\mathrm{I}}]] \sim \frac{t^2_{i,j}}{U} . \tag{2.37b}$$

Up to this point, the expansion of the Hamiltonian $\hat{H}'_{1\mathrm{b}}$ is exact to order $t^3_{i,j}/U^2$. Now, again, we define an effective Hamiltonian

$$\hat{H}^{\mathrm{eff}} = \hat{H}^{\mathrm{eff}}_1 + \hat{H}_J + \hat{H}_3 \tag{2.38}$$

through the condition that $\hat{H}^{\mathrm{eff}}$ and $\hat{H}'_{1\mathrm{b}}$ are the same in the subspace without double occupancy, i.e.,

$$\hat{P}_0 \hat{H}'_{1\mathrm{b}} \hat{P}_0 = \hat{P}_0 \hat{H}^{\mathrm{eff}} \hat{P}_0 . \tag{2.39}$$

The operator $\hat{H}^{\mathrm{eff}}_1$ in (2.38) has already been defined in (2.29). Its two leading corrections, the operators $\hat{H}_J$ and $\hat{H}_3$, are given by

$$\hat{H}_J \equiv \frac{1}{2} \sum_{i,j} \frac{4|t_{i,j}|^2}{U} \left(\hat{\boldsymbol{S}}_i \hat{\boldsymbol{S}}_j - \frac{1}{4} \hat{n}_i \hat{n}_j \right) , \tag{2.40a}$$

$$\hat{H}_3 \equiv - \sum_{i \neq j \neq k (\neq i)} \frac{t_{i,j} t_{j,k}}{U} \sum_{s} \left(\hat{c}^{\dagger}_{i,s} \hat{c}_{k,s} \hat{n}_{j,\bar{s}} - \hat{c}^{\dagger}_{i,s} \hat{c}_{k,\bar{s}} \hat{c}^{\dagger}_{j,\bar{s}} \hat{c}_{j,s} \right) . \tag{2.40b}$$

If one neglects the three-site term $\hat{H}_3$ in (2.38), the 't-J model' results

$$\hat{H}_{t-J} \equiv \hat{H}^{\mathrm{eff}}_1 + \hat{H}_J , \tag{2.41}$$

The three site terms are, however, of the same order $t^2_{i,j}/U$ and, therefore, it is unclear if (or when) it might be justified to neglect them. At half band filling, both operators $\hat{H}^{\mathrm{eff}}_1$ and $\hat{H}_3$ vanish in the subspace without double occupancies and the Heisenberg spin model results.

Chapter 3

Ab-Initio Methods

In the previous chapter, we introduced the general electronic Hamiltonian in theoretical solid-states physics, see equations (2.2) or (2.3). As discussed already in section 2.1, one can either try to simplify that Hamiltonian leading to certain classes of model Hamiltonians or one aims at an 'ab-initio' treatment of the full Hamiltonian. The two most important 'ab-initio' methods are the Hartree-Fock theory and the Density-Functional Theory, which we discuss in sections 3.1 and 3.2, respectively.

3.1 Hartree-Fock Theory

We start this chapter with a derivation of the general Hartree-Fock equations in section 3.1.1. As two simple examples, the Hartree-Fock equations are solved for the jellium model and a two-site Hubbard model in sections 3.1.2 and 3.1.3, respectively. We close the first part of this chapter on ab-initio methods with a discussion of merits and shortcomings of the Hartree-Fock theory in section 3.1.4.

3.1.1 Derivation of the Hartree-Fock Equations

The Hartree-Fock theory can be derived in various ways, all leading to equivalent results. The most transparent derivation is based on a diagrammatic expansion of the single-particle Green's function; see, e.g., reference [30]). It naturally covers systems at finite temperatures and provides a systematic way to investigate dynamical properties. In our derivation, we use a variational approach since it is closely related to the Density-Functional Theory and, more importantly, to the Gutzwiller variational theory.

The Hartree-Fock theory provides variationally the optimal one-particle wave function to the Hamiltonian (2.3). Such a wave function is defined as a Slater determinant

$$|\Psi_0\rangle = \prod_{\gamma(\text{occ.})} \hat{h}^\dagger_\gamma |0\rangle \ , \tag{3.1}$$

in which certain one-particle states $|\gamma\rangle$ are occupied. The operators $\hat{h}^\dagger_\gamma$ and $\hat{c}^\dagger_\sigma$ are related by a unitary transformation

$$\hat{h}^\dagger_\gamma = \sum_\sigma u_{\gamma,\sigma} \hat{c}^\dagger_\sigma \ , \tag{3.2a}$$

$$\hat{c}^\dagger_\sigma = \sum_\gamma u^*_{\gamma,\sigma} \hat{h}^\dagger_\gamma \ . \tag{3.2b}$$

The unitarity of the transformation implies that

$$\sum_{\sigma} u^*_{\gamma,\sigma} u_{\gamma',\sigma} = \delta_{\gamma,\gamma'} \; . \tag{3.3}$$

It is chosen such that the expectation value

$$\left\langle \hat{H}_{\rm el} \right\rangle_{\Psi_0} = \sum_{\sigma_1,\sigma_2} \varepsilon_{\sigma_1,\sigma_2} \left\langle \hat{c}^\dagger_{\sigma_1} \hat{c}_{\sigma_2} \right\rangle_{\Psi_0} + \frac{1}{2} \sum_{\sigma_1,\sigma_2,\sigma_3,\sigma_4} U_{\sigma_1,\sigma_2,\sigma_3,\sigma_4} \left\langle \hat{c}^\dagger_{\sigma_1} \hat{c}^\dagger_{\sigma_2} \hat{c}_{\sigma_3} \hat{c}_{\sigma_4} \right\rangle_{\Psi_0} \tag{3.4}$$

of the Hamiltonian (2.3) with respect to $|\Psi_0\rangle$ is minimal. With Wick's theorem, see equation (A.2) in appendix A, we find

$$\left\langle \hat{c}^\dagger_{\sigma_1} \hat{c}^\dagger_{\sigma_2} \hat{c}_{\sigma_3} \hat{c}_{\sigma_4} \right\rangle_{\Psi_0} = \left\langle \hat{c}^\dagger_{\sigma_1} \hat{c}_{\sigma_4} \right\rangle_{\Psi_0} \left\langle \hat{c}^\dagger_{\sigma_2} \hat{c}_{\sigma_3} \right\rangle_{\Psi_0} - \left\langle \hat{c}^\dagger_{\sigma_1} \hat{c}_{\sigma_3} \right\rangle_{\Psi_0} \left\langle \hat{c}^\dagger_{\sigma_2} \hat{c}_{\sigma_4} \right\rangle_{\Psi_0} \; , \tag{3.5a}$$

with

$$\left\langle \hat{c}^\dagger_{\sigma_i} \hat{c}_{\sigma_j} \right\rangle_{\Psi_0} = \sum_{\gamma({\rm occ.})} u^*_{\gamma,\sigma_i} u_{\gamma,\sigma_j} \; . \tag{3.5b}$$

Therefore, the expectation value (3.4) reads

$$\begin{aligned} \left\langle \hat{H}_{\rm el} \right\rangle_{\Psi_0} \;\; = \;\; & \sum_{\sigma_1,\sigma_2} \varepsilon_{\sigma_1,\sigma_2} \sum_{\gamma({\rm occ.})} u^*_{\gamma,\sigma_1} u_{\gamma,\sigma_2} + \\ & \frac{1}{2} \sum_{\sigma_1,\sigma_2,\sigma_3,\sigma_4} U_{\sigma_1,\sigma_2,\sigma_3,\sigma_4} \sum_{\gamma,\gamma'({\rm occ.})} \left(u^*_{\gamma,\sigma_1} u_{\gamma,\sigma_4} u^*_{\gamma',\sigma_2} u_{\gamma',\sigma_3} - u^*_{\gamma,\sigma_1} u_{\gamma,\sigma_3} u^*_{\gamma',\sigma_2} u_{\gamma',\sigma_4} \right) \; . \end{aligned} \tag{3.6}$$

It must be minimised with respect to $u^*_{\gamma,\sigma}$ (or, equivalently, with respect to $u_{\gamma,\sigma}$) with the additional constraints given by equations (3.3) for $\gamma = \gamma'$. These constraints are implemented by adding Lagrange-parameter terms to (3.6),

$$\frac{\partial}{\partial u^*_{\gamma,\sigma}} \left[\left\langle \hat{H}_{\rm el} \right\rangle_{\Psi_0} - \sum_{\gamma} E_\gamma \left(\sum_{\sigma'} |u_{\gamma,\sigma'}|^2 - 1 \right) \right] = 0 \; . \tag{3.7}$$

Note that equations (3.3) for $\gamma \neq \gamma'$ are implemented by a proper solution of equation (3.9a), see below. With the obvious symmetries

$$U_{\sigma_1,\sigma_2,\sigma_3,\sigma_4} = U_{\sigma_2,\sigma_1,\sigma_4,\sigma_3} \; , \tag{3.8}$$

equation (3.7) yields the effective one-particle Schrödinger equation

$$\sum_{\sigma'} (\varepsilon_{\sigma,\sigma'} + \Sigma_{\sigma,\sigma'}) u_{\gamma,\sigma'} = E_\gamma u_{\gamma,\sigma} \; , \tag{3.9a}$$

where we introduced the Hartree-Fock 'self-energy'

$$\Sigma_{\sigma,\sigma'} \equiv \sum_{\sigma_1,\sigma_2} \left(U_{\sigma,\sigma_1,\sigma_2,\sigma'} - U_{\sigma,\sigma_1,\sigma',\sigma_2} \right) \sum_{\gamma({\rm occ.})} u^*_{\gamma,\sigma_1} u_{\gamma,\sigma_2} \; . \tag{3.9b}$$

The first and the second term in (3.9b) are denoted as the 'Hartree' and the 'Fock' (or 'exchange') contribution, respectively. Note that the self-energy $\Sigma_{\sigma,\sigma'}$ still depends on the wave function (3.1) and, therefore, the 'Hartree-Fock equations' (3.9a) have to be solved self-consistently. From equation (3.9a) it becomes apparent why the Hartree-Fock approximation

is also denoted as a 'mean-field theory'. The electronic interaction appears in eq. (3.9a) solely through the self-energy (3.9b), i.e., it has the form of an effective or 'mean' field.

The Hartree-Fock ground state often has the special form

$$|\Psi_{\mathrm{HF}}\rangle = \prod_{\gamma(E_\gamma<E_\mathrm{F})} \hat{h}_\gamma^\dagger\,|0\rangle \tag{3.10}$$

with a Fermi energy E_F, which is determined by the particle number

$$N = \sum_{\gamma(E_\gamma<E_\mathrm{F})} 1\,. \tag{3.11}$$

For infinite systems, one can prove that the occupied levels are indeed given by a condition $E_\gamma < E_\mathrm{F}$ [31], whereas, for finite systems, a more complicated Hartree-Fock ground state cannot be excluded.

Due to the self-consistency, it is usually impossible to prove rigorously that a certain solution $|\Psi_{\mathrm{HF}}\rangle$ of the Hartree-Fock equations is indeed the one-particle state of lowest energy. At least for translationally invariant systems, which we consider in this work, it will usually be simple to identify the optimum Hartree-Fock state by symmetry arguments. The stability of an assumed variational ground state $|\Psi_{\mathrm{HF}}\rangle$ can also be tested at least with respect to small variations within an RPA calculation, see section 8.2 and, e.g., reference [31].

The Lagrange parameters E_γ in (3.10) and (3.11) appear to be the single-particle energies of an uncorrelated Fermi gas. In fact, one usually interprets these parameters as 'quasi-particle' excitation energies. One way to legitimise this interpretation is based on 'Koopmanns' theorem' [32]. It states that by creating a particle or a hole in the Hartree-Fock ground state the energy changes by E_γ, i.e., we have

$$\big\langle \Psi^{(\gamma)}_{\mathrm{HF},\pm}\big|\hat{H}_\mathrm{el}\big|\Psi^{(\gamma)}_{\mathrm{HF},\pm}\big\rangle - \big\langle \Psi_{\mathrm{HF}}\big|\hat{H}_\mathrm{el}\big|\Psi_{\mathrm{HF}}\big\rangle = \pm E_\gamma \tag{3.12a}$$

for the particle and hole states

$$\big|\Psi^{(\gamma)}_{\mathrm{HF},+}\big\rangle \;\equiv\; \hat{h}_\gamma^\dagger\,|\Psi_{\mathrm{HF}}\rangle\;, \tag{3.12b}$$

$$\big|\Psi^{(\gamma)}_{\mathrm{HF},-}\big\rangle \;\equiv\; \hat{h}_\gamma\,|\Psi_{\mathrm{HF}}\rangle\;. \tag{3.12c}$$

The same result for quasi-particle excitation energies can be derived, more transparently, by means of the diagrammatic Hartree-Fock approximation for the single-particle Green's function. One should keep in mind, however, that the variational ground-state energy in the Hartree-Fock theory is not given by the sum over all occupied energy levels as one might expect from a naive analogy with an uncorrelated Fermi gas. Instead, equations (3.6), (3.9a), and (3.9b), readily give

$$\big\langle \hat{H}_\mathrm{el}\big\rangle_{\Psi_{\mathrm{HF}}} = \frac{1}{2}\sum_{\gamma(\mathrm{occ.})} E_\gamma + \frac{1}{2}\big\langle \hat{H}_0\big\rangle_{\Psi_{\mathrm{HF}}} = \sum_{\gamma(\mathrm{occ.})} E_\gamma - \big\langle \hat{H}_\mathrm{I}\big\rangle_{\Psi_{\mathrm{HF}}} \tag{3.13}$$

for the Hartree-Fock ground-state energy.

When we work with the basis $|\sigma\rangle = |\boldsymbol{r}\rangle\,|s\rangle$ of position space eigenvectors $|\boldsymbol{r}\rangle$ and spinors $|s\rangle = |\uparrow\rangle$ and $|\downarrow\rangle$, the transformation (3.2a) reads

$$\hat{h}_\gamma^\dagger = \sum_s \int d^3\boldsymbol{r}\; u_\gamma(s,\boldsymbol{r})\hat{\psi}_s^\dagger(\boldsymbol{r})\;, \tag{3.14}$$

and the Hartree-Fock equations (3.9a) for the single-particle wave functions $u_\gamma(s,\boldsymbol{r})$ have the form

$$\left(-\frac{\Delta_{\boldsymbol{r}}}{2m}+V(\boldsymbol{r})\right)u_\gamma(s,\boldsymbol{r})+\sum_{s'}\int d^3\boldsymbol{r}'\,\Sigma_{s,s'}(\boldsymbol{r},\boldsymbol{r}')u_\gamma(s',\boldsymbol{r}')=E_\gamma u_\gamma(s,\boldsymbol{r})\;. \tag{3.15}$$

Here, the Hartree contribution to the self-energy $\Sigma=\Sigma^{\mathrm{H}}+\Sigma^{\mathrm{F}}$ is given by

$$\Sigma^{\mathrm{H}}_{s,s'}(\boldsymbol{r},\boldsymbol{r}')=\delta(\boldsymbol{r}-\boldsymbol{r}')\sum_{\tilde{s}}\int d^3\tilde{\boldsymbol{r}}\,\frac{e^2}{|\boldsymbol{r}-\tilde{\boldsymbol{r}}|}n(\tilde{\boldsymbol{r}}) \tag{3.16a}$$

with the particle density

$$n(\boldsymbol{r})=\sum_s\sum_{\gamma(E_\gamma\le E_{\mathrm{F}})}|u_\gamma(s,\boldsymbol{r})|^2\;. \tag{3.16b}$$

For the Fock contribution to the self-energy, we find

$$\Sigma^{\mathrm{F}}_{s,s'}(\boldsymbol{r},\boldsymbol{r}')=-\delta_{s,s'}\frac{e^2}{|\boldsymbol{r}-\boldsymbol{r}'|}\sum_{\gamma(E_\gamma\le E_{\mathrm{F}})}u^*_\gamma(s,\boldsymbol{r}')u_\gamma(s,\boldsymbol{r})\;. \tag{3.16c}$$

Here, we assumed that $|\Psi_{\mathrm{HF}}\rangle$ is an eigenstate of

$$\hat{S}_z=\frac{1}{2}\int d^3\boldsymbol{r}\,\left(\hat{\psi}^\dagger_\uparrow(\boldsymbol{r})\hat{\psi}_\uparrow(\boldsymbol{r})-\hat{\psi}^\dagger_\downarrow(\boldsymbol{r})\hat{\psi}_\downarrow(\boldsymbol{r})\right), \tag{3.17}$$

the operator for the total spin along the spin-quantisation axis. Only with this assumption does the sum over γ in (3.16c) lead to the Kronecker-delta $\delta_{s,s'}$ for the spins.

Obviously, the Hartree and the Fock contribution to the self-energy are fundamentally different. The Hartree term acts like a classical field and could, in principle, be added to the potential $V(\boldsymbol{r})$ in (3.15). By contrast, the Fock contribution is non-local and it further introduces a spin dependence since only electrons with parallel spins are coupled.

In order to assess the accuracy of Hartree-Fock calculations for real materials in section 3.1.4, we first have a look at the results for the free-electron gas and the two-site Hubbard model. The Hartree-Fock results for the free-electron gas will also be needed in order to set up the energy functional in the Local-Density Approximation in section 3.2.2.

3.1.2 Jellium Model

In the 'jellium model', the periodic potential $V(\boldsymbol{r})$ in (3.15) is replaced by a homogeneous background of a positive charge density n_{p} to ensure the charge neutrality of the system. As a consequence, the electronic density $n(\boldsymbol{r})=-n_{\mathrm{p}}$ is also homogeneous and the potential term proportional to $V(\boldsymbol{r})$ just cancels the Hartree contribution to the self-energy in (3.15). It is clear from symmetry arguments that a homogeneous paramagnetic solution of the Hartree-Fock equations must be given by a Slater determinant (3.10) of plane waves

$$u_{\boldsymbol{k}}(s,\boldsymbol{r})=\frac{1}{\sqrt{(2\pi)^3V}}\,e^{\mathrm{i}\boldsymbol{k}\boldsymbol{r}}\;. \tag{3.18}$$

For these single-particle wave functions, the Fock contribution to the self-energy reads

$$\begin{aligned}\Sigma^{\mathrm{F}}_{s,s'}(\boldsymbol{r},\boldsymbol{r}') &= -\delta_{s,s'}\frac{e^2}{(2\pi)^3|\boldsymbol{r}-\boldsymbol{r}'|}\int_{k<k_{\mathrm{F}}}\mathrm{d}^3\boldsymbol{k}\;e^{\mathrm{i}\boldsymbol{k}(\boldsymbol{r}-\boldsymbol{r}')}\\ &= +\delta_{s,s'}\frac{e^2}{2\pi^2}\frac{k_{\mathrm{F}}|\boldsymbol{r}-\boldsymbol{r}'|\cos\left(k_{\mathrm{F}}|\boldsymbol{r}-\boldsymbol{r}'|\right)-\sin\left(k_{\mathrm{F}}|\boldsymbol{r}-\boldsymbol{r}'|\right)}{|\boldsymbol{r}-\boldsymbol{r}'|^4}\end{aligned} \tag{3.19}$$

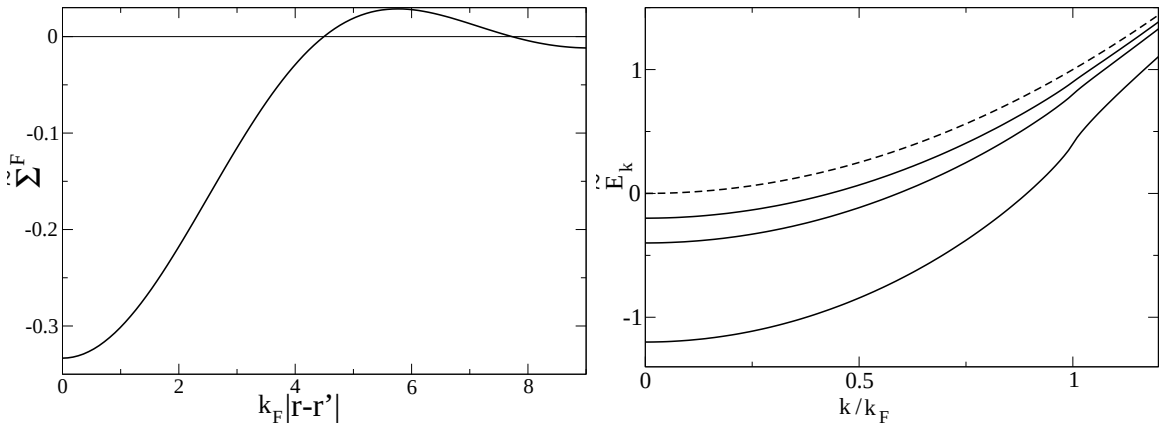

Figure 3.1: Left: Fock self-energy $\tilde{\Sigma}^{\mathrm{F}}(k_{\mathrm{F}}|\boldsymbol{r}-\boldsymbol{r}'|) \equiv \Sigma^{\mathrm{F}}_{s,s}(\boldsymbol{r},\boldsymbol{r}')(2\pi^2|\boldsymbol{r}-\boldsymbol{r}'|)/e^2$ for the jellium model. Right: Quasi-particle dispersion $\tilde{E}_{\boldsymbol{k}} \equiv \frac{2m}{k_{\mathrm{F}}^2}E_{\boldsymbol{k}}$ of the jellium model for values $\frac{me^2k_{\mathrm{F}}}{\pi} = 0, 0.05, 0.1, 0.3$ in descending order.

where we introduced the Fermi wave vector $k_{\mathrm{F}} \equiv \sqrt{2mE_{\mathrm{F}}}$. The spatial dependence of the Fock self-energy is displayed in figure 3.1(left). One clearly sees the pronounced 'attractive' interaction of electrons with the same spin on short distances. By contrast, electrons with opposite spins do not interact at all in the Hartree-Fock approximation, which is obviously an unphysical feature in the high-density limit.

With the result for the self-energy, we can evaluate the integral in (3.15)

$$\int \mathrm{d}^3\boldsymbol{r}'\, \Sigma^{\mathrm{F}}_{s,s}(\boldsymbol{r},\boldsymbol{r}')u_{\boldsymbol{k}}(s,\boldsymbol{r}') = -u_{\boldsymbol{k}}(s,\boldsymbol{r})\frac{e^2k_{\mathrm{F}}}{2\pi}F(k/k_{\mathrm{F}}) \,, \tag{3.20a}$$

where

$$F(x) \equiv 2 + \frac{1-x^2}{x}\ln\left|\frac{1+x}{1-x}\right| . \tag{3.20b}$$

Hence, the plane-wave Ansatz (3.18) is indeed a solution of (3.15) for the jellium model and the eigenvalues $E_\gamma = E_{\boldsymbol{k}}$ are given as

$$E_{\boldsymbol{k}} = E_k = \frac{k^2}{2m} - \frac{e^2k_{\mathrm{F}}}{2\pi}F(k/k_{\mathrm{F}}) \,. \tag{3.20c}$$

The quasi-particle dispersion (3.20c) is displayed in figure 3.1(right). We will discuss this results for the dispersion in section 3.1.4.

Finally, for later use in connection with the Local-Density Approximation, we consider the expectation values of the kinetic and the Coulomb energy in the Hartree-Fock theory. Since our Hartree-Fock ground state (3.10) is a Slater determinant of plane waves, the expectation value of the kinetic energy is that of an uncorrelated Fermi sea,

$$\langle\hat{H}_0\rangle_{\Psi_{\mathrm{HF}}} = \frac{V}{2m\pi^2}\int_{k<k_{\mathrm{F}}} k^4\mathrm{d}k = V\frac{3}{10m}(3\pi^2)^{2/3}n^{5/3} \,. \tag{3.21a}$$

Here, we used

$$n = \frac{N}{V} = \frac{1}{\pi^2}\int_{k<k_{\mathrm{F}}} k^2\mathrm{d}k = \frac{1}{3\pi^2}k_{\mathrm{F}}^3 \,. \tag{3.21b}$$

Equation (3.13) yields the expectation value of the Coulomb interaction,

$$\langle\hat{H}_{\mathrm{I}}\rangle_{\Psi_{\mathrm{HF}}} = \frac{1}{2}\sum_{\boldsymbol{k}(|\boldsymbol{k}|<k_{\mathrm{F}})} E_{\boldsymbol{k}} - \frac{1}{2}\langle\hat{H}_0\rangle_{\Psi_{\mathrm{HF}}} = -\frac{Ve^2k_{\mathrm{F}}^4}{4\pi^3}\int_0^1 x^2F(x)\mathrm{d}x \,. \tag{3.21c}$$

The integral in (3.21c) is equal to unity and, hence, with (3.21b), we find

$$\langle \hat{H}_{\rm I} \rangle_{\Psi_{\rm HF}} = -\frac{3Ve^2}{4\pi} k_{\rm F}^4 = -\frac{3Ve^2}{4\pi} (3\pi)^{1/3} n^{4/3} \; . \tag{3.21d}$$

3.1.3 Hartree-Fock Approximation for the Two-Site Hubbard Model

The two-site Hubbard model was introduced in section 2.3.1 and its exact eigenstates and energies are derived in appendix B. Here, we only consider states with two electrons since all other eigenstates are simple Slater determinants and captured correctly by the Hartree-Fock theory; see appendix B.

For $U = 0$, the two-particle ground state of (2.22) is

$$|\Psi_0\rangle = \hat{h}_1^\dagger \hat{h}_2^\dagger |0\rangle \tag{3.22}$$

in which the two lowest one-particle levels, given by the operators

$$\hat{h}_{1(2)}^\dagger = \frac{1}{\sqrt{2}} \left(\hat{c}_{1\uparrow(\downarrow)}^\dagger - \hat{c}_{2\uparrow(\downarrow)}^\dagger \right) \; , \tag{3.23}$$

are occupied. At finite U, the self-energy (3.9b) contains only a Hartree contribution if we assume that the Hartree-Fock ground state $|\Psi_{\rm HF}\rangle$ is an eigenstate of the spin operator $\hat{S}_z$ in spin-quantisation direction. This ensures that spin-flip expectation values, such as $\Delta_{\uparrow,\downarrow} \equiv \langle \hat{c}_{1\uparrow}^\dagger \hat{c}_{1\downarrow} \rangle$, vanish for $|\Psi_{\rm HF}\rangle$. Note that this condition does not confine our variational space; all solutions with finite $\Delta_{\uparrow,\downarrow}$ are energetically equivalent to some other states that have $\Delta_{\uparrow,\downarrow} = 0$, just with respect to a different spin-quantisation axis.

The self-energy is diagonal and given as

$$\Sigma_{is} \equiv \Sigma_{is,is} = U n_{i,\bar{s}} \; , \tag{3.24}$$

where $n_{i,\bar{s}} = \langle \hat{n}_{i,\bar{s}} \rangle_{\Psi_{\rm HF}}$ and, as before, $\bar{\uparrow} \equiv \downarrow$, $\bar{\downarrow} \equiv \uparrow$. Without spin order, i.e., if $n_{i,\bar{s}} = 1/2$ for all i and s, the self-energy is a constant and also independent of i and s. Then, $|\Psi_{\rm HF}\rangle$ is just the uncorrelated ground state (3.22) and it has the energy

$$E_0 = -2t + \frac{U}{2} \; . \tag{3.25}$$

A comparison with the exact ground-state energy (B.13b) shows that this result is correct up to first order in U/t, but it does not capture any higher-order terms and, in particular, it is wrong in the large-U limit where the exact ground-state energy is proportional to t^2/U.

Obviously, the Hartree-Fock state (3.22) is not favourable energetically for large U because it does not lower the Coulomb energy. This can only be achieved in the Hartree-Fock theory by introducing some spin order. A ferromagnetic order would lower the interaction energy but an antiferromagnetic order is more favourable for both the interaction and the kinetic energy. Therefore, we assume that

$$\Delta \equiv n_{1\uparrow} - n_{1\downarrow} = n_{2\downarrow} - n_{2\uparrow} \neq 0 \; . \tag{3.26}$$

With this antiferromagnetic order, the self-energies are still diagonal but they depend on the spin and orbital indices,

$$\Sigma_{1\uparrow} = \Sigma_{2\downarrow} \;\; = \;\; \frac{U}{2} (1 + \Delta) \; , \tag{3.27a}$$

$$\Sigma_{1\downarrow} = \Sigma_{2\uparrow} \;\; = \;\; \frac{U}{2} (1 - \Delta) \; . \tag{3.27b}$$

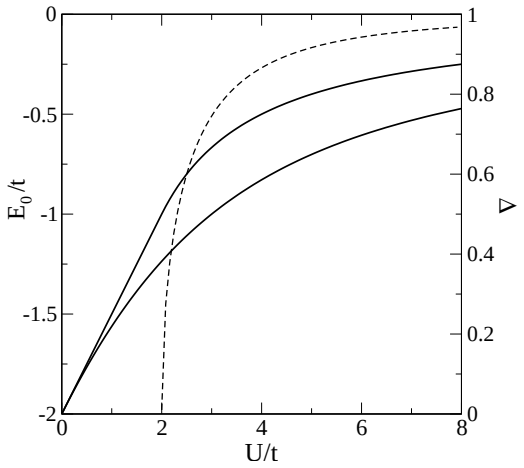

Figure 3.2: Exact ground-state energy and the Hartree-Fock energy of the two-site Hubbard model (solid lines) in ascending order; The dashed line shows the 'magnetisation' Δ.

The solution of the Hartree-Fock equations (3.9a) then leads to the one-particle operators

$$\hat{h}^\dagger_{1(2)} = \cos(\theta)\hat{c}^\dagger_{1\uparrow(2\downarrow)} + \sin(\theta)\hat{c}^\dagger_{2\uparrow(1\downarrow)} \,, \tag{3.28a}$$

where

$$\tan(\theta) = -\frac{U\Delta + \sqrt{U^2\Delta^2 + 4t^2}}{2t} \,. \tag{3.28b}$$

The operators (3.28a) define the new Hartree-Fock ground state (3.22), which determines the 'magnetisation' Δ by the self-consistency condition

$$\Delta = \cos^2(\theta) - \sin^2(\theta) \,. \tag{3.29}$$

Instead of solving the self-consistency equations (3.28b) and (3.29), we could find the same results by minimising the variational energy (3.30) with respect to the parameter Δ; compare the corresponding calculation in the Gutzwiller approximation, section 5.4.2. The self-consistency equations (3.28b) and (3.29) have three solutions, $\Delta = 0$ and $\Delta = \pm\sqrt{1-(2t/U)^2}$. The antiferromagnetic solutions with $\Delta \neq 0$ exist for $U > 2t$ and the Hartree-Fock ground-state energy is therefore given as

$$E_0^\Delta = 4t\sin(\theta)\cos(\theta) + 2U\cos^2(\theta)\sin^2(\theta) = \begin{cases} -2t + U/2 & \text{for} \quad U \leq 2t \\ -2t^2/U & \text{for} \quad U > 2t \end{cases} \,. \tag{3.30}$$

In figure 3.2, the Hartree-Fock energy is compared to the exact ground-state energy (B.13b),

$$E_0^{\text{exact}} = \frac{1}{2}\left(U - \sqrt{U^2 + 16t^2}\right) \overset{U\gg t}{\to} -\frac{4t^2}{U} \,. \tag{3.31}$$

Due to the antiferromagnetic order, the energy (3.30) shows the correct large-U scaling, however, the coefficient is off by a factor of 2,

$$E_0^\Delta \overset{U\gg t}{\to} -\frac{2t^2}{U} \neq -\frac{4t^2}{U} \,. \tag{3.32}$$

This discrepancy is due to the fact that the Hartree-Fock wave function does not capture the spin-fluctuations in the exact singlet ground state. More worrying than this discrepancy in energy, however, is the spurious symmetry breaking that appears in the Hartree-Fock solution. In fact, as we will see throughout this work, it is one of the main problems of effective single-particle theories that they overestimate the instability of many-particle systems with respect to spurious ground states with broken symmetries.

3.1.4 Merits and Shortcomings of the Hartree-Fock Approximation

The Hartree-Fock theory is the natural first-order approximation in order to study systems of interacting particles. However, there are serious shortcomings in this approach, which make it inevitable to seek for more precise many-particle theories. We begin with a discussion of its merits.

Merits

i) The Hartree-Fock theory can be derived starting from a variational wave function. Therefore, the Hartree-Fock energy provides a rigorous upper bound of the exact ground-state energy. However, an exact energy boundary does not ensure that the wave function resembles the exact ground state, not even qualitatively. We have found such a qualitative failure of the Hartree-Fock ground state in the case of the two-site Hubbard model. Other examples will be discussed in later parts of this work, see, e.g., sections 9.1 and 9.2 on spin and orbital order in two-band Hubbard models.

ii) When the Hartree-Fock theory is derived within a diagrammatic perturbation theory, it is found to be the first-order term in such an expansion. In this respect, the Hartree-Fock approximation provides a systematic starting point for more advanced many-particle theories. However, it is not ensured that the first-order contribution does not, e.g., introduce a certain symmetry breaking, which is absent in the true ground state and its excitations. A many-particle theory that is based on such spurious Hartree-Fock results will then suffer from the very same shortcomings.

Shortcomings

i) As a first-order perturbation correction to an uncorrelated Fermi gas the Hartree-Fock theory should qualitatively describe the physics of simple metals, such as sodium or potassium. However, from our results for the jellium model, we can already conclude that it fails this test: The density of states at the Fermi level is given by

$$D(E_{\mathrm{F}}) = \int \mathrm{d}^3\boldsymbol{k}\; \delta(E_{\mathrm{F}} - E_{\boldsymbol{k}}) = 4\pi \int_0^\infty \mathrm{d}k\; k^2 \delta(E_{\mathrm{F}} - E_k) = 4\pi k_{\mathrm{F}}^2 \left| \frac{\partial}{\partial k} E_k \right|^{-1}_{k=k_{\mathrm{F}}} , \quad (3.33)$$

where the derivative of E_k diverges for $k = k_{\mathrm{k}}$ due to the logarithm in equations (3.20). Hence, the density of states vanishes at the Fermi level for the jellium model. A closer inspection of the integrals that have led to the logarithm in (3.20) shows that this non-analyticity is solely caused by the long-range character of the Coulomb potential. Therefore, it seems natural that this result is not bound to the jellium model but shows up in more realistic lattice systems as well. In fact, it has been shown in reference [33] that the Hartree Fock theory yields a vanishing density of states at the Fermi level for all lattice models and band fillings. This is obviously in disagreement with our experimental observations on metals. In order to mend this deficiency, one has to employ more sophisticated many-particle techniques, which properly incorporate the self-screening of the electrons, see, e.g., references [34–36].

To be fair in our assessment of this particular Hartree-Fock failure, it should be mentioned that other methods, which we are going to discuss in this work, 'solve' the self-screening problem rather phenomenologically: The Density-Functional Theory replaces the full non-local exchange interaction by some effective local field, see section 3.2.2; In model-system treatments, the problematic long-range Coulomb interaction is usually cut off by hand, see section 2.2.

ii) Apart from the problems with the long-range nature of the Coulomb interaction, the Hartree-Fock theory also fails to treat the Coulomb interaction properly on short distances. In the self-energy of the jellium model, there is no contribution from the Coulomb interaction for electrons with opposite spin but only the 'attractive' exchange interaction of electrons with the same spin. Therefore, one finds an inherent disposition to build up some form of spin order. In fact, it was shown in references [37, 38] that the homogeneous paramagnetic solution is never the variational ground state of the Hartree-Fock equations for the jellium model. Depending on the particle density, a state of lower energy could be ferromagnetic (at low densities) or showing a spin-density wave (at higher densities). For the jellium model, it is difficult to asses whether these spin orders are spurious Hartree-Fock results. In the case of the two-site model, we have definitely seen that the Hartree-Fock approach tends to spurious symmetry breaking. The reason for these shortcomings is relatively simple from an energetic point of view: Due to the inflexibility of the Hartree-Fock wave function, it is often bound to resort to states with a broken symmetry in order to lower the correlation energy. We observe these features not only in the case of the two-site model but also in other model systems that we are going to discuss in later chapters.

iii) The solution of the Hartree-Fock equations for realistic three-dimensional systems is quite challenging numerically because of the non-local exchange interaction. This is one of the reasons why, in the Density-Functional Theory, one works with a phenomenological local exchange interaction. Furthermore, a comparison of the Hartree-Fock results with experiments on metals and semiconductors show significant discrepancies: band widths and band gaps are usually overestimated; see, e.g., reference [39]. This is the reason why state-of-the-art band-structure theories are all based on the Density-Functional Theory, which will be discussed in the following section.

3.2 Density-Functional Theory

Based on earlier ideas for a Density-Functional Theory (DFT) [40–44], Hohenberg and Kohn published their seminal work on the 'Hohenberg-Kohn theorem' in 1964 [45], as it is generally called nowadays. This theorem states that there is a universal functional $W[n(\boldsymbol{r})]$ of the electronic density $n(\boldsymbol{r})$ such that

$$E[n(\boldsymbol{r})] = \int d^3\boldsymbol{r} V(\boldsymbol{r}) n(\boldsymbol{r}) + W[n(\boldsymbol{r})] \tag{3.34}$$

has its minimum, $E_0 \equiv E[n_0(\boldsymbol{r})]$, at the exact ground state density $n_0(\boldsymbol{r})$ of the Hamiltonian (2.2) and E_0 is the corresponding ground-state energy. The DFT can be viewed as a special case of a more general approach, the 'constrained-search method', see references [46, 47]. We give an introduction into this approach in section 3.2.1. In sections 3.2.2, 3.2.3, and 3.2.4, we discuss the main results of the DFT, which is the basis of most state-of-the-art ab-initio calculations. Another approach that can be derived from the constrained-search method is the Density-matrix Functional Theory (DmFT), which is closely related to our Gutzwiller variational approach, see appendix G.2. We discuss the DmFT in section 3.2.5.

3.2.1 Constrained-Search Method

We consider the general Hamiltonian

$$\hat{H} = \sum_i V_i \hat{Y}_i + \hat{W} \equiv \hat{V} + \hat{W} \,, \tag{3.35}$$

with the real or complex numbers V_i and operators $\hat{W}$ and $\hat{Y}_i$. Note that all results in this section are equally valid if we replace the discrete sum $\sum_i V_i \hat{Y}_i$ in (3.35) by a continuous integral $\int \mathrm{d}x V(x)\hat{Y}(x)$. For our general considerations here, we do not need to further specify the numbers V_i ('fields') or the operators $\hat{Y}_i$ ('densities') and $\hat{W}$. The typical situation will be that the fields V_i are varying, depending on the particular system of interest, while the operators $\hat{Y}_i$ and $\hat{W}$ are universal. For example, the DmFT is obtained if we work with the Hamiltonian (2.3) and set $\hat{W} = \hat{H}_I$, $\hat{Y}_i = \hat{c}^\dagger_{\sigma_1}\hat{c}_{\sigma_2}$ and $V_i = \varepsilon_{\sigma_1,\sigma_2}$. Obviously, with this choice, only the fields V_i change if we consider different periodic potentials (2.2b).

The wave functions $|\Psi\rangle$ in the Hilbert space $\mathcal{H}$ of the Hamiltonian (3.35) define the set Ω_Y of all possible sets

$$\{Y_i\} = \{\langle\Psi|\hat{Y}_i|\Psi\rangle\} \tag{3.36}$$

of density expectation values. A set of densities $\{Y_i\}$ is called 'representable' if it is in Ω_Y, i.e., if there exists a state $|\Psi\rangle \in \mathcal{H}$ that complies with (3.36).

For all representable $\{Y_i\}$, we introduce the set of normalised wave functions $Q[\{Y_i\}]$, which, by definition, all have the same set of expectation values (3.36). For each $\{Y_i\} \in \Omega_Y$, we minimise the expectation value of the operator $\hat{W}$, in order to define the energy functional

$$W[\{Y_i\}] = \min_{|\Psi\rangle \in Q[\{Y_i\}]} \langle\Psi|\hat{W}|\Psi\rangle \; . \tag{3.37}$$

This functional does not depend on $\hat{V}$ in the Hamiltonian (3.35) and, therefore, it is usually denoted as 'universal'. With $W[\{Y_i\}]$, we define the 'ground-state energy functional' as

$$E[\{Y_i\}] \equiv \sum_i V_i Y_i + W[\{Y_i\}] \; . \tag{3.38}$$

If E_0 is the exact ground-state energy of (3.35), we find

$$E_0 \leq E[\{Y_i\}] \tag{3.39}$$

for all $\{Y_i\} \in \Omega_Y$ since, otherwise, there would be a state $|\Psi\rangle$ with an energy lower than the ground state. On the other hand, with the expectation values $\{Y_{i;0}\} \in \Omega_Y$ of the ground-state wave function $|\Phi_0\rangle$, we can further conclude that

$$E_0 = \sum_i V_i Y_{i;0} + \langle\Phi_0|\hat{W}|\Phi_0\rangle \geq \sum_i V_i Y_{i;0} + W[\{Y_{i;0}\}] = E[\{Y_{i;0}\}] \; . \tag{3.40}$$

Both inequalities (3.39) and (3.40) together yield the following result: The energy functional $E[\{Y_i\}]$ has its minimum $E_0 = E[\{Y_{i;0}\}]$ at values $Y_{i;0}$ that are the ground-state expectation values of the operators $\hat{Y}_i$ for the Hamiltonian (3.35) and E_0 is the corresponding ground-state energy. Note that in cases of degenerate ground states, expectation values $Y_{i;0}$ may not be defined uniquely. However, such a degeneracy only complicates the considerations in this section without affecting the main results. Therefore, to simplify matters, we assume from now on that we only deal with systems that have a non-degenerate ground state.

A consequence of our considerations so far is the existence of a map

$$\mathrm{M} : \{V_i\} \to \{Y_{i;0}\} \; , \tag{3.41}$$

which relates each set of fields $\{V_i\}$ in (3.35) to the ground-state expectation values $\{Y_{i;0}\}$ of the density operators $\hat{Y}_i$. It naturally poses the question whether this map is injective. To answer it, we first investigate if, for two different sets of parameters $\{V_i\}$ and $\{V'_i\}$, the ground states $|\Phi_0\rangle$ and $|\Phi'_0\rangle$ of the two corresponding Hamiltonians $\hat{H}$ and $\hat{H}'$ could be the same. If

this was the case, i.e., if $|\Phi_0\rangle = |\Phi_0'\rangle$, by subtraction of the two Schrödinger equations, we would find that

$$(\hat{V} - \hat{V}')\,|\Phi_0\rangle = (E_0 - E_0')\,|\Phi_0\rangle \ . \tag{3.42}$$

Therefore, the ground state $|\Phi_0\rangle$ had to be an eigenstate not only of the Hamiltonian but also of the operator $\hat{V} - \hat{V}'$. In general, such a scenario cannot be excluded. However, in both of our applications, sections 3.2.2 and 3.2.5, $\hat{V} - \hat{V}'$ is a single-particle operator and $|\Phi_0\rangle$ is the ground state of a many-particle Hamiltonian. Therefore, we can safely assume that $|\Phi_0\rangle$ is not an eigenstate of $\hat{V} - \hat{V}'$ and, consequently, the two ground states $|\Phi_0\rangle$ and $|\Phi_0'\rangle$ must be different. Here, we assume that all fields V_i that only differ by a constant are considered as equivalent, i.e., the domain of the map M contains only one element for each class of equivalent fields.

In order to prove the injectivity of the map M, we just have to show that $\{Y_{i;0}\} \neq \{Y_{i;0}'\}$ for the two sets of fields $\{V_i\} \neq \{V_i'\}$ and their respective ground states $|\Phi_0\rangle \neq |\Phi_0'\rangle$. For this proof, let us assume again the opposite, i.e., $\{Y_{i;0}\} = \{Y_{i;0}'\}$. Then we find

$$E_0 < \langle\Phi_0'|\hat{H}|\Phi_0'\rangle = E_0' + \langle\Phi_0'|(\hat{V} - \hat{V}')|\Phi_0'\rangle = E_0' + \sum_i (V_i - V_i')Y_{i;0} \ . \tag{3.43}$$

In exactly the same way, one can show that

$$E_0' < E_0 + \sum_i (V_i' - V_i)Y_{i;0} \ , \tag{3.44}$$

which, together with (3.43), leads to the contradiction

$$E_0 - E_0' < E_0 - E_0' \ . \tag{3.45}$$

Hence, we can conclude that $\{Y_{i;0}\}$ must be different from $\{Y_{i;0}'\}$ and the map M is injective.

All sets of densities $\{Y_i\}$ that belong to the range Ω_Y^v of the map M, are generally denoted as 'v-representable' since they are ground-state expectation values of some Hamiltonian (3.35). Unfortunately, in general, Ω_Y^v is only a subset of Ω_Y, i.e., not all representable densities $\{Y_i\}$ are necessarily v-representable. We come back to the v-representability problem in connection with the DFT and the DmFT in sections 3.2.2 and 3.2.5.

In case that all densities $\{Y_i\} \in \Omega_Y$ are v-representable, i.e., if

$$\Omega_Y^v = \Omega_Y \ , \tag{3.46}$$

we can draw an interesting conclusion, which, in the Density-Functional Theory, leads to the 'Kohn-Sham scheme' [48], see section 3.2.3. We consider two Hamiltonians $\hat{H}$ and $\hat{H}'$, both of the form (3.35), but with different parameters V_i, V_i' and operators $\hat{W}$, $\hat{W}'$. The energy functionals $E[\{Y_i\}]$ and $E'[\{Y_i\}]$ of both Hamiltonians may have their minima at $\{Y_i\} = \{Y_{i;0}\}$ and $\{Y_i\} = \{Y_{i;0}'\}$, respectively. If equation (3.46) holds, the set $\{Y_{i;0}\}$ is also v-representable with respect to the Hamiltonian $\hat{H}'$, it is $\{Y_{i;0}'\} = \{Y_{i;0}\}$ for some set of parameters $\{V_i'\}$. An explicit formula for these parameters $\{V_i'\}$ can be derived as follows. The ground-state conditions for $E[\{Y_i\}]$ and $E'[\{Y_i\}]$ are

$$V_i + \frac{\partial}{\partial Y_i} W[\{Y_i\}]\bigg|_{\{Y_i\}=\{Y_{i;0}\}} = 0 \ , \tag{3.47a}$$

$$V_i' + \frac{\partial}{\partial Y_i} W'[\{Y_i\}]\bigg|_{\{Y_i\}=\{Y_{i;0}'\}} = 0 \ . \tag{3.47b}$$

Since we demand $\{Y_i'\} = \{Y_{i;0}\}$ a subtraction of both equations (3.47) yields

$$V_i' = V_i + \frac{\partial}{\partial Y_i}(W[\{Y_i\}] - W'[\{Y_i\}])\Big|_{\{Y_i\}=\{Y_{i;0}\}} . \tag{3.48}$$

In principle, this formula allows to determine the auxiliary Hamiltonian

$$\hat{H}' = \sum_i \left(V_i + \frac{\partial}{\partial Y_i}(W[\{Y_i\}] - W'[\{Y_i\}])|_{\{Y_i\}=\{Y_{i;0}\}} \right) \hat{Y}_i + \hat{W}' , \tag{3.49}$$

which, by construction, has the same ground-state expectation values $\{Y_{i;0}'\}$ like $\hat{H}$. This procedure could be useful, if the Hamiltonian $\hat{H}'$ can be solved more easily than $\hat{H}$, for example, because it is a single-particle Hamiltonian. In such a case, however, equation (3.49) is not of much use because it already includes the full energy functional of the Hamiltonian $\hat{H}$ itself. We will see that in the DFT the general result (3.49) is indeed merely used as a motivation to work with a simpler auxiliary Hamiltonian. The explicit form of this Hamiltonian is determined by a sophisticated guess and not by an evaluation of equation (3.49).

3.2.2 Density-Functional Theory and Local-Density Approximation

The functional theory, developed by Hohenberg and Kohn [45], follows straightforwardly from our general results on the constrained-search method in the previous section. In this context, it is advisable to distinguish clearly the general results of the Density-Functional Theory, which, in principle, are exact, and, the effective one-particle theory that arises from the Kohn-Sham scheme. Both aspects of the theory will be discusses separately in the present and in the following section. For a review on the DFT, see, e.g., references [49–51].

We use the representation (2.3e) of our general electronic Hamiltonian and choose the operators $\hat{W}$ and $\hat{V}$ in equation (3.35) as

$$\begin{aligned} \hat{W} &= \sum_s \int d^3\boldsymbol{r} \int d^3\boldsymbol{r}' \, \hat{\psi}_s^\dagger(\boldsymbol{r}) \left(-\frac{\Delta_{\boldsymbol{r}'}}{2m} \right) \hat{\psi}_s(\boldsymbol{r}') \\ &\quad + \frac{1}{2} \sum_{s,s'} \int d^3\boldsymbol{r} \, \hat{\psi}_s^\dagger(\boldsymbol{r}) \hat{\psi}_{s'}^\dagger(\boldsymbol{r}) \frac{e^2}{|\boldsymbol{r} - \boldsymbol{r}'|} \hat{\psi}_{s'}(\boldsymbol{r}) \hat{\psi}_s(\boldsymbol{r}) , \end{aligned} \tag{3.50}$$

$$\hat{V} = \sum_s \int d^3\boldsymbol{r} \, V(\boldsymbol{r}) \hat{\psi}_s^\dagger(\boldsymbol{r}) \hat{\psi}_s(\boldsymbol{r}) . \tag{3.51}$$

The operators $\hat{Y}_i$ and fields V_i in (3.35) are therefore given by

$$\hat{Y}_i \rightarrow \hat{Y}(\boldsymbol{r}) \equiv \sum_s \hat{\psi}_s^\dagger(\boldsymbol{r}) \hat{\psi}_s(\boldsymbol{r}) , \tag{3.52a}$$

$$V_i \rightarrow V(\boldsymbol{r}) . \tag{3.52b}$$

With this choice of operators, the expectation values (3.36), which define the constrained search in (3.36), are just the particle densities

$$\{Y_i\} \rightarrow n(\boldsymbol{r}) = \sum_s \langle \Psi | \hat{\psi}_s^\dagger(\boldsymbol{r}) \hat{\psi}_s(\boldsymbol{r}) | \Psi \rangle , \tag{3.53}$$

and the ground-state energy functional has the form

$$E[n(\boldsymbol{r})] = \int d^3\boldsymbol{r} \, V(\boldsymbol{r}) n(\boldsymbol{r}) + W[n(\boldsymbol{r})] . \tag{3.54}$$

Note that the functional $E[n(\boldsymbol{r})]$ is properly defined only when we add the constraint

$$N = \int d^3\boldsymbol{r}\; n(\boldsymbol{r}) \tag{3.55}$$

that fixes the total particle number.

It is impossible to determine exactly the functional $W[n(\boldsymbol{r})]$ for many-particle systems, and one can only hope to find some reasonable approximations. Usually it is written as

$$W[n(\boldsymbol{r})] = T[n(\boldsymbol{r})] + \frac{e^2}{2}\int d^3\boldsymbol{r}\int d^3\boldsymbol{r}'\;\frac{n(\boldsymbol{r})n(\boldsymbol{r}')}{|\boldsymbol{r}-\boldsymbol{r}'|} + E_{\rm xc}[n(\boldsymbol{r})]\;, \tag{3.56}$$

where $T[n(\boldsymbol{r})]$ is the unknown kinetic-energy functional. Equally unknown is the 'exchange-correlation' functional $E_{\rm xc}[n(\boldsymbol{r})]$, which contains all Coulomb-energy contributions apart from the Hartree term that was separated in (3.56).

Approximate expressions for $T[n(\boldsymbol{r})]$ and $E_{\rm xc}[n(\boldsymbol{r})]$ are usually derived by considering the free-electron gas. In section 2.1, we found that the kinetic energy of the free-electron gas in the Hartree-Fock approximation is $\sim n^{5/3}$ where n is the homogeneous density of that system, see equation (3.21a). Therefore, a common approximation for the kinetic-energy functional in (3.56) is

$$T[n(\boldsymbol{r})] = \frac{3}{10m}(3\pi^2)^{2/3}\int \mathrm{d}^3\boldsymbol{r}\; n(\boldsymbol{r})^{5/3}\;. \tag{3.57a}$$

In the same way, i.e., based on the free-electron result equation (3.21d), one usually approximates the exchange-correlation potential as

$$E_{\rm xc}[n(\boldsymbol{r})] = -\beta\int \mathrm{d}^3\boldsymbol{r}\frac{3e^2}{4\pi}(3\pi)^{1/3}n(\boldsymbol{r})^{4/3}\;, \tag{3.57b}$$

where the factor β is adjusted in order to have optimum agreement with experiments. Working with the functional (3.57b) is generally called the X_α-method, which was first proposed by Slater [52, 53]. With respect to the ground-state energy, the X_α-method reproduces the Hartree-Fock result for the free-electron gas. As discussed in section (3.1.2), the major shortcoming of the Hartree-Fock theory for the free-electron gas is the result for the quasi-particle dispersion. As will become clear in the following section, the Kohn-Sham scheme provides a different way to calculate such excitation energies, which are in better agreement with experiments.

To work with the energy functionals (3.57a) and (3.57b), is the simplest example for a 'Local-Density Approximation' (LDA). The exact energy, however, will be a more complicated non-local functional of the density. Systematic improvements of the LDA can, in principle, be derived by calculating the energy of the free-electron gas beyond the simple Hartree-Fock approximation. This, however, is a non-trivial problem that requires more subtle many-particle techniques. Examples for such improvements can be found in references [54–59]. Another way to improve the functionals (3.57a) and (3.57b), is to go beyond the local-density scheme by adding, e.g., gradient corrections. For an overview on these approximations, see, e.g., reference [50].

The DFT, as introduced so far, provides an approximate way to determine the ground-state energy and the electronic density in the ground state. Both of these quantities are of limited interest for most experiments on molecules or solids. At least for all v-representable densities, the potential $V(\boldsymbol{r})$ is uniquely determined by $n(\boldsymbol{r})$. Therefore, one could argue that all eigenstates of the Hamiltonian (2.3e) are also functionals of the density. In the same way, all thermodynamic quantities can be viewed as functionals of $n(\boldsymbol{r})$. These, however, are merely

formal arguments and they do not provide a feasible way to calculate excited states, response functions, or thermodynamic quantities. The immense importance of the Density-Functional Theory is, in fact, not based on such general ideas but it is a result of the Kohn-Sham scheme, which we discuss in the following section.

3.2.3 Kohn-Sham Scheme

The Kohn-Sham scheme is based on the general results, derived at the end of section 3.2, if we chose $\hat{W}' = \hat{T}$ in equation (3.49). In this way, we are led to the auxiliary single-particle Hamiltonian

$$\begin{aligned} \hat{H}' &= \sum_s \int \mathrm{d}^3\boldsymbol{r}\hat{\psi}_s^\dagger(\boldsymbol{r}) \left[-\frac{\Delta_{\boldsymbol{r}}}{2m} + V(\boldsymbol{r})\right] \hat{\psi}_s(\boldsymbol{r}) \\ &\quad + \sum_s \int \mathrm{d}^3\boldsymbol{r}\hat{\psi}_s^\dagger(\boldsymbol{r}) \left[e^2 \int d^3\boldsymbol{r}' \frac{n(\boldsymbol{r}')}{|\boldsymbol{r}-\boldsymbol{r}'|} + V_{\mathrm{x}}^{\mathrm{KS}}[n(\boldsymbol{r})]\right] \hat{\psi}_s(\boldsymbol{r}) \ , \end{aligned} \tag{3.58}$$

which, by construction, has the the same ground-state density $n_0(\boldsymbol{r})$ as the original many-particle Hamiltonian (2.3e) as long as this density is v-representable for both Hamiltonians. In (3.58) we introduced the Kohn-Sham potential

$$V_{\mathrm{xc}}^{\mathrm{KS}}[n(\boldsymbol{r})] = \frac{\partial}{\partial\tilde{n}(\boldsymbol{r})} \left(T[\tilde{n}(\boldsymbol{r})] - T'[\tilde{n}(\boldsymbol{r})] + E_{\mathrm{x}}[\tilde{n}(\boldsymbol{r})]\right)\Big|_{\tilde{n}(\boldsymbol{r})=n(\boldsymbol{r})} \ , \tag{3.59}$$

in which $T'[n(\boldsymbol{r})]$ is the minimum kinetic energy of free non-interacting particles with a density distribution $n(\boldsymbol{r})$. In the context of the DFT, the problem of v-representability has been investigated extensively in the past, see, e.g., references [50, 60, 61]. For practical applications, one usually presumes that v-representability is ensured and the investigation of the effective single-particle Hamiltonian (3.58) is therefore justified. Given the significant approximations that are usually made to set up the Kohn-Sham potential (3.59) the assumption of v-representability seems to be a matter of minor concern.

In first quantisation, the Hamiltonian (3.58) leads to the Schrödinger equation

$$\left[-\frac{\Delta_{\boldsymbol{r}}}{2m} + V(\boldsymbol{r}) + e^2 \int d^3\boldsymbol{r}' \frac{n(\boldsymbol{r}')}{|\boldsymbol{r}-\boldsymbol{r}'|} + V_{\mathrm{xc}}^{\mathrm{KS}}[n(\boldsymbol{r})]\right] \Psi_{s,\alpha}(\boldsymbol{r}) = \varepsilon_\alpha \Psi_{s,\alpha}(\boldsymbol{r}) \ , \tag{3.60}$$

which has to be solved self-consistently since the Hartree and the Kohn-Sham potentials in (3.60) depend on the particle density

$$n(\boldsymbol{r}) = \sum_s \sum_{\alpha(\varepsilon_\alpha<E_{\mathrm{F}})} |\Psi_{s,\alpha}(\boldsymbol{r})|^2 \ . \tag{3.61}$$

The Fermi energy in (3.61) is determined by the condition

$$\sum_s \sum_{\alpha(\varepsilon_\alpha<E_{\mathrm{F}})} 1 = N \ . \tag{3.62}$$

With the approximate functionals (3.57) for $T[n(\boldsymbol{r})]$ and $E_{\mathrm{xc}}[n(\boldsymbol{r})]$, the effective single-particle Schrödinger equation for the jellium model reads

$$\left[-\frac{\Delta_{\boldsymbol{r}}}{2m} + V_0^{\mathrm{KS}}\right] \Psi_{s,\alpha}(\boldsymbol{r}) = \varepsilon_\alpha \Psi_{s,\alpha}(\boldsymbol{r}) \tag{3.63}$$

since $T[n(\boldsymbol{r})]$ and $T'[n(\boldsymbol{r})]$ in (3.59) cancel each other and $V_0^{\mathrm{KS}} = V^{\mathrm{KS}}[n^0(\boldsymbol{r})]$ is the constant Kohn-Sham field with the homogeneous particle density $n^0(\boldsymbol{r}) = n$. The single-particle excitation energies of the jellium model in this approximation are, therefore, those of free particles. This means that this DFT approach avoids the severe shortcomings of the Hartree-Fock approximation for the quasi-particle dispersion, see section 3.1.2. However, the quasi-particle dispersion is not renormalised for all particle densities, which also is questionable. In particular, for larger densities the Coulomb interaction certainly decreases the mobility of the electrons and we expect a renormalisation of the quasi-particle dispersion. It is therefore clear that the LDA, as long as it based on the Hartree-Fock energy functionals (3.57), is not suitable for the investigation of systems with significant Coulomb-interaction effects.

Based on the result for the jellium model, the difference between $T[n(\boldsymbol{r})]$ and $T'[n(\boldsymbol{r})]$ in (3.59) is usually neglected also for lattice models. Furthermore, one often uses the approximation (3.57b) for the Kohn-Sham potential, which leads to

$$V^{\mathrm{KS}}[n(\boldsymbol{r})] = -\beta e^2 \left(\frac{3}{\pi}\right)^{1/3} n(\boldsymbol{r})^{1/3} \,. \tag{3.64}$$

Instead of using a constant fit parameter β one may also work with an adjustable functional $\beta[n(\boldsymbol{r})]$. More systematic improvements of (3.36) can be derived along the lines discussed in connection with the functional (3.57b).

3.2.4 Merits and Shortcomings

The Density-Functional Theory, in connection with the Kohn-Sham scheme, provides an exact way to derive, for any many-particle system, an effective single-particle Hamiltonian that has the same ground-state density as the corresponding many-particle Hamiltonian. In principle, this is a huge step forward since single-particle Schrödinger equations can usually be solved quite accurately by numerical means. Therefore, it is possible to investigate real materials 'ab-initio', i.e., without the need to neglect certain degrees of freedom. However, this quite remarkable achievement is spoiled by two serious shortcomings:

i) An exact determination of the energy functional $W[n(\boldsymbol{r})]$ is impossible for many-particle systems and one is bound to work with rather simple approximations. The most frequently used approximations are based on Hartree-Fock results for the energy of the jellium model, see equations (3.57). As it is well known by comparison to more sophisticated many-particle theories, the Hartree-Fock theory is reliable only for systems with small Coulomb interactions, see, e.g., the results for the two-site Hubbard model in section 3.1.3. Therefore, it appears quite likely that a Density-Functional Theory approach that is based on Hartree-Fock energy expressions will run into similar problems for systems with medium to strong Coulomb-interaction effects. The inclusion of fit parameters may improve results in comparison to experiments but it compromises the ab-initio character of the whole theory.

ii) Even if it was possible to find the exact effective single-particle Hamiltonian (3.58) within the Kohn-Sham scheme, there is no reason to believe that the properties of this Hamiltonian have anything in common with the corresponding many-particle Hamiltonian, except to yield the same ground-state density. Nevertheless, the eigenstates of the Kohn-Sham Hamiltonian are generally interpreted as the quasi-particle excitations of the many-particle system. As we have argued in connection with the jellium model, this assumption is particularly questionable for systems with strong Coulomb-interaction effects.

Despite the obvious conceptual shortcomings of the Density-Functional Theory, a comparison of theoretical and experimental results has revealed a remarkable agreement for a large number of materials. Therefore, the Density-Functional Theory has become the most important tool for the investigation of electronic properties in solid-state physics. There are, however, a few well known problems with certain classes of materials. For example, band gaps in insulators or semiconductors are usually found to be significantly smaller in theory than in experiments. In order to improve the results for semiconductors, one often employs the GW approximation [62–65]; for an overview on this method, see reference [66].

Materials in which the local Coulomb interaction is believed to have an important influence on their electronic properties are also not well described within the Density-Functional Theory. These are, in particular, transition metals, lanthanides and their respective compounds. It is the main purpose of the Gutzwiller theory to improve results for these classes of materials.

3.2.5 Density-Matrix Functional Theory

The constrained search (3.37) that led to the DFT in section 3.2.2 was carried out for a fixed density $n(\boldsymbol{r})$. Instead of the density we now use the single-particle density matrix $\tilde{\rho}$ with the elements

$$\rho_{\sigma_1\sigma_2} \equiv \langle\Psi|\hat{c}^\dagger_{\sigma_1}\hat{c}_{\sigma_2}|\Psi\rangle \ . \tag{3.65}$$

The density matrix was first used in the context of the Hohenberg-Kohn theorem by Gilbert who generalised that theorem for non-local potentials [67]. We can derive it here directly from our constrained-search results in section 3.2.2. Starting from the general many-particle Hamiltonian (2.3), we chose

$$\hat{W} = \frac{1}{2}\sum_{\sigma_1,\sigma_2,\sigma_3,\sigma_4} U_{\sigma_1,\sigma_2,\sigma_3,\sigma_4}\hat{c}^\dagger_{\sigma_1}\hat{c}^\dagger_{\sigma_2}\hat{c}_{\sigma_3}\hat{c}_{\sigma_4} \ , \tag{3.66a}$$

$$\hat{V} = \sum_{\sigma_1,\sigma_2} \varepsilon_{\sigma_1,\sigma_2}\hat{c}^\dagger_{\sigma_1}\hat{c}_{\sigma_2} \tag{3.66b}$$

as the operators in (3.35). The operators $\hat{Y}_i$ and fields V_i in (3.35) are therefore identified as

$$\hat{Y}_i \rightarrow \hat{c}^\dagger_{\sigma_1}\hat{c}_{\sigma_2} \ , \tag{3.67a}$$

$$V_i \rightarrow \varepsilon_{\sigma_1,\sigma_2} \ . \tag{3.67b}$$

The constrained search in (3.36) is then carried out with respect to the density matrix,

$$\{Y_i\} \rightarrow \rho_{\sigma_1\sigma_2} \ , \tag{3.68}$$

and the ground-state energy functional has the form

$$E[\tilde{\rho}] = \sum_{\sigma_1,\sigma_2} \varepsilon_{\sigma_1,\sigma_2}\rho_{\sigma_1\sigma_2} + W[\tilde{\rho}] \ . \tag{3.69}$$

When we work with eigenstates $|\sigma\rangle = |\boldsymbol{r}\rangle\,|s\rangle$ of the position and the spin operator, the ground-state energy functional reads

$$E[\tilde{\rho}] = \sum_s \int \mathrm{d}^3\boldsymbol{r} \int \mathrm{d}^3\boldsymbol{r}' \left[-\delta(\boldsymbol{r}-\boldsymbol{r}')\frac{\Delta_{\boldsymbol{r}}}{2m}\right] \rho_s(\boldsymbol{r},\boldsymbol{r}') + W[\tilde{\rho}] \ , \tag{3.70}$$

where $\rho_s(\boldsymbol{r},\boldsymbol{r}')$ is the density matrix in real space for electrons with spin s.

There are a number of studies in which approximate expressions for $W[\tilde{\rho}]$ have been used in order to minimise the real space functional (3.70) for molecules and crystals [68–82]. In this work, where we are more interested in lattice models, the general functional (3.69) is more appropriate. It allows us to apply the DmFT to lattice systems, for example, to the general class of Hubbard models derived in section 2.2. Such studies have already been carried out for various single-band Hubbard models [47, 83–88] as well as for impurity systems [89]. We will later see that the Gutzwiller variational theory provides a way to set up density-matrix functionals for general multi-band Hubbard models.

The density matrices of single and many-particle Hamiltonians are fundamentally different. For a Slater determinant, which is the ground state of a single-particle Hamiltonian, the density matrix has eigenvalues zero or unity, depending on the occupation of the single-particle levels. In contrast, the density matrix of a many-particle Hamiltonian is genuinely fractional. Therefore, it is impossible to set up a useful Kohn-Sham scheme for the density matrix that would allow to investigate an effective single-particle problem instead of the actual many-particle system. Identical density matrices for single and many-particle Hamiltonians with fractional eigenvalues may be obtained if the single-particle system is highly degenerate at the Fermi level [90]. These, however, are not very physical constructions and they do not seem to be of much use for the investigation of many-particle systems. Therefore, the DmFT is mainly a tool to investigate ground-state properties of many-particle Hamiltonians.

As an example, we consider the one-band Hubbard model (2.20) with the density matrix

$$\rho_{i,j} = \langle \Psi | \hat{c}^\dagger_{i,s} \hat{c}_{j,s} | \Psi \rangle \; . \tag{3.71}$$

Here, we use rotational invariance in spin space, i.e., we assume that spin-flip expectation values vanish and the matrix element (3.71) does not depend on the spin s.

The ground-state energy functional has the form

$$E[\{\rho_{i,j}\}] = 2 \sum_{i,j} t_{i,j} \rho_{i,j} + LUd[\{\rho_{i,j}\}] \; , \tag{3.72}$$

where L is the number of lattice sites. The unknown double-occupancy functional $d[\{\rho_{i,j}\}]$ depends on the dimensionality of the lattice and its structure, but it does not depend on the tight-binding parameters $t_{i,j}$. For practical applications, however, it is more useful to work with the 'effective' density matrix $\bar{\rho}_{i,j}$, which is defined only for those lattice sites i, j that have a finite hopping parameter $t_{i,j}$. We may then define the effective double-occupancy functional

$$d[\{\bar{\rho}_{i,j}\}] \equiv \min_{\{\rho_{i,j}\}(\rho_{i,j}=\bar{\rho}_{i,j})} d[\{\rho_{i,j}\}] \; , \tag{3.73}$$

which, by definition, depends on the topology of the tight-binding matrix but not on their actual values. The effective energy functional with respect to $\bar{\rho}_{i,j}$ has exactly the same form as (3.72) if ρ is replaced by $\bar{\rho}$. In general, a tight-binding Hamiltonian includes hopping terms only up to a certain shell of nearest neighbours and, therefore, the effective energy functional depends on only a few parameters. In case of only nearest-neighbour hopping t, we end up with the simple energy function

$$E(T)/L = 2 n_{\mathrm{nn}} t T + U d(T) \tag{3.74}$$

where T is the hopping expectation value between nearest neighbours and n_{nn} the number of such neighbours. Note that the lattice needs to have a sufficiently high symmetry such that hopping parameters t and expectation values T in all directions are the same. This is the case, e.g., for a hypercubic or a Bethe lattice [91].

As an example, the explicit form of $E(T)$ is derived for the two-site Hubbard model in appendix B.2. We discuss these results in appendix G.2 where we compare them to those of the Gutzwiller theory.

Chapter 4

Gutzwiller Wave Functions

We start this chapter with an overview of notations and definitions, which will turn out to be quite useful for our derivations in the following chapters. In section 4.2, we introduce the Gutzwiller wave function for the one-band model and prove that this wave function yields the exact ground state of the two-site Hubbard model (2.22). The general class of Gutzwiller wave functions, which allow the investigation of multi-band Hubbard models, are introduced in section 4.3. We close this chapter with an overview of various earlier attempts to evaluate Gutzwiller wave functions and to generalise them to more complicated systems in section 4.4.

4.1 Notations and Definitions

The general class of multi-band Hubbard models (2.15), which we study in this work contains a local Hamiltonian of the form

$$\hat{H}_{\mathrm{loc}} = \sum_{\sigma_1,\sigma_2} \varepsilon_{\sigma_1,\sigma_2} \hat{c}^\dagger_{\sigma_1} \hat{c}_{\sigma_2} + \sum_{\sigma_1,\sigma_2,\sigma_3,\sigma_4} U^{\sigma_1,\sigma_2,\sigma_3,\sigma_4} \hat{c}^\dagger_{\sigma_1} \hat{c}^\dagger_{\sigma_2} \hat{c}_{\sigma_3} \hat{c}_{\sigma_4} \tag{4.1}$$

for each lattice site i. Note that throughout this work we frequently drop lattice site indices in formulae for purely local quantities. With the orbital basis $|\sigma\rangle$ that led to the Hamiltonian (2.15), the local one particle term is diagonal, i.e., we have $\varepsilon_{\sigma_1,\sigma_2} \sim \delta_{\sigma_1,\sigma_2}$. For applications, however, it can be more convenient to work with a more general basis that has non-diagonal one particle terms. The explicit form of (4.1) is specified in equations (2.20), (2.23) and (C.3) for orbital numbers $N = 1, 2, 5$, respectively. The general Hamiltonian (4.1) contains $2N$ spin-orbit states σ, which we assume to be ordered in some arbitrary way, $\sigma = 1, \ldots, 2N$. In order to set up a proper basis of the local Hilbert space, we introduce the following notations for the 2^{2N} possible configurations:

i) An atomic configuration I is characterised by the electron occupation of the orbitals,

$$I \in \{\emptyset; (1), \ldots, (2N); (1,2), \ldots, (2,3), \ldots (2N-1, 2N); \ldots; (1, \ldots, 2N)\} \ , \tag{4.2}$$

where the elements in each set $I = (\sigma_1, \sigma_2, \ldots)$ are ordered, i.e., it is $\sigma_1 < \sigma_2 < \ldots$. The symbol $\emptyset$ in (4.2) means that the site is empty. In general, we interpret the indices I as sets in the usual mathematical sense. For example, in the atomic configuration $I \backslash I'$ only those orbitals in I that are not in I' are occupied. The complement of I is $\overline{I} \equiv (1, 2, \ldots, 2N) \backslash I$, i.e., in the atomic configuration $\overline{I}$ all orbitals but those in I are occupied.

ii) The absolute value $|I|$ of a configuration is the number of elements in it, i.e.,

$$|\emptyset| = 0; |(\sigma_1)| = 1; |(\sigma_1, \sigma_2)| = 2; \ldots; |(1, \ldots, 2N)| = 2N \ . \tag{4.3}$$

iii) A state with a specific configuration I is given as

$$|I\rangle = \hat{C}_I^\dagger |0\rangle \equiv \prod_{\sigma\in I} \hat{c}_\sigma^\dagger |0\rangle = \hat{c}_{\sigma_1}^\dagger \dots \hat{c}_{\sigma_{|I|}}^\dagger |0\rangle \ , \tag{4.4}$$

where the operators $\hat{c}_\sigma^\dagger$ are in ascending order, i.e., it is $\sigma_1 < \sigma_2 \dots < \sigma_{|I|}$. Products of annihilation operators, such as

$$\hat{C}_I \equiv \prod_{\sigma\in I} \hat{c}_\sigma = \hat{c}_{\sigma_1} \dots \hat{c}_{\sigma_{|I|}}, \tag{4.5}$$

will always be placed in descending order, i.e., with $\sigma_1 > \sigma_2 \dots > \sigma_{|I|}$. Note that we have introduced the operators $\hat{C}_I^\dagger$ and $\hat{C}_I$ just as convenient abbreviations. They must not be misinterpreted as fermionic creation or annihilation operators.

iv) The sign function

$$\mathrm{sign}(\sigma, I) \equiv \left\langle I \cup \sigma \middle| \hat{c}_\sigma^\dagger \middle| I \right\rangle \tag{4.6}$$

is zero if $\sigma \in I$ and 1 (-1) if it takes an even (odd) number of anticommutations to shift the operator $\hat{c}_\sigma^\dagger$ to its proper place in the sequence (4.4) of electron creation operators for the state $|I \cup \sigma\rangle$. A useful generalisation of $\mathrm{sign}(\sigma, I)$ is

$$\mathrm{sign}(J, I) = \prod_{\sigma\in J} \mathrm{sign}(\sigma, I) \ . \tag{4.7}$$

v) The operator $\hat{m}_{I,I'} \equiv |I\rangle \langle I'|$ describes the transfer between configurations I' and I. It can be written as

$$\hat{m}_{I,I'} = \hat{C}_I^\dagger \hat{C}_{I'} \prod_{\sigma''\in J} (1 - \hat{n}_{\sigma''}) \tag{4.8}$$

where $J \equiv \overline{I \cup I'}$. A special case, which derives from (4.8), is the occupation operator

$$\hat{m}_I \equiv |I\rangle \langle I| = \prod_{\sigma\in I} \hat{n}_\sigma \prod_{\sigma'\in \bar{I}} (1 - \hat{n}_{\sigma'}) \ . \tag{4.9}$$

The states $|I\rangle$ form a basis of the atomic Hilbert space. Therefore, the eigenstates $|\tilde{\Gamma}\rangle$ of the atomic Hamiltonian (4.1) can be written as

$$|\tilde{\Gamma}\rangle = \sum_I T_{I,\tilde{\Gamma}} |I\rangle \tag{4.10}$$

with coefficients $T_{I,\tilde{\Gamma}}$, which have to be determined by a diagonalisation of the Hamilton matrix

$$H_{\mathrm{loc}}^{I,I'} = \langle I| \hat{H}_{\mathrm{loc}} \left| I' \right\rangle . \tag{4.11}$$

As an analytic example for such a diagonalisation, see the results for the two-orbital model in section 2.3.2, or the results in reference [92] for the five-orbital model (C.3). In general, the diagonalisation of the atomic Hamiltonian (4.1) has to be carried out numerically. After diagonalisation, the atomic Hamiltonian can be written as

$$\hat{H}_{\mathrm{loc}} = \sum_{\tilde{\Gamma}} E_{\tilde{\Gamma}} \hat{m}_{\tilde{\Gamma}} \ , \tag{4.12a}$$

where $E_{\tilde{\Gamma}}$ are the eigenvalues of $\hat{H}_{\mathrm{loc}}$ and

$$\hat{m}_{\tilde{\Gamma}} \equiv |\tilde{\Gamma}\rangle\langle\tilde{\Gamma}| = \sum_{I,I'} T_{I,\tilde{\Gamma}} T_{I',\tilde{\Gamma}}^* \hat{m}_{I,I'} \tag{4.12b}$$

is the projector onto the corresponding eigenstates $|\tilde{\Gamma}\rangle$.

4.2 Gutzwiller Wave Function for One-Band Hubbard Models

4.2.1 General One-Band Models

In the Hartree-Fock theory, as introduced in section (3.1), one uses a variational wave function that is a Slater determinant or, in the language of second quantisation, a one-particle product state

$$|\Psi_0\rangle = \prod_\gamma \hat{h}_\gamma^\dagger |0\rangle \ . \tag{4.13}$$

As we have already observed in connection with the two-site Hubbard model, such one-particle wave functions are insufficient for systems with medium to strong Coulomb interaction effects. In the case of our Hubbard models, it is a particular problem of a Hartree-Fock treatment that local charge fluctuations can only be suppressed in that approach by a spurious breaking of symmetries. However, Hartree-Fock wave functions are still a reasonable starting point in order to set up a more sophisticate variational wave function. This leads to the general class of 'Jastrow wave functions' [93, 94], which are given as

$$|\Psi_\mathrm{J}\rangle = \hat{P}_\mathrm{J} |\Psi_0\rangle \ . \tag{4.14}$$

Here, $|\Psi_0\rangle$ is a one-particle product state, such as (4.13), and $\hat{P}_\mathrm{J}$ is a correlation operator, which can be chosen in various ways in order to minimise the variational ground-state energy. Such general Jastrow wave functions are of importance for numerical quantum Monte-Carlo calculations, see, e.g., reference [95].

The 'Gutzwiller wave function' (GWF) is a special Jastrow wave function with a particular choice of the correlation operator $\hat{P}_\mathrm{J}$. In a series of three publications [96–98], Gutzwiller introduced and investigated the wave function

$$\left|\Psi_\mathrm{G}'\right\rangle \equiv \hat{P}_\mathrm{G}' |\Psi_0\rangle = \prod_i \hat{P}_i' |\Psi_0\rangle \tag{4.15a}$$

in order to study ferromagnetism in a one-band Hubbard model. Here

$$\hat{P}_i' \equiv g^{\hat{d}_i} = 1 - (1-g)\hat{d}_i \tag{4.15b}$$

is the local 'Gutzwiller correlation operator' and the operator

$$\hat{d}_i \equiv \hat{n}_{i,\uparrow}\hat{n}_{i,\downarrow} \tag{4.15c}$$

measures doubly-occupied lattice sites. The variational parameter g, with $0 \leq g \leq 1$, allows to optimise the expectation value of local double occupancies that are energetically unfavourable for a finite Hubbard interaction $U > 0$. The Ansatz (4.15) allows two opposing limits to be described correctly, the uncorrelated limit $U \to 0$ (with $g = 1$) and the atomic limit $t \to 0$ (with $g \to 0$). Note that, in the atomic limit $t \to 0$, the ground state is just a simple collection of isolated atoms and different from the ground state at $U \to \infty$, which, in general, is quite difficult to determine, cf. section 2.4.2.

The Hilbert space of the local Hamiltonian for the one-band Hubbard model is four-dimensional where a local basis $|I\rangle$ is given by the states $|\emptyset\rangle$, $|\uparrow\rangle$, $|\downarrow\rangle$, and $|d\rangle$ for empty, singly-occupied and doubly-occupied sites, respectively. By working with the occupation operator $\hat{d} = |d\rangle\langle d|$, Gutzwiller singled out the state $|d\rangle$. A more symmetric definition of the *local* Gutzwiller correlator (4.15b) is given by

$$\hat{P} = \prod_I \lambda_I^{\hat{m}_I} = \sum_I \lambda_I \hat{m}_I \tag{4.16}$$

where the operators $\hat{m}_I = |I\rangle\langle I|$ are the projectors onto the four atomic eigenstates $|I\rangle$. The operator (4.16) contains four parameters λ_I instead of only one parameter g in Gutzwiller's definition (4.15).

For general one-particle states $|\Psi_0\rangle$, which, e.g., could show a complicated spatial spin structure, it is obviously indicated to work with lattice site dependent parameters $\lambda_{i;I}$ or g_i. This leads to our final definition of Gutzwiller wave functions

$$|\Psi_{\mathrm{G}}\rangle = \prod_i \hat{P}_i |\Psi_0\rangle = \prod_{i,I} \lambda_{i;I}^{\hat{m}_{i;I}} |\Psi_0\rangle \tag{4.17a}$$

for the one-band Hubbard model. Note that the local correlation operator can also be written as

$$\hat{P}_i = \sum_I \lambda_{i;I} \hat{m}_{i;I} \tag{4.17b}$$

since the operators $\hat{m}_{i;I}$ are projectors, i.e., we have

$$\hat{m}_{i;I}\hat{m}_{i;I'} = \delta_{I,I'}\hat{m}_{i;I} \ . \tag{4.18}$$

We will start from the definition (4.17) when we generalise the Gutzwiller theory for multi-band models in section 4.3.

Finally, we address the question whether the two Gutzwiller projectors (4.15b) and (4.16) define the same spaces of variational wave functions. Obviously, Gutzwiller's original space of wave functions, given by the projector (4.15b), is included in the Ansatz (4.16) since one can simply chose $\lambda_I = 1$ for all $|I\rangle \neq |d\rangle$. It requires a more lengthy derivation to show that the same is true in the opposite direction. In appendix D, we prove that, in fact, all wave functions (4.17a) can be written in the form of equations (4.15) with lattice-site dependent variational parameters g_i.

4.2.2 Exact Evaluation for the Two-Site Hubbard Model

In general, the true ground state of a single-band Hubbard model cannot be written as a Gutzwiller wave function. The situation is different, however, for the two-site Hubbard model (2.22), which we introduced in section 2.3.1. As we will show now, for this model the Gutzwiller wave function reproduces the exact ground states, in particular, the two-particle ground state $|\Psi_-\rangle$, equation (B.12b). For all particle numbers $N \neq 2$, this is a trivial result, since the eigenstates are Slater determinants. For $N = 2$, we choose the $U = 0$ ground state (3.22),

$$|\Psi_0\rangle = \frac{1}{\sqrt{2}} \left(|2, \mathrm{s}, 1\rangle_1 - |2, \mathrm{s}, 1\rangle_2 \right) \tag{4.19}$$

as the one-particle wave function $|\Psi_0\rangle$ in our Gutzwiller Ansatz $|\Psi_{\mathrm{G}}\rangle = \hat{P}_{\mathrm{G}} |\Psi_0\rangle$. The states $|2, \mathrm{s}, 1\rangle_i$ are defined as

$$|2, \mathrm{s}, 1\rangle_1 = \frac{1}{\sqrt{2}} \left(\hat{c}^\dagger_{1,\uparrow}\hat{c}^\dagger_{2,\downarrow} - \hat{c}^\dagger_{1,\downarrow}\hat{c}^\dagger_{2,\uparrow} \right) |0\rangle \ , \tag{4.20a}$$

$$|2, \mathrm{s}, 1\rangle_2 = \frac{1}{\sqrt{2}} \left(\hat{c}^\dagger_{1,\uparrow}\hat{c}^\dagger_{1,\downarrow} + \hat{c}^\dagger_{2,\uparrow}\hat{c}^\dagger_{2,\downarrow} \right) |0\rangle \ ; \tag{4.20b}$$

compare equation (B.10). We work with a Gutzwiller correlation operator

$$\hat{P}_{\mathrm{G}} = \hat{P}_{\mathrm{G};1}\hat{P}_{\mathrm{G};2} \ , \tag{4.21}$$

with site-independent local operators

$$\hat{P}_{\mathrm{G};b} = \lambda_\emptyset \hat{m}_\emptyset + \lambda_\uparrow \hat{m}_\uparrow + \lambda_\downarrow \hat{m}_\downarrow + \lambda_d \hat{m}_d \; . \tag{4.22}$$

The states $|2,\mathrm{s},1\rangle_i$ are eigenstates of $\hat{P}_\mathrm{G}$,

$$\hat{P}_\mathrm{G} \, |2,\mathrm{s},1\rangle_1 \;\; = \;\; \lambda_\uparrow \lambda_\downarrow \, |2,\mathrm{s},1\rangle_1 \;\; , \tag{4.23a}$$

$$\hat{P}_\mathrm{G} \, |2,\mathrm{s},1\rangle_2 \;\; = \;\; \lambda_\emptyset \lambda_d \, |2,\mathrm{s},1\rangle_2 \;\; . \tag{4.23b}$$

By comparison with the exact solution (B.12b), one finds that $|\Psi_\mathrm{G}\rangle$ yields the exact ground state if we set

$$\lambda_\uparrow = \lambda_\downarrow = \sqrt{\sqrt{2}\cos\left(\phi_-\right)} \tag{4.24a}$$

and

$$\lambda_d = \lambda_\emptyset = \sqrt{\sqrt{2}|\sin\left(\phi_-\right)|} \; , \tag{4.24b}$$

where ϕ_- is defined in equation (B.12c).

4.3 Gutzwiller Wave Functions for Multi-Band Hubbard Models

It is quite obvious how to generalise the Gutzwiller wave function (4.17a) for the investigation of the multi-band Hubbard models (2.15). The starting point is again a single-particle product state $|\Psi_0\rangle$ to which we apply a Jastrow factor that is a product of local correlation operators. Hence, the multi-orbital Gutzwiller wave function has the form

$$|\Psi_\mathrm{G}\rangle = \hat{P}_\mathrm{G} \, |\Psi_0\rangle = \prod_i \hat{P}_i \, |\Psi_0\rangle \;\; . \tag{4.25a}$$

The most general Ansatz for the local correlation operator in (4.25a) is given as

$$\hat{P}_i = \sum_{\Gamma_i, \Gamma_i'} \lambda_{i;\Gamma_i,\Gamma_i'} \hat{m}_{i;\Gamma_i,\Gamma_i'} \; , \tag{4.25b}$$

where we introduced a matrix $\tilde{\lambda}_i$ of variational parameters $\lambda_{i;\Gamma_i,\Gamma_i'}$ and operators

$$\hat{m}_{i;\Gamma_i,\Gamma_i'} \equiv |\Gamma\rangle_{i\,i}\langle\Gamma'| \;\; . \tag{4.25c}$$

With a general variational-parameter matrix $\tilde{\lambda}_i$, one could choose the states

$$|\Gamma_i\rangle = \sum_{I_i} T_{I_i,\Gamma_i} \, |I_i\rangle \tag{4.26}$$

in (4.25c) as the eigenstates (4.10) of the Hamiltonian (4.1) without any loss of variational flexibility. However, the atomic eigenstates are not necessarily best suited for numerical applications of the theory and, therefore, we will derive the variational ground-state energy in the following chapters for an unspecified basis (4.26). Note that in the following we denote

$$|\Gamma| = \sum_I |T_{I,\Gamma}|^2 |I| \tag{4.27}$$

as the number of particles in the state $|\Gamma\rangle$. The configurations $|I\rangle_i$ and the states $|\Gamma\rangle_i$ carry a spatial index i because, in general, there can be various atoms in our Hamiltonian (2.15).

However, in order to keep the notation as transparent as possible, we drop this index in the following.

An alternative definition of the Gutzwiller variational space is given if we work with a diagonal variational-parameter matrix $\lambda_{i;\Gamma,\Gamma}$ and consider the coefficients $T_{I,\Gamma}$ as variational parameters. For practical applications, this definition turns out to be less convenient because one has to obey additional constraints concerning the normalisation and the orthogonality of the states (4.26). However, for general considerations, we will occasionally use this alternative formulation of the Gutzwiller variational space.

For our analytical considerations in the following chapter, and also for later applications, we have to address the question which of the parameters $\lambda_{\Gamma,\Gamma'} = \lambda_{i;\Gamma,\Gamma'}$ for a site i are assumed to be finite. In reference [99], we investigated the wave function (4.25a) for $\lambda_{\Gamma,\Gamma'} = \delta_{\Gamma,\Gamma}$ with states $|\Gamma\rangle$ that were the eigenstates of the atomic Hamiltonian (4.1). At first sight, this Ansatz seems quite natural since it yields the correct atomic limit and the uncorrelated limit of the Hamiltonian (2.15). For all intermediate values of the hopping and the Coulomb parameters, however, it turns out that such a restricted Ansatz can be insufficient; see for example the results for the spin-orbit coupling in iron [100]. For systems without superconductivity, the Gutzwiller wave function should be an eigenstate of the total particle number operator

$$\hat{N} = \sum_{i,\sigma} \hat{n}_{i,\sigma} \tag{4.28}$$

This requires that $\hat{N}$ commutes with $\hat{P}_{\mathrm{G}}$, which leads to

$$\sum_{\Gamma,\Gamma'} \lambda_{\Gamma,\Gamma'} (|\Gamma| - |\Gamma'|) \hat{m}_{\Gamma,\Gamma'} = 0 \; . \tag{4.29}$$

From equation (4.29), we conclude that $\lambda_{\Gamma,\Gamma'}$ can only be finite for states $|\Gamma\rangle, |\Gamma'\rangle$ with the same particle number. In a very similar way, one can show that these states have to belong to the same representation of the point symmetry group, see appendix E.

For superconducting systems, one usually works with BCS-type one-particle wave functions $|\Psi_0\rangle$ for which the particle number is not conserved. In this case, the variational-parameter matrix $\lambda_{\Gamma,\Gamma'}$ also have to be finite for states $|\Gamma\rangle, |\Gamma'\rangle$ with different particle numbers, see appendix F.

4.4 Evaluation of Gutzwiller Wave Functions and Earlier Attempts for a Generalised Gutzwiller Theory

Despite their simplicity, it is impossible, in general, to evaluate expectation values for the single-band Gutzwiller wave functions (4.15) or (4.17a). For this reason, Gutzwiller introduced an approximate evaluation scheme that was based on quasiclassical counting arguments. We will discuss this approximation, which is usually denoted as the 'Gutzwiller approximation', in section 6.1. Gutzwiller used his approach, in order to investigate the stability of ferromagnetic order in one-band Hubbard models. He found that ferromagnetism shows up in such models only under very special circumstances, for example, if there are sharp peaks in the density of states at the paramagnetic Fermi level. These findings are in stark contrast to the Hartree-Fock theory, which predicts the stability of ferromagnetic ground states for all one-band Hubbard models with sufficiently large U parameters.

Whereas the Gutzwiller theory for the one-band model obviously failed to explain ferromagnetism in transition metals, it turned out to yield a qualitatively correct description of the Mott metal-insulator transition [12, 101] at half band filling. This was first shown by

Brinkman and Rice [102] who found that the variational parameter g goes to zero at some critical value U_C of the Hubbard parameter. Although, strictly speaking, the metallic or insulating behaviour is not a simple ground-state property it is possible to derive a connection between the Gutzwiller and the Landau-Fermi-liquid theory, see section 7.3. In this context, one can interpret the behaviour of the Gutzwiller wave function at U_C as a metal to insulator transition. The insulating Gutzwiller state, however, is just a caricature of a realistic insulator since all electrons are completely localised and immobile. Furthermore, it has been shown that such a transition is entirely caused by the Gutzwiller approximation and does not show up if the Gutzwiller wave function is evaluated exactly on lattices in finite spatial dimensions [103].

The Gutzwiller approximation was formulated for a spatially homogeneous para- or ferromagnetic system, see Gutzwiller's own works [96–98] or the articles by Ogawa or by Vollhardt [104, 105]. It is not a straightforward task to generalise the approximation to more complicated situations. For example, the early attempts [104, 106, 107] to work with an antiferromagnetic one-particle product state $|\Psi_0\rangle$ in (4.15) led to some inconsistent and partly unphysical results. Similar problems arose when the Gutzwiller theory was applied [108–113] to a periodic Anderson model [114]. Although, in these works, there was an agreement about the energy functional that had to be minimised, it remained a controversy about the interpretation of the results. In particular, it was not clear to what wave function the derived ground-state properties actually apply.

Vulovic and Abrahams were the first who came up with a consistent analysis [113] of the problems that arise when one aims to generalise the Gutzwiller approximation for more complicated wave functions or Hamiltonians. They pointed out that, for systems (or wave functions) with inequivalent spin-orbital states, i.e., in an antiferromagnet, the Gutzwiller correlation operator changes the orbital occupation and it is not obvious how to cope with this effect in the Gutzwiller-approximation scheme. Vulovic and Abrahams succeeded in formulating the Gutzwiller approximation consistently for the periodic Anderson model. Their formulation, however, could also not be generalised to investigate multi-band Hubbard models.

Chao and Gutzwiller [115–118] tried to generalise the Gutzwiller approximation to investigate a degenerate two-band model. However, they were not able to derive an analytic energy functional and they also did not find a way to include inter-orbital hopping terms. More recent attempts to investigate more general multi-band models with the Gutzwiller approximation also failed to cope with inter-orbital hopping terms in the Hamiltonian [119–121]. Bünemann and Weber derived a Gutzwiller-approximation scheme that allowed to study general multi-band models with purely density-density type Coulomb interaction terms (i.e., terms of the form $\sim \hat{n}_\sigma \hat{n}_{\sigma'}$) without any restrictions on the single-particle Hamiltonian [122–124], see section 6.1.

A very different way to derive the Gutzwiller ground-state energy functional is based on the slave-boson mean-field theory. For the one-band model, this approach was first proposed by Kotliar and Ruckenstein [125]. With the hindsight knowledge of the correct Gutzwiller energy functional, the slave-boson method always turned out to be flexible enough to provide an alternative derivation scheme for more complicated systems. We give an introduction into the slave-boson theory in section 6.2.

Metzner, Gebhard, and Vollhardt were able to evaluate expectation values and correlation functions exactly for Gutzwiller wave functions in one [126–129] and infinite dimensions [130, 131]. The evaluation in one dimension was later generalised to a ferromagnetic wave function in reference [132]. Due to the availability of rather powerful numerical and analytical techniques for one-dimensional systems, however, the Gutzwiller wave function does not provide any relevant insights into the physics of such systems.

The energy functional in infinite dimensions turned out to be same as the one derived

with the Gutzwiller approximation. Gebhard introduced a more elegant evaluation scheme in this limit that allowed to work with arbitrary wave functions $|\Psi_0\rangle$ and could be applied straightforwardly to the periodic Anderson model [133, 133]. In all finite dimensions $1 < D < \infty$, one can evaluate expectation values for Gutzwiller wave functions only numerically by means of variational quantum Monte Carlo simulations; see, e.g., [134–136] and references therein.

Gutzwiller wave functions for multi-band Hubbard models have been evaluated by Bünemann, Gebhard, and Weber in the limit of infinite dimensions for density-density interactions [137] and for general atomic Hamiltonians [99]. The variational wave functions have later been generalised [138], in particular, to study superconducting systems. Note that with the phrase 'Gutzwiller theory' in this work we always mean the evaluation of Gutzwiller wave functions in the limit of infinite spatial dimensions or by means of the Gutzwiller approximation.

Chapter 5

Limit of Infinite Spatial Dimensions

In this chapter, we explain in detail how expectation values for the Gutzwiller wave functions (4.25) can be calculated in the limit of infinite spatial dimensions D. We start our considerations in section 5.1 with the derivation of diagrammatic rules in the large-D limit. These rules are used in section 5.2 where we evaluate all relevant expectation values for Gutzwiller wave functions. The general structure of the Gutzwiller energy functional and a suitable way to minimise it are discussed in section 5.3. Finally, in section 5.4, we consider the simplest conceivable example, a one-band model at half filling, for which the minimisation of the energy functional can be carried out analytically.

5.1 Fermiology in Infinite Dimensions

5.1.1 Scaling in Infinite Dimensions

A systematic investigation of itinerant lattice models in infinite dimensions began with the work by Metzner and Vollhardt [130], Brandt and Mielsch [139–141], and Müller-Hartmann [142, 143]. More recent reviews on this subject can be found in references [11, 12, 144, 145].

Before we start to evaluate Gutzwiller wave functions in the limit of infinite dimensions, we have to address the scaling problem that arises in this limit. The contribution of each lattice site i to the single-particle energy

$$\varepsilon_0 \equiv \sum_{j,s} t_{i,j} \langle \hat{c}^\dagger_{i,s} \hat{c}_{j,s} \rangle \tag{5.1}$$

in a single-band Hubbard model should be finite. Each site i, however, has $2D$ nearest-neighbours j_i. If we assume constant hopping parameters $t_{i,j} = t$ and constant hopping expectation values $\langle \hat{c}^\dagger_{i,s} \hat{c}_{j_i,s} \rangle = P$ the nearest-neighbour contribution to the single-particle energy

$$\varepsilon_0^{n.n} = 2tPD \tag{5.2}$$

obviously diverges for $D \to \infty$. The same divergence is found for the contributions to (5.1) beyond nearest-neighbour hopping. Therefore, one has to introduce a proper scaling of the tight-binding parameters $t_{i,j}$ with the spatial dimension D in order to ensure that (5.1) remains finite.

At first sight, from equation (5.2) one may conclude that the proper scaling (for nearest neighbours) is $t_{i,j} \sim 1/D$. However, this is incorrect because, with a scaling of $t_{i,j}$, the expectation value P also scales to zero with the spatial dimension D. In fact, it turns out that

the correct scaling of the hopping matrix $t_{i,j}$ for a hyper-cubic lattice with lattice constant $a = 1$ is given by

$$t_{i,j} = \frac{\tilde{t}_{i,j}}{\sqrt{2D}^{||i-j||}} \ . \tag{5.3}$$

Here, we introduced the 'New-York metric'

$$||i-j|| \equiv \sum_{l=1}^{D} |\boldsymbol{R}_{i;l} - \boldsymbol{R}_{j;l}| \ , \tag{5.4}$$

where $\boldsymbol{R}_{i;l}$ is the l-th component of the lattice site vector $\boldsymbol{R}_i$. Note that the number of neighbouring sites with distance $||i-j||$ is given by

$$N_{\text{n.n}}^{||i-j||} = D^{||i-j||} \ . \tag{5.5}$$

To motivate the general scaling proposition (5.3), we consider a model with only nearest-neighbour hopping. In this case, the scaling is given by

$$t_{i,j} = t = \frac{\tilde{t}}{\sqrt{2D}} \tag{5.6}$$

where $\tilde{t}$ is a D-independent parameter. Then, the single-particle dispersion in momentum space has the form

$$\varepsilon_{\boldsymbol{k}} = \frac{2\tilde{t}}{\sqrt{2D}} \sum_{l=1}^{D} \cos k_l \ , \tag{5.7}$$

with wave vectors $\boldsymbol{k} = (k_l, \ldots, k_D)$ and $k_l \in (-\pi, \pi)$. For $D \to \infty$, the dispersion $\varepsilon_{\boldsymbol{k}}$ obviously diverges for certain wave vectors, e.g., for $\boldsymbol{k} = (0, 0, \ldots)$. One can show, however, that the average energy per lattice site ε_0 is finite. To this end, we introduce the single-particle density of states

$$D_0(\varepsilon) = \lim_{D\to\infty} \frac{1}{(2\pi)^D} \int \mathrm{d}^D k \, \delta(\varepsilon - \varepsilon_{\boldsymbol{k}}) \ , \tag{5.8}$$

which allows us to write ε_0 as

$$\varepsilon_0 = \int_{-\infty}^{E_\mathrm{F}} \mathrm{d}\varepsilon D_0(\varepsilon) \ . \tag{5.9}$$

Here, E_F is the Fermi energy, which determines the average particle number

$$n = \int_{-\infty}^{E_\mathrm{F}} \mathrm{d}\varepsilon D_0(\varepsilon) \tag{5.10}$$

per lattice site.

In order to evaluate $D_0(\varepsilon)$, we follow reference [142] and consider the Fourier transform

$$D_0(\tau) = \frac{1}{\sqrt{2\pi}} \int_{-\infty}^{\infty} D_0(\varepsilon) \exp(\mathrm{i}\tau\varepsilon) \mathrm{d}\varepsilon \tag{5.11a}$$

$$= \frac{1}{\sqrt{2\pi}} \lim_{D\to\infty} \frac{1}{(2\pi)^D} \left[\int_{-\pi}^{\pi} \mathrm{d}k \exp\left(\mathrm{i}\tau \frac{2\tilde{t}}{\sqrt{2D}} \cos(k) \right) \right]^D \tag{5.11b}$$

of (5.11a). We expand the integrand in (5.11b)

$$\exp\left(\mathrm{i}\tau \frac{2\tilde{t}}{\sqrt{2D}} \cos(k) \right) \approx 1 + \mathrm{i}\tau \frac{2\tilde{t}}{\sqrt{2D}} \cos(k) - \tau^2 \frac{\tilde{t}^2}{D} \cos^2(k) \tag{5.12}$$

to leading order in $1/\sqrt{D}$. The second term ($\sim \tilde{t}$) vanishes in (5.11b). Therefore, with the representation

$$\exp(x) = \lim_{n\to\infty} \left(1 + \frac{x}{n}\right)^n \tag{5.13}$$

of the exponential function, we find

$$D_0(\tau) = \frac{1}{\sqrt{2\pi}} \lim_{D\to\infty} \frac{1}{(2\pi)^D} \left(2\pi - \tilde{t}^2 \frac{\pi}{D}\tau^2\right)^D \tag{5.14a}$$

$$= \frac{1}{\sqrt{2\pi}} \exp\left(-\frac{\tilde{t}^2\tau^2}{2}\right) . \tag{5.14b}$$

Finally, the inverse Fourier transform of (5.14b) yields the Gaussian density of states

$$D_0(\varepsilon) = \frac{1}{\sqrt{2\pi}\tilde{t}} \exp\left(-\frac{\varepsilon^2}{2\tilde{t}^2}\right) . \tag{5.15}$$

Note that the same result can be derived with the central limit theorem, see, e.g., reference [130]. The scaling for more general tight-binding matrices beyond nearest-neighbour hopping is studied in reference [142].

Now, after having shown that the scaling (5.3) yields a finite energy per lattice site, we can conclude that the expectation values in (5.1) scale as

$$\langle \hat{c}^\dagger_{i,s} \hat{c}_{j,s} \rangle \sim \frac{1}{\sqrt{2D}^{||i-j||}} , \tag{5.16}$$

such that the single-particle energy per site is finite,

$$\varepsilon_0 = \sum_{j,s} t_{i,j} \langle \hat{c}^\dagger_{i,s} \hat{c}_{j,s} \rangle < \infty . \tag{5.17}$$

In the following section, we discuss the implications of the scaling (5.16) for the evaluation of many-particle expectation values.

5.1.2 Evaluation of Expectation Values

The evaluation of Gutzwiller wave functions, which we will discuss in section 5.2, leads to expectation values

$$\sum_{i_1,\ldots,i_n} \langle \hat{O}_{i_1} \hat{O}_{i_2} \ldots \hat{O}_{i_n} \rangle_{\Psi_0} \tag{5.18}$$

of many-particle operators with respect to a single-particle product wave functions $|\Psi_0\rangle$. Here, we introduced local operators

$$\hat{O}_{i_l} = \hat{C}^\dagger_{i_l,I_l} \hat{C}_{i_l,I'_l} \tag{5.19}$$

where $\hat{C}^\dagger_{i,I}$ and $\hat{C}_{i,I}$ are defined in equations (4.4) and (4.5).

To evaluate the expectation value in (5.18), we use Wicks's theorem, see appendix A. Note that we can readily bring the operators in (5.18) into the form of equation (A.2) since fermionic operators with different site indices i_l anticommute. All contributions to the expectation value in (5.18), which follow from the application of Wick's theorem, can be visualised by diagrams. These have to be drawn, following the diagrammatic rules:

i) Draw n points, which represent the lattice sites $i_1, \ldots, i_n$ in (5.18).

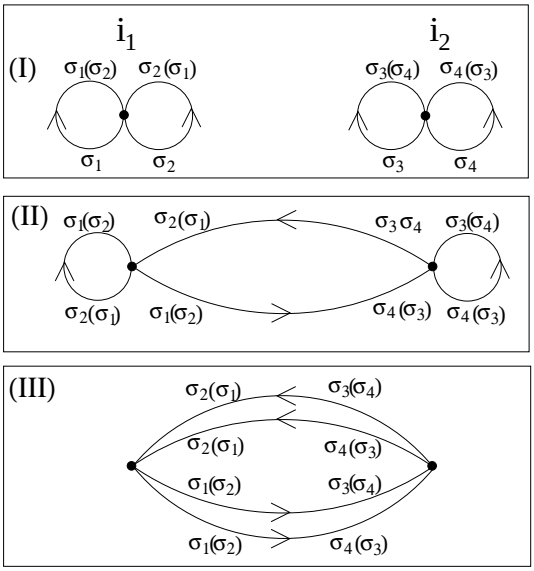

Figure 5.1: Diagrams resulting from the evaluation of (5.21).

ii) For each site i_l, draw $|I_l|$ outgoing and $|I'_l|$ ingoing lines where the lines are carrying indices $\sigma \in I_l$ and $\sigma' \in I'_l$, respectively.

iii) Find all $N_{\rm d}$ topologically different ways to connect each outgoing line to an ingoing line.

iv) The contribution $D^m_{i_1,\ldots,i_n}$ (with $m = 1,\ldots,N_{\rm d}$) of a diagram is given by the product of all lines, where a line represents the expectation value

$$P^{\sigma_l,\sigma'_{l'}}_{i_l,i_{l'}} = \left\langle \hat{c}^\dagger_{i_l,\sigma_l} \hat{c}_{i_{l'},\sigma'_{l'}} \right\rangle_{\Psi_0} . \tag{5.20}$$

To formulate rules for the correct sign of a diagram, is more difficult. As we will show in the following section, however, for our evaluation in the large D limit, the signs of the diagrams are irrelevant and we can leave this question aside.

As an example, we show all diagrams that result from the evaluation of

$$\left\langle \left(\hat{c}^\dagger_{i_1\sigma_1}\hat{c}^\dagger_{i_1\sigma_2}\hat{c}_{i_1\sigma_2}\hat{c}_{i_1\sigma_1}\right)\left(\hat{c}^\dagger_{i_2\sigma_3}\hat{c}^\dagger_{i_2\sigma_4}\hat{c}_{i_2\sigma_4}\hat{c}_{i_2\sigma_3}\right)\right\rangle_{\Psi_0} \tag{5.21}$$

in figure 5.1. Note that the brackets in figure 5.1, for example $\sigma_1(\sigma_2)$, that belong to different lattice sites are unrelated. For example, there are four different diagrams in the first group (I), which, explicitly, are given by an expansion of

$$D^{(1-4)}_{i_1,i_2} = \left(P^{\sigma_1,\sigma_1}_{i_1,i_1}P^{\sigma_2,\sigma_2}_{i_1,i_1} - P^{\sigma_1,\sigma_2}_{i_1,i_1}P^{\sigma_2,\sigma_1}_{i_1,i_1}\right)\left(P^{\sigma_3,\sigma_3}_{i_2,i_2}P^{\sigma_4,\sigma_4}_{i_1,i_1} - P^{\sigma_3,\sigma_4}_{i_2,i_2}P^{\sigma_4,\sigma_3}_{i_1,i_1}\right) . \tag{5.22}$$

Similarly, both the group (II) and (III) contains four different diagrams.

The diagrams (I)-(III) have a different scaling behaviour both with respect to the number of lattice site L and the spatial dimension D. We first consider the scaling behaviour with respect to L. As an example, the evaluation of the sum in (5.18) for the first diagram in group (I) leads to

$$\sum_{i_1,i_2} D^1_{i_1,i_2} = \left(\sum_{i_1} P^{\sigma_1,\sigma_1}_{i_1,i_1}P^{\sigma_2,\sigma_2}_{i_1,i_1}\right)\left(\sum_{i_2} P^{\sigma_3,\sigma_3}_{i_2,i_2}P^{\sigma_4,\sigma_4}_{i_2,i_2}\right) , \tag{5.23}$$

i.e., the lattice sums factorise in this case. Since each of the 'local' lines $P^{\sigma_1,\sigma_1}_{i_1,i_1}$ is of the order unity, the two sums in (5.23) lead to a contribution of order L^2. In contrast, if we assume translational invariance, i.e.,

$$P^{\sigma,\sigma'}_{i,i} = P^{\sigma,\sigma'} \quad (\forall\, i) \tag{5.24}$$

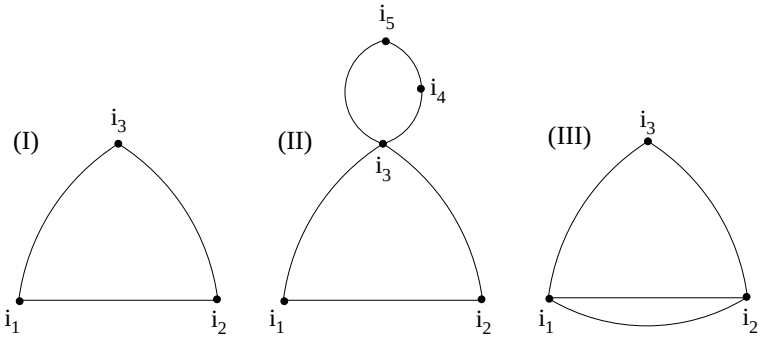

Figure 5.2: Examples for diagrams that, in infinite dimensions, are finite (I)/(II), or that vanish (III). For simplicity, arrows and orbital indices are dropped here.

we find

$$\sum_{i_1,i_2} P^{\sigma_1,\sigma_1}_{i_1,i_1} P^{\sigma_2,\sigma_3}_{i_1,i_2} P^{\sigma_3,\sigma_2}_{i_2,i_1} P^{\sigma_4,\sigma_4}_{i_2,i_2} = P^{\sigma_1,\sigma_1} P^{\sigma_4,\sigma_4} \sum_{i_1,i_2} P^{\sigma_2,\sigma_3}_{i_1,i_2} P^{\sigma_3,\sigma_2}_{i_2,i_1} \tag{5.25}$$

for one of the diagrams in group (II). The evaluation of the sum on the r.h.s. of equation (5.25) yields

$$\sum_{i_1,i_2} P^{\sigma_2,\sigma_3}_{i_1,i_2} P^{\sigma_3,\sigma_2}_{i_2,i_1} = \sum_{\boldsymbol{k},\gamma(\mathrm{occ.})} |u_{\gamma,\sigma_2}(\boldsymbol{k})|^2 |u_{\gamma,\sigma_3}(\boldsymbol{k})|^2 \tag{5.26}$$

where the coefficient $u_{\gamma,\sigma}(\boldsymbol{k})$ defines the creation operators

$$\hat{h}^\dagger_{\boldsymbol{k},\gamma} \equiv \frac{1}{\sqrt{L}} \sum_{i,\sigma} e^{\mathrm{i}\boldsymbol{k}\boldsymbol{R}_i} u_{\gamma,\sigma}(\boldsymbol{k}) \hat{c}^\dagger_{i,\sigma} \,, \tag{5.27}$$

which set up the single-particle product state $|\Psi_0\rangle$. Obviously, (5.26) is of order L and so is the diagram (5.25).

The diagrams in our approach result from the evaluation of expectation values, which, physically, have to be of order L. Therefore, all diagrams of order L^m, with $m \geq 2$, cannot contribute. For example, the diagrams (I) in figure 5.1 must somehow cancel out. As a matter of fact, a scaling $\sim L^m$ with $m \geq 2$ is found for all diagrams that are not totally connected; for a proof of this general statement see, e.g., reference [3]. In our context, the discard of all disconnected diagrams is a result of the linked-cluster theorem, see section 5.2.2.

The connected diagrams (II) and (III) scale differently with respect to the spatial dimension D. Since the local lines (5.24) are of order unity with respect to D, the diagrams (II) in figure 5.1 scale like

$$\sum_{i_1,i_2} P^{\sigma_2,\sigma_3}_{i_1,i_2} P^{\sigma_3,\sigma_2}_{i_2,i_1} \sim L \sum_{i_2} P^{\sigma_2,\sigma_3}_{i_1,i_2} P^{\sigma_3,\sigma_2}_{i_2,i_1} \sim L \sum_{i_2} \frac{1}{D^{||i_1 - i_2||}} \sim L \,, \tag{5.28}$$

i.e., they are of order unity with respect to D. In contrast, the diagrams (III) with four fermionic lines scale at least like $1/D$ and, therefore, they vanish for $D \to \infty$. The general topological rule behind these considerations is:

> *A diagram of order L vanishes in the limit of infinite spatial dimensions if (at least) one pair of sites is connected by three (or more) different paths.*

For example, the diagrams (I) and (II) in figure 5.1.2 are finite, while the diagram (III) vanishes since, here, the sites i_1 and i_2 are connected by three different paths. Note that in our context two paths are denoted as 'different' if they do not share a single part. For example, the two paths $i_5 \to i_3 \to i_1$ and $i_5 \to i_4 \to i_3 \to i_1$ in diagram (II), figure 5.1.2, are *not* different according to this definition because they share the part $i_3 \to i_1$.

5.1.3 Simplifications in Momentum Space

The diagrammatic rules in infinite dimensions, which we formulated in real space in section 5.1.2, have consequences for the evaluation of expectation values in momentum space. We start our considerations with the momentum distribution

$$n^0_{\boldsymbol{k},s} = \langle \hat{n}_{\boldsymbol{k},s} \rangle_{\Psi_0} = \frac{1}{L} \sum_{i,j} e^{\mathrm{i}(\boldsymbol{R}_i - \boldsymbol{R}_j)\boldsymbol{k}} \langle \hat{c}^\dagger_{i,s} \hat{c}_{j,s} \rangle_{\Psi_0} \tag{5.29}$$

for a single-band Hubbard model. This momentum distribution is of order unity. However, the r.h.s. of equation (5.29) seems to diverge in the limit of infinite dimensions because

$$\frac{1}{L} \sum_{i,j} e^{\mathrm{i}(\boldsymbol{R}_i - \boldsymbol{R}_j)\boldsymbol{k}} \langle \hat{c}^\dagger_{i,s} \hat{c}_{j,s} \rangle_{\Psi_0} = \underbrace{\sum_j P^{s,s}_{i,j} \, e^{\mathrm{i}(\boldsymbol{R}_i - \boldsymbol{R}_j)\boldsymbol{k}}}_{\sim \sqrt{D}^{||i-j||} \to \infty} \stackrel{?}{\to} \infty \; . \tag{5.30}$$

Obviously, for a consistent evaluation of expectation values in the limit of infinite dimensions, we have to add the following rule:

An exponential function $e^{\mathrm{i}(\boldsymbol{R}_i - \boldsymbol{R}_j)\boldsymbol{k}}$ *scales like* $1/\sqrt{2D}^{||i-j||}$.

This additional scaling rule has consequences for the evaluation of expectation values in momentum space. For example, we find

$$\langle \hat{n}_{\boldsymbol{k},s} \hat{n}_{\boldsymbol{k}+\boldsymbol{q},s} \rangle_{\Psi_0} = \frac{1}{L^2} \sum_{i,j,l,m} e^{\mathrm{i}(\boldsymbol{R}_i - \boldsymbol{R}_j)\boldsymbol{k}} e^{\mathrm{i}(\boldsymbol{R}_l - \boldsymbol{R}_m)(\boldsymbol{k}+\boldsymbol{q})} \langle \hat{c}^\dagger_{i,s} \hat{c}_{j,s} \hat{c}^\dagger_{l,s} \hat{c}_{m,s} \rangle_{\Psi_0} \; , \tag{5.31a}$$

for $\boldsymbol{q} \neq \boldsymbol{0}$, where the expectation value in the sum is given by

$$\langle \hat{c}^\dagger_{i,s} \hat{c}_{j,s} \hat{c}^\dagger_{l,s} \hat{c}_{m,s} \rangle_{\Psi_0} = P^{s,s}_{i,j} P^{s,s}_{l,m} - P^{s,s}_{i,m} P^{s,s}_{l,j} \; . \tag{5.31b}$$

The two terms in (5.31a), arising from (5.31b), are displayed diagrammatically in the upper part of figure 5.3. The solid lines represent, as before, the expectation values $P^{s,s}_{i,j}$. The exponential functions in (5.31a) are represented by dashed lines. Note that both diagrams are disconnected with respect to the solid lines. For this reason, they are not of order L, unlike connected diagrams, and the diagrammatic rule, formulated in section 5.1.2, cannot be applied here directly. The easiest way to analyse the $D \to \infty$ scaling of such unconnected diagrams is to add a particle (solid) line that links the two disconnected parts of the diagram. This diagrammatic procedure corresponds to a fixing of two sites in the sum (5.31a) and to analyse the large-D scaling of the remaining two sums. To the new (connected) diagrams in figure 5.3 we can apply the diagrammatic rule of the previous section. As a result we find that the diagram (I) is finite, while the diagram (II) vanishes because the sites i and l are connected by three different paths.

Since the second diagram vanishes in infinite dimensions, we find a factorisation of the expectation value in (5.31a),

$$\begin{aligned} \langle \hat{n}_{\boldsymbol{k},s} \hat{n}_{\boldsymbol{k}+\boldsymbol{q},s} \rangle_{\Psi_0} &= \left(\frac{1}{L} \sum_{i,j} e^{\mathrm{i}(\boldsymbol{R}_i - \boldsymbol{R}_j)\boldsymbol{k}} P^{s,s}_{i,j} \right) \left(\frac{1}{L} \sum_{l,m} e^{\mathrm{i}(\boldsymbol{R}_l - \boldsymbol{R}_m)(\boldsymbol{k}+\boldsymbol{q})} P^{s,s}_{l,m} \right) && (5.32a) \\ &= \langle \hat{n}_{\boldsymbol{k},s} \rangle_{\Psi_0} \langle \hat{n}_{\boldsymbol{k}+\boldsymbol{q},s} \rangle_{\Psi_0} \; . && (5.32b) \end{aligned}$$

This result can be generalised to arbitrary products of occupation operators in momentum space. It is the foundation of the 'Random-Dispersion Approximation', see references [12, 22, 146, 147].

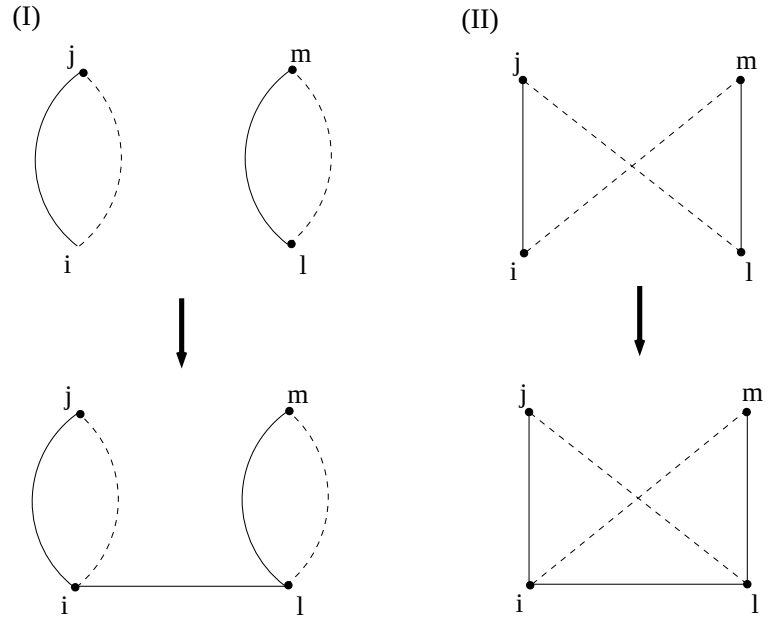

Figure 5.3: Diagrams arising from the evaluation of equation (5.29), see text.

5.2 Evaluation of Gutzwiller Wave Functions

In this section, we evaluate expectation values for the Gutzwiller wave function

$$|\Psi_{\mathrm{G}}\rangle = \hat{P}_{\mathrm{G}}\,|\Psi_0\rangle = \prod_i \hat{P}_i\,|\Psi_0\rangle \tag{5.33}$$

with

$$\hat{P}_i = \sum_{\Gamma,\Gamma'} \lambda_{i;\Gamma,\Gamma'} \hat{m}_{i;\Gamma,\Gamma'} \tag{5.34}$$

in the limit of infinite spatial dimensions. We will confine our considerations to systems without superconductivity. Although, technically, the treatment of wave functions with superconducting pairing does not differ from those without, the notations and results are more complicated. In order to keep the derivation here as simple as possible, we refer the reader to appendix F where the main results for systems with superconductivity are summarised.

The uncorrelated local density matrix $\tilde{C}_i^0$ with the elements

$$C^0_{i;\sigma,\sigma'} \equiv \langle \hat{c}^\dagger_{i,\sigma} \hat{c}_{i,\sigma'} \rangle_{\Psi_0} \tag{5.35}$$

is not diagonal, in general. For a given wave function $|\Psi_0\rangle$, however, one can always find a local basis

$$\hat{h}^\dagger_{i,\gamma} = \sum_\sigma u_{i;\gamma,\sigma} \hat{c}^\dagger_{i,\sigma}\ , \tag{5.36}$$

for which the corresponding density matrix $\tilde{H}_i^0$ with the elements

$$H^0_{i;\gamma,\gamma'} = \langle \hat{h}^\dagger_{i,\gamma} \hat{h}_{i,\gamma'} \rangle_{\Psi_0} = \delta_{\gamma,\gamma'} n^0_{i,\gamma} \tag{5.37}$$

is diagonal. In order to determine the variational ground-state energy, it is most convenient to work with such a local basis because, as we will see below, all expectation values have a much simpler form. Unfortunately, in order to formulate a time dependent Gutzwiller theory

in section 8.3, we need the energy functional for a general orbital basis $|\sigma\rangle$. Therefore, we work with such a basis in our derivation here. In addition, we give the particular form of all essential formulae also for the basis $|\gamma\rangle$ with a diagonal local density matrix. To clearly distinguish equations for the two different basis sets, we denote the configurations states (Slater determinants) defined for the operators (5.36) as $|H\rangle$ instead of $|I\rangle$.

We aim to evaluate expectation values of operators $\hat{O}_i$ and $\hat{O}_{i,j} = \hat{c}^\dagger_{i,\sigma}\hat{c}_{j,\sigma'}$ with respect to the wave function (5.33),

$$\langle \hat{O}_i \rangle_{\mathrm{G}} = \frac{\langle \Psi_0 | \left[\prod_{m\neq i} \hat{P}^\dagger_m \hat{P}_m\right] \hat{P}^\dagger_i \hat{O}_i \hat{P}_i \, |\Psi_0\rangle}{\langle \Psi_0 | \prod_m \hat{P}^\dagger_m \hat{P}_m |\Psi_0\rangle} \,, \tag{5.38a}$$

$$\langle \hat{O}_{i,j} \rangle_{\mathrm{G}} = \frac{\langle \Psi_0 | \left[\prod_{m\neq i,j} \hat{P}^\dagger_m \hat{P}_m\right] \hat{P}^\dagger_j \hat{P}^\dagger_i \hat{O}_{i,j} \hat{P}_i \, \hat{P}_j \, |\Psi_0\rangle}{\langle \Psi_0 | \prod_m \hat{P}^\dagger_m \hat{P}_m |\Psi_0\rangle} \,. \tag{5.38b}$$

In the following, lattice site indices in formulae for local quantities will be generally dropped. The product $\hat{P}^\dagger_i \hat{P}_i$ of a local Gutzwiller correlation operators can be reduced to

$$\hat{P}^\dagger \hat{P} = \sum_{I_1,I_2} \overline{\lambda}_{I_1,I_2} |I_1\rangle\langle I_2| \,, \tag{5.39a}$$

where

$$\overline{\lambda}_{I_1,I_2} = \sum_{\Gamma_1,\Gamma_2} T_{I_1,\Gamma_1} T^*_{I_2,\Gamma_2} \sum_{\Gamma_3} \lambda^*_{\Gamma_3,\Gamma_1} \lambda_{\Gamma_3,\Gamma_2} \,, \tag{5.39b}$$

and the coefficients $T_{I,\Gamma}$ have been introduced in equation (4.26). We evaluate $\langle \hat{O}_i \rangle_{\mathrm{G}}$ and $\langle \hat{O}_{i,j} \rangle_{\mathrm{G}}$ by means of the diagrammatic technique that was introduced in the previous section. In such an approach, the sites $m \neq i, j$ in (5.38) will play the role of inner vertices. Before we start with the investigation of the expectation values (5.38), we first introduce a technique in the following section that will later enable us to get rid of *all* diagrams that contain inner vertices.

5.2.1 Local Constraints

First, we eliminate all local contributions at the inner vertices that arise after the application of Wick's theorem to the expectation values in (5.38). This leads to a number of constraints for the variational parameters $\lambda_{i;\Gamma,\Gamma'}$.

We expand $\hat{P}^\dagger_i \hat{P}_i$ in terms of new local operators,

$$\hat{P}^\dagger \hat{P} = x_{\emptyset,\emptyset} + \left[\hat{P}^\dagger \hat{P}\right]^{\mathrm{HF}} \tag{5.40a}$$

$$\left[\hat{P}^\dagger \hat{P}\right]^{\mathrm{HF}} = \sum_{\substack{I_1,I_2 \\ (|I_i|\geq 1)}} x_{I_1,I_2} \left(\hat{C}^\dagger_{I_1} \hat{C}_{I_2} - \left[\hat{C}^\dagger_{I_1} \hat{C}_{I_2}\right]^{\mathrm{HF}} \right) \tag{5.40b}$$

with operators $\hat{C}^\dagger_{i,I}$ and $\hat{C}_{i,I}$ as defined in (4.4) and (4.5) and expansion coefficients $x_{i;I_1,I_2}$. Here, the Hartree-Fock operator for an even number $n \geq 4$ of fermionic operators is defined recursively,

$$\begin{aligned} [\hat{a}_1 \ldots \hat{a}_n]^{\mathrm{HF}} \equiv\ & \langle \hat{a}_1 \ldots \hat{a}_n \rangle_{\Psi_0} \\ & + {\sum_{\{\gamma_1,\ldots,\gamma_n\}=0}^{1}}' (-1)^{f_{\mathrm{s}}(\{\gamma_i\})} \left\{ \left(\prod_{\ell=1}^{n} \hat{a}^{\gamma_\ell}_\ell \right) - \left[\prod_{\ell=1}^{n} \hat{a}^{\gamma_\ell}_\ell \right]^{\mathrm{HF}} \right\} \left\langle \prod_{\ell=1}^{n} \hat{a}^{1-\gamma_\ell}_\ell \right\rangle_{\Psi_0} \end{aligned} \tag{5.41a}$$

with

$$f_{\mathrm{s}}(\{\gamma_i\}) \equiv \sum_{\ell=1}^{n} \left(\ell - \frac{1}{2}\right) \gamma_\ell \; . \tag{5.41b}$$

The prime in (5.41a) indicates that

$$2 \leq \sum_{\ell=1}^{n} \gamma_\ell \leq n-2 \tag{5.41c}$$

is even. As the starting point of the recursive formula (5.41), we define

$$[\hat{a}_1 \hat{a}_2]^{\mathrm{HF}} \equiv \langle \hat{a}_1 \hat{a}_2 \rangle_{\Psi_0} \tag{5.41d}$$

for $n = 2$ fermionic operators. By construction, the operators

$$\hat{C}^\dagger_{i;I_1} \hat{C}_{i;I_2} - \left[\hat{C}^\dagger_{i;I_1} \hat{C}_{i;I_2}\right]^{\mathrm{HF}} \tag{5.42}$$

in the expansion (5.40) generate diagrams with exactly $|I_1| = |I_2|$ non-local lines that enter (and leave) the lattice site i. All diagrams with trivial local Hartree-Fock bubbles are automatically excluded.

As an example for this procedure, we consider the square of the local correlation operator for the single-band Hubbard model, cf. equation (4.16),

$$\hat{P}^\dagger \hat{P} = \hat{P}^2 = \lambda_d^2 \hat{m}_d + \sum_s \lambda_s^2 \hat{m}_s + \lambda_\emptyset^2 \hat{m}_\emptyset \tag{5.43a}$$

$$= \left(\lambda_d^2 - \sum_s \lambda_s^2 + \lambda_\emptyset^2\right) \hat{c}^\dagger_\uparrow \hat{c}^\dagger_\downarrow \hat{c}_\downarrow \hat{c}_\uparrow + \sum_s (\lambda_s^2 - \lambda_\emptyset^2) \hat{c}^\dagger_s \hat{c}_s + \lambda_\emptyset^2 \; . \tag{5.43b}$$

For the expansion (5.40) of

$$\hat{P}^2 = x_{\emptyset,\emptyset} + x_{d,d} \left(\hat{c}^\dagger_\uparrow \hat{c}^\dagger_\downarrow \hat{c}_\downarrow \hat{c}_\uparrow - \left[\hat{c}^\dagger_\uparrow \hat{c}^\dagger_\downarrow \hat{c}_\downarrow \hat{c}_\uparrow\right]^{\mathrm{HF}}\right) + \sum_s x_{s,s} \left(\hat{c}^\dagger_s \hat{c}_s - \left[\hat{c}^\dagger_s \hat{c}_s\right]^{\mathrm{HF}}\right) \; , \tag{5.44a}$$

we need the Hartree-Fock operators,

$$\left[\hat{c}^\dagger_\uparrow \hat{c}^\dagger_\downarrow \hat{c}_\downarrow \hat{c}_\uparrow\right]^{\mathrm{HF}} = \sum_s \hat{c}^\dagger_s \hat{c}_s \langle \hat{c}^\dagger_{\bar{s}} \hat{c}_{\bar{s}} \rangle_{\Psi_0} - \langle \hat{c}^\dagger_\uparrow \hat{c}_\uparrow \rangle_{\Psi_0} \langle \hat{c}^\dagger_\downarrow \hat{c}_\downarrow \rangle_{\Psi_0} \; , \tag{5.44b}$$

$$\left[\hat{c}^\dagger_s \hat{c}_s\right]^{\mathrm{HF}} = \langle \hat{c}^\dagger_s \hat{c}_s \rangle_{\Psi_0} \; . \tag{5.44c}$$

A comparison of equations (5.43b) and (5.44) yields the relations

$$\lambda_\emptyset^2 = x_{\emptyset,\emptyset} - \sum_s x_{s,s} \langle \hat{c}^\dagger_s \hat{c}_s \rangle_{\Psi_0} + x_{d,d} \langle \hat{c}^\dagger_\uparrow \hat{c}_\uparrow \rangle_{\Psi_0} \langle \hat{c}^\dagger_\downarrow \hat{c}_\downarrow \rangle_{\Psi_0} \; , \tag{5.45a}$$

$$\lambda_s^2 - \lambda_\emptyset^2 = x_{s,s} - x_{d,d} \langle \hat{c}^\dagger_{\bar{s}} \hat{c}_{\bar{s}} \rangle_{\Psi_0} \; , \tag{5.45b}$$

$$\lambda_d^2 - \sum_s \lambda_s^2 + \lambda_\emptyset^2 = x_{d,d} \; , \tag{5.45c}$$

which, in principle, can be used to determine the coefficients $x_{I,I}$ as a function of the parameters $\lambda_{I,I}$, or vice versa. In the following, we will carry out the expansion (5.40) in a way that avoids to work with the expansion coefficients $x_{I,I'}$.

For our diagrammatic evaluation, we demand that there is only a contribution from inner vertices with at least two leaving and/or entering lines. This is ensured if

$$x_{i;\emptyset,\emptyset} = 1 , \tag{5.46a}$$
$$x_{i;I_1,I_2} = 0 \quad \text{for } |I_1| = |I_2| = 1 , \tag{5.46b}$$

and for all lattice sites i. We can fulfill these conditions by restricting the variational parameters $\lambda_{i;\Gamma,\Gamma'}$. Using the expansion (5.40) together with (5.46b) one readily finds that the constraint equations

$$1 = \langle \hat{P}_i^\dagger \hat{P}_i \rangle_{\Psi_0} , \tag{5.47a}$$
$$\langle \hat{c}_{i,\sigma}^\dagger \hat{c}_{i,\sigma'} \rangle_{\Psi_0} = \langle \hat{c}_{i,\sigma}^\dagger \hat{c}_{i,\sigma'} \hat{P}_i^\dagger \hat{P}_i \rangle_{\Psi_0} , \tag{5.47b}$$

must be fulfilled. This follows from the fact that, apart from the trivial term $x_{i;\emptyset,\emptyset} = 1$ in (5.40), at least four lines meet at every vertex; a contraction with the two 'external' fermionic operators $\hat{c}_{i,\sigma}^\dagger$ and $\hat{c}_{i,\sigma'}$ in (5.47b) leaves at least one uncontracted pair whose local contraction, however, vanishes by construction. Note that the same argument applies if we move the operator $\hat{P}_i^\dagger \hat{P}_i$ relative to $\hat{c}_{i,\sigma}^\dagger$ and $\hat{c}_{i,\sigma'}$ in (5.47). Hence, there are three different ways to formulate the group of equations (5.47), which all yield the same physical constraints for the variational parameters $\lambda_{i;\Gamma,\Gamma'}$.

Explicitly, equations (5.47) have the form

$$1 = \sum_{I_1,I_2} \overline{\lambda}_{I_1,I_2} m^0_{I_1,I_2} , \tag{5.48a}$$
$$\langle \hat{c}_\sigma^\dagger \hat{c}_{\sigma'} \rangle_{\Psi_0} = \sum_{I_1,I_2,I_3} \langle I_1 | \hat{c}_\sigma^\dagger \hat{c}_{\sigma'} | I_3 \rangle \overline{\lambda}_{I_3,I_2} m^0_{I_1,I_2} , \tag{5.48b}$$

where we introduced the expectation value

$$m^0_{I_1,I_2} = \big\langle (|I_1\rangle\langle I_2|) \big\rangle_{\Psi_0} , \tag{5.49}$$

which can be evaluated by means of equation (A.10), appendix A.

For the orbital basis $|\gamma\rangle$ with a diagonal density matrix (5.37), the constraints (5.48) read

$$1 = \sum_H \overline{\lambda}_H m^0_{H,H} \tag{5.50a}$$
$$\delta_{\gamma,\gamma'} n^0_\gamma = \sum_{H_1,H_2} \overline{\lambda}_{H_1,H_2} \langle H_2 | \hat{h}_\gamma^\dagger \hat{h}_{\gamma'} | H_1 \rangle \sqrt{m^0_{H_1} m^0_{H_2}} , \tag{5.50b}$$

where we used that

$$m^0_{H,H'} = \delta_{H,H'} m^0_{H,H} \equiv m^0_H , \tag{5.51}$$

and

$$\big\langle (\hat{h}_\gamma^\dagger \hat{h}_{\gamma'} | H_1\rangle\langle H_2|) \big\rangle_{\Psi_0} = \langle H_2 | \hat{h}_\gamma^\dagger \hat{h}_{\gamma'} | H_1 \rangle m^0_{H_2} \tag{5.52a}$$
$$= \sqrt{\frac{n^0_\gamma (1 - n^0_{\gamma'})}{n^0_{\gamma'} (1 - n^0_\gamma)}} \langle H_2 | \hat{h}_\gamma^\dagger \hat{h}_{\gamma'} | H_1 \rangle \sqrt{m^0_{H_1} m^0_{H_2}} . \tag{5.52b}$$

Note that the left square root in (5.52b) does not appear in (5.50b) since it is either unity for $\gamma = \gamma'$, or it can be cancelled for $\gamma \neq \gamma'$. For the one-band model, the constraints (5.50) have

the form

$$1 = \lambda_\emptyset^2 m_\emptyset^0 + \sum_s \lambda_s^2 m_s^0 + \lambda_d^2 m_d^0 \,, \tag{5.53a}$$

$$n_s^0 = \lambda_d^2 m_d^0 + \lambda_s^2 m_s^0 \,, \tag{5.53b}$$

if we assume a diagonal density matrix $\tilde{C}^0$ and work with the correlation operator (4.16). Here, the uncorrelated expectation values m_I^0 are given by

$$m_d^0 = n_\uparrow^0 n_\downarrow^0 \,, \tag{5.54a}$$

$$m_s^0 = n_s^0(1 - n_{\bar{s}}^0) \,, \tag{5.54b}$$

$$m_\emptyset^0 = (1 - n_\uparrow^0)(1 - n_\downarrow^0) \tag{5.54c}$$

with

$$n_s^0 \equiv \langle \hat{n}_s \rangle_{\Psi_0} \,. \tag{5.55}$$

Note that the non-diagonal constraints are automatically fulfilled for the correlation operator (4.16) since it leads to $\bar{\lambda}_{I,I'} \sim \delta_{I,I'}$. This, however, also shows that the Ansatz (4.16) is insufficient for wave functions with non-diagonal elements $\langle \hat{c}_{i,s}^\dagger \hat{c}_{i,\bar{s}} \rangle_{\Psi_0} \neq 0$ of the local density matrix. To cope with such wave functions, one has to work with the correlation operator

$$\hat{P} = \lambda_d \hat{m}_d + \sum_s \lambda_s \hat{m}_s + \lambda_\emptyset \hat{m}_\emptyset + \left(\lambda_{\uparrow,\downarrow} \left|\uparrow\right\rangle \left\langle\downarrow\right| + \text{h.c.} \right) \,, \tag{5.56}$$

which generalises (4.16). A similar generalisation is needed to study systems with superconductivity, see equation (F.7).

5.2.2 Diagrammatic Simplifications

With the help of equations (5.40) and (5.46a), we expand the product over the squares of local Gutzwiller correlation operators in (5.38) in the form

$$\prod_{m \neq i[j]} \hat{P}_m^2 = 1 + {\sum_m}' \left[\hat{P}_m^2\right]^{\text{HF}} + \frac{1}{2} {\sum_{m_1,m_2}}' \left[\hat{P}_{m_1}^2\right]^{\text{HF}} \left[\hat{P}_{m_2}^2\right]^{\text{HF}} + \dots \,, \tag{5.57}$$

where the prime on the sums indicates that all lattice sites are different from each other and from i [and j]. When Wick's theorem is applied to the numerators in (5.38) we can work with the new lines

$$K_{m,n}^{\sigma,\sigma'} = \langle \hat{c}_{n,\sigma}^\dagger \hat{c}_{m,\sigma'} \rangle_{\Psi_0} - \delta_{n,m} \langle \hat{c}_{n,\sigma}^\dagger \hat{c}_{n,\sigma'} \rangle_{\Psi_0} \tag{5.58}$$

instead of $P_{m,n}^{\sigma,\sigma'}$ in our diagrammatic expansion. This is possible since, in those cases where Fermi operators on the same site are contracted, the contribution vanishes by construction of the Hartree-Fock operators $\left[\hat{P}_m^2\right]^{\text{HF}}$.

The application of Wick's theorem thus gives a result that we would have obtained by working with Graßmann operators $\hat{c}_{i,\sigma}^{\text{g}}$ instead of Fermion operators in the definition of the expectation values; all operators $\hat{c}_{i,\sigma}^{\text{g}}$ anti-commute with each other

$$\left[\hat{c}_{i,\sigma}^{\text{g}}, \hat{c}_{j,\sigma'}^{\text{g}}\right]_+ = 0 \,, \tag{5.59}$$

so that local contractions always vanish,

$$\left\langle \hat{c}_{i,\sigma}^{\text{g}} \hat{c}_{i,\sigma'}^{\text{g}} \right\rangle_{\Psi_0} = 0 \,. \tag{5.60}$$

The use of Graßmann operators instead of Fermi operators also shows that we may now drop the restrictions on the lattice sums because all contributions with two lattice sites put equal vanish due to the anti-commutation relation between the corresponding Graßmann operators. In this way, we have generated a diagrammatic theory in which lines between two vertices n and m are given by the one-particle density matrices $K^{\sigma\sigma'}_{m,n}$ defined in (5.58), and $x_{m;I_1,I_2}$ gives the strength of a vertex $(m; I_1, I_2)$ with $|I_1| = |I_2|$ ingoing and outgoing lines.

Now we are in the position to apply the 'linked-cluster theorem', see, e.g., reference [3], so that all disconnected diagrams in the numerators in equations (5.38) cancel the corresponding denominator. Then, the calculation of the expectation values (5.38a) and (5.38b) is reduced to the sum over all *connected* diagrams according to the Feynman rules with lines and vertices as defined above.

By construction, at least four lines meet at every inner vertex. For the operators $\hat{O}_i$ and $\hat{O}_{ij}$ in (5.38) that we investigate in this section, it follows that two inner vertices are always connected by at least three independent paths of lines. Therefore, the contribution of all diagrams with inner vertices vanishes at least proportional to $1/\sqrt{D}$ in the limit of infinite dimensions. Thus, not a single diagram needs to be calculated in infinite dimensions, i.e., we arrive at the result

$$\langle \hat{O}_i \rangle_{\Psi_G} = \langle \Psi_0 | \hat{P}_i^\dagger \hat{O}_i \hat{P}_i \, | \Psi_0 \rangle \, , \tag{5.61a}$$

$$\langle \hat{O}_{i,j} \rangle_{\Psi_G} = \langle \Psi_0 | \hat{P}_j^\dagger \hat{P}_i^\dagger \hat{O}_{i,j} \hat{P}_i \, \hat{P}_j \, | \Psi_0 \rangle \tag{5.61b}$$

in $D = \infty$ dimensions. Note that the arguments that led to equation (5.61b) do not apply to all types of two-site operators $\hat{O}_{ij}$. For example, the evaluation of $\hat{O}_{ij} = \hat{n}_{i,\sigma}\hat{n}_{j,\sigma'}$ leads to an infinite number of diagrams that contribute even in the limit of infinite spatial dimensions. Equation (5.61b) does, however, apply to hopping operators $\hat{O}_{ij} = \hat{c}^\dagger_{i,\sigma}\hat{c}_{j,\sigma'}$. For them, the result (5.61b) can be even further simplified because in $D = \infty$ dimensions, there is only a single line connecting the two external vertices i and j, see below.

5.2.3 Local Energy

For a general atomic basis $|\Gamma\rangle$, the local Hamiltonian (4.1) has the form

$$\hat{H}_{\rm loc} = \sum_{\Gamma,\Gamma'} E^{\rm loc}_{\Gamma,\Gamma'} |\Gamma\rangle\langle\Gamma'| \tag{5.62}$$

with

$$E^{\rm loc}_{\Gamma,\Gamma'} \equiv \langle \Gamma | \hat{H}_{\rm loc} | \Gamma' \rangle \, . \tag{5.63}$$

Since, for this operator, we find

$$\hat{P}^\dagger \hat{H}_{\rm loc} \hat{P} = \sum_{\Gamma_1 \ldots \Gamma_4} \lambda^*_{\Gamma_2,\Gamma_1} \lambda_{\Gamma_3,\Gamma_4} E^{\rm loc}_{\Gamma_2,\Gamma_3} |\Gamma_1\rangle\langle\Gamma_4| \, , \tag{5.64}$$

equation (5.61a) yields the expectation value

$$E_{\rm loc} = \langle \hat{H}_{\rm loc} \rangle_{\Psi_G} = \sum_{\Gamma_1 \ldots \Gamma_4} \lambda^*_{\Gamma_2,\Gamma_1} \lambda_{\Gamma_3,\Gamma_4} E^{\rm loc}_{\Gamma_2,\Gamma_3} m^0_{\Gamma_1,\Gamma_4} \, , \tag{5.65}$$

where we introduced the uncorrelated expectation value

$$m^0_{\Gamma_1,\Gamma_4} \equiv \left\langle \, (|\Gamma_1\rangle\langle\Gamma_4|) \, \right\rangle_{\Psi_0} = \sum_{I_1,I_4} T_{I_1,\Gamma_1} T^*_{I_4,\Gamma_4} m^0_{I_1,I_4} \, , \tag{5.66}$$

and $m^0_{I_1,I_4}$ is calculated in equation (A.10).

For the special case that the states $|\Gamma\rangle$ are the eigenstates of the local Hamiltonian and the variational-parameter matrix is diagonal, i.e., with

$$E^{\mathrm{loc}}_{\Gamma,\Gamma'} = \delta_{\Gamma,\Gamma'} E_\Gamma \,, \tag{5.67a}$$
$$\lambda_{\Gamma,\Gamma'} = \delta_{\Gamma,\Gamma'} \lambda_\Gamma \,, \tag{5.67b}$$

the expectation value of $\hat{H}_{\mathrm{loc}}$ is given by

$$\langle \hat{H}_{\mathrm{loc}} \rangle_{\Psi_{\mathrm{G}}} = \sum_\Gamma E_\Gamma \langle \hat{m}_\Gamma \rangle_{\Psi_{\mathrm{G}}} \,, \tag{5.67c}$$
$$\langle \hat{m}_\Gamma \rangle_{\Psi_{\mathrm{G}}} = \lambda_\Gamma^2 \langle \hat{m}_\Gamma \rangle_{\Psi_0} \,. \tag{5.67d}$$

For example, the expectation values of the projectors onto the four atomic states in a single-band Hubbard model are

$$m_d = \langle \hat{m}_d \rangle_{\Psi_{\mathrm{G}}} = \lambda_d^2 n^0_\uparrow n^0_\downarrow \,, \tag{5.68a}$$
$$m_s = \langle \hat{m}_s \rangle_{\Psi_{\mathrm{G}}} = \lambda_s^2 n^0_s (1 - n^0_{\bar{s}}) \,, \tag{5.68b}$$
$$m_\emptyset = \langle \hat{m}_\emptyset \rangle_{\Psi_{\mathrm{G}}} = \lambda_\emptyset^2 (1 - n^0_\uparrow)(1 - n^0_\downarrow) \,, \tag{5.68c}$$

if we assume a diagonal density matrix $\tilde{C}^0$ and work with the correlation operator (4.16). Note that with these finding we can write the constraints (5.53) in the form

$$1 = m_d + \sum_s m_s + m_\emptyset \,, \tag{5.69a}$$
$$n^0_s = m_d + m_s = n_s \,, \tag{5.69b}$$

i.e., the constraints simply ensure that the orbital densities are the same in the Gutzwiller wave function $|\Psi_{\mathrm{G}}\rangle$ and in the corresponding single-particle product state $|\Psi_0\rangle$. For multi-band models, such an identity of correlated and uncorrelated densities is not guaranteed, in general, as we will show in the following section 5.2.4.

5.2.4 Local Density Matrix

The single-particle wave function $|\Psi_0\rangle$ enters all local expectation values solely through the uncorrelated local density matrix $\tilde{C}^0$, cf. equation (5.35). The occupation of local orbitals, however, is determined by the *correlated* local density matrix

$$C_{\sigma,\sigma'} \equiv \langle \hat{c}^\dagger_\sigma \hat{c}_{\sigma'} \rangle_{\Psi_{\mathrm{G}}} = \langle \hat{P}^\dagger \hat{c}^\dagger_\sigma \hat{c}_{\sigma'} \hat{P} \rangle_{\Psi_0} \,, \tag{5.70}$$

which, in general, is not identical to $C^0_{\sigma,\sigma'}$. Instead, equation (5.61a) yields

$$C_{\sigma,\sigma'} = \sum_{I_1,\ldots,I_4} \lambda^*_{I_4,I_1} \lambda_{I_3,I_2} \langle I_4 | \hat{c}^\dagger_\sigma \hat{c}_{\sigma'} | I_3 \rangle m^0_{I_1,I_2} \tag{5.71}$$

with

$$\lambda_{I_1,I_2} \equiv \sum_{\Gamma_1,\Gamma_2} T_{I_1,\Gamma_1} T^*_{I_2,\Gamma_2} \lambda_{\Gamma_1,\Gamma_2} \,. \tag{5.72}$$

A comparison with equation (5.48b) reveals that we have $C_{\sigma,\sigma'} = C^0_{\sigma,\sigma'}$ only if

$$\sum_{I_3} \langle I_1 | \hat{c}^\dagger_\sigma \hat{c}_{\sigma'} | I_3 \rangle \overline{\lambda}_{I_3,I_2} = \sum_{I_3,I_4} \langle I_4 | \hat{c}^\dagger_\sigma \hat{c}_{\sigma'} | I_3 \rangle \lambda^*_{I_4,I_1} \lambda_{I_3,I_2} \,. \tag{5.73}$$

Even in the case that $C_{\sigma,\sigma'} \neq C^0_{\sigma,\sigma'}$, the total number of particles per site is still conserved, i.e., we find

$$\sum_\sigma C_{\sigma,\sigma} = \sum_\sigma C^0_{\sigma,\sigma} \; . \tag{5.74}$$

This identity follows from the fact that the local number operator

$$\hat{N} \equiv \sum_\sigma \hat{c}^\dagger_\sigma \hat{c}_\sigma \; , \tag{5.75}$$

commutes with the local correlation operator $\hat{P}$. Therefore, we find

$$\langle \hat{P}^\dagger \hat{N} \hat{P} \; \rangle_{\Psi_0} = \langle \hat{P}^\dagger \hat{P} \; \hat{N} \rangle_{\Psi_0} \; , \tag{5.76}$$

where the two sides of this equation yield the correlated and the uncorrelated particle number, see equations (5.47b) and (5.70).

5.2.5 Hopping Expectation Values

Finally, we consider the correlated expectation value

$$\begin{aligned} \bar{P}^{\sigma_1,\sigma_2}_{i,j} &\equiv \left\langle \hat{c}^\dagger_{i,\sigma_1} \hat{c}_{j,\sigma_2} \right\rangle_{\Psi_\mathrm{G}} && \text{(5.77a)} \\ &= \left\langle (\hat{P}^\dagger_i \hat{c}^\dagger_{i,\sigma_1} \hat{P}_i \,)(\hat{P}^\dagger_j \hat{c}_{j,\sigma_2} \hat{P}_j \,) \right\rangle_{\Psi_0} \; , && \text{(5.77b)} \end{aligned}$$

for a hopping operator. Note that the equation (5.77b) follows from (5.61b). In order to evaluate (5.77b), we apply again Wick's theorem. Here, we must keep in mind that eventually we aim at an evaluation of the single-particle Hamiltonian in (2.15) where each hopping operator is multiplied with a hopping amplitude $t^{\sigma,\sigma'}_{i,j}$. Due to the scaling (5.6) of those amplitudes, the only finite contributions from the expectation value (5.77b) contain a single line connecting the two sites i and j. This leads to the expression

$$\left\langle \hat{c}^\dagger_{i,\sigma_1} \hat{c}_{j,\sigma_2} \right\rangle_{\Psi_\mathrm{G}} = \sum_{\sigma'_1,\sigma'_2} q^{\sigma'_1}_{\sigma_1} \left(q^{\sigma'_2}_{\sigma_2} \right)^* \left\langle \hat{c}^\dagger_{i,\sigma'_1} \hat{c}_{j,\sigma'_2} \right\rangle_{\Psi_0} \; , \tag{5.78}$$

in which, to simplify the notation, we dropped the lattice site index of the 'renormalisation matrix' $q^{\sigma'}_\sigma$. In order to determine this matrix, we have to evaluate the expectation value

$$\begin{aligned} \langle \hat{P}^\dagger \hat{c}^\dagger_\sigma \hat{P} \ldots \rangle_{\Psi_0} &= \sum_{\Gamma_1,\ldots,\Gamma_4} \lambda^*_{\Gamma_2,\Gamma_1} \lambda_{\Gamma_3,\Gamma_4} \langle \Gamma_2 | \hat{c}^\dagger_\sigma | \Gamma_3 \rangle && \text{(5.79)} \\ &\quad \times \sum_{I_1,I_4} T_{I_1,\Gamma_1} T^*_{I_4,\Gamma_4} \left\langle (|I_1\rangle \langle I_4|) \ldots \right\rangle_{\Psi_0} \end{aligned}$$

for the a creation operator at site i by means of Wick's theorem. The remaining expectation value in the second line of equation (5.79) leads to a sum over all possibilities to take a creation operator $\hat{c}^\dagger_{i,\sigma'}$ out of $|I_1\rangle \langle I_4|$, see equation (4.8), which then generates a line together with an annihilation operator on site j. This procedure eventually yields the result

$$q^{\sigma'}_\sigma = \sum_{\Gamma_1,\ldots,\Gamma_4} \lambda^*_{\Gamma_2,\Gamma_1} \lambda_{\Gamma_3,\Gamma_4} \langle \Gamma_2 | \hat{c}^\dagger_\sigma | \Gamma_3 \rangle \sum_{I_1,I_4} T_{I_1,\Gamma_1} T^*_{I_4,\Gamma_4} H^{\sigma'}_{I_1,I_4} \; , \tag{5.80a}$$

which, by using equation (5.72), can also be written as

$$q^{\sigma'}_\sigma = \sum_{I_1,\ldots,I_4} \lambda^*_{I_2,I_1} \lambda_{I_3,I_4} \langle I_2 | \hat{c}^\dagger_\sigma | I_3 \rangle H^{\sigma'}_{I_1,I_4} \; . \tag{5.80b}$$

In equations (5.80), we introduced the expectation value $H^{\sigma'}_{I_1,I_4}$, which contains three different contributions, depending on whether the index σ' is an element of $I_1 \cap I_4$, $I_1 \backslash (I_1 \cap I_4)$, or $J = (1,\ldots,N)\backslash(I_1 \cup I_4)$. With the abbreviation $f_{\sigma,I} \equiv \langle I|\hat{c}^\dagger_\sigma \hat{c}_\sigma|I\rangle$, we can write $H^{\sigma'}_{I_1,I_4}$ as

$$\begin{aligned} H^{\sigma'}_{I_1,I_4} \;\equiv\; & (1-f_{\sigma',I_1})\langle I_4|\hat{c}_{\sigma'}|I_4\cup\sigma'\rangle m^0_{I_1,I_4\cup\sigma'} \\ & +\langle I_1\backslash\sigma'|\hat{c}_{\sigma'}|I_1\rangle \left(f_{\sigma',I_4} m^0_{I_1\backslash\sigma',I_4} + (1-f_{\sigma',I_4}) m^{0;\sigma'}_{I_1\backslash\sigma',I_4}\right) . \end{aligned} \tag{5.81}$$

Here, the expectation value $m^{0;\sigma'}_{I_1\backslash\sigma',I_4}$ has the same form as the corresponding one in equation (A.10), except that the index J is replaced by $J\backslash\sigma'$.

For the basis $|\gamma\rangle$ with the diagonal local density matrix (5.37), we find

$$H^{\gamma'}_{H_1,H_4} = \frac{1}{n^0_{\gamma'}} \Big\langle \big(|H_1\rangle \langle H_4| \, \hat{h}_{\gamma'} \big) \Big\rangle_{\Psi_0} \tag{5.82}$$

for the expectation value (5.81) and, accordingly, the renormalisation matrix has the form

$$q^{\gamma'}_{\gamma} = \frac{1}{n^0_{\gamma'}} \sum_{\Gamma_1\ldots\Gamma_4} \lambda^*_{\Gamma_2,\Gamma_1}\lambda_{\Gamma_3,\Gamma_4} \langle\Gamma_2|\hat{h}^\dagger_\gamma|\Gamma_3\rangle \Big\langle \big(|\Gamma_1\rangle\langle\Gamma_4|\hat{h}_{\gamma'}\big)\Big\rangle_{\Psi_0} . \tag{5.83}$$

Note that from this expression, one can readily derive the compact formula

$$q^{\gamma'}_{\gamma} = \frac{1}{n^0_{\gamma'}} \langle \hat{P}^\dagger \hat{h}^\dagger_\gamma \hat{P} \hat{h}_{\gamma'} \rangle_{\Psi_0} \tag{5.84}$$

for the renormalisation matrix, which, however, is valid only for the orbital basis $|\gamma\rangle$.

As an example, we consider the one-band Hubbard model with the correlation operator (4.16) and a diagonal density matrix. From equation (5.84) we find that $q^{s'}_s = \delta_{s,s'} q^s_s$ with

$$q^s_s = \frac{1}{n^0_s}\left(\lambda_\emptyset \lambda_s m^0_s + \lambda_d \lambda_{\bar{s}} m^0_d\right) \tag{5.85a}$$

$$= \frac{1}{\sqrt{n^0_s(1-n^0_s)}}\left(\sqrt{m_\emptyset m_s} + \sqrt{m_d m_{\bar{s}}}\right) \tag{5.85b}$$

where, in the second line, we used equations (5.68).

5.3 Energy Functional in Infinite Dimensions

We now summarise the results of this chapter and discuss the general structure of our minimisation problem. In infinite dimensions, the expectation value

$$E_{\mathrm{G}} \equiv \langle \hat{H}_{\mathrm{H}} \rangle_{\Psi_{\mathrm{G}}} \tag{5.86}$$

of the Hubbard Hamiltonian (2.15) with respect to the Gutzwiller wave function (4.25) is given by

$$E_{\mathrm{G}}\big(\{\tilde{\lambda}_i\},\{\tilde{C}^0_i\},|\Psi_0\rangle\big) = E_0\big(\{\tilde{\lambda}\},\{\tilde{C}^0_i\},|\Psi_0\rangle\big) + \sum_i E_{i;\mathrm{loc}}\big(\tilde{\lambda}_i,\tilde{C}^0_i\big) , \tag{5.87}$$

where

$$E_{\mathrm{loc}}\big(\tilde{\lambda}_i,\tilde{C}^0_i\big) \equiv \sum_i E_{i;\mathrm{loc}}\big(\tilde{\lambda}_i,\tilde{C}^0_i\big) \tag{5.88}$$

is the sum of all local energies (5.65) and

$$E_0(\{\tilde{\lambda}_i\},\{\tilde{C}_i^0\},|\Psi_0\rangle) = \sum_{i\neq j}\sum_{\sigma_1,\sigma_1',\sigma_2,\sigma_2'} t_{i,j}^{\sigma_1,\sigma_2} q_{\sigma_1}^{\sigma_1'} \left(q_{\sigma_2}^{\sigma_2'}\right)^* \langle \hat{c}_{i,\sigma_1'}^\dagger \hat{c}_{j,\sigma_2'}\rangle_{\Psi_0} \tag{5.89}$$

is the single-particle energy functional that derives from the expectation value (5.78) of hopping operators. Note that the functional (5.89) can also be written in the form

$$E_0(\{\tilde{\lambda}_i\},|\Psi_0\rangle) = \sum_{i\neq j}\sum_{\sigma,\sigma'} \tilde{t}_{i,j}^{\sigma,\sigma'} \langle \hat{c}_{i,\sigma}^\dagger \hat{c}_{j,\sigma'}\rangle_{\Psi_0} \ , \tag{5.90}$$

where we introduced the effective hopping parameters

$$\tilde{t}_{i,j}^{\sigma_1',\sigma_2'} \equiv \sum_{\sigma_1,\sigma_2} t_{i,j}^{\sigma_1,\sigma_2} q_{\sigma_1}^{\sigma_1'} \left(q_{\sigma_2}^{\sigma_2'}\right)^* \ . \tag{5.91}$$

Both properties, the renormalisation matrix $q_\sigma^{\sigma'}$, equation (5.80b), and the local energy functional $E_{\rm loc}(\tilde{\lambda}_i,\tilde{C}_i^0)$ are functions of the variational parameter matrices $\tilde{\lambda}_i$ and the uncorrelated density matrices $\tilde{C}_i^0$ on all lattice sites i.

We have to minimise the variational ground-state energy (5.87) with respect to all parameters $\{\tilde{\lambda}_i\}$ and the one-particle states $|\Psi_0\rangle$, whereby the constraints (5.48) have to be obeyed. The latter may be achieved by fixing the parameters $\lambda_{i;\Gamma,\Gamma'}$ for $|\Gamma|,|\Gamma'|\leq 1$, which are then functions of $\tilde{C}_i^0$ and of the remaining *independent* parameters $\lambda_{i;\Gamma,\Gamma'}^{\rm i}$ with $|\Gamma|,|\Gamma'|>1$. Such an explicit solution of the constraints yields an energy functional of the form (5.87)-(5.90) with the argument $\{\tilde{\lambda}_i\}$ replaced by $\{\tilde{\lambda}_i^{\rm i}\}$. Note that this way to obey the constraints is only useful for our formal considerations in this section. In numerical applications, we employ different strategies, see appendix H.

The one-particle states $|\Psi_0\rangle$ enter the energy functional indirectly through the local density matrix $\tilde{C}_i^0$, equation (5.35), and explicitly in the expectation value of hopping operators, equation (5.90). To carry out an unconstrained minimisation with respect to $|\Psi_0\rangle$, we introduce the matrix $\tilde{\eta}_i$ of Lagrange multipliers $\eta_{i;\sigma,\sigma'}$, which ensure that equation (5.35) is fulfilled. The particle numbers in $|\Psi_{\rm G}\rangle$ and $|\Psi_0\rangle$ are the same, see equation (5.74). In order to fix the average number of particles

$$N = \sum_{i,\sigma} \langle \hat{c}_{i,\sigma}^\dagger \hat{c}_{i,\sigma}\rangle_{\Psi_{\rm G}} \ , \tag{5.92}$$

and to ensure the normalisation of $|\Psi_0\rangle$, we use Lagrange multipliers $E_{\rm F}$ and $E^{\rm SP}$, respectively. Then, the variational ground-state energy $E_0^{\rm var}$ is given by

$$E_0^{\rm var} = \underset{\{\tilde{\lambda}_i^{\rm i}\},\{\tilde{C}_i^0\},\{\tilde{\eta}_i\},|\Psi_0\rangle,E_{\rm F},E^{\rm SP}}{\rm Minimum} E_{\rm c}\big(\{\tilde{\lambda}_i^{\rm i}\},\{\tilde{C}_i^0\},\{\tilde{\eta}_i\},|\Psi_0\rangle,E_{\rm F},E^{\rm SP}\big) \tag{5.93}$$

with

$$\begin{aligned} E_{\rm c}(\ldots) \;=\; & E_{\rm G}\big(\{\tilde{\lambda}_i^{\rm i}\},\{\tilde{C}_i^0\},|\Psi_0\rangle\big) + \sum_{i,\sigma,\sigma'} \eta_{i;\sigma,\sigma'}\big(C_{i;\sigma,\sigma'}^0 - \langle\Psi_0|\hat{c}_{i,\sigma}^\dagger\hat{c}_{i,\sigma'}|\Psi_0\rangle\big) \\ & + E_{\rm F}\left(N - \sum_{i,\sigma}\langle\Psi_0|\hat{c}_{i,\sigma}^\dagger\hat{c}_{i,\sigma}|\Psi_0\rangle\right) - E^{\rm SP}\big(\langle\Psi_0|\Psi_0\rangle - 1\big) \ . \end{aligned} \tag{5.94}$$

Note that, strictly speaking, one has to find a stationary point and not a minimum of $E_{\rm c}(\ldots)$ in equation (5.93).

The minimisation with respect to $|\Psi_0\rangle$ can now be carried out explicitly and leads to the effective one-particle Schrödinger equation

$$\hat{H}_0^{\mathrm{eff}}\big|\Psi_0\big\rangle = E^{\mathrm{SP}}\big(\{\tilde{\lambda}_i^{\mathrm{i}}\},\{\tilde{C}_i^0\},\{\tilde{\eta}_i\}\big)\big|\Psi_0\big\rangle\;, \tag{5.95}$$

with the effective single-particle Hamiltonian

$$\hat{H}_0^{\mathrm{eff}} \equiv \sum_{i\neq j}\sum_{\sigma,\sigma'} \tilde{t}_{i,j}^{\sigma,\sigma'}\,\hat{c}_{i,\sigma}^{\dagger}\hat{c}_{j,\sigma'} - \sum_i(\eta_{i;\sigma,\sigma'}+\delta_{\sigma,\sigma'}E_{\mathrm{F}})\hat{c}_{i,\sigma}^{\dagger}\hat{c}_{i,\sigma'}\;. \tag{5.96}$$

For translationally invariant systems, the effective Hamiltonian (5.96) in momentum space has the form

$$\hat{H}_0^{\mathrm{eff}} = \sum_{\boldsymbol{k},\sigma,\sigma'}\Bigg(\sum_{\tilde{\sigma},\tilde{\sigma}'} Q_{\tilde{\sigma},\tilde{\sigma}'}^{\sigma,\sigma'}\varepsilon_{\boldsymbol{k};\tilde{\sigma},\tilde{\sigma}'} - \eta_{\sigma,\sigma'} - \delta_{\sigma,\sigma'}E_{\mathrm{F}}\Bigg)\hat{c}_{\boldsymbol{k},\sigma}^{\dagger}\hat{c}_{\boldsymbol{k},\sigma'}\;, \tag{5.97}$$

where

$$Q_{\tilde{\sigma},\tilde{\sigma}'}^{\sigma,\sigma'} \;\equiv\; q_{\tilde{\sigma}}^{\sigma}(q_{\tilde{\sigma}}^{\sigma'})^*\;, \tag{5.98a}$$

$$\varepsilon_{\boldsymbol{k};\sigma,\sigma'} \;\equiv\; \frac{1}{L}\sum_{i\neq j} t_{i,j}^{\sigma,\sigma'}\,e^{\mathrm{i}\boldsymbol{k}(\boldsymbol{R}_i-\boldsymbol{R}_j)}\;, \tag{5.98b}$$

and the operators $\hat{c}_{\boldsymbol{k},\sigma}^{(\dagger)}$ have been defined in equation (2.17b). The Hamiltonian (5.97) can be readily diagonalised

$$\hat{H}_0^{\mathrm{eff}} = \sum_{\boldsymbol{k},\gamma}(E_{\boldsymbol{k},\gamma}-E_{\mathrm{F}})\hat{h}_{\boldsymbol{k},\gamma}^{\dagger}\hat{h}_{\boldsymbol{k},\gamma}\;, \tag{5.99}$$

by a proper unitary transformation

$$\hat{h}_{\boldsymbol{k},\gamma}^{\dagger} = \sum_{\sigma} u_{\gamma,\sigma}(\boldsymbol{k})\hat{c}_{\boldsymbol{k},\sigma}^{\dagger} \tag{5.100}$$

such that the eigenvalues $E_{\boldsymbol{k},\gamma}$ of $\hat{H}_0^{\mathrm{eff}}$ and the band-energy matrix (5.98b) are related through

$$E_{\boldsymbol{k},\gamma} = \sum_{\sigma,\sigma'}\Bigg(\sum_{\tilde{\sigma},\tilde{\sigma}'} Q_{\tilde{\sigma},\tilde{\sigma}'}^{\sigma,\sigma'}\varepsilon_{\boldsymbol{k};\tilde{\sigma},\tilde{\sigma}'} - \eta_{\sigma,\sigma'}\Bigg)u_{\gamma,\sigma}(\boldsymbol{k})u_{\gamma,\sigma'}^*(\boldsymbol{k})\;. \tag{5.101}$$

We assume that the wave function $|\Psi_0\rangle$ is the ground state

$$|\Psi_0\rangle = \prod_{\substack{\boldsymbol{k},\gamma\\(E_{\boldsymbol{k},\gamma}\leq E_{\mathrm{F}})}} \hat{h}_{\boldsymbol{k},\gamma}^{\dagger}\,|0\rangle \tag{5.102}$$

of the effective single-particle Hamiltonian (5.99). This assumption is motivated by the corresponding result in the Hartree-Fock theory, see reference [31]. So far, however, it has not been formally proven in the context of the Gutzwiller theory. In this way, $|\Psi_0\rangle$ becomes a function of $\{\tilde{\lambda}_i^{\mathrm{i}}\},\{\tilde{C}_i^0\},\{\tilde{\eta}_i\}$, and, in principle, the remaining task is to find the minimum

$$E_0^{\mathrm{var}} = \underset{\{\tilde{\lambda}_i^{\mathrm{i}}\},\{\tilde{C}_i^0\},\{\tilde{\eta}_i\},E_{\mathrm{F}}}{\mathrm{Minimum}} E_{\mathrm{c}}\big(\{\tilde{\lambda}_i^{\mathrm{i}}\},\{\tilde{C}_i^0\},\{\tilde{\eta}_i\},E_{\mathrm{F}}\big) \tag{5.103}$$

of the function

$$E_{\mathrm{c}}(\ldots) = E^{\mathrm{SP}}\big(\{\tilde{\lambda}_i^{\mathrm{i}}\},\{\tilde{C}_i^0\},\{\tilde{\eta}_i\}\big) + E_{\mathrm{loc}}\big(\{\tilde{\lambda}_i^{\mathrm{i}}\},\{\tilde{C}_i^0\}\big) + \sum_{i,\sigma,\sigma'}\eta_{i;\sigma,\sigma'}C_{i;\sigma,\sigma'}^0 + E_{\mathrm{F}}N\;. \tag{5.104}$$

Note that the minimisation of (5.104) with respect to $\eta_{i;\sigma,\sigma'}$ and E_{F} just recaptures the physical definition of the density matrix, equation (5.35), and fixes the particle number, equation (5.92).

The minimisation of E_{c} in this straightforward way requires rather time-consuming calculations of expectation values in $|\Psi_0\rangle$ for every single variation of our parameters. Such a strategy is therefore prohibitive, in particular due to the large number of variational parameters $\{\tilde{\lambda}^{\mathrm{i}}\}$. Therefore, one needs more sophisticated numerical strategies when our general theory is applied to realistic model system. Such strategies are discussed in detail in appendix H.

So far, the effective single-particle Hamiltonian (5.96) is just an auxiliary object, which is needed for the determination of the variational ground state. However, as we will explain in section 7.3, the eigenvalues $E_{\boldsymbol{k},\gamma}$ of that Hamiltonian can be interpreted as quasi-particle energies within a Landau Fermi-liquid theory and, therefore, they are of great importance for the interpretation of experiments.

5.4 Example: Single-Band Hubbard Model

In the previous sections of this chapter, we have already evaluated all general results for the special case of a single-band Hubbard model. Therefore, we can readily summarise them as follows: The variational ground-state energy of the single-band Hubbard model (2.20) is given by

$$E_{1\mathrm{B}} = \langle \hat{H}_{1\mathrm{B}} \rangle_{\Psi_{\mathrm{G}}} = \sum_{i,j} \sum_{s} (q_s^s)^2 \, t_{i,j} \langle \hat{c}_{i,s}^{\dagger} \hat{c}_{j,s} \rangle_{\Psi_0} + ULm_d \; , \tag{5.105}$$

where q_s^s is defined in equation (5.85b). Equations (5.69) allow us to write the occupation expectation values

$$m_{\emptyset} = 1 - \sum_{s} n_s^0 + m_d \; , \tag{5.106a}$$

$$m_s = n_s^0 - m_d \tag{5.106b}$$

as a function of the only remaining variational parameter, m_d. Note that in equations (5.105) and (5.106) we assumed a diagonal local density matrix with respect to our single-particle wave function $|\Psi_0\rangle$.

Starting from the energy functional (5.105) we now discuss the Brinkman-Rice metal-insulator transition at half filling and we evaluate the Gutzwiller energy functional for the two-site Hubbard model (2.22). In both cases, the minimisation of the energy functional (5.105) can be carried out analytically.

5.4.1 The Brinkman-Rice Transition

As first shown by Brinkman and Rice [102], the Gutzwiller theory for the single-band model at half band filling contains a metal-insulator transition. For $n_s^0 = 1/2$ and a translationally invariant ground state without spin order, the variational ground-state energy (5.105) is given by

$$E_{1\mathrm{B}} = 16(1 - 2m_d) m_d \varepsilon_0 + U m_d \; , \tag{5.107}$$

where

$$\varepsilon_0 \equiv \sum_{i,j} t_{i,j} \langle \hat{c}_{i,s}^{\dagger} \hat{c}_{j,s} \rangle_{\Psi_0} = \frac{1}{L} \sum_{\boldsymbol{k}(\varepsilon_{\boldsymbol{k}} < E_{\mathrm{F}})} \varepsilon_{\boldsymbol{k}} \tag{5.108}$$

and $\varepsilon_{\boldsymbol{k}}$ is the Fourier transform of $t_{i,j}$. The minimisation of the energy (5.107) with respect to m_d leads to

$$m_d = \frac{1}{4} \left(1 - \frac{U}{U_{\mathrm{BR}}} \right) \; , \tag{5.109}$$

and

$$(q_s^s)^2 \equiv q^2 = 1 - \left(\frac{U}{U_{\mathrm{BR}}}\right)^2 , \tag{5.110}$$

where we introduced the critical interaction strength $U_{\mathrm{BR}} \equiv 16|\varepsilon_0|$. When U approaches U_{BR} from below, the average number of doubly-occupied lattice sites and the renormalisation factor q both go to zero. As will be shown in chapter 7, the square q^2 of the renormalisation factor is related to the effective mass m^* of quasi-particle excitations, $m^* \sim 1/q^2$. Therefore, one interprets the result (5.110) as a metal-to-insulator transition.

At values $U > U_{\mathrm{BR}}$, the Gutzwiller theory depicts a collection of isolated and singly-occupied sites, which is certainly not a satisfactory description of a Mott insulator. In addition, it has been shown for the single-band model that the Brinkman–Rice transition at finite interaction strength is the consequence of the large-D limit, i.e., it is not contained in the wave function for any finite dimension [103]. Hence, statements on metal-insulator transitions based on our variational description must be taken with care.

5.4.2 Two-Site Hubbard Model

An approximation that becomes exact in the limit of infinite spatial dimensions is certainly not the method of choice for the investigation of a one-dimensional system, such as the two-site model (2.22). Therefore, the results in this section should be seen as a benchmark test on how the Gutzwiller theory copes with a model system for which it is actually most inappropriate.

We focus again on the half-filled case. Without antiferromagnetic order, i.e., when we work with the one-particle wave function (4.19), the approximate energy functional for the two-site Hubbard model reads

$$E_{\mathrm{G}}(d) = -2tq(d) + 2Ud , \tag{5.111}$$

where

$$q(d) = 8d(1 - 2d) . \tag{5.112}$$

As in the previous section, the minimisation of (5.111) leads to a Brinkman-Rice transition at a critical interaction strength $U_{\mathrm{BR}} = 8t$ where the double occupancy,

$$d = d_{\mathrm{BR}} = \frac{1}{4}\left(1 - \frac{U}{8t}\right) , \tag{5.113}$$

and the ground-state energy

$$E_{\mathrm{G}}(d_{\mathrm{BR}}) = -2t + \frac{U}{2} - \frac{U^2}{32t} , \tag{5.114}$$

vanish. This result is already an improvement over the Hartree-Fock theory, equation (3.25), however, it still does not yield the correct second-order contribution, which is $\sim 1/(16t)$, as can be seen from the exact ground-state energy

$$E_0^{\mathrm{exact}} = \frac{1}{2}\left(U - \sqrt{U^2 + 16t^2}\right) , \tag{5.115}$$

equation (B.13b).

The energy (5.111) goes to zero for $U = U_{\mathrm{BR}}$ and, therefore, it becomes larger than the corresponding Hartree-Fock ground-state energy (3.30) beyond a certain value of U. Since the space of Gutzwiller wave functions contains the whole Hartree-Fock space, the optimum Gutzwiller energy must be lower than the Hartree-Fock energy. Consequently, there must be

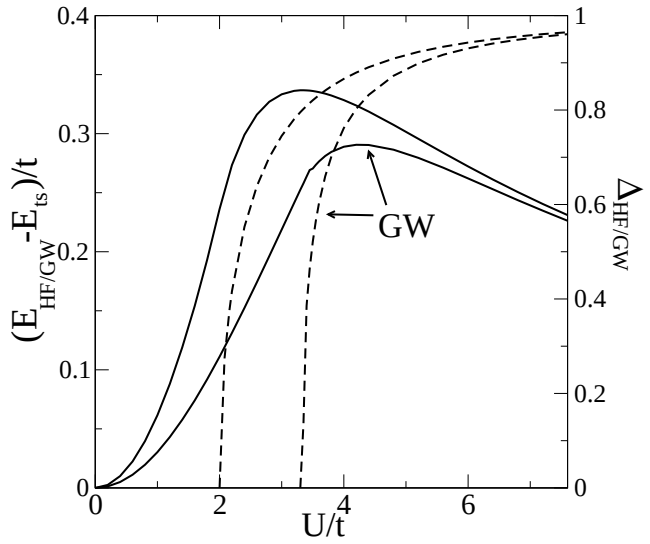

Figure 5.4: Deviation of Gutzwiller and Hartree-Fock energy from the exact ground-state energy, equation (B.13b) (solid lines); magnetisation Δ in Gutzwiller and Hartree-Fock approximation (dashed lines).

an antiferromagnetic solution for this model in the Gutzwiller theory as well. To determine it, we have to minimise the energy functional

$$E_{\mathrm{G}}(\eta, d) = 4tq(\eta, d)\sin(\theta)\cos(\theta) + 2Ud\,, \tag{5.116}$$

with

$$q(\eta, d) = \frac{2d\left(\sqrt{1-2d+2\Delta(\eta)}+\sqrt{1-2d-2\Delta(\eta)}\right)^2}{1-\Delta(\eta)^2}\,, \tag{5.117}$$

and $\Delta(\eta)$ as defined in (3.29). The angle $\theta = \theta(\eta)$ in (3.29) and (5.116) is given by

$$\tan(\theta) = -\frac{\eta+\sqrt{\eta^2+t^2}}{t}\,. \tag{5.118}$$

For $d = d_{\mathrm{BR}}$, a second-order expansion of $E_{\mathrm{G}}(\eta, d)$ with respect to η indicates that the non-magnetic state becomes unstable if $U > U_{\mathrm{C}}$ where $U_{\mathrm{C}} = 8(\sqrt{2}-1)t \approx 3.3t$. For $U > U_{\mathrm{C}}$, the minimisation of (5.116) with respect to η and d has to be carried out numerically.

The difference between the Gutzwiller and the exact ground-state energy as a function of U/t is shown in figure 5.4. For comparison, the figure also shows the energy difference for the Hartree-Fock wave function. The dotted lines are the magnetisation curves in both theories. Obviously, both theories do not capture the physics of the true ground state correctly since they break the SU(2) spin-symmetry. The Gutzwiller theory result is quantitatively superior to the Hartree-Fock theory. The spurious phase transition is shifted to larger values of U/t and, energetically, the deviation from the exact results is smaller, in particular, for medium interaction strengths.

5.5 Non-Local Interaction Terms

As shown in section 2.4, non-local interaction terms naturally arise either, as a direct consequence of the Coulomb interaction, e.g., in equation (2.27), or in effective models, such as $\hat{H}_J$ and $\hat{H}_3$ in (2.40). In this section, we focus on the t-J model (2.41). The evaluation of other terms, e.g., those in the Hamiltonian (2.27) or the three site terms in (2.40b) can be readily derived from our considerations here.

The t-J model and the additional three-site operator (2.40b) have been studied extensively by means of Gutzwiller wave functions both numerically, in 'variational quantum Monte-Carlo' calculations, and analytically, by means of the Gutzwiller approximation, see references [27, 136, 148–150]. As will be shown in section 6.1.3, the Gutzwiller approximation scheme does not yield unambiguous results for the expectation values of non-local operators. Therefore, the exact evaluation in infinite dimensions is essential to assess the validity of the analytical expressions derived in the Gutzwiller approximation scheme.

The evaluation of non-local operators, e.g., of the operator

$$\hat{H}_J = \sum_{i,j} J_{i,j} \hat{\boldsymbol{S}}_i \hat{\boldsymbol{S}}_j \tag{5.119a}$$

$$= \sum_{i,j} J_{i,j} \left[\frac{1}{4} (\hat{n}_{i,\uparrow} - \hat{n}_{i,\downarrow})(\hat{n}_{j,\uparrow} - \hat{n}_{j,\downarrow}) + (\hat{c}^\dagger_{i,\uparrow} \hat{c}_{i,\downarrow} \hat{c}^\dagger_{j,\downarrow} \hat{c}_{j,\uparrow} + \text{h.c.}) \right] \tag{5.119b}$$

in the limit of infinite dimensions leads to a general problem concerning the proper scaling of coupling parameters with respect to the lattice dimension D. For the t-J model, the exchange parameters in (5.119a) are given as $J_{i,j} = t^2_{i,j}/U$, from which we can derive

$$J_{i,j} = \bar{J}_{i,j} \frac{1}{D^{||i-j||}} \,, \tag{5.120}$$

where $\bar{J}_{i,j}$ is independent of D. With such a scaling, however, the evaluation of $\hat{H}_J$ leads to a rather trivial result; only the Ising-terms in the Hamiltonian (5.119a) lead to a finite contribution,

$$\sum_{i,j} J_{i,j} \langle \hat{n}_{i,s} \hat{n}_{j,s'} \rangle_{\Psi_\mathrm{G}} = \sum_{i,j} J_{i,j} \langle \hat{n}_{i,s} \rangle_{\Psi_\mathrm{G}} \langle \hat{n}_{j,s'} \rangle_{\Psi_\mathrm{G}} \,, \tag{5.121}$$

which is of order unity in the large-D limit. From (5.121) one readily finds that, for a paramagnetic ground state, the expectation value of $\hat{H}_J$ vanishes.

In order to derive the energy expressions that are used in references [27, 136, 148–150], we have to assume that $J_{i,j}$ is independent of D. Note that such a scaling leads to sensible results in infinite dimensions only for paramagnetic ground states since, for spin-ordered states, the terms (5.121) diverge in the large-D limit. With D-independent parameters $J_{i,j}$, the leading terms of order unity in the expectation value of $\hat{H}_J$ have the form

$$\sum_{i,j} J_{i,j} \langle \hat{n}_{i,s} \hat{n}_{j,s} \rangle_{\Psi_\mathrm{G}} = \sum_{i,j} J_{i,j} \langle \hat{P}_i \hat{n}_{i,s} \hat{P}_i \hat{P}_j \hat{n}_{j,s} \hat{P}_j \rangle_{\Psi_0} \tag{5.122}$$

Here, we used the fact that $J_{i,j}$ is finite only up to a certain shell of nearest neighbours, which restricts the sum in (5.122). For an unrestricted sum, we had to take into account diagrams with internal vertices from operators $\hat{P}^2_l$ on lattice sites $l \neq i, j$; see reference [151] on spin-wave excitations where, unlike here, such diagrams need to be evaluated.

For the t-J model, the local Gutzwiller correlation operator is given as

$$\hat{P} = \lambda_\emptyset \hat{m}_\emptyset + \sum_s \lambda_s \hat{m}_s \tag{5.123}$$

since there are no doubly-occupied sites ($\lambda_d = 0$). The constraints (5.53) then yield

$$\lambda^2_\emptyset = \frac{1-2n}{(1-n)^2} \,, \tag{5.124a}$$

$$\lambda^2_s = \frac{1}{1-n} \,, \tag{5.124b}$$

and the expectation value (5.121) reads

$$\sum_{i,j} J_{i,j} \langle \hat{n}_{i,s} \hat{n}_{j,s} \rangle_{\Psi_{\mathrm{G}}} = g_J \sum_{i,j} J_{i,j} \langle \hat{n}_{i,s} \hat{n}_{j,s} \rangle_{\Psi_0} \; . \tag{5.125}$$

Here, we introduced the renormalisation factor

$$g_J = \lambda_s^4 = \frac{1}{(1-n)^2} \; . \tag{5.126}$$

All other terms in the expectation value of $\hat{H}_J$ lead to the same renormalisation factor g_J. Therefore, one finds

$$\sum_{i,j} J_{i,j} \langle \hat{\boldsymbol{S}}_i \hat{\boldsymbol{S}}_j \rangle_{\Psi_{\mathrm{G}}} = g_J \sum_{i,j} J_{i,j} \langle \hat{\boldsymbol{S}}_i \hat{\boldsymbol{S}}_j \rangle_{\Psi_0} \tag{5.127}$$

for the expectation value of $\hat{H}_J$ in the Gutzwiller theory. This result is in agreement with the one derived within the Gutzwiller approximation, see section (6.1.3).

Starting from the expectation value (5.127) one finds ground-state wave functions $|\Psi_0\rangle$ with finite superconducting order parameters

$$\Delta_{i,j}^0 = \langle \hat{c}_{i,\uparrow}^\dagger \hat{c}_{i,\uparrow}^\dagger \rangle_{\Psi_0} \neq 0 \; . \tag{5.128}$$

Therefore, the Gutzwiller theory for a two-dimensional t-J model was put forward in references [27, 136, 148–150] as a reasonable approach to describe high superconductivity in cuprates.

The main deficiency of the Gutzwiller wave function is the missing of non-local terms in the correlation operator. In particular, for the treatment of non-local interactions, a generalisation of the variational wave function is certainly desirable. There have been various attempts for such a generalisation in the past, e.g., the 'Baeriswyl-Gutzwiller wave function' [152] or the local Ansatz [153]. However, an exact evaluation of such wave functions in a well-defined limit, such as infinite D, did not succeed, so far.

Chapter 6

Alternative Evaluation Techniques

In this chapter, we consider the evaluation schemes that lead to the same energy functionals as the exact evaluation in the limit of infinite dimensions: the Gutzwiller approximation and the slave-boson mean-field theory.

6.1 Combinatorial Counting: Gutzwiller Approximation

The approximation was originally introduced by Gutzwiller [96–98]. It was formulated in a more physical way in references [104, 105]. The derivation in those works, however, did not provide a clear recipe how to generalise the approximation for more complicated systems, e.g, for the multi-band Hubbard models (2.15).

It is an ongoing debate how the Gutzwiller approximation can be further generalised; in recent references [136, 148–150, 154–156], e.g., the proper treatment of non-local interaction terms has been addressed. Those works indicate that it is possible to derive different results depending on how non-local terms are treated in a generalised Gutzwiller approximation scheme. These contradictory results, therefore, just show that the Gutzwiller approximation itself is rather uncontrolled and only a comparison to an exact evaluation, for example, in infinite dimensions may justify it a posteriori. One may rightly argue that the Gutzwiller approximation is redundant. However, as it is still very often used in the literature, it is certainly appropriate to present a derivation in this review as well.

In this section, we give a mathematical formulation of the Gutzwiller approximation for the one-band model that can be applied to multi-band Hubbard models with a local Coulomb interaction of the form

$$\hat{H}_{\mathrm{I}} = \sum_{\sigma,\sigma'} U_{\sigma,\sigma'} \hat{n}_{\sigma} \hat{n}_{\sigma'} \ . \tag{6.1}$$

We start with a formulation of the Gutzwiller approximation for the single-band Hubbard model in section 6.1.1. In section 6.1.2, the approach is generalised to multi-band models with a local Hamiltonian of the form (6.1). The treatment of non-local terms in the Hamiltonian is discussed in section 6.1.3.

6.1.1 Gutzwiller Approximation for the One-Band Hubbard Model

We study the single-band Hubbard model

$$\hat{H}_{1\mathrm{B}} = \sum_{i,j} \sum_{\sigma=1}^{2} t_{i,j} \hat{c}^{\dagger}_{i,\sigma} \hat{c}_{j,\sigma} + U \hat{M}_{12} = \hat{H}_0 + \hat{H}_{\mathrm{I}} \ , \tag{6.2a}$$

as derived in section 2.3.1. Here, the operator

$$\hat{M}_{12} = \sum_i \hat{m}_{i;12} \tag{6.2b}$$

with $\hat{m}_{i;12} = \hat{n}_{i,\uparrow}\hat{n}_{i,\downarrow}$ counts the total number of doubly-occupied lattice sites. Note that, for our later treatment of the multi-band model, we have replaced the spin index $s \in \uparrow, \downarrow$ with the general index $\sigma \in \uparrow, \downarrow$ following the notations introduced in section 4.1.

Within the Gutzwiller approximation scheme, it is most convenient to work with Gutzwiller's original form

$$|\Psi_{\mathrm{G}}\rangle = g^{\hat{M}_{12}} |\Psi_0\rangle \tag{6.3}$$

for his variational wave function, see equation (4.15). Our aim is to calculate the expectation value

$$\langle \hat{H}_{1\mathrm{B}} \rangle_{\Psi_{\mathrm{G}}} = \frac{\langle \Psi_{\mathrm{G}} | \hat{H}_{1\mathrm{B}} | \Psi_{\mathrm{G}} \rangle}{\langle \Psi_{\mathrm{G}} | \Psi_{\mathrm{G}} \rangle} = \sum_{i,j} \sum_{\sigma=1}^{2} t_{i,j} \langle \hat{c}^{\dagger}_{i,\sigma} \hat{c}_{j,\sigma} \rangle_{\Psi_{\mathrm{G}}} + U \sum_i \langle \hat{m}_{i;12} \rangle_{\Psi_{\mathrm{G}}} \tag{6.4}$$

for the wave function (6.3).

To formulate a well-defined mathematical description of the Gutzwiller approximation, we introduce a local basis for our many-particle Hilbert space,

$$|\Phi_{\mathcal{N}_1,\mathcal{N}_2}\rangle \equiv \prod_{i_1 \in \mathcal{N}_1} \prod_{i_2 \in \mathcal{N}_2} \hat{c}^{\dagger}_{i_1,1} \hat{c}^{\dagger}_{i_2,2} |0\rangle \ . \tag{6.5}$$

Here, $\mathcal{N}_1$ and $\mathcal{N}_2$ are sets of lattice sites with $N_i = |\mathcal{N}_1|$ elements. Since the basis (6.5) is complete, we can expand the one particle wave function in the form

$$|\Psi_0\rangle = \sum_{\mathcal{N}_1,\mathcal{N}_2} A(\mathcal{N}_1,\mathcal{N}_2) |\Phi_{\mathcal{N}_1,\mathcal{N}_2}\rangle \ , \tag{6.6}$$

with expansion coefficients $A(\mathcal{N}_1,\mathcal{N}_2)$. The sum over $\mathcal{N}_\sigma$ in (6.6) includes all subsets of the whole set of lattice sites $\mathcal{L}$ ($|\mathcal{L}| = L$) with N_σ elements. In this way, we fix the numbers N_σ of particles in $|\Psi_0\rangle$, which is reasonable since the Hamiltonian (6.2a) commutes with the corresponding operators $\hat{N}_\sigma = \sum_i \hat{n}_{i,\sigma}$.

Using the expansion (6.6) we can write the Gutzwiller wave function (6.3) as

$$|\Psi_{\mathrm{G}}\rangle = \sum_{\mathcal{N}_1,\mathcal{N}_2} g^{M_{12}(\mathcal{N}_1,\mathcal{N}_2)} A(\mathcal{N}_1,\mathcal{N}_2) |\Phi_{\mathcal{N}_1,\mathcal{N}_2}\rangle \ , \tag{6.7}$$

where the function $M_{12}(\mathcal{N}_1,\mathcal{N}_2)$ counts the number of doubly-occupied sites when the up (down) electrons are placed at the sites belonging to $\mathcal{N}_1(\mathcal{N}_2)$. We use the fact that the states (6.5) are orthogonal and normalised in order to write the expectation values and the norm in (6.4) as

$$\langle \Psi_{\mathrm{G}} | \Psi_{\mathrm{G}} \rangle = \sum_{\mathcal{N}_1,\mathcal{N}_2} g^{2M_{12}(\mathcal{N}_1,\mathcal{N}_2)} |A(\mathcal{N}_1,\mathcal{N}_2)|^2 \ , \tag{6.8a}$$

$$\langle \Psi_{\mathrm{G}} | \hat{c}^{\dagger}_{i,\sigma} \hat{c}_{j,\sigma} | \Psi_{\mathrm{G}} \rangle = \sum_{\mathcal{N}_1',\mathcal{N}_2} g^{M_{12}(\mathcal{N}_1'\cup i,\mathcal{N}_2)} g^{M_{12}(\mathcal{N}_1'\cup j,\mathcal{N}_2)} A^*(\mathcal{N}_1'\cup i,\mathcal{N}_2) A(\mathcal{N}_1'\cup j,\mathcal{N}_2), \tag{6.8b}$$

$$\langle \Psi_{\mathrm{G}} | \hat{m}_{i;12} | \Psi_{\mathrm{G}} \rangle = \sum_{\mathcal{N}_1',\mathcal{N}_2'} g^{2M_{12}(\mathcal{N}_1'\cup i,\mathcal{N}_2'\cup i)} \left| A(\mathcal{N}_1'\cup i,\mathcal{N}_2'\cup i) \right|^2 \ . \tag{6.8c}$$

Here, we have

$$i,j \notin \mathcal{N}_1' \quad \text{and} \quad |\mathcal{N}_1'| = N_1 - 1 \tag{6.9a}$$

in (6.8b) and

$$i \notin \mathcal{N}'_\sigma \quad \text{and} \quad |\mathcal{N}'_\sigma| = N_\sigma - 1 \tag{6.9b}$$

in (6.8c). To make further progress, we need expressions for the two types of products between coefficients A in (6.8). They can be obtained from the corresponding expectation values in the uncorrelated wave function $|\Psi_0\rangle$. First, we address the norm

$$\langle\Psi_0|\Psi_0\rangle = \sum_{\mathcal{N}_1,\mathcal{N}_2} |A(\mathcal{N}_1,\mathcal{N}_2)|^2 = 1 \; . \tag{6.10}$$

The Gutzwiller approximation is defined by the assumption that each term in (6.10) is independent of the particular sets $\mathcal{N}_1, \mathcal{N}_2$. This means that all local distributions of electrons have the same probability in the uncorrelated state $|\Psi_0\rangle$. As a result, equation (6.10) yields

$$|A(\mathcal{N}_1,\mathcal{N}_2)|^2 = \binom{L}{N_1}\binom{L}{N_2} \equiv P(L,N_1)P(L,N_2) \; . \tag{6.11}$$

As a second step, we make a similar assumption for the terms in the expectation value

$$\langle\Psi_0|\hat{c}^\dagger_{i,\sigma}\hat{c}_{j,\sigma}|\Psi_0\rangle \equiv \langle\hat{c}^\dagger_{i,\sigma}\hat{c}_{j,\sigma}\rangle_{\Psi_0} = \sum_{\mathcal{N}'_1,\mathcal{N}_2} A^*(\mathcal{N}'_1 \cup i, \mathcal{N}_2) A(\mathcal{N}'_1 \cup j, \mathcal{N}_2) \; , \tag{6.12}$$

for a hopping operator. Again, we assume that the terms in (6.12) do not depend on the sets $\mathcal{N}'_1, \mathcal{N}_2$. This leads to the equation

$$A^*(\mathcal{N}'_1 \cup i, \mathcal{N}_2) A(\mathcal{N}'_1 \cup j, \mathcal{N}_2) = P(L, N_1 - 1) P(L, N_2) \langle\hat{c}^\dagger_{i,\sigma}\hat{c}_{j,\sigma}\rangle_{\Psi_0} \tag{6.13}$$

for the product of coefficients in (6.8b). Equations (6.11) and (6.13) constitute the Gutzwiller approximation for the single-band Hubbard model.

Now we are in the position to evaluate equations (6.8). First, the norm of the Gutzwiller wave function becomes

$$\langle\Psi_\mathrm{G}|\Psi_\mathrm{G}\rangle = P(L,N_1)P(L,N_2) \sum_{\mathcal{N}_1,\mathcal{N}_2} g^{2M_{12}(\mathcal{N}_1,\mathcal{N}_2)} \; . \tag{6.14}$$

The sum over the sets N_σ can be replaced by a sum over the number of doubly-occupied sites M_{12} if we introduce the combinatorial factor

$$C_{M_{12}}(L,N_1,N_2) = \frac{L!}{M_{12}!(N_1 - M_{12})!(N_2 - M_{12})!(L - N_1 - N_2 + M_{12})!} \tag{6.15a}$$

$$= \frac{L!}{M_{12}!M_1!M_2!M_\emptyset!} \tag{6.15b}$$

This factor counts the number of possibilities to distribute N_1 (N_2) electrons with spin up (down) on the lattice such that M_{12} sites are doubly occupied. It allows us to write (6.14) as

$$\langle\Psi_\mathrm{G}|\Psi_\mathrm{G}\rangle = P(L,N_1)P(L,N_2) \sum_{M_{12}} g^{2M_{12}} C_{M_{12}}(L,N_1,N_2) \; . \tag{6.16}$$

For the expectation value (6.8c) of a double-occupancy operator, equation (6.11) yields

$$\langle\Psi_\mathrm{G}|\hat{m}_{i;12}|\Psi_\mathrm{G}\rangle = P(L,N_1)P(L,N_2) \sum_{\mathcal{N}'_1,\mathcal{N}'_2} g^{2M_{12}(\mathcal{N}'_1\cup i,\mathcal{N}'_2\cup i)} \tag{6.17a}$$

$$= P(L,N_1)P(L,N_2) \sum_{M_{12}} g^{2M_{12}+2} C_{M_{12}}(L-1,N_1-1,N_2-1) \; . \tag{6.17b}$$

To relate this expression to (6.16), we recast (6.17b) into the form

$$\langle\Psi_{\mathrm{G}}|\hat{m}_{i;12}|\Psi_{\mathrm{G}}\rangle = P(L,N_1)P(L,N_2)\sum_{M_{12}} g^{2M_{12}} C_{M_{12}}(L,N_1,N_2) f_{\mathrm{c}}(M_{12}) \;, \tag{6.18a}$$

with

$$f_{\mathrm{c}}(M_{12}) \equiv g^2 \frac{(N_1-M_{12})(N_2-M_{12})}{L(L-N_1-N_2+M_{12})} \;. \tag{6.18b}$$

Here, we used the fact that, in the thermodynamic limit, we can set

$$\begin{aligned} L-N_1-N_2+M_{12}+1 &\approx L-N_1-N_2+M_{12} \;, & (6.19a)\\ N_\sigma - M_{12} - 1 &\approx N_\sigma - M_{12} & (6.19b) \end{aligned}$$

in equation (6.18b). Note that the factors $P(L,N_\sigma)^{-1}$ and $C_{M_{12}}(L,N_1,N_2)$ are 'macroscopic' quantities, i.e., they are of order $\mathcal{O}(\exp(L))$. This will be used to replace the sum in (6.16) and (6.18a) by its maximum term, see below.

A similar form as equation (6.18a) can be derived for the expectation value of a hopping term. Using equation (6.13), we find

$$\langle\Psi_{\mathrm{G}}|\hat{c}^\dagger_{i,1}\hat{c}_{j,1}|\Psi_{\mathrm{G}}\rangle = \langle\hat{c}^\dagger_{i,1}\hat{c}_{j,1}\rangle_{\Psi_0} P(L-2,N_1-1)P(L,N_2) \sum_{\mathcal{N}_1',\mathcal{N}_2} g^{M_{12}(\mathcal{N}_1'\cup i,\mathcal{N}_2)} g^{M_{12}(\mathcal{N}_1'\cup j,\mathcal{N}_2)} \;. \tag{6.20}$$

Again, the sum over the sets $\mathcal{N}_1', \mathcal{N}_2$ can be replaced by a sum over M_{12}. To this end, we have to distinguish four different cases in (6.20) because the sites i and j can either be occupied with the opposite spin ($\sigma = 2$) or empty when the hopping process takes place. Hence, we have to address the cases (i) $i,j \notin N_2$; (ii) $i \in N_2, j \notin N_2$; (iii) $j \in N_2, i \notin N_2$; (iv) $i,j \in N_2$. Altogether, (6.20) can be written as

$$\begin{aligned} \langle\Psi_{\mathrm{G}}|\hat{c}^\dagger_{i,1}\hat{c}_{j,1}|\Psi_{\mathrm{G}}\rangle &= \langle\hat{c}^\dagger_{i,1}\hat{c}_{j,1}\rangle_{\Psi_0} P(L-2,N_1-1)P(L,N_2) \qquad (6.21)\\ &\quad \times \sum_{M_{12}} g^{2M_{12}} \big[C_{M_{12}}(L-2,N_1-1,N_2) + 2gC_{M_{12}}(L-2,N_1-1,N_2-1) \\ &\qquad + g^2 C_{M_{12}}(L-2,N_1-1,N_2-2)\big] \;. \end{aligned}$$

We extract the factors equivalent to the norm (6.16) and arrive at

$$\begin{aligned} \langle\Psi_{\mathrm{G}}|\hat{c}^\dagger_{i,1}\hat{c}_{j,1}|\Psi_{\mathrm{G}}\rangle &= \langle\hat{c}^\dagger_{i,1}\hat{c}_{j,1}\rangle_{\Psi_0} P(L,N_1)P(L,N_2)\frac{L^2}{N_1(L-N_1)} \qquad (6.22a)\\ &\quad \times \sum_{M_{12}} g^{2M_{12}} C_{M_{12}}(L,N_1,N_2) f_{\mathrm{h}}(M_{12}) \;, \end{aligned}$$

with

$$\begin{aligned} f_{\mathrm{h}}(M_{12}) &\equiv \frac{(N_1-M_{12})(L-N_1-N_2+M_{12})}{L^2} + 2g\frac{(N_1-M_{12})(N_2-M_{12})}{L^2} \qquad (6.22b)\\ &\quad + g^2 \frac{(N_1-M_{12})(N_2-M_{12})^2}{L^2(L-N_1-N_2+M_{12})} \;. \end{aligned}$$

Again, we neglected terms of order unity in (6.22b).

Now we are in the position to exploit the simplifications in the thermodynamic limit when we divide (6.18a) and (6.22b) by the norm. The sum in equation (6.16) has a macroscopic maximum for a certain value $\bar{M}_{12}$ (and resulting values $\bar{M}_1, \bar{M}_1, \bar{M}_\emptyset$). The same holds for the

expectation values (6.18a) and (6.22b) because the functions $f_{\rm h}(M_{12})$ and $f_{\rm c}(M_{12})$, which are of order unity do not affect the macroscopic peak position. Hence, we can replace the sum by its maximum term in all three cases. After the application of Stirling's formula $X! \approx X^X$ [157], we find that the maximum term problem has the general form

$$\frac{\partial}{\partial x}\left(p^x \prod_i r_i(x)^{\alpha_i r_i(x)}\right) = 0 \,, \tag{6.23a}$$

where the linear functions $r_i(x)$ obey the additional condition

$$\sum_i \alpha_i \frac{\partial}{\partial x} r_i(x) = 0 \,. \tag{6.23b}$$

For example, for the norm we obtain from (6.15a) and (6.16) that $r_1(x) = m_{12} = x$, $r_2(x) = n_1 - x$, $r_3(x) = n_2 - x$, $r_4(x) = 1 - n_1 - n_2 + x$, and $p = g^2$ where $m_I = M_I/L$ and $n_\sigma = N_\sigma/L$. By means of elementary calculus, equation (6.23a) yields the condition

$$p \prod_i r_i(x)^{\alpha_i r_i(x)} = 1 \,. \tag{6.23c}$$

In the case of the norm, this leads to the maximum-term condition

$$g^2 = \frac{m_{12} m_\emptyset}{m_1 m_2} \,, \tag{6.24}$$

which allows the original variational parameter g to be replaced by the new parameter m_{12}.

We replace the sums in the expectation value (6.18a) by its maximum term, divide it by the norm, and find

$$\langle \hat{m}_{i;12} \rangle_{\Psi_{\rm G}} = g^2 \frac{m_1 m_2}{m_\emptyset} = m_{12} \tag{6.25}$$

for the mean number of double occupancies. In the same way, we derive from (6.22),

$$\langle \hat{c}^\dagger_{i,\sigma} \hat{c}_{j,\sigma} \rangle_{\Psi_{\rm G}} = q_\sigma^2 \langle \hat{c}^\dagger_{i,\sigma} \hat{c}_{j,\sigma} \rangle_{\Psi_0} \tag{6.26}$$

with the Gutzwiller loss factors

$$\begin{aligned} q_1^2 &= \frac{1}{n_1(1-n_1)} \left(m_1 m_\emptyset + 2g m_1 m_2 + g^2 \frac{m_1 m_2^2}{m_\emptyset} \right) && (6.27a) \\ &= \frac{1}{n_1(1-n_1)} \left(\sqrt{m_1 m_\emptyset} + \sqrt{m_2 m_{12}} \right) \,, && (6.27b) \\ q_2^2 &= \frac{1}{n_2(1-n_2)} \left(\sqrt{m_2 m_\emptyset} + \sqrt{m_1 m_{12}} \right) \,. && (6.27c) \end{aligned}$$

Thus, we finally obtain the same result as in the limit of infinite dimensions,

$$\langle \hat{H}_{\rm 1B} \rangle_{\Psi_{\rm G}} = \sum_{i(\neq)j} t_{i,j} \sum_{\sigma=1}^{2} q_\sigma^2 \langle \hat{c}^\dagger_{i,\sigma} \hat{c}_{j,\sigma} \rangle_{\Psi_0} + L\varepsilon \sum_{\sigma=1}^{2} n_\sigma + LU m_{12} \tag{6.28}$$

for the variational ground-state energy within the Gutzwiller approximation. Here, we separated the site-independent on-site energies $\varepsilon = t_{i,i}$.

6.1.2 Gutzwiller Approximation for Multi-Band Hubbard Models

For a multi-band model with the Coulomb interaction (6.1), the atomic eigenstates $|\Gamma\rangle$ are configurations $|I\rangle$, as defined in (4.4). Then, if we work with diagonal and site-independent variational parameters $\lambda_I \equiv \lambda_{i;I,I}$, the Gutzwiller wave function (4.25a) has the form

$$|\Psi_{\mathrm{G}}\rangle = \prod_I \lambda_I^{\hat{M}_I} |\Psi_0\rangle \ , \tag{6.29}$$

where $\hat{M}_I = \sum_i \hat{m}_{i,I}$. For the derivation of the multi-band Gutzwiller approximation, it is convenient to write the wave function (6.29) as

$$|\Psi_{\mathrm{G}}\rangle = \eta_\emptyset \prod_\sigma \eta_\sigma^{\hat{N}_\sigma} \prod_{I(|I|\geq 2)} g_I^{\hat{M}_I} |\Psi_0\rangle \ , \tag{6.30a}$$

where

$$\eta_\emptyset = \lambda_\emptyset^L \ , \tag{6.30b}$$

$$\eta_\sigma = \lambda_\sigma/\lambda_\emptyset \ , \tag{6.30c}$$

$$g_I = \lambda_I/\lambda_\emptyset \prod_{\sigma\in I} (\lambda_\emptyset/\lambda_\sigma) \ , \tag{6.30d}$$

and $\hat{N}_\sigma \equiv \sum_i \hat{n}_{i,\sigma}$. Here, we used the operator identities

$$\hat{M}_\sigma = \hat{N}_\sigma - \sum_{I(|I|\geq 2,\sigma\in I)} \hat{M}_I \ , \tag{6.31a}$$

$$\hat{M}_\emptyset = L - \sum_\sigma \hat{N}_\sigma + \sum_{I(|I|\geq 2)} (|I|-1)\hat{M}_I \ . \tag{6.31b}$$

As in the one-band case, we introduce a local basis,

$$\left|\Phi_{\tilde{\mathcal{N}}}\right\rangle \equiv \prod_\sigma \prod_{i\in\mathcal{N}_\sigma} \hat{c}_{i,\sigma}^\dagger |0\rangle \ , \tag{6.32}$$

in order to expand the one-particle wave function

$$|\Psi_0\rangle = \sum_{\tilde{\mathcal{N}}} A(\tilde{\mathcal{N}}) \left|\Phi_{\tilde{\mathcal{N}}}\right\rangle \ . \tag{6.33}$$

Here, and in the following, we use the abbreviations

$$\tilde{\mathcal{N}} \equiv \{\mathcal{N}_1, \ldots, \mathcal{N}_{2N}\} \ , \tag{6.34a}$$

$$\tilde{N} \equiv \{N_1, \ldots, N_{2N}\} \ , \tag{6.34b}$$

for all subsets $\mathcal{N}_\sigma$ of lattice sites with the orbital σ occupied, and, the corresponding set of numbers $N_\sigma = |\mathcal{N}_\sigma|$. Hybridisation terms $\sim \hat{c}_{i,\sigma}^\dagger \hat{c}_{i,\sigma'}$ in the kinetic energy part of the Hamiltonian (2.15) lead to a major difference between equations (6.6) and (6.33). In (6.33) the sum over $\mathcal{N}_1, \ldots, \mathcal{N}_{2N}$ includes all possible number distributions $N_1, \ldots, N_{2N}$ of electrons on the lattice, since, in general, the operators $\hat{N}_\sigma$ do not commute with the Hamiltonian.

In close analogy to the one-band case, we need to derive expressions for certain products of the coefficients A in (6.33). Again, we consider the one-particle state $|\Psi_0\rangle$ to set up the Gutzwiller approximation. First, the norm becomes

$$\langle\Psi_0|\Psi_0\rangle = \sum_{\tilde{\mathcal{N}}} \left|A(\tilde{\mathcal{N}})\right|^2 = \sum_{\tilde{N}} \Omega(\tilde{N}) \ , \tag{6.35}$$

where

$$\Omega(\tilde{N}) \equiv \sum_{\tilde{\mathcal{N}}} \left| A(\tilde{\mathcal{N}}) \right|^2 \prod_{\sigma} \delta_{|\tilde{\mathcal{N}}_\sigma|,\tilde{N}_\sigma} \tag{6.36}$$

is the probability to find exactly $N_1, \ldots, N_{2N}$ electrons in the orbitals $\sigma = 1, \ldots, 2N$. The Gutzwiller approximation is defined by

$$\left| A(\tilde{\mathcal{N}}) \right|^2 = \Omega(\tilde{N}) \prod_{\sigma} P(L, N_\sigma) \; ; \tag{6.37}$$

compare equation (6.11) for the one-band case.

In general, there are certain constraints on the occupation densities N_σ in the wave functions $|\Psi_{\mathrm{G}}\rangle$ and $|\Psi_0\rangle$. For example, the total number of spin-up and spin-down electrons is usually conserved for systems without spin-orbit coupling. In this case, the number distribution $\Omega(\tilde{N})$ is non-zero only in a d-dimensional subspace ($d < 2N$) of the total space of occupancies $\{N_1, \ldots, N_{2N}\}$ where $2N - d$ is the number of constraints.

While one can implement the constraints exactly, i.e., in a 'micro-canonical' way, here we use a more concise derivation, which corresponds to a 'grand-canonical' ensemble in statistical physics. We allow the wave functions $|\Psi_{\mathrm{G}}\rangle$ and $|\Psi_0\rangle$ to include components with any numbers of occupancies $\{N_1, \ldots, N_{2N}\}$. In this way, even the total number of electrons $\sum_\sigma N_\sigma$ is not a good quantum number for these wave functions. In the thermodynamic limit, however, only expectation values matter and, therefore, the micro-canonical and the grand-canonical derivation are equivalent.

In our grand-canonical description, we consider the number distribution $\Omega(\tilde{N})$ as a continuous function in the entire $2N$-dimensional space $\{N_1, \ldots, N_{2N}\}$. As a macroscopic probability distribution, $\Omega(\tilde{N})$ has a sharp maximum around the expectation values

$$\bar{N}^0_\sigma = \langle \hat{N}_\sigma \rangle_{\Psi_0} \; . \tag{6.38}$$

For these occupancies $\tilde{\bar{N}}^0 \equiv \{\bar{N}^0_1, \ldots, \bar{N}^0_{2N}\}$, we have

$$\frac{\partial}{\partial N_\sigma} \Omega(\tilde{N}) \bigg|_{\tilde{N} = \tilde{\bar{N}}^0} = 0 \; . \tag{6.39a}$$

Moreover,

$$\frac{\Omega(\bar{N}_1 + \Delta N_1, \ldots, \bar{N}_{2N} + \Delta N_{2N})}{\Omega(\tilde{\bar{N}}^0)} = 1 + \mathcal{O}\left(\frac{1}{L}\right) \tag{6.39b}$$

is fulfilled in the thermodynamic limit if the numbers $\Delta N_1, \ldots, \Delta N_{2N}$ are of order unity. For the following derivation, we need not determine the explicit form of the function $\Omega(\tilde{N})$ but only the two equations (6.39).

Apart from equation (6.37) we need expressions for products of the coefficients in (6.33) that result from the evaluation of hopping terms. Again, we consider the respective uncorrelated expectation values

$$\langle \Psi_0 | \hat{c}^\dagger_{i,\sigma} \hat{c}_{j,\sigma'} | \Psi_0 \rangle = \sum_{\tilde{\mathcal{N}}'} A^*(\tilde{\mathcal{N}}'_{i,\sigma}) A(\tilde{\mathcal{N}}'_{j,\sigma'}) = \sum_{\tilde{N}} \Omega^{\sigma,\sigma'}_{i,j}(\tilde{N}) \; , \tag{6.40a}$$

where we introduced the probability distribution

$$\Omega^{\sigma,\sigma'}_{i,j}(\tilde{N}) = \sum_{\tilde{\mathcal{N}}'} A^*(\tilde{\mathcal{N}}'_{i,\sigma}) A(\tilde{\mathcal{N}}'_{j,\sigma'}) \prod_{\sigma''} \delta_{|\mathcal{N}'_{\sigma''}|,N_{\sigma''}} \; , \tag{6.40b}$$

with $i \notin \tilde{\mathcal{N}}'_{i,\sigma}$, $j \notin \tilde{\mathcal{N}}'_{j,\sigma'}$, and the notation

$$\tilde{\mathcal{N}}_{i(j),\sigma(\sigma')} \equiv \{\mathcal{N}'_1 \ldots, \mathcal{N}'_{\sigma(\sigma')} \cup i(j), \ldots \mathcal{N}'_{2N}\} \; . \tag{6.40c}$$

We can write the distribution (6.40b) as

$$\Omega_{i,j}^{\sigma,\sigma'}(\tilde{N}) = \omega_{i,j}^{\sigma,\sigma'}(\tilde{N})\Omega(\tilde{N}) \; , \tag{6.41}$$

where the function $\omega_{i,j}^{\sigma,\sigma'}$ is of order unity and gives the conditional probability for the hopping transfer of an electron from orbital σ' on site j into an orbital σ on site i if the number distribution of the remaining electrons is given by $\tilde{N} = \{N_1, \ldots, N_{2N}\}$. For the expectation values $\tilde{\tilde{N}}^0$, one finds, in particular,

$$\omega_{i,j}^{\sigma,\sigma'}(\tilde{\tilde{N}}^0) = \langle \Psi_0 | \hat{c}_{i,\sigma}^{\dagger} \hat{c}_{j,\sigma'} | \Psi_0 \rangle \; . \tag{6.42}$$

Since the probability factors in (6.40a) have the same form

$$P(L-1, N_\sigma)P(L-1, N_{\sigma'}) = \frac{L^2}{(L-N_\sigma)(L-N_{\sigma'})} P(L, N_\sigma)P(L, N_{\sigma'}) \; , \tag{6.43a}$$

$$P(L-2, N_\sigma) = \frac{L^2}{(L-N_\sigma)^2} P(L, N_\sigma) \; , \tag{6.43b}$$

for both cases $\sigma \neq \sigma'$ and $\sigma = \sigma'$, the Gutzwiller approximation can be written in the compact form

$$A^*(\tilde{\mathcal{N}}'_{i,\sigma})A(\tilde{\mathcal{N}}'_{j,\sigma'}) = \Omega_{i,j}^{\sigma,\sigma'}(\tilde{N}) \frac{L^2}{(L-N_\sigma)(L-N_{\sigma'})} \prod_{\sigma''} P(L, N_{\sigma''}) \; . \tag{6.44}$$

Equations (6.37) and (6.44) define the Gutzwiller approximation for multi-band system. The remaining steps of the derivation are exact as in the one-band case.

First, equation (6.37) allows us to write the norm as

$$\langle \Psi_{\mathrm{G}} | \Psi_{\mathrm{G}} \rangle = \sum_{\tilde{\mathcal{N}}} \left| A(\tilde{\mathcal{N}}) \right|^2 \prod_{\sigma} \eta_\sigma^{2N_\sigma} \prod_{I(|I|\geq 2)} g_I^{2Z_I^{\mathcal{L}}(\tilde{\mathcal{N}})} \tag{6.45a}$$

$$= \sum_{\tilde{N}} \Omega(\tilde{N}) \prod_{\sigma} P(L, N_\sigma) \eta_\sigma^{2N_\sigma} \sum_{\tilde{\mathcal{N}}(|\mathcal{N}_\sigma|=N_\sigma)} \prod_{I(|I|\geq 2)} g_I^{2Z_I^{\mathcal{L}}(\tilde{\mathcal{N}})} \; , \tag{6.45b}$$

where $Z_I^{\mathcal{X}}(\tilde{\mathcal{N}})$ is the number of sites (included in $\mathcal{X}$) with a multiple occupancy I provided that the distribution of all electrons is given by $\tilde{\mathcal{N}}$. In equation (6.45b), we have $\mathcal{X} = \mathcal{L}$, the set of all lattice sites.

The sum over $\tilde{\mathcal{N}}$ in (6.45b) can be replaced by sums over all possible multiple occupancies $\tilde{M} \equiv \{M_{12}, \ldots, M_{1\ldots 2N}\}$,

$$\langle \Psi_{\mathrm{G}} | \Psi_{\mathrm{G}} \rangle = \sum_{\tilde{N}} \Omega(\tilde{N}) \prod_{\sigma} P(L, N_\sigma) \eta_\sigma^{2N_\sigma} \sum_{\tilde{M}} C_{\tilde{M}}(L, \tilde{N}) \prod_{I(|I|\geq 2)} g_I^{2M_I} \; , \tag{6.46a}$$

where we introduced the combinatorial factor

$$C_{\tilde{M}}(L, \tilde{N}) \equiv L! \left[\prod_I M_I! \right]^{-1} \; . \tag{6.46b}$$

It counts the number of possibilities to put $N_1, \ldots, N_{2N}$ electrons onto the lattice for a given number M_I of sites with multiple occupancies $I \in \{(12), \ldots, (1 \ldots 2N)\}$. Here, the numbers of empty and singly-occupied sites are determined by the completeness relations

$$M_\emptyset = L - \sum_\sigma N_\sigma + \sum_{I(|I|\geq 2)} (|I|-1) M_I \,, \tag{6.47a}$$

$$M_\sigma = N_\sigma - \sum_{I(|I|\geq 2, \sigma \in I)} M_I \,, \tag{6.47b}$$

which follow from (6.31).

As in the one-band case, all relevant expectation values have the same form as the norm, apart from factors of order unity in the respective sums, see below. Again, we will be able to replace all these sums by their maximum terms. From equation (6.46a), we see that one has to find the maximum term with respect to $\tilde{M}$ and $\tilde{N}$. We first consider the sum over $\tilde{M}$ in (6.46a). The maximum term condition for each of these multiple occupancies has the form of equation (6.23a) if we use Stirling's formula and equations (6.47). This leads directly to

$$g_I^2 = m_I m_\emptyset^{|I|-1} \prod_{\sigma \in I} m_\sigma^{-1} \,, \tag{6.48}$$

where the values $\bar{M}_I = L m_I$ are the numbers for which the sum in (6.46a) takes its maximum.

The evaluation of the sum with respect to the 'gross' occupancies $\tilde{N}$ in (6.46a) is, in general, quite complicated because it requires an explicit evaluation of the distribution $\Omega(\tilde{N})$. The evaluation becomes much easier if we choose the parameters η_σ such that the sum (6.46a) takes its maximum at values $\tilde{\bar{N}} = \tilde{\bar{N}}^0$. In this way, we ensure that the orbital densities in the Gutzwiller wave function $|\Psi_{\mathrm{G}}\rangle$ and the corresponding one particle wave function $|\Psi_0\rangle$ are the same. Then, the maximum term condition for the sum in (6.46a) with respect to $\tilde{N}$ reads

$$0 = \frac{\partial}{\partial N_\sigma} \left(\Omega(\tilde{N}) \eta_\sigma^{2N_\sigma} \frac{P(L, N_\sigma)}{M_\sigma! M_\emptyset!} \right) \Bigg|_{\tilde{\bar{N}} = \tilde{\bar{N}}^0} \tag{6.49a}$$

$$= \frac{\partial}{\partial N_\sigma} \left(\eta_\sigma^{2N_\sigma} \frac{(L-N_\sigma)^{L-N_\sigma} N_\sigma^{N_\sigma}}{M_\sigma^{M_\sigma} M_\emptyset^{M_\emptyset}} \right) \Bigg|_{\tilde{\bar{N}} = \tilde{\bar{N}}^0} \,, \tag{6.49b}$$

where we used Stirling's formula and equation (6.39a). To evaluate (6.49b), we use again equations (6.23) and find

$$\eta_\sigma^2 = \frac{1 - n_\sigma}{n_\sigma} \frac{m_\sigma}{m_\emptyset} \,. \tag{6.50}$$

We skip the straightforward proof here that the numbers $\bar{N}_\sigma$ and $\bar{M}_I$ that maximise the sum in (6.46a) are, in fact, the expectation values of the corresponding operators, i.e.,

$$\bar{M}_I = L m_I = \frac{\langle \Psi_{\mathrm{G}} | \hat{M}_I | \Psi_{\mathrm{G}} \rangle}{\langle \Psi_{\mathrm{G}} | \Psi_{\mathrm{G}} \rangle} \,, \tag{6.51a}$$

$$\bar{N}_\sigma = L n_\sigma = \frac{\langle \Psi_{\mathrm{G}} | \hat{N}_\sigma | \Psi_{\mathrm{G}} \rangle}{\langle \Psi_{\mathrm{G}} | \Psi_{\mathrm{G}} \rangle} \,. \tag{6.51b}$$

The results derived so far, agree with those that we found in the exact evaluation of the Gutzwiller wave functions in infinite dimensions. Equations (6.30c), (6.30d), (6.48), and (6.50) lead to

$$\lambda_I^2 = \frac{m_I}{m_I^0} \lambda_\emptyset^2 \frac{m_\emptyset^0}{m_\emptyset} \,, \tag{6.52}$$

which is equivalent to (5.67d) if we choose $\lambda_\emptyset^2 = m_\emptyset/m_\emptyset^0$. This is possible since $\lambda_\emptyset$ just leads to a different norm of $|\Psi_\mathrm{G}\rangle$ and does not affect expectation values.

Finally, we have to evaluate the expectation value for an electronic hopping operator. With the help of equation (6.44), we find

$$\langle\Psi_\mathrm{G}|\hat{c}_{i,\sigma}^\dagger\hat{c}_{j,\sigma'}|\Psi_\mathrm{G}\rangle = \sum_{\tilde{N}} \frac{H_{i,j}^{\sigma,\sigma'}(\tilde{N})\Omega_{i,j}^{\sigma,\sigma'}(\tilde{N})\eta_\sigma\eta_{\sigma'}}{(L-N_\sigma)(L-N_{\sigma'})} \prod_{\sigma''} P(L,N_{\sigma''})L^2\eta_{\sigma''}^{2N_{\sigma''}} \;, \tag{6.53a}$$

where

$$H_{i,j}^{\sigma,\sigma'}(\tilde{N}) \equiv \sum_{\tilde{\mathcal{N}}'(|\mathcal{N}_\sigma=N_\sigma|)} \prod_{I(|I|\geq 2)} g_I^{\left[2Z_I^{\mathcal{L}\setminus\{i,j\}}(\tilde{\mathcal{N}}')+Z_I^{\{i,j\}}(\tilde{\mathcal{N}}'_{i,\sigma})+Z_I^{\{i,j\}}(\tilde{\mathcal{N}}'_{j,\sigma})\right]} \;. \tag{6.53b}$$

Again, the sum over $\tilde{\mathcal{N}}'$ in (6.53b) can be replaced by a sum over the multiple occupancies $\tilde{M}$. As in the one-band case, we have to distinguish the different occupancies of the sites i and j. Depending on these occupancies different arguments occur in the respective combinatorial factors (6.46b). We set $g_I \equiv 1$ for $|I| \leq 1$ and use the abbreviation $\delta_\sigma^I \equiv |\sigma \cap I|$. Then, equation (6.53b) can be written as

$$\begin{aligned} H_{i,j}^{\sigma,\sigma'}(\tilde{N}) = &\sum_{\tilde{M}} \left(\prod_I g_I^{2M_I}\right) \sum_{I_i(\sigma\notin I_i)} \sum_{I_j(\sigma'\notin I_j)} g_{I_i\cup\sigma} g_{I_i} g_{I_j\cup\sigma'} g_{I_j} \\ &\times C_{\tilde{M}}\left(L-2, \{N_1-\delta_1^{I_i}-\delta_1^{I_j}, \ldots, N_\sigma-\delta_\sigma^{I_j}, \ldots, N_{\sigma'}-\delta_{\sigma'}^{I_i}, \ldots, N_{2N}-\delta_{2N}^{I_i}-\delta_{2N}^{I_j}\}\right) \;. \end{aligned} \tag{6.54}$$

In the case that $\sigma = \sigma'$, the terms $\delta_\sigma^{I_j}$ and $\delta_{\sigma'}^{I_i}$ obey $\delta_\sigma^{I_j} = \delta_{\sigma'}^{I_i} = 0$ because of the summation restriction in (6.54). In the thermodynamic limit, it follows that

$$\begin{aligned} &C_{\tilde{M}}\left(L-2, \{N_1-\delta_1^{I_i}-\delta_1^{I_j}, \ldots, N_\sigma-\delta_\sigma^{I_j}, \ldots, N_{\sigma'}-\delta_{\sigma'}^{I_i}, \ldots, N_{2N}-\delta_{2N}^{I_i}-\delta_{2N}^{I_j}\}\right) \\ &\qquad = C_{\tilde{M}}(L,\tilde{N}) \left(\frac{M_\sigma}{M_\emptyset}\right)^{\delta_\sigma^{I_j}} \left(\frac{M_{\sigma'}}{M_\emptyset}\right)^{\delta_{\sigma'}^{I_i}} \frac{M_\emptyset^2}{L^2} \prod_{\sigma''(\neq\sigma,\sigma')} \left(\frac{M_{\sigma''}}{M_\emptyset}\right)^{\delta_{\sigma''}^{I_i}+\delta_{\sigma''}^{I_j}} \;. \end{aligned} \tag{6.55}$$

Hence, equation (6.53a) becomes

$$\begin{aligned} \langle\Psi_\mathrm{G}|\hat{c}_{i,\sigma}^\dagger\hat{c}_{j,\sigma'}|\Psi_\mathrm{G}\rangle \;&=\; \sum_{\tilde{N}} \Omega(\tilde{N}) \prod_{\sigma''} P(L,N_{\sigma''})\eta_{\sigma''}^{2N_{\sigma''}} \\ &\quad\times \sum_{\tilde{M}} \prod_I g_I^{2M_I} C_{\tilde{M}}(L,\tilde{N}) h_{i,j}^{\sigma,\sigma'}(\tilde{N},\tilde{M}) \end{aligned} \tag{6.56a}$$

with

$$\begin{aligned} h_{i,j}^{\sigma,\sigma'}(\tilde{N},\tilde{M}) \;&\equiv\; \frac{\omega_{i,j}^{\sigma,\sigma'}(\tilde{N})L^2\eta_\sigma\eta_{\sigma'}}{(L-N_\sigma)(L-N_{\sigma'})} \sum_{I_i(\sigma\notin I_i)} \sum_{I_j(\sigma'\notin I_j)} g_{I_i\cup\sigma} g_{I_i} g_{I_j\cup\sigma'} g_{I_j} \\ &\quad\times \left(\frac{M_\sigma}{M_\emptyset}\right)^{\delta_\sigma^{I_j}} \left(\frac{M_{\sigma'}}{M_\emptyset}\right)^{\delta_{\sigma'}^{I_i}} \frac{M_\emptyset^2}{L^2} \prod_{\sigma''(\neq\sigma,\sigma')} \left(\frac{M_{\sigma''}}{M_\emptyset}\right)^{\delta_{\sigma''}^{I_i}+\delta_{\sigma''}^{I_j}} \;. \end{aligned} \tag{6.56b}$$

Apart from the factor (6.56b), which is of order unity, equation (6.56a) is identical to the norm (6.46a). Thus, in the thermodynamic limit we can replace the whole sum by its maximum

term, which has the same position as the norm with respect to $\tilde{N}$ and $\tilde{M}$. When we use equation (6.50) for the factors η_σ and the relation

$$\begin{aligned} g_{I_i\cup\sigma} g_{I_i} g_{I_j\cup\sigma'} g_{I_j} &= \left(\frac{M_\emptyset}{M_\sigma}\right)^{\delta_\sigma^{I_j}} \left(\frac{M_\emptyset}{M_{\sigma'}}\right)^{\delta_{\sigma'}^{I_i}} \prod_{\sigma''(\neq\sigma,\sigma')} \left(\frac{M_\emptyset}{M_{\sigma''}}\right)^{\delta_{\sigma''}^{I_i}+\delta_{\sigma''}^{I_j}} \\ &\quad \times \sqrt{\frac{M_{I_i\cup\sigma} M_{I_i}}{M_\emptyset M_\sigma}} \sqrt{\frac{M_{I_j\cup\sigma'} M_{I_j}}{M_\emptyset M_{\sigma'}}} \,, \end{aligned} \tag{6.57}$$

the expectation value for a hopping term finally becomes

$$\frac{\langle\Psi_{\mathrm{G}}|\hat{c}_{i,\sigma}^\dagger \hat{c}_{j,\sigma'}|\Psi_{\mathrm{G}}\rangle}{\langle\Psi_{\mathrm{G}}|\Psi_{\mathrm{G}}\rangle} = q_\sigma q_{\sigma'} \langle\Psi_0|\hat{c}_{i,\sigma}^\dagger \hat{c}_{j,\sigma'}|\Psi_0\rangle \,. \tag{6.58}$$

Here, the renormalisation factors,

$$q_\sigma^2 = \frac{1}{n_\sigma(1-n_\sigma)} \left[\sum_{I(\sigma\notin I)} \sqrt{m_{I\cup\sigma} m_I}\right]^2 \,, \tag{6.59a}$$

are the same as in equation (5.83) if we work with $|\Gamma\rangle = |I\rangle$ and

$$\lambda_{I,I'} = \delta_{I,I'}\lambda_I = \delta_{I,I'} \sqrt{\frac{m_I}{m_I^0}} \,. \tag{6.60}$$

This completes the proof that the Gutzwiller approximation leads to the same results for the energy functionals as obtained in the limit of infinite dimensions.

6.1.3 Non-Local Terms in the Hamiltonian

The Gutzwiller approximation scheme, as introduced in sections 6.1.1 and 6.1.2, can also be used to calculate the expectation values of non-local operators. As an example, we consider the expectation value of the single-band operator

$$\hat{J}_{i,j}^{+-} = \hat{c}_{i,\uparrow}^\dagger \hat{c}_{i,\downarrow} \hat{c}_{j,\downarrow}^\dagger \hat{c}_{j,\uparrow} = \hat{c}_{i,1}^\dagger \hat{c}_{i,2} \hat{c}_{j,2}^\dagger \hat{c}_{j,1} \tag{6.61}$$

as it appears, e.g., in the t-J model, equation (2.40a).

Following the arguments in section 6.1.1, we first consider the uncorrelated expectation value

$$\langle\Psi_0|\hat{J}_{i,j}^{+-}|\Psi_0\rangle = \sum_{\mathcal{N}_1',\mathcal{N}_2'} A^*(\mathcal{N}_1'\cup i, \mathcal{N}_2'\cup j) A(\mathcal{N}_1'\cup j, \mathcal{N}_2'\cup i) \,, \tag{6.62}$$

where the sets $\mathcal{N}_1'$ and $\mathcal{N}_2'$ do not contain the lattice sites i and j. We apply the usual Gutzwiller approximation assumption that the sum in (6.62) does not depend on $\mathcal{N}_1'$ and $\mathcal{N}_2'$. This leads to

$$\begin{aligned} &A^*(\mathcal{N}_1'\cup i, \mathcal{N}_2'\cup j) A(\mathcal{N}_1'\cup j, \mathcal{N}_2'\cup i) \\ &= P(L-2, N_1-1) P(L-2, N_2-1) \langle\Psi_0|\hat{J}_{i,j}^{+-}|\Psi_0\rangle \,. \end{aligned} \tag{6.63}$$

The expectation value of (6.61) with respect to the Gutzwiller wave function(6.3) is then given by

$$\begin{aligned} \langle\Psi_{\mathrm{G}}|\hat{J}_{i,j}^{+-}|\Psi_{\mathrm{G}}\rangle &= \langle\Psi_0|\hat{J}_{i,j}^{+-}|\Psi_0\rangle P(L-2, N_1-2) P(L-2, N_2) \\ &\quad \times \sum_{M_{12}} g^{2M_{12}} C_{M_{12}}(L-2, N_1-1, N_2-1) \,. \end{aligned} \tag{6.64}$$

If we replace the sum by its maximum term and divide it by the norm, we end up with

$$\frac{\langle\Psi_{\mathrm{G}}|\hat{J}^{+-}_{i,j}|\Psi_{\mathrm{G}}\rangle}{\langle\Psi_{\mathrm{G}}|\Psi_{\mathrm{G}}\rangle} = \frac{m_1 m_2}{n_1(1-n_2)n_2(1-n_2)}\langle\Psi_0|\hat{J}^{+-}_{i,j}|\Psi_0\rangle \ . \tag{6.65}$$

The factor

$$g_J = \frac{m_1 m_2}{n_1(1-n_2)n_2(1-n_2)} = \lambda_1^2\lambda_2^2 \tag{6.66}$$

in (6.65) is the same as the one derived in the limit of infinite dimensions, see equation (5.126).

Other non-local terms can be evaluated within the Gutzwiller approximation along the same lines as the expectation value (6.64). The results, however, do not necessarily agree with those in the limit of infinite dimensions. For example, in the Gutzwiller approximation, the expectation value of the correlated hopping operator

$$\hat{T}^{\mathrm{c}}_{i,j} \equiv \hat{n}_{i,2}\hat{c}^{\dagger}_{i,1}\hat{n}_{j,2}\hat{c}_{j,1} \ , \tag{6.67}$$

is given by

$$\langle\hat{T}^{\mathrm{c}}_{i,j}\rangle_{\Psi_{\mathrm{G}}} = \lambda_d^2\lambda_2^2\langle\hat{n}_{i,2}\hat{c}^{\dagger}_{i,1}\hat{n}_{j,2}\hat{c}_{j,1}\rangle_{\Psi_0} \ . \tag{6.68}$$

In contrast, the corresponding evaluation in infinite dimensions leads to

$$\langle\hat{T}^{\mathrm{c}}_{i,j}\rangle_{\Psi_{\mathrm{G}}} = \lambda_d^2\lambda_2^2\langle\hat{c}^{\dagger}_{i,1}\hat{c}_{j,1}\rangle_{\Psi_0} \ . \tag{6.69}$$

Equations (6.68) and (6.69) only agree if the diagrammatic rules in infinite dimensions are taken into account when the uncorrelated expectation value in (6.68) is evaluated by means of Wick's theorem. This means that the second term in

$$\begin{aligned}\langle\hat{n}_{i,2}\hat{c}^{\dagger}_{i,1}\hat{n}_{j,2}\hat{c}_{j,1}\rangle_{\Psi_0} &= \langle\hat{n}_{i,2}\rangle_{\Psi_0}\langle\hat{n}_{i,2}\rangle_{\Psi_0}\langle\hat{c}^{\dagger}_{i,1}\hat{c}_{j,1}\rangle_{\Psi_0} \\ &\quad -\langle\hat{c}^{\dagger}_{i,2}\hat{c}_{j,2}\rangle_{\Psi_0}\langle\hat{c}^{\dagger}_{j,2}\hat{c}_{i,2}\rangle_{\Psi_0}\langle\hat{c}^{\dagger}_{i,1}\hat{c}_{j,1}\rangle_{\Psi_0}\end{aligned} \tag{6.70}$$

has to be dropped. Note that without adding such 'infinite-dimension-rules' to the combinatorial Gutzwiller approximation one can easily derive contradictory results. For example, the hopping operator can be written in the form

$$\begin{aligned}\hat{c}^{\dagger}_{i,1}\hat{c}_{i,1} &= \hat{n}_{i,2}\hat{c}^{\dagger}_{i,1}\hat{c}_{i,1}\hat{n}_{j,2} + (1-\hat{n}_{i,2})\hat{c}^{\dagger}_{i,1}\hat{c}_{i,1}\hat{n}_{j,2} \\ &\quad +\hat{n}_{i,2}\hat{c}^{\dagger}_{i,1}\hat{c}_{i,1}(1-\hat{n}_{j,2}) + (1-\hat{n}_{i,2})\hat{c}^{\dagger}_{i,1}\hat{c}_{i,1}(1-\hat{n}_{j,2}) \ .\end{aligned} \tag{6.71}$$

If we evaluate each of the four terms on the r.h.s. of equation (6.71) by means of the Gutzwiller approximation we find

$$\begin{aligned}\langle\hat{c}^{\dagger}_{i,1}\hat{c}_{i,1}\rangle_{\Psi_{\mathrm{G}}} &= q_1^2\langle\hat{c}^{\dagger}_{i,1}\hat{c}_{i,1}\rangle_{\Psi_0} \\ &\quad -\left(\lambda_d^2\lambda_2^2 - 2\lambda_d\lambda_2\lambda_1\lambda_{\emptyset} + \lambda_1^2\lambda_{\emptyset}^2\right)\langle\hat{c}^{\dagger}_{i,2}\hat{c}_{j,2}\rangle_{\Psi_0}\langle\hat{c}^{\dagger}_{j,2}\hat{c}_{i,2}\rangle_{\Psi_0}\langle\hat{c}^{\dagger}_{i,1}\hat{c}_{j,1}\rangle_{\Psi_0}\end{aligned} \tag{6.72}$$

with q_1 as introduced in (6.27). The additional terms, in comparison to equation (6.26), i.e., the second line of (6.72), only vanish in the uncorrelated limit ($\lambda_I = 1$) or if we apply the diagrammatic rules in infinite dimensions. The combinatorial Gutzwiller approximation itself is not able to resolve the contradiction between the two expressions, equations (6.26) and (6.72).

6.2 Slave-boson Mean-Field Theories

The main problem in the investigation of many-particle systems arises from two-particle terms in the Hamiltonian, e.g., the operator $\hat{H}_I$ in (2.14). As we will show in this section, it is possible to get rid of such two-particle terms by introducing certain auxiliary (bosonic or fermionic) degrees of freedom, which are coupled to the physical particles. In this way, the quantum mechanical problem usually does not become simpler because a model of coupled fermions and bosons is just as difficult to tackle as the original physical system. Such a reformulation of the problem, however, may open ways to tackle it by means of approximate solutions that cannot be formulated for the original system.

For the derivation of theories with auxiliary particles, one may either use functional integral techniques or rewrite the Hamiltonian directly in terms of physical and auxiliary operators. We briefly summarise the ideas behind the functional integral method in section 6.2.1. In section 6.2.2, we introduce the Kotliar-Ruckenstein (KR) theory [125] for the single-band Hubbard model, which is based on a reformulation of the fermionic operators and most clearly related to the Gutzwiller variational approach. Note that Barnes and Coleman introduced an alternative slave-boson scheme for impurity systems, which will not be addressed in this work; we refer the interested reader to references [158–167].

A generalisation of the Kotliar-Ruckenstein method for multi-band Hubbard models is straightforward for systems with density-density type interaction, as we will show in section 6.2.3. In a more recent work [168], the approach has also been generalised for the investigation of multi-band models with general on-site interactions. We will discuss the main ideas behind this approach in section 6.2.4. Unfortunately, the derivation in [168] is mathematically not well-defined. Therefore, we propose an alternative slave-boson scheme for general multi-band models in section 6.2.4, which quite naturally reproduces the Gutzwiller energy functional, derived in chapter 5.

6.2.1 Slave Bosons and Functional Integrals

Quantum mechanical problems can be formulated quite elegantly by means of functional integrals. For an introduction into this field see, e.g., reference [3]. Here, we consider the single-band Hubbard model in order to illustrate the basic concepts behind the use of auxiliary fields in the context of functional-integral representations.

As shown, e.g., in reference [3], the partition function for the Hubbard model can be written as the functional integral

$$Z = \int \mathcal{D}(\Phi^*_{i,\sigma}\Phi_{i,\sigma}) \exp[-S_0 - S_\mathrm{I}] \,, \tag{6.73a}$$

with

$$S_0 = \int_0^\beta \mathrm{d}\tau \sum_{i,j,s} \Phi^*_{i,\sigma}(\tau) \left(\delta_{i,j} \frac{\partial}{\partial \tau} - t_{i,j} \right) \Phi_{j,\sigma}(\tau) \,, \tag{6.73b}$$

and

$$S_\mathrm{I} = U \int_0^\beta \mathrm{d}\tau \sum_i \Phi^*_{i,\uparrow}(\tau)\Phi^*_{i,\downarrow}(\tau)\Phi_{i,\downarrow}(\tau)\Phi_{i,\uparrow}(\tau) \,. \tag{6.73c}$$

Here, $\beta = 1/(k_\mathrm{B}T)$ is the inverse temperature and $\Phi^*_{i,\sigma}(\tau)$ and $\Phi_{i,\sigma}(\tau)$ are Graßmann variables, which represent the fermionic operators $\hat{c}^\dagger_{i,\sigma}$ and $\hat{c}_{i,\sigma}$, respectively. In order to get rid of the two-particle term in (6.73c), we write it as

$$\Phi^*_{i,\uparrow}(\tau)\Phi^*_{i,\downarrow}(\tau)\Phi_{i,\downarrow}(\tau)\Phi_{i,\uparrow}(\tau) = \frac{1}{4}(A^\mathrm{c}_i(\tau)^2 + A^\mathrm{s}_i(\tau)^2) \tag{6.74a}$$

with

$$A_i^{\mathrm{c}}(\tau) \equiv \Phi_{i,\uparrow}^*(\tau)\Phi_{i,\uparrow}(\tau) + \Phi_{i,\downarrow}^*(\tau)\Phi_{i,\downarrow}(\tau) \,, \tag{6.74b}$$

$$A_i^{\mathrm{s}}(\tau) \equiv \mathrm{i}(\Phi_{i,\uparrow}^*(\tau)\Phi_{i,\uparrow}(\tau) - \Phi_{i,\downarrow}^*(\tau)\Phi_{i,\downarrow}(\tau)) \,. \tag{6.74c}$$

Note that $A_i^{\mathrm{c}}(\tau)$ and $A_i^{\mathrm{s}}(\tau)$ describe the charge and the spin density on site i. At each imaginary time step in the integral (6.73c) we may replace the two quadratic terms in (6.74a) by means of a 'Hubbard-Stratonovich transformation' [169, 170]

$$\exp\left[\frac{(A_i^{\mathrm{c/s}}(\tau))^2}{2}\right] = \sqrt{2\pi}\int_{-\infty}^{\infty} \mathrm{d}[x_i^{\mathrm{c/s}}(\tau)] \exp\left[-\frac{(x_i^{\mathrm{c/s}}(\tau))^2}{2} - (x_i^{\mathrm{c/s}}(\tau))A_i^{\mathrm{c/s}}(\tau)\right] \,. \tag{6.75}$$

If we consider $x_i^{\mathrm{c}}(\tau)$ and $x_i^{\mathrm{s}}(\tau)$ as the real and the imaginary part of a complex field $\tilde{x}_i(\tau)$ we can write the partition function (6.73a) as

$$Z = \int \mathcal{D}(\tilde{x}_i^*\tilde{x}_i) \int \mathcal{D}(\Phi_{i,\sigma}^*\Phi_{j,\sigma}) \exp\big[-S^{\mathrm{eff}}\big] \tag{6.76}$$

with

$$S^{\mathrm{eff}} = S_0 + \sum_i \int_0^\beta \mathrm{d}\tau \left[\frac{1}{2}\tilde{x}_i^*(\tau)\tilde{x}_i(\tau) + \frac{U}{\sqrt{2}}\big(\tilde{x}_i^*(\tau)\Phi_{i,\uparrow}^*(\tau)\Phi_{i,\uparrow}(\tau) + \tilde{x}_i(\tau)\Phi_{i,\downarrow}^*(\tau)\Phi_{i,\downarrow}(\tau)\big)\right] \,. \tag{6.77}$$

The effective action S^{eff} belongs to a system of free (i.e., uncorrelated) fermions, which, at each lattice site i, are coupled to bosonic degrees of freedom described by the field $\tilde{x}_i(\tau)$. Note that there is a large amount of arbitrariness in the choice of both the rearrangement (6.74a) and the type of Hubbard-Stratonovich transformation that is used. For example, instead of the integral in (6.75), one can also work with a discrete sum over Ising variables $s = \pm 1$ [171]. All these functional-integral techniques are of great importance for quantum Monte-Carlo calculations [171–173] and field-theoretical approaches to the Hubbard model, see, for example, reference [174].

For a physical system of fermions and bosons, which are locally coupled, the action would contain a term

$$S_0^x = \int_0^\infty \mathrm{d}\tau \sum_i \tilde{x}_i^* \frac{\partial}{\partial\tau}\tilde{x}_i \,. \tag{6.78}$$

Such a term is missing in the effective action (6.77) and, therefore, it does not correspond to a quantum mechanical system with a well-defined Hamiltonian for physical fermions and bosons. In the following section, we introduce an auxiliary-particle method that avoids the functional integral technique and addresses directly the physical Hamiltonian.

6.2.2 Kotliar-Ruckenstein Theory for the One-Band Hubbard Model

In this section, we introduce the auxiliary particle method, which was proposed by Kotliar and Ruckenstein in order to investigate the single-band Hubbard model. We shall show that the ground-state energy functional in this approach agrees with the Gutzwiller variational energy.

We start from the single-band Hubbard model (6.2a) with its four-dimensional local Hilbert space $\mathcal{H}_i$ for each lattice site i represented by the four states $|I\rangle = |\emptyset\rangle\,, |\sigma\rangle\,, |12\rangle$ (with $\sigma = 1, 2$ for the two spin directions). The Hilbert space of the whole lattice system is given as the tensor product

$$\mathcal{H} \equiv \bigotimes_i \mathcal{H}_i \,. \tag{6.79}$$

Kotliar and Ruckenstein introduced auxiliary bosonic operators $\hat{\phi}^\dagger_{i;I}$, $\hat{\phi}_{i;I}$, which led to an enlarged local Hilbert space $\mathcal{H}_i^{\mathrm{FB}}$ defined by the basis states

$$\left|I, I'\right\rangle_{i;\mathrm{FB}} \equiv |I\rangle_i \otimes \left|I'\right\rangle_{i;\mathrm{B}} \ . \tag{6.80a}$$

Here, $|I\rangle_i$ is the fermionic configuration state, defined in equation (4.4), and $|I\rangle_{i;\mathrm{B}}$ is the bosonic state

$$|I\rangle_{i;\mathrm{B}} \equiv \hat{\phi}^\dagger_{i;I} \, |0\rangle_{i;\mathrm{B}} \ . \tag{6.80b}$$

with the bosonic vacuum state $|0\rangle_{i;\mathrm{B}}$. The original quantum mechanical problem can be recovered in the following way:

i) One has to find a subspace $\underline{\mathcal{H}}_i$ of $\mathcal{H}_i^{\mathrm{FB}}$ that is isomorphic to the physical Hilbert space $\mathcal{H}_i$ for each lattice site i. Kotliar and Ruckensstein defined this subspace by means of the constraints

$$\hat{F}_{i,0} \equiv 1 - \sum_I \hat{n}^{\mathrm{B}}_{i;I} = 0 \ , \tag{6.81a}$$

$$\hat{F}_{i,\sigma} \equiv \hat{c}^\dagger_{i,s} \hat{c}_{i,s} - \hat{n}^{\mathrm{B}}_{i;12} + \hat{n}^{\mathrm{B}}_{i;\sigma} = 0 \ , \tag{6.81b}$$

where we introduced the bosonic occupation operators

$$\hat{n}^{\mathrm{B}}_{i;I} \equiv \hat{\phi}^\dagger_{i;I} \hat{\phi}_{i;I} \ . \tag{6.82}$$

The constraints (6.81) define the subspace $\underline{\mathcal{H}}_i$ by the condition

$$\hat{F}_{i,\tilde{\sigma}} \, |\underline{\Psi}\rangle = 0 \tag{6.83}$$

for each $|\underline{\Psi}\rangle \in \underline{\mathcal{H}}_i$ and $\tilde{\sigma} \in (0, 1, 2)$. Alternatively, we can define $\underline{\mathcal{H}}_i$ directly by specifying its basis

$$|\underline{I}\rangle_i \equiv |I, I\rangle_{i;\mathrm{FB}} = |I\rangle_i \otimes |I\rangle_{i;\mathrm{B}} \ . \tag{6.84}$$

The corresponding Hilbert space for the lattice system is given by

$$\underline{\mathcal{H}} \equiv \bigotimes_i \underline{\mathcal{H}}_i \ . \tag{6.85}$$

Note that, by this construction, we now have a one-to-one correspondence of all physical states $|\Psi\rangle \in \mathcal{H}$ and their counterparts $|\underline{\Psi}\rangle \in \underline{\mathcal{H}}$.

ii) With the auxilliary Hilbert spaces $\underline{\mathcal{H}}_i$ and $\underline{\mathcal{H}}$ properly defined, one can find operators $\underline{\hat{O}}_i$ in $\underline{\mathcal{H}}_i$ that are *similar* to the physical operators $\hat{O}_i$ in $\mathcal{H}_i$. Here, 'similarity' means that

$${}_i\langle \underline{I}|\underline{\hat{O}}_i|\underline{I}'\rangle_i = {}_i\langle I|\hat{O}_i|I'\rangle_i \tag{6.86}$$

for all configurations $|I\rangle$, $|I'\rangle$. With similar local operators $\underline{\hat{O}}_i$, we can set up an 'effective' Hamiltonian $\underline{\hat{H}}_{1\mathrm{B}}$ that is similar to the physical Hamiltonian $\hat{H}_{1\mathrm{B}}$, i.e., it obeys

$$\langle\Psi|\hat{H}_{1\mathrm{B}}|\Psi'\rangle = \langle\underline{\Psi}|\underline{\hat{H}}_{1\mathrm{B}}|\underline{\Psi}'\rangle \tag{6.87}$$

for all physical states $|\Psi\rangle, |\Psi'\rangle \in \mathcal{H}$ and their counterparts $|\underline{\Psi}\rangle, |\underline{\Psi}'\rangle \in \underline{\mathcal{H}}$. In this way, we have introduced an exact mapping of the original physical problem, described by the Hamiltonian $\hat{H}_{1\mathrm{B}}$ in its Hilbert space $\mathcal{H}$ and the effective Hamiltonian $\underline{\hat{H}}_{1\mathrm{B}}$ in $\underline{\mathcal{H}}$.

To set up $\hat{\underline{H}}_{1\mathrm{B}}$, we start with an identification of operators that are similar to the fermionic operators $\hat{c}^{(\dagger)}_{i,\sigma}$ in $\mathcal{H}_i$. Their counterparts $\hat{\underline{c}}^{(\dagger)}_{i,\sigma}$ in $\underline{\mathcal{H}}_i$ can be chosen as

$$\hat{\underline{c}}^{\dagger}_{i,\sigma} = \hat{r}_{i,\sigma}\hat{c}^{\dagger}_{i,\sigma} \quad , \quad \hat{\underline{c}}_{i,\sigma} = \hat{r}^{\dagger}_{i,\sigma}\hat{c}_{i,\sigma} \; , \tag{6.88a}$$

where we introduced the bosonic operators

$$\hat{r}_{i,\sigma} \equiv \hat{\phi}^{\dagger}_{i;12}\hat{\phi}_{i;\bar{\sigma}} + \hat{\phi}^{\dagger}_{i;\sigma}\hat{\phi}_{i;\emptyset} \; , \tag{6.88b}$$

$$\hat{r}^{\dagger}_{i,\sigma} = \hat{\phi}^{\dagger}_{i;\bar{\sigma}}\hat{\phi}_{i;12} + \hat{\phi}^{\dagger}_{i;\emptyset}\hat{\phi}_{i;\sigma} \; . \tag{6.88c}$$

As required, the operators $\hat{\underline{c}}^{(\dagger)}_{i,\sigma}$ obey equation (6.86). To set up the Hamiltonian $\hat{\underline{H}}_{1\mathrm{B}}$ in $\underline{\mathcal{H}}_i$, we need to further find an operator $\hat{\underline{m}}_{i;12}$ that is similar to $\hat{m}_{i;12} = \hat{n}_{i,1}\hat{n}_{i,2}$. The most obvious choice is

$$\hat{\underline{m}}_{i;12} = \hat{n}^{\mathrm{B}}_{i;12} \; . \tag{6.89}$$

Note, however, that there is a large amount of arbitrariness. For example, the operators

$$\hat{\underline{m}}_{i;12} = \hat{n}^{\mathrm{B}}_{i;I}\hat{m}_{i;12} \quad \text{or} \quad \hat{\underline{m}}_{i;12} = \hat{m}_{i;12} \tag{6.90}$$

are also similar to $\hat{m}_{i;12}$ since both obey equation (6.86). The same ambiguity arises for the operators (6.88a). For example, they may equally well be chosen as

$$\hat{\underline{c}}^{\dagger}_{i,\sigma} = \hat{q}_{i,\sigma}\hat{c}^{\dagger}_{i,\sigma} \quad , \quad \hat{\underline{c}}_{i,\sigma} = \hat{q}^{\dagger}_{i,\sigma}\hat{c}_{i,\sigma} \tag{6.91a}$$

with

$$\hat{q}_{i,\sigma} \equiv (\hat{\Delta}_{i,\sigma})^{-1/2}\hat{r}_{i,\sigma}(1-\hat{\Delta}_{i,\sigma})^{-1/2} \; , \tag{6.91b}$$

$$\hat{q}^{\dagger}_{i,\sigma} = (1-\hat{\Delta}_{i,\sigma})^{-1/2}\hat{r}^{\dagger}_{i,\sigma}(\hat{\Delta}_{i,\sigma})^{-1/2} \; , \tag{6.91c}$$

and

$$\hat{\Delta}_{i,\sigma} \equiv \hat{n}^{\mathrm{B}}_{i;12} + \hat{n}^{\mathrm{B}}_{i;\sigma} \; . \tag{6.91d}$$

In fact, this is a better choice than (6.88a) since it yields the correct ground-state energy in the uncorrelated limit $U = 0$ if the resulting effective Hamiltonian

$$\hat{\underline{H}}_{1\mathrm{B}} = \sum_{i,j,\sigma} t_{i,j}\hat{q}_{i,\sigma}\hat{c}^{\dagger}_{i,\sigma}\hat{q}^{\dagger}_{j,\sigma}\hat{c}_{j,\sigma} + U\sum_{i}\hat{n}^{\mathrm{B}}_{i;12} \tag{6.92}$$

is investigated on a mean-field level, see below.

Kotliar and Ruckenstein [125] used a functional integral approach to calculate the free energy of the Hamiltonian (6.92). For ground-state properties, i.e., at zero temperature, their saddle-point approach is equivalent to an evaluation of the Hamiltonian (6.92) by means of the variational wave function

$$\left|\Psi^{\mathrm{FB}}_0\right\rangle \equiv \left|\Psi^{\mathrm{B}}_0\right\rangle \otimes \left|\Psi_0\right\rangle \; . \tag{6.93a}$$

Here, we introduced a fermionic single-particle product state $|\Psi_0\rangle$ and a coherent bosonic state

$$\left|\Psi^{\mathrm{B}}_0\right\rangle \equiv \prod_i \hat{D}_i \left|0\right\rangle \tag{6.93b}$$

with

$$\hat{D}_i \equiv \prod_I \exp\left(\varphi_{i;I}\hat{\phi}^{\dagger}_{i;I}\right) . \tag{6.93c}$$

Note that, by construction, (6.93b) is an eigenstate of $\hat{\phi}_{i;I}$ with eigenvalues $\varphi_{i;I}$; see, e.g., reference [3]. Therefore, the coefficients $\varphi_{i;I}$ give the bosonic occupation

$$|\varphi_{i;I}|^2 = \langle \hat{n}^{\mathrm{B}}_{i;I} \rangle_{\Psi^{\mathrm{B}}_0} = n^{\mathrm{B}}_{i;I} \; , \tag{6.94}$$

which is determined by a minimisation of the ground-state energy functional

$$\langle \hat{\underline{H}}_{1\mathrm{B}} \rangle_{\Psi^{\mathrm{FB}}_0} = \sum_{i,j,s} t_{i,j} q^*_{i,\sigma} q_{j,s} \langle \hat{c}^\dagger_{i,\sigma} \hat{c}_{j,s} \rangle_{\Psi_0} + U \sum_i n^{\mathrm{B}}_{i;12} \; . \tag{6.95}$$

Here, the factors $q^*_{i,\sigma}$ and $q_{i,\sigma}$ are given in (6.91) with the operators $\hat{\phi}^{(\dagger)}_{i;I}$ replaced by their expectation values $\varphi^{(*)}_{i;I}$. Note that all quantities in this section are real and the asterisks, for example in equation (6.95), are only used for an easy comparison with the corresponding multi-band results in section 6.2.4.

In general, the wave function (6.93a) is not entirely in the physical Hilbert space $\underline{\mathcal{H}}$ and, hence, it violates the constraints (6.81). Therefore, instead of dealing with the exact constraints (6.81), we only satisfy them for their expectation values

$$1 = \sum_I n^{\mathrm{B}}_{i;I} \; , \tag{6.96a}$$

$$n^0_{i,\sigma} = n^{\mathrm{B}}_{i;12} + n^{\mathrm{B}}_{i;\sigma} \; , \tag{6.96b}$$

with respect to $\left|\Psi^{\mathrm{FB}}_0\right\rangle$ in the 'slave-boson mean-field theory' by Kotliar and Ruckenstein.

The constraints (6.96) and the energy functional (6.95) are the same as those derived for the Gutzwiller wave function in the limit of infinite spatial dimensions or evaluated by means of the Gutzwiller approximation in sections 5.2 and 6.1.1.

6.2.3 Hubbard Models with a Density-Density Interaction

A generalisation of the slave-boson theory is straightforward [175, 176] for multi-band Hubbard models with a local Coulomb interaction of the form

$$\hat{H}_{\mathrm{I}} = \sum_{\sigma,\sigma'} U_{\sigma,\sigma'} \hat{n}_\sigma \hat{n}_{\sigma'} = \sum_I U_I \hat{m}_I \; , \tag{6.97}$$

where

$$U_I = \sum_{\sigma,\sigma' \in I} U_{\sigma,\sigma'} \; . \tag{6.98}$$

For each atomic configuration $|I\rangle_i$, we introduce bosonic operators $\phi^{(\dagger)}_{i;I}$, which define an enlarged local Hilbert space $\mathcal{H}^{\mathrm{FB}}_i$ in the same way as in equations (6.80). A subspace $\underline{\mathcal{H}}_i$ of $\mathcal{H}^{\mathrm{FB}}_i$ that is isomorphic to the physical Hilbert space $\mathcal{H}_i$ is then given by the basis states $|\underline{I}\rangle_i$, defined in equation (6.84). For the mean-field treatment, one needs to define $\underline{\mathcal{H}}_i$ also by a set of constraints, which, as a generalisation of equations (6.81), are given as

$$\hat{F}_{i,0} \equiv 1 - \sum_I \hat{n}^{\mathrm{B}}_{i;I} = 0 \; , \tag{6.99a}$$

$$\hat{F}_{i,\sigma} \equiv \hat{c}^\dagger_{i,\sigma} \hat{c}_{i,\sigma} - \sum_{I(\sigma \in I)} \hat{n}^{\mathrm{B}}_{i;I} = 0 \; . \tag{6.99b}$$

The proper operators $\hat{\underline{c}}^{\dagger}_{i,\sigma}$ in $\underline{\mathcal{H}}_i$ that are similar to $\hat{c}^{\dagger}_{i,\sigma}$ and, eventually, lead to the correct mean-field results, have the form of equations (6.91) with

$$\hat{r}_{i,\sigma} \equiv \sum_{I(\sigma\notin I)} \hat{\phi}^{\dagger}_{i;I\cup\sigma}\hat{\phi}_{i;I} = \sum_{I,I'} {}_i\langle I|\hat{c}^{\dagger}_{i,\sigma}|I'\rangle_i\, \hat{\phi}^{\dagger}_{i;I}\hat{\phi}_{i;I'} \;, \tag{6.100a}$$

$$\hat{\Delta}_{i,\sigma} \equiv \sum_{I(\sigma\in I)} \hat{\phi}^{\dagger}_{i;I}\hat{\phi}_{i;I} \;. \tag{6.100b}$$

Altogether, we find the effective Hamiltonian

$$\hat{\underline{H}}_{\mathrm{H}} = \sum_{i,j}\sum_{\sigma,\sigma'} t^{\sigma,\sigma'}_{i,j}\, q^{\dagger}_{i,\sigma} q_{j,\sigma'} \hat{c}^{\dagger}_{i,\sigma}\hat{c}_{j,\sigma} + \sum_i \sum_I U_I \hat{n}^{\mathrm{B}}_{i;I} \tag{6.101}$$

with $\hat{n}^{\mathrm{B}}_{i;I}$ as defined in (6.82). A variational wave function of the form (6.93) yields the same energy functional as derived within the Gutzwiller theory.

6.2.4 General Multi-Band Hubbard Models

A generalisation of the slave-boson mean-field theory for the treatment of general multi-band Hubbard models has been derived by Dai et al. [177] and, more successfully, by Lechermann et al. [168]. As demonstrated in the previous sections, the slave-boson approach contains a number of adjustable objects. These rather flexible elements of the theory are the definition of the extended Hilbert space $\mathcal{H}_i$, the definition of its physical subspace $\underline{\mathcal{H}}_i$, the form of the constraint equations $\hat{F}_{i,\sigma} = 0$ and, finally, the particular definition of similar operators $\hat{\underline{Q}}_i$. Despite this huge flexibility, in both works the authors fail to derive an exact mapping of Hilbert spaces and Hamiltonians that, on a mean-field level, leads to satisfactory results.

Dai et al. use constraint equations that do not define the correct physical Hilbert space. This problem has been pointed out and solved by Lechermann et al. In their work, however, they fail to derive proper fermionic operators $\hat{\underline{c}}^{(\dagger)}_i$. Instead, certain symmetry arguments are employed to guess the form of certain operators $\hat{\underline{c}}^{(\dagger)}_i$, which yield a reasonable energy functional on mean-field level. These operators, however, are *not* similar to the physical operators $\hat{c}^{(\dagger)}_i$ and the whole derivation appears to be even less controlled than for the models discussed in the previous sections. Here, we summarise the main ideas of the slave-boson mean-field theory introduced by Lechermann et al. and show that their energy functional at zero temperature agrees with the results of the Gutzwiller theory; see also reference [178].

As in case of the Hubbard models discussed in the previous sections, one has to set up a local Hamiltonian $\underline{\mathcal{H}}_i$ that is isomorphic to the physical fermionic Hamiltonian $\mathcal{H}_i$ with its basis $|\Gamma\rangle_i$. Lechermann et al. discuss various possibilities to define such local Hilbert spaces consisting of bosons and fermions. At first sight, it seems that $\underline{\mathcal{H}}_i$ is most naturally defined as a generalisation of (6.84) through a basis

$$|\underline{\Gamma}\rangle_i \equiv |\Gamma\rangle_i \otimes |\Gamma\rangle_{i;\mathrm{B}} \tag{6.102}$$

with bosonic operators $\hat{\phi}^{(\dagger)}_{i;\Gamma}$ and the corresponding states $|\Gamma\rangle_{i;\mathrm{B}} \equiv \hat{\phi}^{\dagger}_{i;\Gamma}|0\rangle_{i;\mathrm{B}}$. However, the Hilbert-space $\underline{\mathcal{H}}_i$ defined by this basis is discarded by Lechermann et al. on the grounds that there is no way to find a reasonable set of constraint equations as an alternative definition of $\underline{\mathcal{H}}_i$. In section 6.2.5, we show that the basis (6.102) can, in fact, be used for a slave-boson theory, which, however, deviates significantly from the original scheme introduced by Kotliar and Ruckenstein.

Instead of (6.102), Lechermann et al. introduced the basis

$$|\underline{\Gamma}\rangle_i \equiv \frac{1}{\sqrt{|\Gamma|}} \sum_{I(|I|=|\Gamma|)} \hat{\phi}^\dagger_{i;\Gamma,I} \, |0\rangle_{i;\mathrm{B}} \otimes |I\rangle_i \tag{6.103}$$

as a definition of their Hilbert space $\underline{\mathcal{H}}_i$. Note that in their derivation they draw a distinction between physical particles and quasi-particles, described by operators $\hat{d}^{(\dagger)}_{i,\sigma}$ and $\hat{f}^{(\dagger)}_{i,\sigma}$, respectively. Our derivation in this section indicates that this distinction is unnecessary and confusing.

The Ansatz (6.103) employs bosonic operators $\hat{\phi}_{i;\Gamma,I}$ for each pair of multiplet states $|\Gamma\rangle$ and configurations states $|I\rangle$ with the same particle number $|\Gamma| = |I|$. The number of these operators is much larger than the dimension of the local Hilbert space, which is obviously different from the scheme introduced by Kotliar and Ruckenstein. Despite this large number of operators, the space $\underline{\mathcal{H}}_i$ is isomorphic to the physical Hilbert space $\mathcal{H}_i$ with its basis $|\Gamma\rangle_i$. Therefore, it is possible to find operators $\underline{\hat{O}}_i$ in $\underline{\mathcal{H}}_i$ that are *similar* to the physical operators $\hat{O}_i$ in $\mathcal{H}_i$, see below.

For the mean-field treatment, one has to find constraints that define the Hilbert space $\underline{\mathcal{H}}_i$ in a unique way. As shown in [168], this is achieved by means of the operator identities

$$\hat{F}_{i,0} = 1 - \sum_{\Gamma,I} \hat{\phi}^\dagger_{i;\Gamma,I} \hat{\phi}_{i;\Gamma,I} = 0 \, , \tag{6.104a}$$

$$\hat{F}_{i;\sigma,\sigma'} = \hat{c}^\dagger_{i,\sigma} \hat{c}_{i,\sigma'} - \sum_{\Gamma,I,I'} \hat{\phi}^\dagger_{i;\Gamma,I'} \hat{\phi}_{i;\Gamma,I} \; {}_i\langle I|\hat{c}^\dagger_{i,\sigma} \hat{c}_{i,\sigma'}|I'\rangle_i = 0 \, . \tag{6.104b}$$

The representation $\underline{\hat{m}}_{i;\Gamma,\Gamma'}$ of local operators $\hat{m}_{i;\Gamma,\Gamma'} = |\Gamma\rangle_{i\,i}\langle\Gamma|$ in $\underline{\mathcal{H}}_i$ is readily given by

$$\underline{\hat{m}}_{i;\Gamma,\Gamma'} = \sum_I \hat{\phi}^\dagger_{i;\Gamma,I} \hat{\phi}_{i;\Gamma',I} \, . \tag{6.105}$$

This result leads to

$$\underline{\hat{H}}_{i;\mathrm{loc}} = \sum_{\Gamma,\Gamma'} E^{\mathrm{loc}}_{i;\Gamma,\Gamma'} \sum_I \hat{\phi}^\dagger_{i;\Gamma,I} \hat{\phi}_{i;\Gamma',I} \tag{6.106}$$

for the representation of the local Hamiltonian (5.62).

In order to set up the effective Hamiltonian $\underline{\hat{H}}_{\mathrm{H}}$, one needs representations $\underline{\hat{c}}^\dagger_{i,\sigma}$ of fermionic creation operators. As proven in [168], a conceivable choice for $\underline{\hat{c}}^\dagger_{i,\sigma}$ is

$$\underline{\hat{c}}^\dagger_{i,\sigma} = \sum_{\sigma'} \hat{r}^{\sigma'}_{i,\sigma} \hat{c}^\dagger_{i,\sigma'} \, , \tag{6.107a}$$

where

$$\hat{r}^{\sigma'}_{i,\sigma} = \sum_{\Gamma,\Gamma'} \sum_{I,I'} \frac{{}_i\langle\Gamma|\hat{c}^\dagger_{i,\sigma}|\Gamma'\rangle_i \; {}_i\langle I|\hat{c}^\dagger_{i,\sigma}|I'\rangle_i}{\sqrt{|\Gamma|(N-|\Gamma'|)}} \hat{\phi}^\dagger_{i;\Gamma,I} \hat{\phi}_{i;\Gamma',I'} \tag{6.107b}$$

is a bosonic operator and N is the number of spin-orbital states $|\sigma\rangle$ per site. Evaluated on mean-field level, the expression (6.107) does not lead to a reasonable energy functional; it does not provide the correct results in the uncorrelated limit. The situation here, however, is different from the models discussed in the previous sections. There, it was possible to find improved expressions for the operator $\underline{\hat{c}}^\dagger_{i,\sigma}$, which were still similar to the physical operators $\hat{c}^\dagger_{i,\sigma}$, but lead to a satisfactory energy functional. In case of the operators (6.107), it seems impossible to improve them accordingly. Instead, Lechermann et al. introduce an 'improved'

expression for (6.107), which, though leading to reasonable results on the mean-field level, is mathematically *not* similar to $\hat{c}^\dagger_{i,\sigma}$. To work with such an improper operator, brings an element of arbitrariness into the whole slave-boson derivation, which is certainly unsatisfactory. We refer the reader to the work of Lechermann et al. where the 'improved' expression of $\underline{\hat{c}}^\dagger_{i,\sigma}$ is motivated in detail and just introduce their final result in our considerations here. Instead of $\hat{r}^{\sigma'}_{i,\sigma}$ in (6.107b) it is suggested in [168] to work with

$$\hat{q}^{\sigma'}_{i,\sigma} = \sum_{\Gamma,\Gamma'} \sum_{I,I'} \sum_{\gamma} {}_i\langle\Gamma|\hat{c}^\dagger_{i,\sigma}|\Gamma'\rangle_i \; {}_i\langle I|\hat{c}^\dagger_{i,\gamma}|I'\rangle_i \, \hat{\phi}^\dagger_{i;\Gamma,I}\hat{\phi}_{i;\Gamma',I'}\hat{M}_{i;\gamma,\sigma'} \;, \tag{6.108}$$

where

$$\hat{M}_{i;\sigma,\sigma'} \equiv \left(\frac{1}{2}[\hat{\Delta}^{(\mathrm{p})}_i\hat{\Delta}^{(\mathrm{h})}_i + \hat{\Delta}^{(\mathrm{h})}_i\hat{\Delta}^{(\mathrm{p})}_i]^{-1/2}\right)_{\sigma,\sigma'} \;, \tag{6.109}$$

and

$$\hat{\Delta}^{(\mathrm{p})}_{i;\sigma,\sigma'} = \sum_{\Gamma,I,I'} \hat{\phi}^\dagger_{i;\Gamma,I}\hat{\phi}_{i;\Gamma,I'} \, {}_i\langle I'|\hat{c}^\dagger_{i,\sigma}\hat{c}_{i,\sigma'}|I\rangle_i \;, \tag{6.110a}$$

$$\hat{\Delta}^{(\mathrm{h})}_{i;\sigma,\sigma'} = \sum_{\Gamma,I,I'} \hat{\phi}^\dagger_{i;\Gamma,I}\hat{\phi}_{i;\Gamma,I'} \, {}_i\langle I'|\hat{c}_{i,\sigma'}\hat{c}^\dagger_{i,\sigma}|I\rangle_i \;. \tag{6.110b}$$

Note that $\hat{\Delta}^{(\mathrm{h/p})}_{i;\sigma,\sigma'}$ and $\hat{M}_{i;\sigma,\sigma'}$ are considered as matrices with respect to the indices σ,σ' whose elements are bosonic operators. The square root and the inversion $[\ldots]^{-1/2}$ in (6.109) are defined with respect to this matrix structure.

The operators (6.106) and (6.108) define an effective Hamiltonian

$$\underline{\hat{H}}_{\mathrm{H}} = \sum_{i,j} t^{\sigma,\sigma'}_{i,j} \sum_{\sigma,\sigma'} \sum_{\gamma,\gamma'} \hat{q}^{\gamma}_{i,\sigma} \left(\hat{q}^{\gamma'}_{j,\sigma'}\right)^\dagger \hat{c}^\dagger_{i,\gamma}\hat{c}_{j,\gamma'} + \sum_i \underline{\hat{H}}_{i;\mathrm{loc}} \tag{6.111}$$

that can now be evaluated on mean-field level, i.e., by means of a wave function as defined in equation (6.93a) with the bosonic operator

$$\hat{D}_i \equiv \prod_{\Gamma,I} \exp\left(\varphi_{i;\Gamma,I}\hat{\phi}^\dagger_{i;\Gamma,I}\right) . \tag{6.112}$$

Like for the single-band model, the constraints (6.104) and the Hamiltonian (6.111) are readily evaluated with respect to the bosonic wave function by a replacement of the operators $\hat{\phi}^{(\dagger)}_{i;\Gamma,I}$ by their corresponding amplitudes $\varphi^{(*)}_{i;\Gamma,I}$. These amplitudes then serve as variational parameters.

We close this section with a proof that the energy functional that results from the mean-field treatment of the constraints (6.104) and of the Hamiltonian (6.111) agrees with our Gutzwiller variational results derived in section 5.2. For the rest of this section, we drop all lattice site indices since we are only dealing with local quantities.

As discussed before, the uncorrelated local density matrix $C^0_{\sigma,\sigma'}$, equation (5.35), is not diagonal, in general. It is therefore often useful to introduce a second orbital basis, defined by the operators $\hat{h}^{(\dagger)}_\gamma$ that, by construction, have a diagonal local density matrix, see equations (5.35)-(5.37). In order to show the equivalence of the Gutzwiller theory with the slave-boson results of this section, we have to work with both representations simultaneously. The operators $\hat{h}^\dagger_\gamma$ define Fock states $|H\rangle$, which can be used to write the multiplet states (4.26) as

$$|\Gamma\rangle = \sum_H T_{H,\Gamma}|H\rangle \;, \tag{6.113}$$

where the coefficients $T_{H,\Gamma}$ and $T_{I,\Gamma}$ are related through

$$T_{H,\Gamma} = \sum_I \Omega_{H,I} T_{I,\Gamma} \quad , \quad \Omega_{H,I} \equiv \langle H|I\rangle \; . \tag{6.114}$$

We start our comparison with the functional for the local energy, which has been derived in equation (5.65). The expectation value $m^0_{\Gamma_1,\Gamma_4}$ in that equation can be written as

$$\begin{aligned} m^0_{\Gamma_1,\Gamma_4} &= \sum_{H_1,H_4} T_{H_1,\Gamma_1} T^*_{H_4,\Gamma_4} m^0_{H_1,H_4} \; . \\ &= \sum_H T_{H,\Gamma_1} T^*_{H,\Gamma_4} m^0_H \end{aligned} \tag{6.115}$$

because, for a diagonal local density matrix in the h-representation, one finds

$$m^0_{H,H'} = \delta_{H,H'} m^0_H \; , \tag{6.116a}$$

$$m^0_H \equiv \prod_{\gamma(\text{occ.})} n^0_\gamma \prod_{\gamma'(\text{unocc.})} (1 - n^0_{\gamma'}) \; . \tag{6.116b}$$

In order to make contact with the slave-boson results, we need to bring (6.115) in the seemingly more complicated form

$$m^0_{\Gamma_1,\Gamma_4} = \sum_{H,H',I} T_{H,\Gamma_1} \Omega^*_{H,I} \sqrt{m^0_H} T^*_{H',\Gamma_4} \Omega_{H',I} \sqrt{m^0_{H'}} \; , \tag{6.117}$$

which is equivalent to (6.115) because of the completeness relation

$$\sum_I \Omega_{H',I} \Omega^*_{H,I} = \delta_{H,H'} \; . \tag{6.118}$$

We now introduce the new variational parameters

$$\varphi_{\Gamma,I} \equiv \sum_{\Gamma',H} \lambda_{\Gamma,\Gamma'} T^*_{H,\Gamma'} \Omega_{H,I} \sqrt{m^0_H} \; , \tag{6.119}$$

which allow us to write the expectation value (5.65) as

$$\langle \hat{H}_{\text{loc},i} \rangle_{\Psi_\text{G}} = \sum_{\Gamma,\Gamma'} \sum_I \varphi^*_{\Gamma,I} \varphi_{\Gamma',I} E^{\text{loc}}_{\Gamma,\Gamma'} \; . \tag{6.120}$$

This equation has the same form as equation (6.106) after the bosonic operators $\hat{\phi}^{(\dagger)}_{\Gamma,I}$ have been replaced by their mean-field expectation values $\varphi^{(*)}_{\Gamma,I}$.

We now address the constraints (5.47). The first constraint (5.47a) can be written as

$$\sum_{\Gamma,\Gamma_1,\Gamma_2} \lambda^*_{\Gamma,\Gamma_1} \lambda_{\Gamma,\Gamma_2} m^0_{\Gamma_1,\Gamma_2} = 1 \; , \tag{6.121}$$

which, by use of equations (6.117) and (6.119), is found to be equivalent to

$$\sum_{\Gamma,I} \varphi^*_{\Gamma,I} \varphi_{\Gamma,I} = 1 \; . \tag{6.122}$$

This is the equation (6.104a) at mean-field level.

A set of constraints equivalent to (5.47a) is obtained when we use the operators $\hat{h}_\gamma^{(\dagger)}$,

$$\langle \hat{h}_\gamma^\dagger \hat{h}_{\gamma'} \hat{P}^\dagger \hat{P} \rangle_{\Psi_0} = \langle \hat{h}_\gamma^\dagger \hat{h}_{\gamma'} \rangle_{\Psi_0} \ . \tag{6.123}$$

As shown in section 5.2.1, this equation leads to

$$\sum_{\Gamma,\Gamma_1,\Gamma_2} \sum_{H_1,H_2} \lambda^*_{\Gamma,\Gamma_1} \lambda_{\Gamma,\Gamma_2} T_{H_1,\Gamma_1} T^*_{H_2,\Gamma_2} \langle H_2 | \hat{h}_\gamma^\dagger \hat{h}_{\gamma'} | H_1 \rangle \sqrt{m^0_{H_1} m^0_{H_2}} = \langle \hat{h}_\gamma^\dagger \hat{h}_{\gamma'} \rangle_{\Psi_0} \ . \tag{6.124}$$

Then, the identity

$$\langle H_2 | \hat{h}_\gamma^\dagger \hat{h}_{\gamma'} | H_1 \rangle = \sum_{I_1,I_2} \Omega_{H_2,I_2} \langle I_2 | \hat{h}_\gamma^\dagger \hat{h}_{\gamma'} | I_1 \rangle \Omega^*_{H_1,I_1} \tag{6.125}$$

transforms equation (6.124) into the form

$$\sum_\Gamma \sum_{I,I'} \varphi^*_{\Gamma,I} \varphi_{\Gamma,I'} \langle I' | \hat{h}_\gamma^\dagger \hat{h}_{\gamma'} | I \rangle = \langle \hat{h}_\gamma^\dagger \hat{h}_{\gamma'} \rangle_{\Psi_0} \ . \tag{6.126}$$

These equations can be transformed to the c-representation, which leads to

$$\sum_\Gamma \sum_{I,I'} \varphi^*_{\Gamma,I'} \varphi_{\Gamma,I} \langle I | \hat{c}_\sigma^\dagger \hat{c}_{\sigma'} | I' \rangle = \langle \hat{c}_\sigma^\dagger \hat{c}_{\sigma'} \rangle_{\Psi_0} \ , \tag{6.127}$$

and is equivalent to equation (6.104b) at mean-field level.

Finally, we consider the renormalisation matrix $q_\sigma^{\sigma'}$ in the c-representation, see equation (5.80a), which is related to the corresponding matrix $\tilde{q}_\gamma^{\gamma'}$ in the h-representation, see in equation (5.83), via

$$q_\sigma^{\sigma'} = \sum_{\gamma,\gamma'} \tilde{q}_\gamma^{\gamma'} u^*_{\gamma,\sigma} u_{\gamma',\sigma'} \ . \tag{6.128}$$

We write the expectation value in (5.83) as

$$\left\langle \left(|\Gamma_1\rangle\langle\Gamma_4| \hat{h}_{\gamma'} \right) \right\rangle_{\Psi_0} = \sum_{H_1,H_4} T_{H_1,\Gamma_1} T^*_{H_4,\Gamma_4} \langle H_4 | \hat{h}_{\gamma'} | H_1 \rangle \sqrt{m^0_{H_1} m^0_{H_4}} \sqrt{\frac{n^0_{\gamma'}}{1-n^0_{\gamma'}}} \ . \tag{6.129}$$

Together with equations (6.118) and (6.119) this leads to

$$\tilde{q}_\gamma^{\gamma'} = \sqrt{\frac{1}{n^0_{\gamma'}(1-n^0_{\gamma'})}} \sum_{\Gamma,\Gamma'} \sum_{I,I'} \varphi^*_{\Gamma,I} \varphi_{\Gamma',I'} \langle \Gamma | \hat{h}_\gamma^\dagger | \Gamma' \rangle \langle I' | \hat{h}_{\gamma'} | I \rangle \ . \tag{6.130}$$

The transformation (6.128) from the h-representation back to the c-representation is not as straightforward as the corresponding transformation from equation (6.126) to equation (6.127), whereas the transformation with respect to the lower index γ is still simple,

$$\langle \Gamma | \hat{c}_\sigma^\dagger | \Gamma' \rangle = \sum_\gamma \langle \Gamma | \hat{h}_\gamma^\dagger | \Gamma' \rangle u^*_{\gamma,\sigma} \ . \tag{6.131}$$

For the upper index γ', we need to take into account the factor $\sqrt{1/(n^0_{\gamma'}(1-n^0_{\gamma'}))}$ in (6.130), which also depends on γ'. For this purpose, we introduce the hole density matrix $\tilde{D}^0$ with the elements

$$D^0_{\sigma,\sigma'} \equiv \langle \hat{c}_{\sigma'} \hat{c}_\sigma^\dagger \rangle_{\Psi_0} \ , \tag{6.132}$$

in addition to the density matrix $\tilde{C}^0$ already defined in (5.35). Then, the transformation (6.128) for the upper index γ' can be carried out along the lines

$$\begin{aligned}\sum_{\gamma'} u_{\gamma',\sigma'} \frac{\hat{h}_{\gamma'}}{\sqrt{n^0_{\gamma'}(1-n^0_{\gamma'})}} &= \sum_{\gamma',\tilde{\sigma}} \frac{u_{\gamma',\sigma'} u^*_{\gamma',\tilde{\sigma}}}{\sqrt{n^0_{\gamma'}(1-n^0_{\gamma'})}} \hat{c}_{\tilde{\sigma}} \\ &\equiv \sum_{\tilde{\sigma}} \left((\tilde{C}^0 \tilde{D}^0)^{-\frac{1}{2}} \right)_{\tilde{\sigma},\sigma'} \hat{c}_{\tilde{\sigma}} \; .\end{aligned} \tag{6.133}$$

Here, we used the notation

$$\sum_{\gamma'} \frac{u_{\gamma',\sigma'} u^*_{\gamma',\tilde{\sigma}}}{\sqrt{n^0_{\gamma'}(1-n^0_{\gamma'})}} = \left((\tilde{C}^0 \tilde{D}^0)^{-\frac{1}{2}} \right)_{\tilde{\sigma},\sigma'} \; . \tag{6.134}$$

With equation (6.134) and $\langle I'|\hat{c}_{\tilde{\sigma}}|I\rangle = \langle I|\hat{c}^\dagger_{\tilde{\sigma}}|I'\rangle$, we can finally write the renormalisation-matrix in the c-representation as

$$q^{\sigma'}_{\sigma} = \sum_{\Gamma,\Gamma'} \sum_{I,I'} \varphi^*_{\Gamma,I} \varphi_{\Gamma',I'} \langle \Gamma|\hat{c}^\dagger_{\sigma}|\Gamma'\rangle \sum_{\tilde{\sigma}} \left((\tilde{C}^0 \tilde{D}^0)^{-\frac{1}{2}} \right)_{\tilde{\sigma},\sigma'} \langle I|\hat{c}^\dagger_{\tilde{\sigma}}|I'\rangle \; . \tag{6.135}$$

This expression matches equation (6.108) at mean-field level, apart from the fact that the constraints have been used to write the matrices $\Delta^{(\mathrm{p})} (\hat{=} \tilde{C}^0)$ and $\Delta^{(\mathrm{h})} (\hat{=} \tilde{D}^0)$ as a function of the fields $\varphi_{\Gamma,I}$; see equations (6.110). However, as long as the constraints are fulfilled, this makes no difference because it does not change the variational energy functional.

6.2.5 Alternative Slave-Boson Scheme for Multi-Band Hubbard Models

As discussed in the previous section, a generalisation of the Kotliar-Ruckenstein scheme for the investigation of multi-band models faces significant problems that, up to now, have not been resolved satisfactorily. In this section, we show that, due to the enormous flexibility of the slave-boson approach, it is, in fact, relatively easy to reproduce the Gutzwiller energy functional for multi-band Hubbard models. To this end, however, one has to approach the problem in a different way from Kotliar and Ruckenstein. We start with a reconsideration of the slave-boson theory for the one-band model as discussed in section 6.2.2

As pointed out before, there is a large amount of arbitrariness in the choice, e.g., of the constraints (6.81). Instead of those equations, we can also work with

$$\hat{F}_{i,0} \equiv 1 - \sum_I \hat{m}_{i;I} \hat{n}^{\mathrm{B}}_{i;I} \; , \tag{6.136a}$$

$$\hat{F}_{i,\sigma} \equiv \hat{n}_{i,\sigma} - \hat{n}_{i,\sigma} \sum_I \hat{m}_{i;I} \hat{n}^{\mathrm{B}}_{i;I} \; , \tag{6.136b}$$

where $\hat{m}_{i;I}$ and $\hat{n}^{\mathrm{B}}_{i;I}$ are defined in equations (4.9) and (6.82) respectively. Note that the Hilbert space $\underline{\hat{H}}_i$ given by the basis (6.84), is already uniquely defined by the first constraint, equation (6.136a). In $\underline{\hat{H}}_i$, however, the second equation is equally valid, i.e., it is $\hat{F}_{i,\sigma} \, |\underline{I}\rangle_i = 0$ for all states (6.84).

In the Kotliar-Ruckenstein scheme, the operators $\underline{\hat{m}}_{i;I}$ are chosen as $n^{\mathrm{B}}_{i;I}$. In our approach, we work with

$$\underline{\hat{m}}_{i;I} \equiv \hat{m}_{i;I} \hat{n}^{\mathrm{B}}_{i;I} \; . \tag{6.137}$$

Evaluated on mean-field level, i.e., with the wave function (6.93a), one finds

$$\langle \underline{\hat{m}}_{i;I} \rangle_{\Psi^{\mathrm{FB}}_0} = \langle \hat{m}_{i;I} \rangle_{\Psi_0} n^{\mathrm{B}}_{i;I} \; , \tag{6.138}$$

where $n^{\mathrm{B}}_{i;I} = |\varphi_{i;I}|^2$. A comparison with the corresponding results in the Gutzwiller theory, equations (5.68), shows that the bosonic amplitudes in our alternative slave-boson scheme correspond to the Gutzwiller variational parameters λ_I,

$$\lambda_{i;I} \hat{=} \varphi_{i;I} \ . \tag{6.139}$$

This equivalence leads to the constraints (6.136),

$$1 = \sum_I |\varphi_{i;I}|^2 \langle \hat{m}_{i;I} \rangle_{\Psi_0} \ , \tag{6.140a}$$

$$\hat{n}^0_{i,\sigma} = |\varphi_{i;\sigma}|^2 \langle \hat{m}_{i;\sigma} \rangle_{\Psi_0} + |\varphi_{i;12}|^2 \langle \hat{m}_{i;12} \rangle_{\Psi_0} \tag{6.140b}$$

on mean-field level, which agree with those in the Gutzwiller theory, see equations (5.53).

We choose the operators $\underline{\hat{c}}^\dagger_{i;\sigma}$ in $\underline{\hat{H}}_i$ as

$$\underline{\hat{c}}^\dagger_{i,\sigma} = \hat{q}_{i,\sigma} \hat{c}^\dagger_{i,\sigma} \quad , \quad \underline{\hat{c}}_{i,\sigma} = \hat{r}^\dagger_{i,\sigma} \hat{c}_{i,\sigma}; \tag{6.141a}$$

where

$$\hat{q}_{i,\sigma} \equiv \hat{\phi}^\dagger_{i;12} \hat{\phi}_{i;\bar{\sigma}} \hat{n}_{i,\bar{\sigma}} + \hat{\phi}^\dagger_{i;\sigma} \hat{\phi}_{i;\emptyset} (1 - \hat{n}_{i,\bar{\sigma}}) \ . \tag{6.141b}$$

Note that here, unlike in the Kotliar-Ruckenstein scheme, the operators $\hat{q}^{(\dagger)}_{i,\sigma}$ contain both fermionic and bosonic degrees of freedom. Evaluated with the wave function (6.93a), one finds

$$\hat{q}_{i,\sigma} = \langle \hat{q}_{i,\sigma} \rangle_{\Psi_0^{\mathrm{FB}}} = \varphi^*_{i;12} \varphi_{i;\bar{\sigma}} n^0_{i,\bar{\sigma}} + \varphi^*_{i;\sigma} \varphi_{i;\emptyset} (1 - n^0_{i,\bar{\sigma}}) \ , \tag{6.142}$$

which agrees with equation (5.85a). However, the expectation value of a hopping operator is the same as in the Gutzwiller theory,

$$\langle \underline{\hat{c}}^\dagger_{i,\sigma} \underline{\hat{c}}_{j,\sigma'} \rangle_{\Psi_0^{\mathrm{FB}}} = \hat{q}_{i,\sigma} \hat{q}^*_{j,\sigma} \langle \hat{c}^\dagger_{i,\sigma} \hat{c}_{j,\sigma} \rangle_{\Psi_0} \ , \tag{6.143}$$

only if we neglect the 'three-line' contributions

$$(\varphi^*_{i;12} \varphi_{i;\bar{\sigma}} - \varphi^*_{i;\sigma} \varphi_{i;\emptyset})^2 |\langle \hat{c}^\dagger_{i,\bar{\sigma}} \hat{c}_{j,\bar{\sigma}} \rangle_{\Psi_0}|^2 \langle \hat{c}^\dagger_{i,\sigma} \hat{c}_{j,\sigma} \rangle_{\Psi_0} \approx 0 \ . \tag{6.144}$$

These terms emerge when the expectation value $\langle \hat{n}_{i,\bar{\sigma}} \hat{c}^\dagger_{i,\sigma} \hat{c}_{j,\sigma} \hat{n}_{j,\bar{\sigma}} \rangle_{\Psi_0}$ is evaluated by means of Wick's theorem,

$$\langle \hat{n}_{i,\bar{\sigma}} \hat{c}^\dagger_{i,\sigma} \hat{c}_{j,\sigma} \hat{n}_{j,\bar{\sigma}} \rangle_{\Psi_0} = n^0_{i,\bar{\sigma}} n^0_{j,\bar{\sigma}} \langle \hat{c}^\dagger_{i,\sigma} \hat{c}_{j,\sigma} \rangle_{\Psi_0} + |\langle \hat{c}^\dagger_{i,\bar{\sigma}} \hat{c}_{j,\bar{\sigma}} \rangle_{\Psi_0}|^2 \langle \hat{c}^\dagger_{i,\sigma} \hat{c}_{j,\sigma} \rangle_{\Psi_0} \ . \tag{6.145}$$

Since the three-line terms vanish in the limit of infinite spatial dimensions, our slave-boson approach and the Gutzwiller theory yield the same variational ground-state energy.

A generalisation of our new slave-boson scheme for multi-band models is straightforward. We work with an arbitrary set of local multiplet states $|\Gamma\rangle_i$, which define the basis (6.102) of a Hilbert space $\underline{\mathcal{H}}_i$. As a generalisation of (6.136), we introduce the constraints

$$\hat{F}_{i,0} \equiv 1 - \sum_\Gamma \hat{m}_{i;\Gamma} \hat{n}^{\mathrm{B}}_{i;\Gamma} \ , \tag{6.146a}$$

$$\hat{F}_{i;\sigma,\sigma'} \equiv \hat{c}^\dagger_{i,\sigma} \hat{c}_{i,\sigma'} - \hat{c}^\dagger_{i,\sigma} \hat{c}_{i,\sigma'} \sum_\Gamma \hat{m}_{i;\Gamma} \hat{n}^{\mathrm{B}}_{i;\Gamma} \ , \tag{6.146b}$$

which yield an alternative way to define the Hilbert space $\underline{\mathcal{H}}_i$.

The operators $\hat{m}_{i;\Gamma,\Gamma'}$ are properly represented in $\underline{\mathcal{H}}_i$ by

$$\underline{\hat{m}}_{i;\Gamma,\Gamma'} \equiv \hat{m}_{i;\Gamma,\Gamma'} \hat{\phi}^\dagger_{i;\Gamma} \hat{\phi}_{i;\Gamma'} \ . \tag{6.147}$$

An evaluation of these operators on mean-field level, i.e, by means of a wave function (6.93), with

$$\hat{D}_i \equiv \prod_{\Gamma} \exp\left(\varphi_{i;\Gamma}\hat{\phi}^{\dagger}_{i;\Gamma}\right) , \tag{6.148}$$

leads to

$$m_{i;\Gamma,\Gamma'} = \langle \underline{\hat{m}}_{i;\Gamma,\Gamma'}\rangle_{\Psi_0^{\mathrm{FB}}} = \langle \hat{m}_{i;\Gamma,\Gamma'}\rangle_{\Psi_0}\varphi^{*}_{i;\Gamma}\varphi_{i;\Gamma'} . \tag{6.149}$$

Through a comparison with the corresponding Gutzwiller result,

$$m_{i;\Gamma,\Gamma'} = \langle \hat{m}_{i;\Gamma,\Gamma'}\rangle_{\Psi_0}\lambda^{*}_{i;\Gamma}\lambda_{i;\Gamma'}, \tag{6.150}$$

for a diagonal variational-parameter matrix $\lambda_{i;\Gamma,\Gamma'} \equiv \delta_{\Gamma,\Gamma'}\lambda_{i;\Gamma}$, we find the correspondence

$$\lambda_{i;\Gamma} \hat{=} \varphi_{i;\Gamma} \tag{6.151}$$

of the variational parameters $\lambda_{i;\Gamma,\Gamma'}$ in the Gutzwiller theory and the amplitudes $\varphi_{i;\Gamma}$ in our slave-boson mean-field theory. An evaluation of the constraints (6.146) on mean-field level leads to

$$1 = \sum_{\Gamma} \varphi^{*}_{i;\Gamma}\varphi_{i;\Gamma}\langle \hat{m}_{i;\Gamma,\Gamma'}\rangle_{\Psi_0} , \tag{6.152a}$$

$$\langle \hat{c}^{\dagger}_{i,\sigma}\hat{c}_{i,\sigma'}\rangle_{\Psi_0} = \sum_{\Gamma} \varphi^{*}_{i;\Gamma}\varphi_{i;\Gamma}\langle \hat{c}^{\dagger}_{i,\sigma}\hat{c}_{i,\sigma'}\hat{m}_{i;\Gamma,\Gamma'}\rangle_{\Psi_0} , \tag{6.152b}$$

which matches the Gutzwiller constraints, see equations (5.48), for a diagonal variational-parameter matrix.

Finally, we define the operator

$$\underline{\hat{c}}^{\dagger}_{i,\sigma} \equiv \sum_{\sigma'} \hat{q}^{\sigma'}_{i,\sigma}\hat{c}^{\dagger}_{i,\sigma} \tag{6.153a}$$

with

$$\hat{q}^{\sigma'}_{\sigma} = \sum_{\Gamma,\Gamma'} \hat{\phi}^{\dagger}_{\Gamma}\hat{\phi}_{\Gamma'}\langle\Gamma|\hat{c}^{\dagger}_{\sigma}|\Gamma'\rangle \sum_{I,I'} T_{I,\Gamma}T^{*}_{I',\Gamma'}\hat{H}^{\sigma'}_{I,I'} . \tag{6.153b}$$

Here, we dropped the site index i and introduced the operator

$$\begin{aligned} \hat{H}^{\sigma'}_{I,I'} \equiv\ & (1-f_{\sigma',I})\langle I'|\hat{c}_{\sigma'}|I'\cup\sigma'\rangle\hat{m}_{I,I'\cup\sigma'} \\ & +\langle I\backslash\sigma'|\hat{c}_{\sigma'}|I\rangle\left(f_{\sigma',I'}\hat{m}_{I\backslash\sigma',I'} + (1-f_{\sigma',I'})\hat{m}^{\sigma'}_{I\backslash\sigma',I'}\right) . \end{aligned} \tag{6.154}$$

Note that the expectation value of $\hat{H}^{\sigma'}_{I,I'}$ has already been introduced in equation (5.81), section 5.2.5. There, we also used the abbreviation $f_{\sigma,I} = \langle I|\hat{c}^{\dagger}_{\sigma}\hat{c}_{\sigma}|I\rangle$ and the expectation value of the operator

$$\hat{m}^{\sigma}_{I,I'} \equiv \hat{C}^{\dagger}_{I}\hat{C}_{I'}\prod_{\sigma'\in J\backslash\sigma}(1-\hat{n}_{\sigma'}) , \tag{6.155}$$

which is defined for $\sigma \in J \equiv \overline{I\cup I'}$. The operator $\underline{\hat{c}}^{\dagger}_{i,\sigma}$ in $\underline{\mathcal{H}}_i$ is similar to the physical creation operator $\hat{c}^{\dagger}_{i,\sigma}$. This follows from the fact that the sums over σ' and I, I' in equations (6.153) are just a complicated expression for

$$|\Gamma\rangle\langle\Gamma'| = \sum_{\sigma'}\sum_{I,I'} T_{I,\Gamma}T^{*}_{I',\Gamma'}\hat{H}^{\sigma'}_{I,I'}\hat{c}^{\dagger}_{\sigma'} . \tag{6.156}$$

A mean-field evaluation of (6.153b) leads to the renormalisation matrix

$$q_\sigma^{\sigma'} = \sum_{\Gamma,\Gamma'} \varphi^*_{i;\Gamma}\varphi_{i;\Gamma'} \langle \Gamma | \hat{c}^\dagger_{i,\sigma} | \Gamma' \rangle \sum_{I,I'} T_{I,\Gamma} T^*_{I',\Gamma'} H^{0;\sigma'}_{I,I'} \;, \tag{6.157}$$

which matches equation (5.81) in the Gutzwiller theory. As in the single-band model, the expectation values of hopping operators agree with those in the Gutzwiller theory

$$\langle \hat{\underline{c}}^\dagger_{i,\sigma_1} \hat{\underline{c}}_{i,\sigma_2} \rangle_{\Psi_0^{\mathrm{FB}}} = \sum_{\sigma_1',\sigma_2'} q^{\sigma_1'}_{i,\sigma_1} \left(q^{\sigma_2'}_{j,\sigma_2} \right)^* \langle \hat{c}^\dagger_{i,\sigma_1'} \hat{c}_{j,\sigma_2'} \rangle_{\Psi_0} \;, \tag{6.158}$$

only if we neglect the contributions with more than one line connecting the sites i and j. This is ensured in the limit of infinite spatial dimensions, where both approaches then yield the same ground-state energy functional.

6.2.6 Merits and Shortcomings of Slave-Boson Theories

As we have shown in the previous sections, the slave-boson mean-field theory provides an alternative way to determine the Gutzwiller ground-state energy functional for multi-band Hubbard models. We believe, however, that there are good reasons to prefer the derivation based on Gutzwiller wave functions over the slave-boson mean-field theory. These wave functions are well defined and they are evaluated exactly in the unambiguous limit of infinite spatial dimensions, $D \to \infty$. In contrast, the slave-boson mean-field derivation is uncontrolled and, as we have seen, quite adjustable in its outcome. Of all the different equations that one may derive within such an approach, the 'right ones' are usually identified by some sophisticated guess. This guess, not surprisingly, always turns out to be equivalent to the Gutzwiller theory. This very equivalence is by far the most convincing argument for the credibility of the slave-boson results.

The derivation by Lechermann et al. is particularly problematic because it works with an inaccurate representation of the fermionic creation and annihilation operators. This shortcoming also prevents an improvement of the results by computing fluctuations around the saddle point within a functional integral representation. It should be mentioned, however, that the promise of such an expansion, although often made, has never materialised in any convincing improvement of the results, not even for the one-band Hubbard model [179]. In contrast, it is possible to calculate systematically $1/D$ corrections for Gutzwiller wave functions for all physical quantities [133, 180]. Such calculations allow one to estimate the accuracy of the results in infinite dimensions and to improve them systematically, if necessary.

The Gutzwiller theory can also be used to calculate quasi-particle excitations within a Fermi-liquid approach, see section 7.3. The quasi-particle bands in the Gutzwiller theory coincide with those derived in the slave-boson mean-field theory by Lechermann et al. Therefore, the zero-temperature spectral properties are equivalent in both approaches.

The functional integral representation of the slave-boson mean-field theory provides a way to investigate systems at finite temperatures. On the other hand, the Gutzwiller ground-state energy functional also provides the Landau parameters for the description of thermodynamic properties [105]. Therefore, both approaches are equivalent in the Fermi-liquid regime when the temperatures T is much smaller than the Fermi temperature T_{F}. Although the slave-boson mean-field equations can also be solved for $T \approx T_{\mathrm{F}}$ or even for $T \gg T_{\mathrm{F}}$, the approximation breaks down in this temperature regime [181].

Chapter 7

Single-Particle Excitations

As we will show in this chapter, the Gutzwiller theory does not only provide an approximate ground-state description of multi-band Hubbard models, but it also allows us to calculate quasi-particle excitation energies. To this end, we first summarise the basic results of the microscopic Fermi-liquid theory in section 7.1 and Landau's phenomenological approach in section 7.2. In section 7.3, we introduce our Gutzwiller quasi-particle theory.

7.1 Spectral Function of a Fermi Liquid

7.1.1 Definitions

The essential quantity for the investigation of the Hubbard models (2.15) with respect to single-particle excitations is the retarded Green's function,

$$G_{i,j}^{\sigma,\sigma'}(t) \equiv -\mathrm{i}\Theta(t)\langle\Phi_0|\{\hat{c}_{i,\sigma}(t), \hat{c}_{j,\sigma'}^{\dagger}(0)\}|\Phi_0\rangle \;, \tag{7.1}$$

or its Fourier transform,

$$G_{\boldsymbol{k}}^{\sigma,\sigma'}(\omega) \equiv \frac{1}{L}\sum_{i,j} e^{\mathrm{i}\boldsymbol{k}(\boldsymbol{R}_i-\boldsymbol{R}_j)} \int_0^{\infty} \mathrm{d}t\, e^{\mathrm{i}\omega t} G_{i,j}^{\sigma,\sigma'}(t) \;. \tag{7.2}$$

Here, $|\Phi_0\rangle$ is the exact ground state of our Hamiltonian (2.15), $\hat{H} \equiv \hat{H}_{\mathrm{H}}$, and

$$\hat{c}_{i,\sigma}^{(\dagger)}(t) = e^{\mathrm{i}\hat{H}t}\hat{c}_{i,\sigma}^{(\dagger)}e^{-\mathrm{i}\hat{H}t} \tag{7.3}$$

are the Heisenberg representations of the operators $\hat{c}_{i,\sigma}^{(\dagger)}$. For a comparison with experiments, the spectral density

$$S_{\boldsymbol{k}}(\omega) \equiv -\frac{1}{\pi}\sum_{\sigma} \mathrm{Im}\left[G_{\boldsymbol{k}}^{\sigma,\sigma}(\omega)\right] \tag{7.4}$$

is of particular interest because it can be measured, e.g., by 'angle-resolved photoemission spectroscopy' (ARPES) [182]. Note that the spectral density (7.4) obeys the sum rule

$$\int_{-\infty}^{\infty} \mathrm{d}\omega S_{\boldsymbol{k}}(\omega) = N \;, \tag{7.5}$$

where N is the number of bands or spin-orbitals in the Hubbard Hamiltonian (2.15).

In the uncorrelated limit, $\hat{H}_{\mathrm{I}} = 0$, the spectral function

$$S_{\boldsymbol{k}}^{0}(\omega) = \sum_{\gamma} \delta\left(\omega - E_{\boldsymbol{k},\gamma}^{0}\right) \tag{7.6}$$

has sharp δ-peaks at the band energies $E^0_{\boldsymbol{k},\gamma}$ of the single-particle Hamiltonian $\hat{H}_0$, see equation (2.16). This explains the term 'spectral function' for $S_{\boldsymbol{k}}(\omega)$. The corresponding non-interacting Green's function is given by

$$G^{\sigma,\sigma'}_{0;\boldsymbol{k}}(\omega) = \sum_\gamma u^*_{\gamma,\sigma}(\boldsymbol{k}) \frac{1}{\omega - E^0_{\boldsymbol{k},\gamma} + \mathrm{i}\delta} u_{\gamma,\sigma'}(\boldsymbol{k}) \;, \tag{7.7}$$

where the unitary matrix $u_{\gamma,\sigma}(\boldsymbol{k})$ was introduced in equation (2.18) and $\delta = 0^+$ is an infinitesimal increment. Note that we may consider the Green's functions (7.2) as the elements of a matrix $\tilde{G}_{\boldsymbol{k}}(\omega)$ with respect to the indices σ, σ'. Then, the uncorrelated Green's function matrix can also be written as

$$\tilde{G}_{0;\boldsymbol{k}}(\omega) = [\omega - \tilde{\varepsilon}^0_{\boldsymbol{k}} + \mathrm{i}\delta]^{-1} \;, \tag{7.8}$$

where the elements $\tilde{\varepsilon}^0_{\boldsymbol{k};\sigma,\sigma'}$ of the matrix $\tilde{\varepsilon}^0_{\boldsymbol{k}}$ were introduced in equation (2.17a).

7.1.2 Single-Band Greens's Function

We start our considerations with the single-band Hubbard model where $\sigma = \uparrow, \downarrow$ is a spin-index and the unitary matrix $u_{\gamma,\sigma}(\boldsymbol{k}) = \delta_{\gamma,\sigma}$ is diagonal. For this model, we can write the Green's function as

$$G^\sigma_{\boldsymbol{k}}(\omega) = \frac{1}{\omega - \varepsilon^0_{\boldsymbol{k}} - \Sigma_\sigma(\boldsymbol{k},\omega)} \;, \tag{7.9}$$

where, by definition, the entire influence of the Coulomb interaction is encoded in the 'self-energy' $\Sigma_\sigma(\boldsymbol{k},\omega)$. The spin index of the self-energy only matters for systems with ferromagnetic order, whereas in paramagnetic systems we have $\Sigma_\sigma(\boldsymbol{k},\omega) = \Sigma(\boldsymbol{k},\omega)$. Note that equation (7.9) is equivalent to

$$G^\sigma_{\boldsymbol{k}}(\omega)^{-1} = G^\sigma_{0;\boldsymbol{k}}(\omega)^{-1} - \Sigma_\sigma(\boldsymbol{k},\omega) \;, \tag{7.10}$$

which can be read as a definition of the self-energy.

In a diagrammatic expansion of the (time-ordered) Green's function, the self-energy can be expressed as a sum of a well-defined class of diagrams; see any text book on many-particle physics, e.g., references [3, 30, 183]. In fermionic systems, it turns out [34, 36, 184, 185] that the self-energy in the thermodynamic limit has the form

$$\Sigma_\sigma(\boldsymbol{k}, \omega \to E_\mathrm{F}) = \Sigma^0_\sigma(\boldsymbol{k}) + \Sigma^\mathrm{R}_\sigma(\boldsymbol{k})(\omega - E_\mathrm{F}) + \mathrm{i}\Sigma^\mathrm{I}_\sigma(\boldsymbol{k})(\omega - E_\mathrm{F})^2 \tag{7.11}$$

around the Fermi energy E_F, provided that the diagrammatic expansion converges properly. Note that the very existence of such a Fermi energy for a correlated system is already a profoundly non-trivial result of the diagrammatic expansion. With the self-energy (7.11), the Green's function near the Fermi energy reads

$$G^\sigma_{\boldsymbol{k}}(\omega \to E_\mathrm{F}) = \frac{1}{\omega - E^0_{\boldsymbol{k},\sigma} - \Sigma^\mathrm{R}_\sigma(\boldsymbol{k})(\omega - E_\mathrm{F}) - \mathrm{i}\Sigma^\mathrm{I}_\sigma(\boldsymbol{k})(\omega - E_\mathrm{F})^2} \;, \tag{7.12}$$

where we introduced the shifted energies $E^0_{\boldsymbol{k},\sigma} = \varepsilon^0_{\boldsymbol{k}} + \Sigma^0_\sigma(\boldsymbol{k})$. The identity

$$\mathrm{Im}\left[\frac{1}{x + \mathrm{i}\delta}\right] \to -\pi\delta(x) \quad \text{for} \quad \delta \to 0^+ \tag{7.13}$$

holds in our case because $\delta = -\Sigma^\mathrm{I}(\boldsymbol{k})(\omega - E_\mathrm{F})^2 \to 0^+$ and $\Sigma^\mathrm{I} < 0$ follows from the analyticity of $G_{\boldsymbol{k}}(z)$ in the upper complex plane. Equation (7.12) leads to the spectral density

$$S_{\boldsymbol{k}}(\omega \to E_\mathrm{F}) = \sum_\sigma \delta\left(\omega - E^0_{\boldsymbol{k},\sigma} - \Sigma^\mathrm{R}_\sigma(\boldsymbol{k})(\omega - E_\mathrm{F})\right) \tag{7.14}$$

for values of ω around $E_{\rm F}$. The δ-function gives finite contributions for $\omega = E_{\boldsymbol{k},\sigma}$ with

$$E_{\boldsymbol{k},\sigma} - E_{\rm F} = z_\sigma(\boldsymbol{k})(E^0_{\boldsymbol{k},\sigma} - E_{\rm F}) \tag{7.15}$$

and

$$z_\sigma(\boldsymbol{k}) \equiv \frac{1}{1 - \Sigma^{\rm R}_\sigma(\boldsymbol{k})} \; . \tag{7.16}$$

It allows the spectral density (7.14) to be written in the form

$$S_{\boldsymbol{k}}(\omega \to E_{\rm F}) = \sum_\sigma z_\sigma(\boldsymbol{k}) \delta \left(\omega - E_{\boldsymbol{k},\sigma}\right) + S^{\rm inc}_{\boldsymbol{k}}(\omega) \; . \tag{7.17}$$

A comparison with (7.6) shows that, near the Fermi energy, the correlated spectral density resembles that of an uncorrelated system. The bare single-particle energies $\varepsilon^0_{\boldsymbol{k}}$ are shifted by $\Sigma^0_\sigma(\boldsymbol{k})$ and renormalised by the factor $z_\sigma(\boldsymbol{k})$, which defines the 'quasi-particle energy' $E_{\boldsymbol{k},\sigma}$, equation (7.15). The contribution of a quasi-particle to the sum rule (7.5) is reduced from unity, in the uncorrelated limit to $z_\sigma(\boldsymbol{k}) < 1$ in the correlated system. Therefore, $z_\sigma(\boldsymbol{k})$ is denoted as the 'quasi-particle weight'. The rest of the spectral weight lies in the 'incoherent background' $S^{\rm inc}_{\boldsymbol{k}}(\omega)$. The quasi-particle behaviour near the Fermi energy is a direct consequence of the specific form (7.11) of the self-energy. Systems with such self-energies are usually denoted as 'Fermi liquids'.

7.1.3 Multi-Band Green's Functions

The quasi-particle or Fermi-liquid theory for multi-band Hubbard models is technically more difficult but, in principle, very similar to that of the single-band model. In multi-band models, the Green's function matrix $\tilde{G}_{\boldsymbol{k}}(\omega)$ and the self-energy matrix $\tilde{\Sigma}(\boldsymbol{k},\omega)$, with their respective elements $G^{\sigma,\sigma}_{\boldsymbol{k}}(\omega)$ and $\Sigma_{\sigma,\sigma'}(\boldsymbol{k},\omega)$, are related via

$$\tilde{G}_{\boldsymbol{k}}(\omega)^{-1} = \tilde{G}_{0;\boldsymbol{k}}(\omega)^{-1} - \tilde{\Sigma}(\boldsymbol{k},\omega) \; , \tag{7.18}$$

which generalises equation (7.10) for the single-band model. Near the Fermi energy, the self-energy matrix of a Fermi liquid has the form

$$\tilde{\Sigma}(\boldsymbol{k},\omega \to E_{\rm F}) = \tilde{\Sigma}^0(k) + \tilde{\Sigma}^{\rm R}(\boldsymbol{k})(\omega - E_{\rm F}) + {\rm i}\tilde{\Sigma}^{\rm I}(\boldsymbol{k})(\omega - E_{\rm F})^2 \; , \tag{7.19}$$

where, as we will see below, a Fermi-liquid behaviour requires that the matrices $\tilde{\Sigma}^0(k)$ and $\tilde{\Sigma}^{\rm R}(\boldsymbol{k})$ are Hermitian. Note that ${\rm i}\tilde{\Sigma}^{\rm I}(\boldsymbol{k})$ is not necessarily an imaginary matrix but we write it in analogy to the corresponding equation (7.11) for the single-band model. The self-energy (7.19) leads to the following equation for the inverse of the Green's function near the Fermi energy,

$$[\tilde{G}_{\boldsymbol{k}}(\omega \to E_{\rm F})]^{-1} = \omega - \tilde{E}^0_{\boldsymbol{k}} - \tilde{\Sigma}^{\rm R}(\boldsymbol{k})(\omega - E_{\rm F}) + {\rm i}\tilde{\Sigma}^{\rm I}(\boldsymbol{k})(\omega - E_{\rm F})^2 \; , \tag{7.20}$$

where we introduced the shifted energies

$$\tilde{E}^0_{\boldsymbol{k}} \equiv \tilde{\varepsilon}^0_{\boldsymbol{k}} + \tilde{\Sigma}^0(\boldsymbol{k}) \; . \tag{7.21}$$

For fixed values of $\boldsymbol{k}$ and ω, we can diagonalise the first two (Hermitian) matrices on the right hand side of equation (7.20)

$$\tilde{u}(\boldsymbol{k},\omega)[\tilde{E}^0_{\boldsymbol{k}} + \tilde{\Sigma}^{\rm R}(\boldsymbol{k})(\omega - E_{\rm F})]\tilde{u}^\dagger(\boldsymbol{k},\omega) = \tilde{R}(\boldsymbol{k},\omega) \; . \tag{7.22}$$

by means of a unitary matrix $\tilde{u}(\boldsymbol{k},\omega)$, which, to leading order in $(\omega - E_{\rm F})$, has the matrix elements

$$u_{\gamma,\sigma}(\boldsymbol{k},\omega \to E_{\rm F}) = u_{0;\gamma,\sigma}(\boldsymbol{k}) + u_{1;\gamma,\sigma}(\boldsymbol{k})(\omega - E_{\rm F}) \; . \tag{7.23}$$

The elements $R_{\gamma,\gamma}(\boldsymbol{k},\omega) \equiv R_\gamma(\boldsymbol{k},\omega)$ of the diagonal matrix $\tilde{R}(\boldsymbol{k},\omega)$ are given by

$$R_\gamma(\boldsymbol{k},\omega \to E_\mathrm{F}) = R_{0;\gamma}(\boldsymbol{k}) + R_{1;\gamma}(\boldsymbol{k})(\omega - E_\mathrm{F}) \;, \tag{7.24}$$

where

$$R_{0;\gamma}(\boldsymbol{k})\delta_{\gamma,\gamma'} = \sum_{\sigma,\sigma'} u_{0;\gamma,\sigma}(\boldsymbol{k}) E^0_{\boldsymbol{k};\sigma,\sigma'} u^*_{0;\gamma',\sigma'}(\boldsymbol{k}) \;, \tag{7.25a}$$

$$R_{1;\gamma}(\boldsymbol{k}) = \sum_{\sigma,\sigma'} u_{0;\gamma,\sigma}(\boldsymbol{k}) \Sigma^\mathrm{R}_{\sigma,\sigma'}(\boldsymbol{k}) u^*_{0;\gamma,\sigma'}(\boldsymbol{k}) \;. \tag{7.25b}$$

Note that $\tilde{E}^0_{\boldsymbol{k}}$ is diagonalised by $\tilde{u}^0_{\boldsymbol{k}}$, as indicated in equation (7.25a), whereas equation (7.25b) only holds for the diagonal elements.

After the diagonalisation (7.22), we can write $\tilde{G}_{\boldsymbol{k}}(\omega \to E_\mathrm{F})$ as

$$\tilde{G}_{\boldsymbol{k}}(\omega \to E_\mathrm{F}) = \tilde{u}^\dagger(\boldsymbol{k},\omega)\tilde{K}(\boldsymbol{k},\omega)\tilde{u}(\boldsymbol{k},\omega) \;, \tag{7.26}$$

where

$$\tilde{K}(\boldsymbol{k},\omega) \equiv [\omega - \tilde{R}(\boldsymbol{k},\omega) - \tilde{I}(\boldsymbol{k},\omega)]^{-1} \;, \tag{7.27a}$$

$$\tilde{I}(\boldsymbol{k},\omega) \equiv \mathrm{i}\tilde{u}_0(\boldsymbol{k})\tilde{\Sigma}^\mathrm{I}(\boldsymbol{k})\tilde{u}^\dagger_0(\boldsymbol{k})(\omega - E_\mathrm{F})^2 \;. \tag{7.27b}$$

In order to determine the spectral function (7.4), we have to calculate the imaginary part of the matrix $\tilde{K}(\boldsymbol{k},\omega)$. By construction, the matrix $\tilde{R}$ in (7.27a) is real and diagonal. For the calculation of $\mathrm{Im}[\tilde{K}(\boldsymbol{k},\omega)]$, we may safely assume that $\tilde{I}$ is imaginary and also diagonal for the following reason: Any real part of $\tilde{I}(\boldsymbol{k},\omega)$ is negligible as compared to the dominant linear term in $\tilde{R}(\boldsymbol{k},\omega)$. Although non-diagonal imaginary elements of $\tilde{I}$ lead to non-diagonal elements in $\mathrm{Im}[\tilde{K}(\boldsymbol{k},\omega)]$, they vanish in the limit $\omega \to E_\mathrm{F}$ as long as the emerging quasi-particle energies (7.31) are non-degenerate. This leads to the imaginary part

$$\mathrm{Im}[K_{\gamma,\gamma'}(\boldsymbol{k},\omega)] = -\pi\delta_{\gamma,\gamma'}\delta(\omega - R_{\gamma,\gamma}(\boldsymbol{k},\omega)) \tag{7.28}$$

of $\tilde{K}(\boldsymbol{k},\omega)$ near the Fermi energy. Like in the one-band model, we can evaluate the δ-function, which leads to

$$\mathrm{Im}[K_{\gamma,\gamma'}(\boldsymbol{k},\omega)] = -\pi\delta_{\gamma,\gamma'} z_\gamma(\boldsymbol{k})\delta(\omega - E_\gamma(\boldsymbol{k})) \;, \tag{7.29}$$

where

$$z_\gamma(\boldsymbol{k}) \equiv \frac{1}{1 - R_{1;\gamma}(\boldsymbol{k})} = \left[\tilde{u}_0(\boldsymbol{k})[1 - \tilde{\Sigma}^\mathrm{R}(\boldsymbol{k})]^{-1}\tilde{u}^\dagger_0(\boldsymbol{k})\right]_{\gamma,\gamma} \tag{7.30}$$

gives the quasi-particle weight and

$$E_{\boldsymbol{k},\gamma} = E_\mathrm{F} + z_\gamma(\boldsymbol{k})(R_{0;\gamma}(\boldsymbol{k}) - E_\mathrm{F}) \tag{7.31}$$

is the quasi-particle dispersion. These notations are obviously justified from our final result for the spectral function

$$S_{\boldsymbol{k}}(\omega \to E_\mathrm{F}) = \sum_\gamma z_\gamma(\boldsymbol{k})\delta(\omega - E_{\boldsymbol{k},\gamma}) + S^\mathrm{inc}_{\boldsymbol{k}}(\omega) \;. \tag{7.32}$$

The quasi-particle dispersion $E_{\boldsymbol{k},\gamma}$ belongs to an effective single-particle Hamiltonian,

$$\hat{H}^\mathrm{eff}_0 = \sum_{\boldsymbol{k},\sigma,\sigma'} \varepsilon^\mathrm{eff}_{\boldsymbol{k};\sigma,\sigma'} \hat{c}^\dagger_{\boldsymbol{k},\sigma}\hat{c}_{\boldsymbol{k},\sigma'} \tag{7.33a}$$

in the original basis $|\sigma\rangle$ with effective energies

$$\varepsilon^{\text{eff}}_{\boldsymbol{k};\sigma,\sigma'} = \eta_{\sigma,\sigma'}(\boldsymbol{k}) + \sum_{\tilde{\sigma},\tilde{\sigma}'} \bar{z}_{\sigma,\tilde{\sigma}}(\boldsymbol{k})\varepsilon^{0}_{\boldsymbol{k};\tilde{\sigma},\tilde{\sigma}'}\bar{z}_{\sigma',\tilde{\sigma}'}(\boldsymbol{k}) \ . \tag{7.33b}$$

Here, we introduced the renormalisation matrix

$$\bar{z}_{\sigma,\sigma'}(\boldsymbol{k}) \equiv \sum_{\gamma} u^{*}_{0;\gamma,\sigma}(\boldsymbol{k})\sqrt{z_{\gamma}(\boldsymbol{k})}u_{0;\gamma,\sigma'}(\boldsymbol{k}) \tag{7.33c}$$

and the energy shifts

$$\eta_{\sigma,\sigma'}(\boldsymbol{k}) \equiv \sum_{\tilde{\sigma},\tilde{\sigma}'} \bar{z}_{\sigma,\tilde{\sigma}}(\Sigma^{0}_{\tilde{\sigma},\tilde{\sigma}'}(\boldsymbol{k}) - \delta_{\tilde{\sigma},\tilde{\sigma}'}E_{\text{F}})\bar{z}_{\sigma',\tilde{\sigma}'} \ . \tag{7.33d}$$

7.2 Landau Theory

In this section, we briefly remind the reader of Landau's phenomenological energy functional in section 7.2.1. This functional is based on the idea that it exists a one-to-one correspondence between elementary excitations of a Fermi liquid and the excitations of a non-interacting Fermi gas. The correspondence between Fermi liquids and Fermi gases becomes mathematically more explicit when we introduce the operators for quasi-particle excitations in section 7.2.2. With such operators, we write the quasi-particle excitations energies as expectation values of the Hamiltonian in section 7.2.3. These exact relations are needed for the implementation of the quasi-particle concept into our Gutzwiller theory in section 7.3.

7.2.1 Landau Energy Functional

As shown in the previous section, the low-energy excitations of Fermi liquids are quasi-particles, which, qualitatively, resemble the excitations of a Fermi gas without Coulomb interaction. Landau used this observation as a starting point of his phenomenological approach in which he assumed that there exists a one-to-one correspondence of excitations in a correlated Fermi liquid and a fictitious non-interacting Fermi gas. At zero temperature, both are then described by a Fermi distribution in momentum space

$$n^{0}_{\boldsymbol{k},\gamma} = \langle \hat{n}_{\boldsymbol{k},\gamma} \rangle = \Theta(E_{\text{F}} - E_{\boldsymbol{k},\gamma}) \ . \tag{7.34}$$

For a Fermi gas, such a distribution is correct for all $(\boldsymbol{k},\gamma)$ while, for a Fermi liquid, it only applies to the vicinity of the Fermi surface.

Low-energy excitations of a Fermi liquid are described by changes

$$\delta n_{\boldsymbol{k},\gamma} = n_{\boldsymbol{k},\gamma} - n^{0}_{\boldsymbol{k},\gamma} \tag{7.35}$$

of the distribution $n_{\boldsymbol{k},\gamma}$. The expectation values of observables, e.g., of the energy, may then be expanded in a power series with respect to $\delta n_{\boldsymbol{k},\gamma}$,

$$\delta E = \sum_{\boldsymbol{k},\gamma} E_{\boldsymbol{k},\gamma}\delta n_{\boldsymbol{k},\gamma} + \sum_{\gamma,\gamma';\boldsymbol{k},\boldsymbol{k}'} f_{\gamma,\gamma'}(\boldsymbol{k},\boldsymbol{k}')\delta n_{\boldsymbol{k},\gamma}\delta n_{\boldsymbol{k}',\gamma'} + \mathcal{O}(\delta n^{3}) \ . \tag{7.36}$$

For sufficiently simple Fermi surfaces, for instance, a sphere in case of the free-electron gas, the coupling constants $f_{\gamma,\gamma'}(\boldsymbol{k},\boldsymbol{k}')$ can be expressed by a small number of parameters, the so-called 'Landau-parameters'. In this way, one can investigate quite a number of phenomena, which are related to weak perturbations of the Fermi liquid both at zero and finite temperature; see references [35, 36, 186, 187]. For a single-band model, Landau parameters have been calculated in the Gutzwiller theory and successfully applied for an investigation of ^{3}He in reference [105].

7.2.2 Quasi-Particle Excitations

In order to formulate a quasi-particle approach in the context of our multi-band Gutzwiller theory, we first address the question how Landau's quasi-particle ideas are mathematically connected to the Fermi-liquid theory discussed in the previous section. The excitations of the Fermi gas are described by the bare fermionic operators $\hat{c}^{(\dagger)}_{\boldsymbol{k},\gamma}$, which, in the ground state, obey equation (7.34) with $\hat{n}_{\boldsymbol{k},\gamma} = \hat{c}^{\dagger}_{\boldsymbol{k},\gamma}\hat{c}_{\boldsymbol{k},\gamma}$. It raises the question wether or not such creation and annihilation operators also exist for the quasi-particles. They have to obey equation (7.34) but with the expectation value carried out with respect to the true many-particle ground state $|\Phi_0\rangle$. It turns out that, near the Fermi surface, it is indeed possible to define such operators.

To keep the notations simple, we consider only a paramagnetic single-band model and skip the spin index σ. In this case, we can define quasi-particle creation and annihilation operators via

$$\hat{h}^{\dagger}_{\boldsymbol{k}} \equiv \frac{\alpha}{\sqrt{z(\boldsymbol{k})}} \int_{-\infty}^{0} \mathrm{d}t\; e^{-\mathrm{i}E_{\boldsymbol{k}}t} e^{\alpha t} \hat{c}^{\dagger}_{\boldsymbol{k}}(t) \;, \tag{7.37a}$$

$$\hat{h}_{\boldsymbol{k}} \equiv \frac{\alpha}{\sqrt{z(\boldsymbol{k})}} \int_{-\infty}^{0} \mathrm{d}t\; e^{\mathrm{i}E_{\boldsymbol{k}}t} e^{\alpha t} \hat{c}_{\boldsymbol{k}}(t) \;, \tag{7.37b}$$

where $E_{\boldsymbol{k}}$ and $z(\boldsymbol{k})$ are the quasi-particle energy and the quasi-particle weight defined in (7.15) and (7.16), respectively. As we will see below, the real parameter α can be chosen arbitrarily as long as it obeys the conditions

$$|E_{\boldsymbol{k}} - E_{\mathrm{F}}| < \alpha \tag{7.38a}$$

and

$$\left| \int_{E_{\mathrm{F}}}^{\pm\infty} \mathrm{d}\omega S^{\mathrm{inc}}_{\boldsymbol{k}}(\omega) \frac{\alpha^2 (\omega/E_{\mathrm{F}})^n}{(\omega - E_{\mathrm{F}})^2 + \alpha^2} \right| \ll 1 \tag{7.38b}$$

for $n = 0$ and $n = 1$. Obviously, both conditions (7.38) together can only be met in the immediate vicinity of the Fermi surface.

In order to show that $\hat{h}^{\dagger}_{\boldsymbol{k}}$ creates and $\hat{h}_{\boldsymbol{k}}$ annihilates a quasi-particle, we calculate

$$\begin{aligned} \langle\Phi_0|\hat{h}^{\dagger}_{\boldsymbol{k}}\hat{h}_{\boldsymbol{k}}|\Phi_0\rangle &= \frac{\alpha^2}{z(\boldsymbol{k})} \sum_n |\langle\Phi_n|\hat{c}_{\boldsymbol{k}}|\Phi_0\rangle|^2 \qquad (7.39a) \\ &\quad \times \int_{-\infty}^{0} \mathrm{d}t \int_{-\infty}^{0} \mathrm{d}t' e^{(-\mathrm{i}E_{\boldsymbol{k}}+\alpha)t} e^{(\mathrm{i}E_{\boldsymbol{k}}+\alpha)t'} e^{-\mathrm{i}(E_n - E_0)(t-t')} \\ &= \frac{1}{z(\boldsymbol{k})} \sum_n |\langle\Phi_n|\hat{c}_{\boldsymbol{k}}|\Phi_0\rangle|^2 \frac{\alpha^2}{(E_{\boldsymbol{k}} + E_n - E_0)^2 + \alpha^2} \;, \qquad (7.39b) \end{aligned}$$

where $|\Phi_n\rangle$ is a basis of eigenstates of our single-band Hamiltonian $\hat{H} \equiv \hat{H}_{1\mathrm{B}}$ with energies E_n. A comparison with the Lehmann representation of the spectral function

$$\frac{1}{2} S_{\boldsymbol{k}}(\omega) = \sum_n |\langle\Phi_n|\hat{c}_{\boldsymbol{k}}|\Phi_0\rangle|^2 \delta(\omega + (E_n - E_0)) + \sum_n |\langle\Phi_n|\hat{c}^{\dagger}_{\boldsymbol{k}}|\Phi_0\rangle|^2 \delta(\omega - (E_n - E_0)) \tag{7.40}$$

allows equation (7.39b) to be written as

$$\langle\Phi_0|\hat{h}^{\dagger}_{\boldsymbol{k}}\hat{h}_{\boldsymbol{k}}|\Phi_0\rangle = \frac{1}{2z(\boldsymbol{k})} \int_{-\infty}^{E_{\mathrm{F}}} \mathrm{d}\omega S_{\boldsymbol{k}}(\omega) \frac{\alpha^2}{(E_{\boldsymbol{k}} - \omega)^2 + \alpha^2} \;. \tag{7.41}$$

The factor 1/2 in (7.40) replaces the σ-sum in the definition (7.4) of the spectral function. Note that we have $E_n - E_0 = -E_{\mathrm{F}} + E'_n$ with energies $E'_n > 0$ in (7.39b) and in the first sum of equation (7.40). The second sum in equation (7.40) only contributes for $\omega > E_{\mathrm{F}}$.

If α obeys equation (7.38a), we can use the spectral function (7.17) to evaluate the expectation value (7.41). This leads to

$$\langle\Phi_0|\hat{h}_{\boldsymbol{k}}^\dagger\hat{h}_{\boldsymbol{k}}|\Phi_0\rangle = \Theta(E_\mathrm{F}-E_{\boldsymbol{k}}) + \frac{1}{2z(\boldsymbol{k})}\int_{-\infty}^{E_\mathrm{F}}\mathrm{d}\omega S_{\boldsymbol{k}}^\mathrm{inc}(\omega)\frac{\alpha^2}{(E_{\boldsymbol{k}}-\omega)^2+\alpha^2} \tag{7.42a}$$

$$\approx \Theta(E_\mathrm{F}-E_{\boldsymbol{k}})\;, \tag{7.42b}$$

where the second line follows because α also obeys equation (7.38b). In the same way as in (7.39a), we can show that near the Fermi surface the quasi-particle operators satisfy the equations

$$\langle\Phi_0|\hat{h}_{\boldsymbol{k}}^\dagger\hat{h}_{\boldsymbol{k}'}|\Phi_0\rangle = \delta_{\boldsymbol{k},\boldsymbol{k}'}\Theta(E_\mathrm{F}-E_{\boldsymbol{k}}) \tag{7.43a}$$

$$\langle\Phi_0|\hat{h}_{\boldsymbol{k}}\hat{h}_{\boldsymbol{k}'}^\dagger|\Phi_0\rangle = \delta_{\boldsymbol{k},\boldsymbol{k}'}\Theta(E_{\boldsymbol{k}}-E_\mathrm{F})\;, \tag{7.43b}$$

$$\langle\Phi_0|\hat{h}_{\boldsymbol{k}}^\dagger\hat{h}_{\boldsymbol{k}'}^\dagger|\Phi_0\rangle = \langle\Phi_0|\hat{h}_{\boldsymbol{k}}\hat{h}_{\boldsymbol{k}'}|\Phi_0\rangle = 0\;. \tag{7.43c}$$

7.2.3 Quasi-Particle Energies

Finally, we calculate the expectation value

$$E_-(\boldsymbol{k}) \equiv \langle\hat{H}\rangle_{\Phi_-^{(\boldsymbol{k})}} - E_0 = \frac{\langle\Phi_-^{(\boldsymbol{k})}|\hat{H}|\Phi_-^{(\boldsymbol{k})}\rangle}{\langle\Phi_-^{(\boldsymbol{k})}|\Phi_-^{(\boldsymbol{k})}\rangle} - E_0 \tag{7.44}$$

of our single-band Hamiltonian $\hat{H}$ with respect to the state

$$|\Phi_-^{(\boldsymbol{k})}\rangle \equiv \hat{h}_{\boldsymbol{k}}\,|\Phi_0\rangle\;, \tag{7.45}$$

in which a quasi-particle is removed from (i.e., a quasi-hole added to) the ground state $|\Phi_0\rangle$. With the definition (7.37) of the quasi-particle operators, and using the Lehmann representation (7.40) of the spectral function, we find

$$\langle\Phi_-^{(\boldsymbol{k})}|\hat{H}|\Phi_-^{(\boldsymbol{k})}\rangle = \frac{1}{z(\boldsymbol{k})}\sum_n|\langle\Phi_n|\hat{c}_{\boldsymbol{k}}|\Phi_0\rangle|^2\frac{E_n\alpha^2}{(E_{\boldsymbol{k}}+E_n-E_0)^2+\alpha^2}\;, \tag{7.46a}$$

$$= \frac{1}{2z(\boldsymbol{k})}\int_{-\infty}^{E_\mathrm{F}}\mathrm{d}\omega S_{\boldsymbol{k}}(\omega)\frac{(E_0-\omega)\alpha^2}{(E_{\boldsymbol{k}}-\omega)^2+\alpha^2}\;. \tag{7.46b}$$

Evaluated with the spectral function (7.17), the expectation value (7.46a) becomes

$$\langle\Phi_-^{(\boldsymbol{k})}|\hat{H}|\Phi_-^{(\boldsymbol{k})}\rangle = E_0 - E_{\boldsymbol{k}} + \frac{1}{2z(\boldsymbol{k})}\int_{-\infty}^{E_\mathrm{F}}\mathrm{d}\omega S_{\boldsymbol{k}}^\mathrm{inc}(\omega)\frac{(E_0-\omega)\alpha^2}{(E_{\boldsymbol{k}}-\omega)^2+\alpha^2} \tag{7.47}$$

In order to calculate (7.44), we expand the inverse of the denominator by means of equation (7.42b),

$$\frac{1}{\langle\Phi_-^{(\boldsymbol{k})}|\Phi_-^{(\boldsymbol{k})}\rangle} \approx \Theta(E_\mathrm{F}-E_{\boldsymbol{k}}) - \frac{1}{2z(\boldsymbol{k})}\int_{-\infty}^{E_\mathrm{F}}\mathrm{d}\omega S_{\boldsymbol{k}}^\mathrm{inc}(\omega)\frac{\alpha^2}{(E_{\boldsymbol{k}}-\omega)^2+\alpha^2}\;. \tag{7.48}$$

This equation, together with (7.47) and (7.38b), leads to

$$E_-(\boldsymbol{k}) = -E_{\boldsymbol{k}}\;. \tag{7.49}$$

In the same way, we can show that adding a quasi-particle also leads to the expectation value

$$E_+(\boldsymbol{k}) \equiv \langle\hat{H}\rangle_{\Phi_+^{(\boldsymbol{k})}} - E_0 = +E_{\boldsymbol{k}} \tag{7.50}$$

for the state

$$|\Phi_+^{(\boldsymbol{k})}\rangle \equiv \hat{h}_{\boldsymbol{k}}^\dagger\,|\Phi_0\rangle\;. \tag{7.51}$$

We will use the exact equations (7.49) and (7.51) when we derive our approximate Gutzwiller-Landau quasi-particle theory in the following section.

7.3 Landau-Gutzwiller Quasi-Particles

The Gutzwiller theory provides approximate ground states

$$|\Psi_{\mathrm{G}}\rangle = \hat{P}_{\mathrm{G}}|\Psi_0\rangle \tag{7.52}$$

for the general class of multi-band Hubbard models (2.15). As discussed in section 5.3, the single-particle wave function $|\Psi_0\rangle$ is the ground state of an effective single-particle Hamiltonian, see equation (5.96). Based on the exact results on quasi-particle excitations, as discussed in the previous section, we now develop a scheme to calculate such excitations for our approximate Gutzwiller ground state. We first identify the quasi-particle operators that belong to $|\Psi_{\mathrm{G}}\rangle$. With these operator, we then calculate the quasi-particle excitation energies. In the following, we restrict our derivation to systems without superconducting order parameters. A more general derivation can be found in reference [138].

7.3.1 Operators for Quasi-Particle Creation and Annihilation

We define quasi-particle and quasi-hole creation operators

$$\hat{e}^{\dagger}_{\boldsymbol{k},\gamma} := \hat{P}_{\mathrm{G}}\hat{h}^{\dagger}_{\boldsymbol{k},\gamma}(\hat{P}_{\mathrm{G}})^{-1} , \tag{7.53a}$$

$$\hat{v}_{\boldsymbol{k},\gamma} := \hat{P}_{\mathrm{G}}\hat{h}_{\boldsymbol{k},\gamma}(\hat{P}_{\mathrm{G}})^{-1} , \tag{7.53b}$$

to which the Gutzwiller wave function behaves like an uncorrelated Fermi gas, see below. These operators obey usual Fermi anti-commutation relations,

$$[\hat{e}^{\dagger}_{\boldsymbol{k},\gamma}, \hat{v}_{\boldsymbol{k}',\gamma'}]_+ = \delta_{\boldsymbol{k},\boldsymbol{k}'}\delta_{\gamma\gamma'} , \tag{7.54a}$$

$$[\hat{e}^{\dagger}_{\boldsymbol{k},\gamma}, \hat{e}^{\dagger}_{\boldsymbol{k}',\gamma'}]_+ = [\hat{v}_{\boldsymbol{k},\gamma}, \hat{v}_{\boldsymbol{k}',\gamma'}]_+ = 0 , \tag{7.54b}$$

and they create quasi-particles/quasi-holes in the variational Gutzwiller ground state, as can be seen from

$$\hat{e}^{\dagger}_{\boldsymbol{k},\gamma}\hat{v}_{\boldsymbol{k},\gamma}|\Psi_{\mathrm{G}}\rangle = \Theta(E_{\mathrm{F}} - E_{\boldsymbol{k},\gamma})|\Psi_{\mathrm{G}}\rangle , \tag{7.55a}$$

$$\hat{v}_{\boldsymbol{k},\gamma}\hat{e}^{\dagger}_{\boldsymbol{k},\gamma}|\Psi_{\mathrm{G}}\rangle = \Theta(E_{\boldsymbol{k},\gamma} - E_{\mathrm{F}})|\Psi_{\mathrm{G}}\rangle . \tag{7.55b}$$

With these operators, we define the states

$$|\Psi^{(\boldsymbol{k},\gamma)}_{\mathrm{G},+}\rangle \equiv \hat{e}^{\dagger}_{\boldsymbol{k},\gamma}|\Psi_{\mathrm{G}}\rangle = \hat{P}_{\mathrm{G}}\hat{h}^{\dagger}_{\boldsymbol{k},\gamma}|\Psi_0\rangle \equiv \hat{P}_{\mathrm{G}}|\Psi^{(\boldsymbol{k},\gamma)}_{0,+}\rangle , \tag{7.56a}$$

$$|\Psi^{(\boldsymbol{k},\gamma)}_{\mathrm{G},-}\rangle \equiv \hat{v}_{\boldsymbol{k},\gamma}|\Psi_{\mathrm{G}}\rangle = \hat{P}_{\mathrm{G}}\hat{h}_{\boldsymbol{k},\gamma}|\Psi_0\rangle \equiv \hat{P}_{\mathrm{G}}|\Psi^{(\boldsymbol{k},\gamma)}_{0,-}\rangle , \tag{7.56b}$$

in which a quasi-particle or quasi-hole is added to the variational ground state. The single-particle state $|\Psi_0\rangle$ is defined in terms of the operators $\hat{h}^{\dagger}_{\boldsymbol{k},\gamma}$ in equation (5.102). Note that $|\Psi_0\rangle$ and $\hat{h}^{\dagger}_{\boldsymbol{k},\gamma}$ have to be used with their optimum values, given by the parameters

$$x_i \equiv \{\tilde{\lambda}^{\mathrm{i}}_i, \tilde{\eta}_i, \tilde{C}^0_i, E_{\mathrm{F}}\} \tag{7.57}$$

that minimise (5.104),

$$\left.\frac{\partial E_{\mathrm{c}}(\ldots)}{\partial x_i}\right|_{x_i = x_i^0} = 0 . \tag{7.58}$$

Equations (7.56) unveil that our approach is a microscopic realisation of Landau's phenomenological concept: the excitations of a correlated system, described by $|\Psi_{\mathrm{G}}\rangle$, are uniquely connected to the excitations of a Fermi gas, described by $|\Psi_0\rangle$.

In analogy to the exact equations (7.49) and (7.50), we define the quasi-particle or quasi-hole excitation energies as

$$E^{\mathrm{qp}}_{\boldsymbol{k},\gamma} \equiv \pm \left(E^{\mathrm{var}}_{\pm}(\boldsymbol{k},\gamma) - E^{\mathrm{var}}_{0} \right) \ , \tag{7.59}$$

where the upper and lower signs correspond to quasi-particles and quasi-holes, respectively. Here,

$$E^{\mathrm{var}}_{\pm}(\boldsymbol{k},\gamma) = \frac{\langle \Psi^{(\boldsymbol{k},\gamma)}_{\mathrm{G},\pm} | \hat{H}_{\mathrm{H}} | \Psi^{(\boldsymbol{k},\gamma)}_{\mathrm{G},\pm} \rangle}{\langle \Psi^{(\boldsymbol{k},\gamma)}_{\mathrm{G},\pm} | \Psi^{(\boldsymbol{k},\gamma)}_{\mathrm{G},\pm} \rangle} \tag{7.60}$$

is the expectation value of our Hamiltonian with respect to the wave functions (7.56) and E^{var}_0 is the variational ground state energy (5.103).

7.3.2 Quasi-Particle Energies

In this section, we prove that the quasi-particle energies, as defined in equation (7.59), are the eigenvalues

$$E^{\mathrm{qp}}_{\boldsymbol{k},\gamma} = E_{\boldsymbol{k},\gamma} \tag{7.61}$$

of the effective single-particle Hamiltonian (5.96). In the orbital band basis (2.17a), this effective Hamiltonian has the form

$$\hat{H}^{\mathrm{eff}}_0 = \sum_{\boldsymbol{k},\sigma,\sigma'} \varepsilon^{\mathrm{eff}}_{\boldsymbol{k};\sigma,\sigma'} \hat{c}^{\dagger}_{\boldsymbol{k},\sigma} \hat{c}_{\boldsymbol{k},\sigma'} \tag{7.62}$$

with the effective band energies

$$\varepsilon^{\mathrm{eff}}_{\boldsymbol{k};\sigma,\sigma'} = \eta_{\sigma,\sigma'} + \sum_{\tilde{\sigma},\tilde{\sigma}'} q^{\sigma}_{\tilde{\sigma}} \varepsilon_{\boldsymbol{k};\tilde{\sigma},\tilde{\sigma}'} \left(q^{\sigma'}_{\tilde{\sigma}'} \right)^* \ . \tag{7.63}$$

This results is in agreement with the general form (7.33) of a quasi-particle Hamiltonian energies in Fermi-liquid theory. Note that $\varepsilon^0_{\boldsymbol{k};\sigma,\sigma'}$ in (7.33) differs from $\varepsilon_{\boldsymbol{k};\sigma,\sigma'}$ in (7.63) by the inclusion of local terms, see equations (2.17b) and (5.98b). This is compensated in the Gutzwiller theory by a proper adjustment of the fields $\eta_{\sigma,\sigma'}$.

We close this section with the proof of equation (7.61). In the following, we drop all lattice site indices and set symbols $\{\}$ of the quantities (7.57). For example, the set of independent variational parameters $\{\tilde{\lambda}^{\mathrm{i};0}_i\}$ that minimises the variational energy is denoted as $\tilde{\lambda}^{\mathrm{i};0}$. We write the energies E^{var}_0 and $E^{\mathrm{var}}_{\pm}(\boldsymbol{k},\gamma)$ in (7.59) as

$$E^{\mathrm{var}}_0 = \sum_{\sigma,\sigma',\tilde{\sigma},\tilde{\sigma}'} Q^{\sigma,\sigma'}_{\tilde{\sigma},\tilde{\sigma}'}(\tilde{\lambda}^{\mathrm{i};0}, \tilde{C}^{0;0})\, K^{\sigma,\sigma'}_{\tilde{\sigma},\tilde{\sigma}'} + E_{\mathrm{loc}}(\tilde{\lambda}^{\mathrm{i};0}, \tilde{C}^{0;0}) \ , \tag{7.64a}$$

$$\begin{aligned} E^{\mathrm{var}}_{\pm}(\boldsymbol{k},\gamma) = {} & \sum_{\sigma,\sigma',\tilde{\sigma},\tilde{\sigma}'} Q^{\sigma,\sigma'}_{\tilde{\sigma},\tilde{\sigma}'}(\tilde{\lambda}^{\mathrm{i};0}, \tilde{C}^{0;0} + \tilde{\Delta}^{(\boldsymbol{k},\gamma)}_{\pm}) \sum_{\boldsymbol{k}'} \varepsilon_{\boldsymbol{k}';\tilde{\sigma},\tilde{\sigma}'} \langle \Psi^{(\boldsymbol{k},\gamma)}_{0,\pm} | \hat{c}^{\dagger}_{\boldsymbol{k}',\sigma} \hat{c}_{\boldsymbol{k}',\sigma'} | \Psi^{(\boldsymbol{k},\gamma)}_{0,\pm} \rangle \\ & + E_{\mathrm{loc}}(\tilde{\lambda}^{\mathrm{i};0}, \tilde{C}^{0;0} + \tilde{\Delta}^{(\boldsymbol{k},\gamma)}_{\pm}) \ , \end{aligned} \tag{7.64b}$$

where

$$K^{\sigma,\sigma'}_{\tilde{\sigma},\tilde{\sigma}'} = \sum_{\boldsymbol{k}} \varepsilon_{\boldsymbol{k};\tilde{\sigma},\tilde{\sigma}'} \langle \hat{c}^{\dagger}_{\boldsymbol{k},\sigma} \hat{c}_{\boldsymbol{k},\sigma'} \rangle_{\Psi_0} \ , \tag{7.64c}$$

and $Q^{\sigma,\sigma'}_{\tilde{\sigma},\tilde{\sigma}'}$ is defined in equation (5.98a). The matrix $\tilde{\Delta}^{(\boldsymbol{k},\gamma)}_{\pm}$ describes the change of the uncorrelated local-density matrix $\tilde{C}^0$ due to the creation of a quasi-particle or a quasi-hole. Its elements are given by

$$\Delta^{(\boldsymbol{k},\gamma)}_{\pm;\sigma,\sigma'} = \pm u_{\gamma,\sigma}(\boldsymbol{k}) u^*_{\gamma,\sigma'}(\boldsymbol{k}) \ , \tag{7.65}$$

where the coefficients $u_{\gamma,\sigma'}(\boldsymbol{k})$ have been introduced in (5.100).

The sum over $\boldsymbol{k}$ in (2.14) is readily evaluated,

$$\sum_{\boldsymbol{k}'} \varepsilon^0_{\boldsymbol{k}';\tilde{\sigma},\tilde{\sigma}'} \langle \Psi^{(\boldsymbol{k},\gamma)}_{0,\pm} | \hat{c}^\dagger_{\boldsymbol{k}',\sigma} \hat{c}_{\boldsymbol{k}',\sigma'} | \Psi^{(\boldsymbol{k},\gamma)}_{0,\pm} \rangle = K^{\sigma,\sigma'}_{\tilde{\sigma},\tilde{\sigma}'} \pm \varepsilon_{\boldsymbol{k};\tilde{\sigma},\tilde{\sigma}'} u_{\gamma,\sigma}(\boldsymbol{k}) u^*_{\gamma,\sigma'}(\boldsymbol{k}) \,. \tag{7.66}$$

Therefore, to order $(1/L)^0$, the expansion of $\pm E^{\rm qp}_{\boldsymbol{k},\gamma} = E^{\rm var}_{\pm}(\boldsymbol{k},\gamma) - E^{\rm var}_0$ with respect to $u^{(*)}_{\gamma,\sigma'}(\boldsymbol{k})$ yields

$$\begin{aligned} \pm E^{\rm qp}_{\boldsymbol{k},\gamma} \;&=\; \pm \sum_{\sigma,\sigma',\tilde{\sigma},\tilde{\sigma}'} Q^{\sigma,\sigma'}_{\tilde{\sigma},\tilde{\sigma}'} \varepsilon_{\boldsymbol{k};\tilde{\sigma},\tilde{\sigma}'} u^*_{\gamma,\sigma}(\boldsymbol{k}) u_{\gamma,\sigma'}(\boldsymbol{k}) \\ &\quad + \sum_{\rho,\rho'} \left[\sum_{\sigma,\sigma',\tilde{\sigma},\tilde{\sigma}'} K^{\sigma,\sigma'}_{\tilde{\sigma},\tilde{\sigma}'} \left. \frac{\partial Q^{\sigma,\sigma'}_{\tilde{\sigma},\tilde{\sigma}'}}{\partial C^0_{\rho,\rho'}} \right|_{\tilde{C}^0=\tilde{C}^{0;0}} + \left. \frac{\partial E_{\rm loc}}{\partial C^0_{\rho,\rho'}} \right|_{\tilde{C}^0=\tilde{C}^{0;0}} \right] \Delta^{(\boldsymbol{k},\gamma)}_{\pm;\rho,\rho'} \,. \end{aligned} \tag{7.67}$$

From equation (5.101), we find

$$\pm \sum_{\sigma,\sigma',\tilde{\sigma},\tilde{\sigma}'} Q^{\sigma,\sigma'}_{\tilde{\sigma},\tilde{\sigma}'} \varepsilon_{\boldsymbol{k};\tilde{\sigma},\tilde{\sigma}'} u_{\gamma,\sigma}(\boldsymbol{k}) u^*_{\gamma,\sigma'}(\boldsymbol{k}) = \pm E_{\boldsymbol{k},\gamma} + \sum_{\sigma,\sigma'} \eta^0_{\sigma,\sigma'} \Delta^{(\boldsymbol{k},\gamma)}_{\pm;\sigma,\sigma'} \,, \tag{7.68}$$

which allows us to evaluate the first line in (7.67). For the second line, we employ

$$\sum_{\sigma,\sigma',\tilde{\sigma},\tilde{\sigma}'} K^{\sigma,\sigma'}_{\tilde{\sigma},\tilde{\sigma}'} \left. \frac{\partial Q^{\sigma,\sigma'}_{\tilde{\sigma},\tilde{\sigma}'}}{\partial C^0_{\rho,\rho'}} \right|_{\tilde{C}^0=\tilde{C}^{0;0}} = \left\langle \frac{\partial}{\partial C^0_{\rho,\rho'}} \hat{H}^{\rm eff}_0 \right\rangle_{\Psi_0} = \left. \frac{\partial E^{\rm SP}}{\partial C^0_{\rho,\rho'}} \right|_{\tilde{C}^0=\tilde{C}^{0;0}} \,, \tag{7.69}$$

where we have used the fact that the dependence of $K^{\sigma,\sigma'}_{\tilde{\sigma},\tilde{\sigma}'}$ on $\tilde{C}$ can be ignored in the derivative of $E^{\rm SP}$ with respect to $\tilde{C}^0$ because $|\Psi_0\rangle$ is an exact eigenstate of $\hat{H}^{\rm eff}_0$, and $E^{\rm SP}$ is its eigenvalue. Using (5.104) and (7.58) we can rewrite this expression as

$$\left. \frac{\partial E^{\rm SP}}{\partial C^0_{\rho,\rho'}} \right|_{\tilde{C}^0=\tilde{C}^{0;0}} = - \left. \frac{\partial E_{\rm loc}}{\partial C^0_{\rho,\rho'}} \right|_{\tilde{C}^0=\tilde{C}^{0;0}} - \eta^0_{\rho,\rho'} \,, \tag{7.70}$$

which, together with equations (7.67)-(7.69), proves (7.61)

Chapter 8

Two-Particle Excitations

Two-particle excitations are described by two-particle Green's functions, which we introduce in section 8.1. In section 8.2, we derive the time-dependent Hartree-Fock approximation, which provides a feasible way to calculate two-particle Green's functions for many-particle systems. In section 8.3, we employ an evaluation scheme, very similar to that of the time-dependent Hartree-Fock approximation, in order to develop a time-dependent Gutzwiller theory.

8.1 Two-Particle Green's Functions

For the theoretical interpretation of various experiments, one has to consider two-particle Green's functions of the form

$$G^{\sigma_3,\sigma_4}_{\sigma_2,\sigma_1}(t-t') \equiv -\mathrm{i}\Theta(t-t')\langle\Phi_0|[\hat{c}^\dagger_{\sigma_1}(t)\hat{c}_{\sigma_2}(t),\hat{c}^\dagger_{\sigma_3}(t')\hat{c}_{\sigma_4}(t')]|\Phi_0\rangle \;, \tag{8.1}$$

where, as in the previous chapter, $|\Phi_0\rangle$ is the exact ground state of the time-independent Hamiltonian $\hat{H}$, e.g., the multi-band Hubbard Hamiltonian (2.15), and $\hat{c}^{(\dagger)}_\sigma(t)$ is the Heisenberg representation of the operator $\hat{c}^{(\dagger)}_\sigma$ with respect to $\hat{H}$. The Green's functions (8.1) naturally arise in 'linear-response theory' because they describe the time-dependent changes of expectation values

$$\delta\langle\hat{c}^\dagger_{\sigma_1}\hat{c}_{\sigma_2}\rangle_t \equiv \langle\hat{c}^\dagger_{\sigma_1}\hat{c}_{\sigma_2}\rangle_t - \langle\hat{c}^\dagger_{\sigma_1}\hat{c}_{\sigma_2}\rangle_{-\infty} = \sum_{\sigma_3,\sigma_4}\int_\infty^\infty \mathrm{d}t' G^{\sigma_3,\sigma_4}_{\sigma_2,\sigma_1}(t-t')f_{\sigma_3,\sigma_4}(t') \tag{8.2}$$

in the presence of a small time-dependent perturbation

$$\hat{V}(t) = \sum_{\sigma,\sigma'} f_{\sigma,\sigma'}(t)\hat{c}^\dagger_\sigma\hat{c}_{\sigma'} \tag{8.3}$$

added to $\hat{H}$ [30, 188, 189]. After a Fourier transformation, equation (8.2) reads

$$\delta\langle\hat{c}^\dagger_{\sigma_1}\hat{c}_{\sigma_2}\rangle(\omega) = \sum_{\sigma_3,\sigma_4} G^{\sigma_3,\sigma_4}_{\sigma_2,\sigma_1}(\omega)f_{\sigma_3,\sigma_4}(\omega) \tag{8.4}$$

with

$$G^{\sigma_3,\sigma_4}_{\sigma_2,\sigma_1}(\omega) \equiv \int_{-\infty}^\infty \mathrm{d}t\, G^{\sigma_3,\sigma_4}_{\sigma_2,\sigma_1}(t)e^{\mathrm{i}\omega t} \;, \tag{8.5}$$

and $f_{\sigma_3,\sigma_4}(\omega)$ and $\delta\langle\hat{c}^\dagger_{\sigma_1}\hat{c}_{\sigma_2}\rangle(\omega)$ defined accordingly.

The general definition (8.1) can be used to set up more special two-particle Green's functions, which are of interest for specific experiments. For example, for the investigation of magnetic excitations in lattice models, the transversal susceptibility

$$G_{\mathrm{T}}(\boldsymbol{q},\omega) = -\frac{\mathrm{i}}{L}\int_0^\infty \mathrm{d}t\, e^{\mathrm{i}\omega t} \left\langle \Psi_0 \left| \left[\hat{S}^+_{\boldsymbol{q}}(t), \hat{S}^-_{\boldsymbol{q}}(0) \right] \right| \Psi_0 \right\rangle \tag{8.6}$$

is of importance [190]. Here, we introduced the $\boldsymbol{q}$-dependent spin-flip operators

$$\hat{S}^+_{\boldsymbol{q}} = \sum_i e^{\mathrm{i}\boldsymbol{q}\boldsymbol{R}_i} \hat{S}^+_i = \sum_{i,b} e^{\mathrm{i}\boldsymbol{q}\boldsymbol{R}_i} \hat{c}^\dagger_{i;(b\uparrow)} \hat{c}_{i;(b\downarrow)} \,, \tag{8.7a}$$

$$\hat{S}^-_{\boldsymbol{q}} = (\hat{S}^+_{\boldsymbol{q}})^+ = \sum_{i,b} e^{-\mathrm{i}\boldsymbol{q}\boldsymbol{R}_i} \hat{c}^\dagger_{i;(b\downarrow)} \hat{c}_{i;(b\uparrow)} \tag{8.7b}$$

in the Heisenberg representation, where the sum runs over all L lattice sites $\boldsymbol{R}_i$ and orbitals b. Magnetic excitations are found as poles of the Green's function $G_{\mathrm{ret}}(\boldsymbol{q}, E)$, or, equivalently, as peaks in

$$\chi_T(\boldsymbol{q}, E) = \mathrm{Im}\, G_{\mathrm{T}}(\boldsymbol{q}, E) \tag{8.8}$$

at energies $E > 0$. They can be measured, e.g., in neutron scattering experiments.

8.2 Time-Dependent Hartree-Fock Approximation

An approximation, frequently applied to two-particle Green's functions, is the 'random-phase approximation' (RPA). This approach can be derived in various ways, e.g., by an equation of motion technique or in diagrammatic perturbation theory; see, e.g., reference [191], where we derived the RPA equations for the Green's function (8.6).

In this section, we use a different derivation in which the RPA turns out to be a time-dependent generalisation of the Hartree-Fock theory; see, e.g., references [192, 193]. If derived in this way, the approach can be generalised quite naturally in order to set up a time-dependent Gutzwiller theory, as we will show in section 8.3.

8.2.1 Equation of Motion for the Density Matrix

We consider the general Hamiltonian $\hat{H}_{\mathrm{el}}$, equation (2.3a), which was investigated within the Hartree-Fock theory in section 3.1. Here, we want to calculate the time dependence of the density matrix $\tilde{\rho}(t)$ with the elements

$$\rho_{\sigma',\sigma}(t) \equiv \langle \Psi(t) | \hat{c}^\dagger_\sigma \hat{c}_{\sigma'} | \Psi(t) \rangle \,, \tag{8.9}$$

where $|\Psi(t)\rangle$ is the solution of the time-dependent Schrödinger equation for the Hamiltonian

$$\hat{H}(t) = \hat{H}_{\mathrm{el}} + \hat{V}(t) \,. \tag{8.10}$$

To be in line with previous works on time-dependent Hartree-Fock and Gutzwiller theories, we use a different order of subscripts in the definition (8.9) of density matrices than in other parts of this work; compare, e.g., equation (3.65).

The expectation value (8.9) obeys the Heisenberg equation

$$-\mathrm{i}\dot{\rho}_{\sigma',\sigma}(t) = \langle \Psi(t) | [\hat{H}, \hat{c}^\dagger_\sigma \hat{c}_{\sigma'}] | \Psi(t) \rangle \,, \tag{8.11}$$

which contains the commutator

$$\begin{aligned}[\hat{H}(t), \hat{c}^\dagger_\sigma \hat{c}_{\sigma'}] &= \sum_{\sigma_1} \Big[\big(\varepsilon_{\sigma_1,\sigma} + f_{\sigma_1,\sigma}(t)\big) \hat{c}^\dagger_{\sigma_1} \hat{c}_{\sigma'} - \big(\varepsilon_{\sigma',\sigma_1} + f_{\sigma',\sigma_1}(t)\big) \hat{c}^\dagger_{\sigma} \hat{c}_{\sigma_1} \Big] \\ &+ \frac{1}{2} \sum_{\sigma_1,\sigma_2,\sigma_3} \left(U_{\sigma_1,\sigma_2,\sigma,\sigma_3} - U_{\sigma_1,\sigma_2,\sigma_3,\sigma}\right) \hat{c}^\dagger_{\sigma_1} \hat{c}^\dagger_{\sigma_2} \hat{c}_{\sigma'} \hat{c}_{\sigma_3} \\ &+ \frac{1}{2} \sum_{\sigma_1,\sigma_2,\sigma_3} \left(U_{\sigma',\sigma_1,\sigma_2,\sigma_3} - U_{\sigma_1,\sigma',\sigma_2,\sigma_3}\right) \hat{c}^\dagger_{\sigma_1} \hat{c}^\dagger_{\sigma} \hat{c}_{\sigma_2} \hat{c}_{\sigma_3} \, . \end{aligned} \tag{8.12}$$

In the time-dependent Hartree-Fock approximation, we assume that the solution $|\Psi(t)\rangle$ of the Schrödinger equation at any time t is approximately given by a single-particle product wave function. In this case, the expectation value of the commutator (8.12) can be evaluated by means of Wick's theorem. This leads to the equation of motion

$$\mathrm{i}\dot{\tilde{\rho}}(t) = [\tilde{h}(t), \tilde{\rho}(t)] \tag{8.13a}$$

for $\tilde{\rho}(t)$, where the matrix $\tilde{h}(t)$ has the elements

$$h_{\sigma,\sigma'}(t) = \varepsilon_{\sigma,\sigma'} + f_{\sigma,\sigma'}(t) + \sum_{\sigma_1,\sigma_2} W^{\sigma_2,\sigma_1}_{\sigma,\sigma'} \rho_{\sigma_2,\sigma_1}(t) \tag{8.13b}$$

with

$$W^{\sigma_2,\sigma_1}_{\sigma,\sigma'} \equiv U_{\sigma,\sigma_1,\sigma_2,\sigma'} - U_{\sigma,\sigma_1,\sigma',\sigma_2} \, . \tag{8.13c}$$

Note the symmetries

$$W^{\sigma_1,\sigma_2}_{\sigma_3,\sigma_4} = W^{\sigma_4,\sigma_3}_{\sigma_2,\sigma_1} = -W^{\sigma_4,\sigma_2}_{\sigma_3,\sigma_1} \, , \tag{8.14}$$

which we have used already to derive equations (8.13). We introduce the abbreviation $\boldsymbol{\sigma} = (\sigma, \sigma')$ for pairs of single-particle indices, which allows equation (8.13b) to be written as

$$h_{\boldsymbol{\sigma}}(t) = \varepsilon_{\boldsymbol{\sigma}} + f_{\boldsymbol{\sigma}}(t) + \sum_{\boldsymbol{\sigma}'} W^{\boldsymbol{\sigma}'}_{\boldsymbol{\sigma}} \rho_{\boldsymbol{\sigma}'}(t) \, . \tag{8.15}$$

The matrix $\tilde{h}(t)$ is related to the expectation value

$$E[\tilde{\rho}(t)] = \langle \hat{H}(t) \rangle_{\Psi(t)} = \sum_{\boldsymbol{\sigma}} (\varepsilon_{\boldsymbol{\sigma}} + f_{\boldsymbol{\sigma}}(t)) \rho_{\bar{\boldsymbol{\sigma}}}(t) + \frac{1}{2} \sum_{\boldsymbol{\sigma},\boldsymbol{\sigma}'} \rho_{\bar{\boldsymbol{\sigma}}}(t) W^{\bar{\boldsymbol{\sigma}}'}_{\boldsymbol{\sigma}} \rho_{\bar{\boldsymbol{\sigma}}'}(t) \tag{8.16}$$

of our Hamiltonian with respect to a wave function $|\Psi(t)\rangle$, which, again, is assumed to be a single-particle product state. In (8.16) we introduced the notation $\bar{\boldsymbol{\sigma}} \equiv (\sigma', \sigma)$ for $\boldsymbol{\sigma} = (\sigma, \sigma')$. A comparison of equations (8.13b) and (8.16) shows that the matrix (8.15) can also be determined through

$$h_{\boldsymbol{\sigma}}(t) = \frac{\partial}{\partial \rho_{\bar{\boldsymbol{\sigma}}}(t)} E[\tilde{\rho}(t)] \tag{8.17}$$

which will become an essential equation for the formulation of a time-dependent Gutzwiller theory in the following section.

8.2.2 Expansion for Weak Perturbations

We are only interested in cases where $\hat{V}(t)$ is a weak perturbation to the time independent Hamiltonian $\hat{H}_{\mathrm{el}}$. In this case, the density matrix $\tilde{\rho}(t)$ and the Hamilton matrix $\tilde{h}(t)$ are given by

$$\tilde{\rho}(t) \approx \tilde{\rho}^0 + \delta\tilde{\rho}(t) \, , \tag{8.18a}$$

$$\tilde{h}(t) \approx \tilde{h}^0 + \tilde{f}(t) + \delta\tilde{h}(t) \, , \tag{8.18b}$$

where $\delta\tilde{\rho}(t)$ describes a 'small' time-dependent perturbation around the ground-state density matrix $\tilde{\rho}^0$ and

$$h^0_{\boldsymbol{\sigma}} = \varepsilon_{\boldsymbol{\sigma}} + \sum_{\boldsymbol{\sigma}'} W^{\boldsymbol{\sigma}'}_{\boldsymbol{\sigma}} \rho^0_{\boldsymbol{\sigma}'} \,, \tag{8.19a}$$

$$\delta h_{\boldsymbol{\sigma}}(t) = \sum_{\boldsymbol{\sigma}'} W^{\boldsymbol{\sigma}'}_{\boldsymbol{\sigma}} \delta\rho_{\boldsymbol{\sigma}'}(t) \,. \tag{8.19b}$$

With the expansion (8.18), the equation of motion (8.13a) becomes

$$0 = [\tilde{h}^0, \tilde{\rho}^0] \,, \tag{8.20a}$$

$$\mathrm{i}\delta\dot{\tilde{\rho}}(t) = [\tilde{h}^0, \delta\tilde{\rho}(t)] + [\delta\tilde{h}(t) + \tilde{f}(t), \tilde{\rho}^0] \,. \tag{8.20b}$$

We have to solve equations (8.20) for density matrices that belong to a single-particle product state. Such density matrices are idempotent, i.e., they obey the matrix equation

$$\tilde{\rho} = \tilde{\rho}^2 \,. \tag{8.21}$$

With the expansion (8.18a), this condition reads

$$\tilde{\rho}^0 = \left(\tilde{\rho}^0\right)^2 \,, \tag{8.22a}$$

$$\delta\tilde{\rho}(t) = \tilde{\rho}^0\delta\tilde{\rho}(t) + \delta\tilde{\rho}(t)\tilde{\rho}^0 + \left(\delta\tilde{\rho}(t)\right)^2 \,. \tag{8.22b}$$

The condition (8.22a) and equation (8.20a) just recover the time-independent Hartree-Fock equations derived in section 3.1. Their solution yields a basis $|\gamma\rangle$ of states for which the ground-state density matrix

$$\rho^0_{\gamma,\gamma'} = \rho^0_{\boldsymbol{\gamma}} = \delta_{\gamma,\gamma'}\Theta(E_\gamma - E_\mathrm{F}) \tag{8.23}$$

and the Hamilton matrix

$$h^0_{\gamma,\gamma'} = h^0_{\boldsymbol{\gamma}} = \delta_{\gamma,\gamma'}E_\gamma \tag{8.24}$$

are diagonal. Here, E_F is the Fermi energy and E_γ are the eigenvalues of the Hartree-Fock equations (3.9a).

8.2.3 RPA Equations

Mathematically, the density matrix $\tilde{\rho}_\mathrm{h} \equiv \tilde{\rho}^0$ is a projector onto 'hole'-states. In addition, we define the projector onto 'particle'-states as

$$\tilde{\rho}_\mathrm{p} \equiv 1 - \tilde{\rho}^0 \,. \tag{8.25}$$

With these two operators, we can decompose all matrices into their four components

$$\delta\tilde{\rho}^{vw}(t) \equiv \tilde{\rho}_v\delta\tilde{\rho}(t)\tilde{\rho}_w \,, \tag{8.26a}$$

$$\tilde{f}^{vw}(t) \equiv \tilde{\rho}_v\tilde{f}(t)\tilde{\rho}_w \,, \tag{8.26b}$$

$$\tilde{h}^{0;vw} \equiv \tilde{\rho}_v\tilde{h}^0\tilde{\rho}_w \tag{8.26c}$$

with $v, w \in \{\mathrm{p}, \mathrm{h}\}$. Note that $\tilde{h}^{0;vw}$ has the elements

$$h^{0;vw}_{\gamma,\gamma'} = \delta_{v,w}\delta_{\gamma,\gamma'}E_\gamma \,. \tag{8.27}$$

An evaluation of the condition (8.22b) for the components $\delta\tilde{\rho}^{vw}(t)$ yields

$$\delta\tilde{\rho}^{vw}(t) = \delta\tilde{\rho}^{vw}(t) + \delta\tilde{\rho}^{vv}(t)\delta\tilde{\rho}^{vw}(t) + \delta\tilde{\rho}^{vw}(t)\delta\tilde{\rho}^{ww}(t) \,, \tag{8.28a}$$

and

$$\delta\tilde{\rho}^{ww}(t) = \pm\delta\tilde{\rho}^{wv}(t)\delta\tilde{\rho}^{vw}(t) \tag{8.28b}$$

for $v \neq w$. From equations (8.28) we conclude that the components $\delta\tilde{\rho}^{\rm pp}(t)$ and $\delta\tilde{\rho}^{\rm hh}(t)$ can be neglected in the following since they are quadratic with respect to the leading fluctuations $\delta\tilde{\rho}^{\rm hp}(t)$ and $\delta\tilde{\rho}^{\rm ph}(t)$.

We express the time-dependent quantities $\delta\tilde{\rho}^{vw}(t)$ and $\delta\tilde{f}^{vw}(t)$ by their respective Fourier transforms $\delta\tilde{\rho}^{vw}(\omega)$ and $\delta\tilde{f}^{vw}(\omega)$. The equation of motion (8.20b) can then be written as

$$\left[(\omega - \tilde{E})\begin{pmatrix} 1 & 0 \\ 0 & -1 \end{pmatrix} - \tilde{U}\right]\begin{pmatrix} \tilde{\rho}^{\rm ph}(\omega) \\ \tilde{\rho}^{\rm hp}(\omega) \end{pmatrix} = -\begin{pmatrix} \tilde{f}^{\rm ph}(\omega) \\ \tilde{f}^{\rm hp}(\omega) \end{pmatrix} . \tag{8.29}$$

where we introduced the matrices (tensors) $\tilde{E}$ and $\tilde{W}$ with the elements

$$U^{\gamma'}_{\gamma} = -W^{\gamma_1',\gamma_2'}_{\gamma_1,\gamma_2} = -\sum_{\sigma_1,\sigma_2,\sigma_1',\sigma_2'} u^*_{\gamma_1,\sigma_1} u_{\gamma_2,\sigma_2} W^{\sigma_1',\sigma_2'}_{\sigma_1,\sigma_2} u_{\gamma_1',\sigma_1'} u^*_{\gamma_2',\sigma_2'} \tag{8.30}$$

and

$$E^{\gamma'}_{\gamma} = E^{\gamma_1',\gamma_2'}_{\gamma_1,\gamma_2} = \delta_{\gamma_1,\gamma_1'}\delta_{\gamma_2,\gamma_4}(E_{\gamma_1} - E_{\gamma_2}) . \tag{8.31}$$

The coefficients $u^{(*)}_{\gamma,\sigma}$ in (8.30) determine the solutions $|\gamma\rangle$ of the Hartree-Fock equations and have been introduced in equations (3.2).

By comparison of equation (8.31) with (8.4) we find

$$\tilde{G}^{-1}(\omega) = \left[(\omega + {\rm i}\delta - \tilde{E})\begin{pmatrix} -1 & 0 \\ 0 & 1 \end{pmatrix} + \tilde{U}\right] \tag{8.32}$$

for the inverse of the two-particle Green's function

$$G^{\gamma'}_{\gamma}(\omega) = G^{\gamma_1',\gamma_2'}_{\gamma_1,\gamma_2}(\omega) = \sum_{\sigma_1,\sigma_2,\sigma_1',\sigma_2'} u_{\gamma_1,\sigma_1} u^*_{\gamma_2,\sigma_2} G^{\sigma_1',\sigma_2'}_{\sigma_1,\sigma_2}(\omega) u^*_{\gamma_1',\sigma_1'} u_{\gamma_2',\sigma_2'} . \tag{8.33}$$

Note that we have added an increment ${\rm i}\delta$ with $\delta = 0^+$ in (8.32), to ensure that $\tilde{G}(\omega)$ obeys the boundary conditions of a retarded Green's function. For $\tilde{U} = 0$, the Green's function (8.32) reads

$$\tilde{\Gamma}^{-1}(\omega) \equiv \mp(\omega + {\rm i}\delta - \tilde{E}) \tag{8.34}$$

and has the elements

$$\Gamma^{\gamma'}_{\gamma}(\omega) = \Gamma^{\gamma_1',\gamma_2'}_{\gamma_1,\gamma_2}(\omega) = \delta_{\gamma_1,\gamma_1'}\delta_{\gamma_2,\gamma_2'}\frac{\rho^0_{\gamma_2,\gamma_2} - \rho^0_{\gamma_1,\gamma_1}}{\omega + {\rm i}\delta - (E_{\gamma_1} - E_{\gamma_2})} . \tag{8.35}$$

The Green's function $\tilde{\Gamma}$ is not exact for the single-particle Hamiltonian $\hat{H}_0$ since we just set $\tilde{U} = 0$ in (8.32), and kept finite the Hartree-Fock self-energy, which influences the eigenvalues E_γ. due to the Hartree-Fock self-energy contributions to the eigenvalues E_γ, the Green's function $\tilde{\Gamma}$ is not exact for the single-particle Hamiltonian $\hat{H}_0$ in (2.3). With the 'uncorrelated' Green's function (8.35), we can write (8.32) as

$$\tilde{G}(\omega) = \tilde{\Gamma}(\omega)[1 + \tilde{U}\tilde{\Gamma}(\omega)]^{-1} \tag{8.36a}$$

$$= \tilde{\Gamma} + \tilde{\Gamma}(\omega)\tilde{U}\tilde{G}(\omega) \tag{8.36b}$$

where, in the second line, we expanded the denominator $[1+\tilde{U}\tilde{\Gamma}(\omega)]^{-1}$ into a power series with respect to $\tilde{U}\tilde{G}$. Both equations (8.36) are standard formulations for the two-particle Green's function in the random-phase approximation.

The derivation of the RPA as a time dependent Hartree-Fock theory illustrates that it is a reliable approximation only for systems with a ground state that is properly described by a mean-field approximation. Therefore, the RPA has to be discarded for the correlated systems we are interested in. Just as we succeeded to improve the ground-state description by means of a Gutzwiller wave function, we will now introduce a time-dependent generalisation of the Gutzwiller theory as an improved method for the investigation of two-particle excitations.

8.3 Time-Dependent Gutzwiller Theory

The time-dependent Gutzwiller approximation has been developed for single-band Hubbard models by Seibold et al. [194, 195]. It was applied, with astonishing success, to a number of such models and response functions [195–206]. In this section, we give a derivation of the time-dependent Gutzwiller theory for multi-band models. To this end, we set up an effective energy functional of the density matrix in sections 8.3.1-8.3.3, which eventually leads to Gutzwiller RPA equations in section 8.3.4.

8.3.1 Energy Functional

As shown in section 5, the expectation value of the multi-band Hamiltonian (2.15) in the Gutzwiller theory is a function of the variational parameters $\lambda_{\Gamma,\Gamma'}$ and of the one-particle wave function $|\Psi_0\rangle$, see equations (5.86)-(5.89), (5.80b), and (5.65). The single-particle wave function $|\Psi_0\rangle$ enters the energy functional solely through elements

$$\rho_Y \equiv \rho_{i,\sigma;j,\sigma'} \equiv \langle \hat{c}^\dagger_{j,\sigma'} \hat{c}_{i,\sigma} \rangle_{\Psi_0} \tag{8.37}$$

of the non-interacting density matrix, where Y is an abbreviation for $(i,\sigma;j,\sigma')$. It is therefore possible to consider the energy

$$E = E(\boldsymbol{\lambda}, \tilde{\rho}) \tag{8.38}$$

as a functional of the density matrix $\tilde{\rho}$ and the vector $\boldsymbol{\lambda}$ of variational parameters λ_Z, with Z as an abbreviation for (Γ,Γ'). The density matrix in the energy functional (8.38) must be derived from a single-particle wave function and, therefore, it has to obey the condition (8.21).

Note that, in the following considerations, the density matrix will either be considered as a matrix (with respect to its two indices (i,σ) and (j,σ')) or as a vector (with respect to its single index Y). To distinguish between both cases, we denote (8.37) as $\tilde{\rho}$ or as $\boldsymbol{\rho}$ for the respective matrix and vector interpretation.

The constraints (5.48) are also functionals of $\boldsymbol{\lambda}$ and $\boldsymbol{\rho}$ and will be denoted as

$$g_i(\boldsymbol{\lambda}, \boldsymbol{\rho}) = 0 \quad , \quad 1 \leq i \leq n_\mathrm{c} \; . \tag{8.39}$$

Here, n_c is the number of independent constraints, which, due to symmetries, will usually be smaller than its maximum value $2N^2+1$, where N is the number of spin-orbital states per lattice site.

By solving equations (5.48) we can, at least in principle, express n_c of the parameters λ_Z through the density matrix $\boldsymbol{\rho}$ and the remaining 'independent' parameters λ^i_Z. In this way, we find an energy functional $E^\mathrm{GA}(\boldsymbol{\lambda}^\mathrm{i}, \boldsymbol{\rho})$, which has to be minimised with the only constraint (8.21) for the density matrix. This leads to

$$\delta\{E^\mathrm{GA}(\boldsymbol{\lambda}^\mathrm{i}, \boldsymbol{\rho}) - \mathrm{tr}\Lambda(\tilde{\rho}^2 - \tilde{\rho})\} = 0 \; , \tag{8.40}$$

where we introduced the Lagrange-parameter matrix Λ. In full analogy to the treatment of the one-band model [197], one finds that equation (8.40) leads to

$$0 = [\tilde{h}^0, \tilde{\rho}^0] \,, \tag{8.41a}$$

$$0 = \left.\frac{\partial E^{\mathrm{GA}}}{\partial \lambda^{\mathrm{i}}_z}\right|_{\lambda^{\mathrm{i}}_z = \lambda^{\mathrm{i};0}_z} \,, \tag{8.41b}$$

where we introduced the matrix $\tilde{h}^0$ with the elements

$$h^0_Y = \left.\frac{\partial E^{\mathrm{GA}}}{\partial \rho_{\bar{Y}}}\right|_{\rho_{\bar{Y}} = \rho^0_{\bar{Y}}} \,. \tag{8.42}$$

Here, we used again the notation $\bar{Y} \equiv (j, \sigma'; i, \sigma)$ for $Y = (i, \sigma; j, \sigma')$ and introduced the parameters $\tilde{\rho}^0$ (or $\boldsymbol{\rho}^0$) and $\boldsymbol{\lambda}^{\mathrm{i};0}$ that minimise $E^{\mathrm{GA}}(\boldsymbol{\lambda}^{\mathrm{i}}, \boldsymbol{\rho})$. The matrix $\tilde{h}^0$ further defines the single-particle 'Gutzwiller-Hamiltonian'

$$\hat{h}^0 \equiv \sum_{i,j;\sigma,\sigma'} h_{i,\sigma;j,\sigma'} \hat{c}^\dagger_{i,\sigma} \hat{c}_{j,\sigma'} \,. \tag{8.43}$$

8.3.2 Second-Order Expansion of the Energy Functional

In order to study excitations, we add a small time-dependent field

$$\hat{H}_f(t) = \sum_{i,j;\sigma,\sigma'} f'_{i,\sigma;j,\sigma'}(t) \hat{c}^\dagger_{i,\sigma} \hat{c}_{j,\sigma'} + \mathrm{h.c.} \tag{8.44}$$

to our multi-band Hamiltonian (2.15). With the time dependence $f_{i,\sigma;j,\sigma'}(t) = f_{i,\sigma;j,\sigma'} e^{-\mathrm{i}\omega t}$, the expectation value of $\hat{H}_f(t)$ reads

$$E_f(\boldsymbol{\lambda}^{\mathrm{i}}, \boldsymbol{\rho}) = \sum_{i,j;\sigma,\sigma'} f_{i,\sigma;j,\sigma'} e^{-\mathrm{i}\omega t} \rho_{j,\sigma';i,\sigma} + \mathrm{c.c.} \,, \tag{8.45}$$

where

$$f_{i,\sigma_1;j,\sigma_2} = \delta_{i,j} f'_{i,\sigma_1;i,\sigma_2} \frac{C_{i,\sigma_2;i,\sigma_1}}{\rho_{i,\sigma_2;i,\sigma_1}} + (1 - \delta_{i,j}) \sum_{\sigma'_1,\sigma'_2} f'_{i,\sigma'_1;j,\sigma'_2} q^{\sigma_1}_{\sigma'_1} \left(q^{\sigma_2}_{\sigma'_2}\right)^* \,. \tag{8.46}$$

The renormalisation matrix $\tilde{q}$ and the (correlated) local density matrix $\tilde{C}$ are defined in equations (5.80) and (5.70), respectively.

The time-dependent field induces small amplitude fluctuations of $\boldsymbol{\rho}$ and $\boldsymbol{\lambda}^{\mathrm{i}}$,

$$\rho_Y = \rho^0_Y + \delta\rho_Y(t) \,, \tag{8.47a}$$

$$\lambda^{\mathrm{i}}_Z = \lambda^0_Z + \delta\lambda^{\mathrm{i}}_Z(t) \,. \tag{8.47b}$$

In order to set up the RPA equations, we have to expand E^{GA} up to second order with respect to $\delta\rho_Y$ and $\delta\lambda^{\mathrm{i}}_Z$,

$$\begin{aligned} E^{\mathrm{GA}}(\boldsymbol{\rho}, \boldsymbol{\lambda}^{\mathrm{i}}) = {} & E_0 + \mathrm{tr}(\tilde{h}^0 \delta\tilde{\rho}) + \frac{1}{2} \sum_{Y,Y'} \delta\rho_Y M^{\rho,\rho}_{Y,Y'} \delta\rho_{Y'} \\ & + \frac{1}{2} \sum_{Z,Y} \left(\delta\lambda^{\mathrm{i}}_Z M^{\lambda,\rho}_{Z,Y} \delta\rho_Y + \delta\rho_Y M^{\rho,\lambda}_{Y,Z} \delta\lambda^{\mathrm{i}}_Z \right) \\ & + \frac{1}{2} \sum_{Z,Z'} \delta\lambda^{\mathrm{i}}_Z M^{\lambda,\lambda}_{Z,Z'} \delta\lambda^{\mathrm{i}}_{Z'} \,. \end{aligned} \tag{8.48}$$

Here, we introduced the matrices $\tilde{M}^{\rho\rho}$, $\tilde{M}^{\lambda\rho}$, $\tilde{M}^{\rho\lambda}$, $\tilde{M}^{\lambda\lambda}$ with the elements

$$M^{\rho\rho}_{Y,Y'} = \frac{\partial^2 E^{\mathrm{GA}}}{\partial\rho_Y \partial\rho_{Y'}} , \tag{8.49a}$$

$$M^{\lambda\rho}_{Z,Y} = \frac{\partial^2 E^{\mathrm{GA}}}{\partial\lambda^{\mathrm{i}}_Z \partial\rho_Y} , \tag{8.49b}$$

$$M^{\rho\lambda}_{Y,Z} = \frac{\partial^2 E^{\mathrm{GA}}}{\partial\rho_Y \partial\lambda^{\mathrm{i}}_Z} , \tag{8.49c}$$

$$M^{\lambda\lambda}_{Z,Z'} = \frac{\partial^2 E^{\mathrm{GA}}}{\partial\lambda^{\mathrm{i}}_Z \partial\lambda^{\mathrm{i}}_{Z'}} , \tag{8.49d}$$

where the second derivatives on the r.h.s. are evaluated for $\boldsymbol{\rho} = \boldsymbol{\rho}^0$ and $\boldsymbol{\lambda}^{\mathrm{i}} = \boldsymbol{\lambda}^{\mathrm{i};0}$. Note that there is no linear term $\sim \lambda^{\mathrm{i}}_Z$ in (8.48) because of the minimisation condition (8.41b). For our further evaluation, it is useful to write equation (8.48) in a more compact form by means of matrix-vector products,

$$\begin{aligned} E^{\mathrm{GA}}(\boldsymbol{\rho},\boldsymbol{\lambda}) &= E_0 + \mathrm{tr}(\tilde{h}^0\delta\tilde{\rho}) + \frac{1}{2}\delta\boldsymbol{\rho}^T\tilde{M}^{\rho\rho}\delta\boldsymbol{\rho} \\ &\quad + (\delta\boldsymbol{\lambda}^{\mathrm{i}})^T\tilde{M}^{\lambda\rho}\delta\boldsymbol{\rho} + \frac{1}{2}(\delta\boldsymbol{\lambda}^{\mathrm{i}})^T\tilde{M}^{\lambda\lambda}\delta\boldsymbol{\lambda} . \end{aligned} \tag{8.50}$$

Here, we used the symmetry $\tilde{M}^{\lambda,\rho} = \left[\tilde{M}^{\rho,\lambda}\right]^T$.

Like in the one-band model, we assume that the local multiplet dynamics, described by the amplitudes $\delta\lambda^{\mathrm{i}}_Z(t)$, are fast compared to those of the local density matrix. This leads to the 'antiadiabaticity assumption'

$$\frac{\partial}{\partial\delta\lambda^{\mathrm{i}}_Z} E^{\mathrm{GA}}(\boldsymbol{\rho},\boldsymbol{\lambda}^{\mathrm{i}}) = 0 , \tag{8.51}$$

which gives us the multiplet amplitude fluctuations

$$\delta\boldsymbol{\lambda}^{\mathrm{i}} = -\left[\tilde{M}^{\lambda,\lambda}\right]^{-1}\tilde{M}^{\lambda,\rho}\delta\boldsymbol{\rho} \tag{8.52}$$

as a linear function of the densities $\delta\boldsymbol{\rho}$. This result, together with equation (8.50), finally leads to the energy expansion

$$E^{\mathrm{GA}}(\boldsymbol{\rho}) = E_0 + \mathrm{tr}(\tilde{h}^0\delta\tilde{\rho}) + \frac{1}{2}\delta\boldsymbol{\rho}^T\tilde{K}^{\rho\rho}\delta\boldsymbol{\rho} , \tag{8.53a}$$

$$\tilde{K}^{\rho\rho} \equiv \tilde{M}^{\rho\rho} - \tilde{M}^{\rho\lambda}\left[\tilde{M}^{\lambda\lambda}\right]^{-1}\tilde{M}^{\lambda\rho} , \tag{8.53b}$$

solely as a function of the density fluctuations $\delta\boldsymbol{\rho}$.

8.3.3 Invariance of the Second-Order Expansion

Before we continue our derivation, we need to address the question whether or not the second-order energy expansion (8.53a)-(8.53b) depends on the particular choices that we have made with respect to our variational parameters. For example, in our numerical minimisations for transition metals, we found it convenient to work with the variational parameters $\lambda_{\Gamma,\Gamma}/\sqrt{m^0_\Gamma m^0_{\Gamma'}}$ instead of $\lambda_{\Gamma,\Gamma}$. Furthermore, in the previous section we had to choose a certain set of dependent and independent parameters in order to fulfil the constraints (5.48).

While the variational ground state is obviously not affected by such an arbitrary choice of the independent variational parameters, the same is not obvious for the matrix $K^{\rho\rho}$.

Mathematically, both of the changes that we could make, i.e., defining different variational parameters, or, introducing another set of independent parameters, are described by a general transformation

$$\boldsymbol{\lambda}^{\mathrm{i}} = \boldsymbol{\lambda}^{\mathrm{i}}(\bar{\boldsymbol{\lambda}}^{\mathrm{i}}, \boldsymbol{\rho}) \tag{8.54}$$

from some old (λ^{i}_Z) to new variational parameters $\bar{\lambda}^{\mathrm{i}}_Z$. The energy functional

$$\bar{E}^{\mathrm{GA}}(\boldsymbol{\rho}, \bar{\boldsymbol{\lambda}}^{\mathrm{i}}) = E^{\mathrm{GA}}(\boldsymbol{\rho}, \lambda(\boldsymbol{\rho}, \bar{\boldsymbol{\lambda}}^{\mathrm{i}})) \tag{8.55}$$

changes accordingly. The second derivatives (8.49a)-(8.49d) with respect to the new and the old parameters are related to each other. One finds

$$\begin{aligned}
\bar{M}^{\rho\rho} &= \tilde{M}^{\rho\rho} + \tilde{V}^T \tilde{M}^{\lambda\rho} + \tilde{M}^{\rho\lambda}\tilde{V} + \tilde{V}^T \tilde{M}^{\lambda\lambda}\tilde{V} \,, && (8.56a)\\
\bar{M}^{\rho\bar{\lambda}} &= \tilde{M}^{\rho\lambda}\tilde{W} + \tilde{V}^T \tilde{M}^{\lambda\lambda}\tilde{W} \,, && (8.56b)\\
\bar{M}^{\bar{\lambda}\rho} &= \tilde{W}^T \tilde{M}^{\lambda\rho} + \tilde{W}^T \tilde{M}^{\lambda\lambda}\tilde{V} \,, && (8.56c)\\
\bar{M}^{\bar{\lambda}\bar{\lambda}} &= \tilde{W}^T \tilde{M}^{\lambda\lambda}\tilde{W} \,, && (8.56d)
\end{aligned}$$

where we introduced the matrices V and W with the elements

$$\begin{aligned}
\tilde{V}_{Z,Y} &\equiv \frac{\partial \bar{\lambda}_Z}{\partial \rho_Y} \,, && (8.57a)\\
\tilde{W}_{Z,Z'} &\equiv \frac{\partial \bar{\lambda}_Z}{\partial \lambda_{Z'}} \,. && (8.57b)
\end{aligned}$$

Note that for the derivation of equations(8.56a)-(8.56d) we explicitly used equation (8.41b). For the second-order terms in the expansion (8.53a), we now readily find

$$\begin{aligned}
\bar{M}^{\rho\bar{\lambda}} \left[\bar{M}^{\bar{\lambda}\bar{\lambda}}\right]^{-1} \bar{M}^{\bar{\lambda}\rho} &= \tilde{V}^T \tilde{M}^{\lambda\rho} + \tilde{M}^{\rho\lambda}\tilde{V} + \tilde{V}^T \tilde{M}^{\lambda\lambda}\tilde{V} \\
&\quad + \tilde{M}^{\rho\lambda} \left[\tilde{M}^{\lambda\lambda}\right]^{-1} \tilde{M}^{\lambda\rho} \,, && (8.58)
\end{aligned}$$

which, together with equation (8.56a), yields the equivalence

$$\bar{K}^{\rho\rho} = \tilde{K}^{\rho\rho} \tag{8.59}$$

of the second-order expansion.

8.3.4 Gutzwiller RPA Equations

The derivation of RPA-type equations within the time-dependent Gutzwiller theory goes along the same lines as discussed in section 8.2 for the time-dependent Hartree-Fock theory. The energy functional (8.53) defines a Hamilton matrix $\tilde{h}(t)$ with the elements

$$h_Y(t) = \frac{\partial E^{\mathrm{GA}}}{\partial \rho_{\bar{Y}}} E^{\mathrm{GA}}(\tilde{\rho}) = h^0_Y + \sum_{Y'} K^{\rho\rho}_{\bar{Y},Y'} \delta\rho_{Y'}(t) = h^0_Y + \delta h_Y(t) \,, \tag{8.60}$$

which we assume to obey the same equation of motion,

$$\mathrm{i}\delta\dot{\tilde{\rho}}(t) = [\tilde{h}^0, \delta\tilde{\rho}(t)] + [\delta\tilde{h}(t) + \tilde{f}(t), \tilde{\rho}^0] \,, \tag{8.61}$$

as the density matrix in the time-dependent Hartree-Fock theory, see equation (8.20b). The diagonalisation of the matrix $\tilde{h}^0$ yields a basis $|\gamma\rangle$ with

$$h^0_{\gamma,\gamma'} = h^0_{\boldsymbol{\gamma}} = \delta_{\gamma,\gamma'} E_\gamma \tag{8.62}$$

and

$$\rho^0_{\gamma,\gamma'} = \rho^0_{\boldsymbol{\gamma}} = \delta_{\gamma,\gamma'} \Theta(E_\gamma - E_\mathrm{F}) \; . \tag{8.63}$$

With the projectors $\tilde{\rho}_\mathrm{h} \equiv \tilde{\rho}^0$ and $\tilde{\rho}_\mathrm{p} \equiv 1 - \tilde{\rho}^0$, we can define the particle and hole components of all matrices, as we did in equations (8.26). The components $\delta\tilde{\rho}^{vw}(t)$ of the density-matrix fluctuations obey equations (8.28), i.e., to leading order we can neglect $\delta\tilde{\rho}^{\mathrm{hh}}(t)$ and $\delta\tilde{\rho}^{pp}(t)$. Hence, after a Fourier transformation we end up with the same form of RPA equations,

$$\left[(\omega - \tilde{E}) \begin{pmatrix} 1 & 0 \\ 0 & -1 \end{pmatrix} - \tilde{K}^{\rho\rho} \right] \begin{pmatrix} \tilde{\rho}^{\mathrm{ph}}(\omega) \\ \tilde{\rho}^{\mathrm{hp}}(\omega) \end{pmatrix} = - \begin{pmatrix} \tilde{f}^{\mathrm{ph}}(\omega) \\ \tilde{f}^{\mathrm{hp}}(\omega) \end{pmatrix} \; . \tag{8.64}$$

as in equation (8.29). Here, however, the bare matrix of Coulomb parameters $\tilde{U}$ is replaced by the matrix $\tilde{K}^{\rho\rho}$ and the energies E_γ in the matrix $\tilde{E}$, equation (8.31), are not the eigenvalues of the Hartree-Fock but of the Gutzwiller Hamiltonian (8.43).

For a comparison with (8.4), we must keep in mind that $\tilde{f}(\omega)$ in (8.64) is renormalised, i.e., it is not the bare field as it appears in (8.4), see equation (8.46). On the other hand, on the l.h.s. of equation (8.4) appears the 'correlated' expectation value of the density matrix, whereas in (8.64) we work with the fluctuations of the uncorrelated density matrix. Therefore, we define

$$\underline{\tilde{G}}^{-1}(\omega) \equiv \left[(\omega + \mathrm{i}\delta - \tilde{E}) \begin{pmatrix} -1 & 0 \\ 0 & 1 \end{pmatrix} + \tilde{K}^{\rho\rho} \right] \; . \tag{8.65}$$

which yields the elements of $\tilde{G}(\omega)$,

$$G^{Y'}_{Y}(\omega) = c_{Y,Y'} \underline{G}^{Y'}_{Y}(\omega) \; , \tag{8.66}$$

apart from frequency independent factors $c_{Y,Y'}$. We can calculate these factors ab-initio if we assume that correlated and uncorrelated density-matrix fluctuations are related through the same renormalisation factors as the corresponding ground-state density matrices. Alternatively, the factors $c_{Y,Y'}$ could be determined by a consideration of sum rules. Ideally, both ways lead to the same results. At the moment, due to the lack of numerical experience for multi-band systems, we cannot make any substantial statements on how the factors $c_{Y,Y'}$ ought to be determined in general. Note, however, that this question is of minor importance since it only affects the overall spectral weight and not the frequency dependence of the Green's function matrix $\tilde{G}(\omega)$.

A numerical evaluation of our time-dependent Gutzwiller theory for multi-band systems is under way and will be published elsewhere [207]. Results for single-band models can be found in references [195–206].

8.4 Spin-Wave Excitations in Itinerant Ferromagnets

For the investigation of spin-wave excitations in itinerant ferromagnets, the Gutzwiller theory provides an alternative scheme, which resembles the Bijn-Feynman approach [208–210] for the investigation of density excitations in Bose superfluids.

The theoretical examination of spin-wave excitations requires the analysis of the imaginary part $\chi_T(\boldsymbol{q}, \omega)$ of the Green' function $G_\mathrm{T}(\boldsymbol{q}, \omega)$, see equations (8.6)-(8.8). The magnetic excitations of a system are represented by poles of $G_\mathrm{T}(\boldsymbol{q}, \omega)$ at frequencies $\omega > 0$. For our further

analysis, we expand the 'spin-wave state'

$$\left|\Phi_{\boldsymbol{q}}^{0}\right\rangle \equiv \hat{S}_{\boldsymbol{q}}^{-}\left|\Phi_{0}\right\rangle \tag{8.67}$$

in terms of exact energy eigenstates

$$\left|\Phi_{\boldsymbol{q}}^{0}\right\rangle = \sum_{n} W_{n}\left|\Phi_{n}\right\rangle \ , \tag{8.68a}$$

$$\hat{H}\left|\Phi_{n}\right\rangle = E_{n}\left|\Phi_{n}\right\rangle \ . \tag{8.68b}$$

The Lehmann-representation of (8.6),

$$G_{T}(\boldsymbol{q},\omega) = -\frac{i}{L}\sum_{n}\left[\frac{|\ \langle\Phi_{n}\mid\hat{S}_{\boldsymbol{q}}^{-}\mid\Phi_{0}\rangle\ |^{2}}{\omega-(E_{n}-E_{0})+i\delta} - \frac{|\ \langle\Phi_{n}\mid\hat{S}_{\boldsymbol{q}}^{+}\mid\Phi_{0}\rangle\ |^{2}}{\omega+(E_{n}-E_{0})+i\delta}\right] \ , \tag{8.69}$$

shows that there are poles in $G_{T}(\boldsymbol{q},\omega)$ for the energies $E_{n}-E_{0}>0$ with weights

$$|W_{n}|^{2} = \left|\langle\Phi_{n}|\hat{S}_{\boldsymbol{q}}^{-}|\Phi_{0}\rangle\right|^{2} \ . \tag{8.70}$$

In a ferromagnetic system without spin-orbit coupling, the state $|\Phi_{\boldsymbol{q}=\boldsymbol{0}}^{0}\rangle$ is also a ground state of $\hat{H}$, since the operator $\hat{S}_{\boldsymbol{q}=\boldsymbol{0}}^{-}$ just flips a spin in the spin-multiplet of the ground state $|\Phi_{0}\rangle$. Therefore, we can conclude that $G_{T}(\boldsymbol{0},\omega)$ has one isolated pole for $\omega-E_{0}=0$. Now we consider finite but small values of $\boldsymbol{q}$, and assume that the expansion (8.69) is still dominated by a narrow distribution of low-energy states. This scenario explains the pronounced peak in $\chi_{T}(\boldsymbol{q},\omega)$ for small values of ω and $|\boldsymbol{q}\,|$, which is seen in experiments and interpreted as a spin-wave excitation, see, e.g., reference [211]. Then, the spin-wave dispersion $E_{\boldsymbol{q}}$ can be identified as the position of this peak, and $E_{\boldsymbol{q}}$ is approximately determined by the first moment of the distribution $|W_{n}|^{2}$,

$$E_{\boldsymbol{q}} = \frac{\sum_{n} E_{n}\ |W_{n}|^{2}}{\sum_{n}|W_{n}|^{2}} - \frac{\langle\Phi_{0}|\hat{H}|\Phi_{0}\rangle}{\langle\Phi_{0}\mid\Phi_{0}\rangle} \tag{8.71a}$$

$$= \frac{\langle\Phi_{0}|\hat{S}_{\boldsymbol{q}}^{+}\hat{H}\hat{S}_{\boldsymbol{q}}^{-}|\Phi_{0}\rangle}{\langle\Phi_{0}|\hat{S}_{\boldsymbol{q}}^{+}\hat{S}_{\boldsymbol{q}}^{-}|\Phi_{0}\rangle} - \frac{\langle\Phi_{0}|\hat{H}|\Phi_{0}\rangle}{\langle\Phi_{0}\mid\Phi_{0}\rangle} \ . \tag{8.71b}$$

It is still impossible to derive the spin-wave dispersion $E_{\boldsymbol{q}}$ from equation (8.71) since we do not know the ground state $|\Phi_{0}\rangle$ of our multi-band Hamiltonian (2.15). If we assume, however, that the variational wave function $|\Psi_{\mathrm{G}}\rangle$ is a good approximation for $|\Phi_{0}\rangle$, we may substitute $|\Phi_{0}\rangle$ in equation (8.71a) by the variational wave function $|\Psi_{\mathrm{G}}\rangle$. In this way, we define the 'variational' spin-wave dispersion

$$E_{\boldsymbol{q}}^{\mathrm{var}} = \frac{\langle\Psi_{\mathrm{G}}|\hat{S}_{\boldsymbol{q}}^{+}\hat{H}\hat{S}_{\boldsymbol{q}}^{-}|\Psi_{\mathrm{G}}\rangle}{\langle\Psi_{\mathrm{G}}|\hat{S}_{\boldsymbol{q}}^{+}\hat{S}_{\boldsymbol{q}}^{-}|\Psi_{\mathrm{G}}\rangle} - \frac{\langle\Psi_{\mathrm{G}}|\hat{H}|\Psi_{\mathrm{G}}\rangle}{\langle\Psi_{\mathrm{G}}\mid\Psi_{\mathrm{G}}\rangle} \ . \tag{8.72}$$

Note that this quantity obeys no strict upper-bound properties. Nevertheless, we expect that $E_{\boldsymbol{q}}^{\mathrm{exp}} < E_{\boldsymbol{q}}^{\mathrm{var}}$ is fulfilled because the expectation value (8.71) includes high-energy states that do not belong to the spin-wave excitation seen in experiments.

In principle, transversal spin-excitations are given as peaks both in $\chi_{T}(\boldsymbol{q},\omega)$ and $\chi_{T}(\boldsymbol{q},E_{0}-\omega)$ for frequencies $\omega > E_{0}$. The latter contributions are identical to the second term in equation (8.69) and we could include them by using the proper spin-wave state

$$\left|\tilde{\Psi}_{\boldsymbol{q}}^{0}\right\rangle \equiv \left(\hat{S}_{\boldsymbol{q}}^{-}+\hat{S}_{\boldsymbol{q}}^{+}\right)\left|\Psi_{G}\right\rangle \tag{8.73}$$

in our variational approach. However, the contributions from the second operator in (8.73) vanish for $\boldsymbol{q} = \boldsymbol{0}$ and may be neglected for small values of $|\boldsymbol{q}|$, where spin-wave excitations are observed in experiments.

The variational spin-wave dispersion (8.71) can be evaluated in the limit of infinite spatial dimensions by means of the diagrammatic techniques developed in chapter 5. The results of this tedious but straightforward evaluation can be found in reference [151]. We will present numerical results for a two-band model in section 9.1.4.

Note that, in general, the Gutzwiller wave function is not an eigenstate of the operator

$$\hat{\boldsymbol{S}}^2 = \left(\sum_i \hat{\boldsymbol{S}}_i \right)^2 \tag{8.74}$$

for the total spin and its z-component

$$\hat{S}^z = \sum_i \hat{S}_{i,z} \ . \tag{8.75}$$

Here, $\hat{\boldsymbol{S}}_i = (\hat{S}_{i,x}, \hat{S}_{i,y}, \hat{S}_{i,z})$ is the local spin operator defined by the z-component

$$\hat{S}_{i,z} \equiv \frac{1}{2} \sum_b \hat{c}^\dagger_{i;(b\uparrow)} \hat{c}_{i;(b\uparrow)} - \hat{c}^\dagger_{i;(b\downarrow)} \hat{c}_{i;(b\downarrow)} \tag{8.76}$$

and the two spin-flip operators

$$\hat{S}^{+/-}_i = \sum_b \hat{c}^\dagger_{i;(b\uparrow/\downarrow)} \hat{c}_{i;(b\downarrow/\uparrow)} \tag{8.77}$$

through

$$\hat{S}_{i,x} = \frac{1}{2}(\hat{S}^+_i + \hat{S}^-_i) \ , \tag{8.78a}$$

$$\hat{S}_{i,y} = \frac{1}{2\mathrm{i}}(\hat{S}^+_i - \hat{S}^-_i) \ . \tag{8.78b}$$

With a Gutzwiller wave function that violates the global spin-symmetry, the variational spin-wave dispersion (8.71) has no Goldstone mode, i.e., it will usually yield the unphysical result $E^{\mathrm{var}}_{\boldsymbol{0}} \neq 0$. This shortcoming is not bound to the variational spin-wave theory, but will also appear if we calculate the transversal susceptibility within the time-dependent Gutzwiller theory of section (8.3). Therefore, it is of importance for both approaches, to ensure that the Gutzwiller wave function is an eigenstate of $\hat{\boldsymbol{S}}^2$ and $\hat{S}^z$. In appendix (E.3), we discuss how this can be achieved by introducing certain constraints on our variational parameters $\lambda_{\Gamma,\Gamma'}$.

Chapter 9

Model Studies

In this chapter, we address four different questions that naturally arise in connection with a two-orbital system. In section 9.1, we investigate the stability of the paramagnetic ground state with respect to ferromagnetic spin order. Instabilities with respect to orbital order are discussed in section 9.2. In section 9.3, we consider metal-insulator transitions in degenerate two-band models. Finally, in section 9.4, we investigate the scenario of an orbital selective Mott transition and study the effects of a finite local hybridisation between orbitals.

9.1 Ferromagnetism in a Two-Band Hubbard Model

It is well known that ferromagnetic order appears in single-band Hubbard models only under very special circumstances, e.g., if the density of states has a sharp peak at the Fermi level and the Coulomb interaction is much larger than the band width. This is seen not only in the Gutzwiller theory, but also in the Dynamical-Mean-Field-Theory, see, e.g., references [212, 213].

From these results, we can already conclude that ferromagnetism, as it is observed in transition metals, is closely related to the orbital degeneracy of the partially filled 3d-shell in these systems. Therefore, it is quite instructive to study ferromagnetic instabilities in a system with two orbitals, as a first step from the simple one-band model towards a realistic description of materials with partially filled 3d-shells.

9.1.1 Model Specification

We consider a Hubbard model with two degenerate e_g orbitals per site on a simple cubic lattice. The local (atomic) Hamiltonian for this system is given in equation (2.23). Using the notations introduced by Slater and Koster in reference [214], we find

$$\begin{aligned}
\varepsilon^0_{\boldsymbol{k};u,u} &= t^{(1)}_{dd\sigma}((1/2)\cos k_x + (1/2)\cos k_y + 2\cos k_z) + (3/2)t^{(1)}_{dd\delta}(\cos k_x + \cos k_y) \\
&\quad + t^{(2)}_{dd\sigma}\cos k_x \cos k_y + [(1/4)t^{(2)}_{dd\sigma} + 3t^{(2)}_{dd\pi}](\cos k_x + \cos k_y)\cos k_z \\
&\quad + 3t^{(2)}_{dd\delta}(\cos k_x \cos k_y + (1/4)\cos k_x \cos k_z + (1/4)\cos k_y \cos k_z)\ , \qquad (9.1a) \\
\varepsilon^0_{\boldsymbol{k};v,v} &= (3/2)t^{(1)}_{dd\sigma}(\cos k_x + \cos k_y) + t^{(1)}_{dd\delta}((1/2)\cos k_x + (1/2)\cos k_y + 2\cos k_z) \qquad (9.1b) \\
&\quad + 4t^{(2)}_{dd\pi}\cos k_x \cos k_y + [(3/4)t^{(2)}_{dd\sigma} + t^{(2)}_{dd\pi} + (9/4)t^{(2)}_{dd\delta}](\cos k_x + \cos k_y)\cos k_z\ , \\
\varepsilon^0_{\boldsymbol{k};u,v} &= \varepsilon^0_{\boldsymbol{k},vu} = (\sqrt{3}/2)[-t^{(1)}_{dd\sigma} + t^{(1)}_{dd\delta}](\cos k_x - \cos k_y) \\
&\quad + [(\sqrt{3}/4)t^{(2)}_{dd\sigma} - \sqrt{3}t^{(2)}_{dd\pi} + (3\sqrt{3}/4)t^{(2)}_{dd\delta}](\cos k_x - \cos k_y)\cos k_z\ . \qquad (9.1c)
\end{aligned}$$

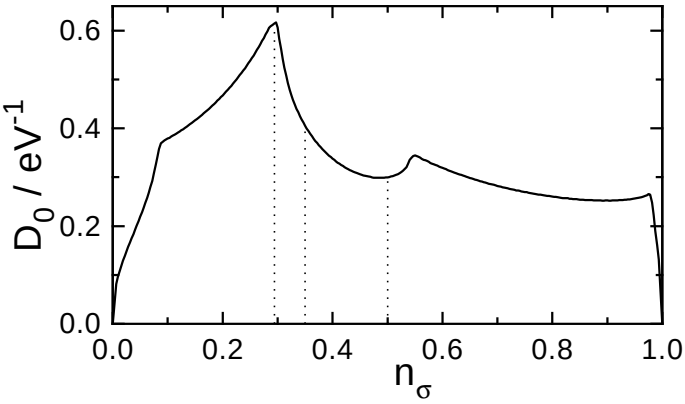

Figure 9.1: Model density of states at the Fermi energy as a function of the orbital filling n_σ. The dashed lines indicate the fillings used in sections 9.1 and 9.3. The total bandwidth is $W = 6.8$ eV.

for the bare (spin independent) band energies (2.17a). Here, we included hopping parameters to the nearest and second-nearest neighbours, and set the cubic lattice constant equal to unity.

As in references [99, 122, 123] we choose the hopping parameters according to general experience for transition metal energy bands, $t^{(1)}_{dd\sigma} = 1\,\mathrm{eV}$, $t^{(2)}_{dd\sigma} = 0.25\,\mathrm{eV}$, and $t^{(1),(2)}_{dd\sigma} : t^{(1),(2)}_{dd\pi} : t^{(1),(2)}_{dd\delta} = 1 : (-0.3) : 0.1$. This choice avoids pathological features in the energy bands, such as perfect nesting at half band filling. The single-particle part of the Hamiltonian (9.1) is easily diagonalised in momentum space and leads to a density of states $D_0(\varepsilon)$ that is shown as a function of the band filling in figure 9.1. Later, we will study the half-filled case, $n \equiv (n_\uparrow + n_\downarrow)/2 = 0.5$, in the context of the Brinkman–Rice metal-to-insulator transition, and the fillings $n \approx 0.29$ and $n \approx 0.35$ for ferromagnetism. The case $n = 0.29$ corresponds to a maximum in the density of states at the Fermi energy. For this band filling, we expect the strongest tendency to ferromagnetism.

9.1.2 Variational Energy Functional

For a two-band model, it is possible to give a manageable explicit expression of the variational energy as a function of the variational parameters. The eigenstates of the two-particle spectrum all belong to different representations of the point symmetry group, see table 2.3.2. Therefore, one can safely assume that the variational-parameter matrix $\lambda_{\Gamma,\Gamma'} = \delta_{\Gamma,\Gamma'}$ is diagonal and we have $\lambda_\Gamma = \lambda_{\Gamma'}$ for all states $|\Gamma\rangle$, $|\Gamma'\rangle$ that are degenerate due to the cubic symmetry. Then, we have to deal with 11 independent variational parameters $m_\Gamma = \lambda^2_\Gamma m^0_\Gamma$:

i) two parameters for an empty and a fully occupied site: $m_\emptyset$, f;

ii) four parameters for singly and triply occupied sites: m_s and t_s with $s = \uparrow, \downarrow$;

iii) five parameters for doubly-occupied sites: $d^{\uparrow,\uparrow}_t$, $d^{\downarrow,\downarrow}_t$, d^0_t (for the triplet ${}^3A_2$), d_E (for the doublet ${}^1E$), and d_A (for the singlet ${}^1A_1$).

In this section, we work with an uncorrelated local density matrix

$$\left\langle \hat{c}^\dagger_{i,(b,s)} \hat{c}_{i,(b',s')} \right\rangle_{\Psi_0} = \delta_{s,s'} \delta_{b,b'} n_s \ , \tag{9.2}$$

which is diagonal and orbital independent Then, the constraint equations (5.47) can be solved explicitely, e.g., by considering the occupations

$$m_\emptyset = 1 - 2n_\uparrow - 2n_\downarrow + d^{\uparrow\uparrow}_t + d^{\downarrow\downarrow}_t + d^0_t + d_A + 2d_E + 4t_\uparrow + 4t_\downarrow + 3f \ , \tag{9.3a}$$

$$m_s = n_s - \left[d^{ss}_t + t_{\bar{s}} + 2t_{\bar{s}} + f + \frac{1}{2}\left(d_A + 2d_E + d^0_t \right) \right] \tag{9.3b}$$

as functions of the remaining nine independent parameters.

The expectation value of the two-band Hubbard Hamiltonian is given by

$$\begin{aligned} E^{\mathrm{2b}} &= \sum_s q_s^s \varepsilon_{s,0} + (U'-J)(d_t^{\uparrow\uparrow} + d_t^{\downarrow\downarrow} + d_t^0) \\ &\quad +2(U'+J)d_E + (U+J)d_A + (2U+4U'-2J)(t_\uparrow + t_\downarrow + f) \;, \end{aligned} \tag{9.4}$$

where we introduced the orbital-independent elements

$$\begin{aligned} q_s^s &= \frac{1}{n_s(1-n_s)}\Bigg[\left(\sqrt{t_s}+\sqrt{m_{\bar{s}}}\right)\frac{1}{2}\left(\sqrt{d_A}+2\sqrt{d_E}+\sqrt{d_t^0}\right) \\ &\qquad + \sqrt{m_s}\left(\sqrt{m_\emptyset}+\sqrt{d_t^{ss}}\right) + \sqrt{t_{\bar{s}}}\left(\sqrt{d_t^{\bar{s}\bar{s}}}+\sqrt{f}\right)\Bigg]^2 \end{aligned} \tag{9.5}$$

of the diagonal renormalisation matrix and the bare band energies

$$\varepsilon_{s,0} = \int_{-\infty}^{E_{\mathrm{F},s}} \mathrm{d}\varepsilon\, \varepsilon D_0(\varepsilon) \;. \tag{9.6}$$

For comparison, we also consider the energy

$$\begin{aligned} E^{\mathrm{dens}} &= \sum_s \bar{q}_s^s \varepsilon_{s,0} + (U'-J)(d_1^{\uparrow\uparrow} + d_1^{\downarrow\downarrow}) \\ &\quad +2U'd_0 + 2Ud_c + (2U+4U'-2J)(t_\uparrow + t_\downarrow + f) \end{aligned} \tag{9.7}$$

of a two-band model without the terms in the second line of the atomic Hamiltonian (2.23). Here, the renormalisation factors are given by

$$\begin{aligned} \bar{q}_s^s &= \frac{1}{n_s(1-n_s)}\Bigg[\left(\sqrt{t_s}+\sqrt{m_{\bar{s}}}\right)\left(\sqrt{d_c}+\sqrt{d_0}\right) \\ &\qquad + \sqrt{m_s}\left(\sqrt{m_\emptyset}+\sqrt{d_1^{ss}}\right) + \sqrt{t_{\bar{s}}}\left(\sqrt{d_1^{\bar{s}\bar{s}}}+\sqrt{f}\right)\Bigg]^2 . \end{aligned} \tag{9.8}$$

In this case, there are seven variational parameters $d_1^{\uparrow\uparrow}$, $d_1^{\downarrow\downarrow}$, d_0, d_c, $t_\uparrow$, $t_\downarrow$, and f, which represent the occupation of the configuration states $|I\rangle$. The probabilities for an empty site $m_\emptyset$ and a singly-occupied site m_s are related to the variational parameters by

$$m_s = n_s - [d_1^{ss} + t_{\bar{s}} + 2t_s + f + d_c + d_0] \;, \tag{9.9a}$$

$$m_\emptyset = 1 - 2n_\uparrow - 2n_\downarrow + d_1^{\uparrow\uparrow} + d_1^{\downarrow\downarrow} + 2d_0 + 2d_c + 4t_\uparrow + 4t_\downarrow + 3f \;. \tag{9.9b}$$

In the following, we compare the results from the two Gutzwiller wave functions to those from the Hartree-Fock theory.

9.1.3 Ground-State Properties

The energies (9.4) and (9.7) have to be minimised with respect to their respective (nine or seven) independent variational parameters m_Γ and the magnetisation

$$M \equiv (n_\uparrow - n_\downarrow)/2 \;, \tag{9.10}$$

for example, by means of the algorithm introduced in appendix E. In figure 9.2(left), the magnetisation M is shown as a function of U for fixed $J/U = 0.2$ ($U'/U = 0.6$).

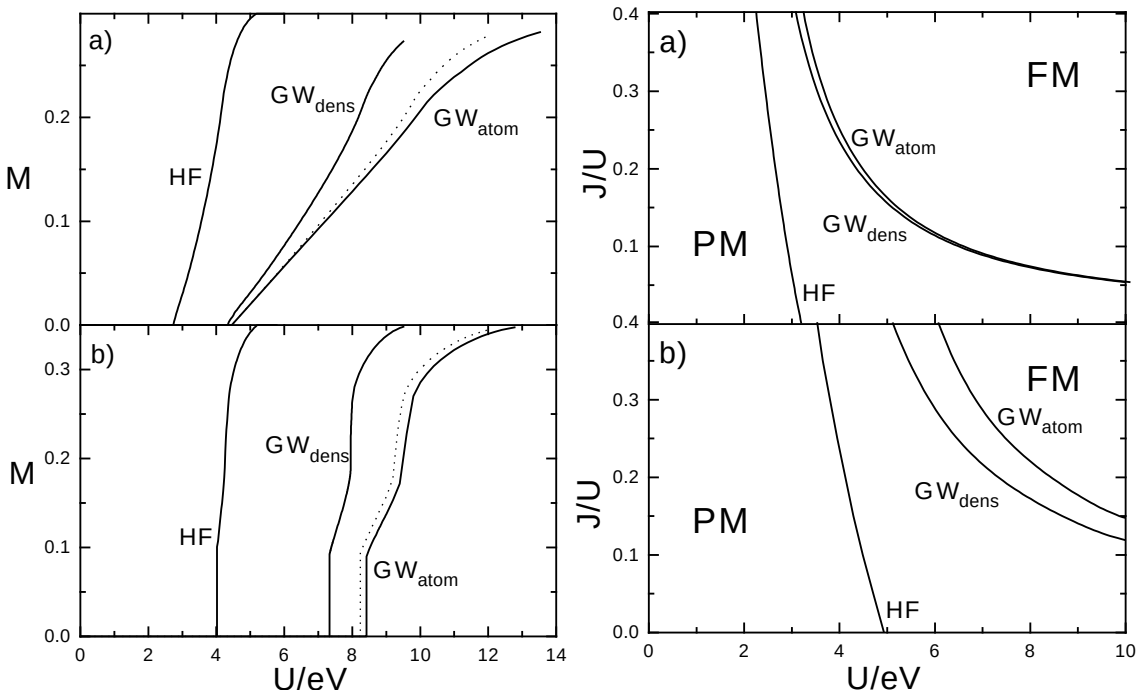

Figure 9.2: Left: Magnetisation density per band as a function of U for the Hartree–Fock solution (HF), the Gutzwiller wave function with pure density correlations ($\mathrm{GW_{dens}}$), and the Gutzwiller wave function with atomic correlations ($\mathrm{GW_{atom}}$) for (a) $n_s = 0.29$ and (b) $n_s = 0.35$. The dotted line indicates the results for $\mathrm{GW_{atom}}$ with $J_\mathrm{C} = 0$. The local exchange interaction is $J = 0.2U$ in all curves. Right: Phase diagram as a function of U and J for the Hartree–Fock solution (HF) and the two Gutzwiller wave functions ($\mathrm{GW_{dens}}$, $\mathrm{GW_{atom}}$) for (a) $n = 0.29$ and (b) $n = 0.35$; PM: paramagnet, FM: ferromagnet.

The critical interaction for the ferromagnetic transition, $U_\mathrm{F}^\mathrm{atom}$, is about a factor two larger than its value U_F^HF as obtained from the Hartree–Fock–Stoner theory. The corresponding values $U_\mathrm{F}^\mathrm{dens}$ always lie somewhat below the values for the Gutzwiller wave function with atomic correlations. In general, the relation $M_\mathrm{HF}(U) > M_\mathrm{dens}(U) > M_\mathrm{atom}(U)$ holds, i.e., for all interaction strengths, the tendency to ferromagnetism is the strongest within the Hartree–Fock theory and weakest for Gutzwiller wave functions with atomic correlations. Furthermore, the slopes of $M(U)$ are much steeper in the Hartree–Fock results than in the presence of correlations.

The properties of the ferromagnetic phase strongly depend on the spectrum of the atomic two-electron configurations. To further analyse this point, we have included the case of $J_\mathrm{C} = 0$, which changes only the excited two-electron states. A shift of the curve $M(U)$ results towards smaller interaction strengths; for a given magnetisation density, a smaller interaction strength is required as compared to the correct symmetry case $J = J_\mathrm{C}$, see figure 9.2(left). The effect is more pronounced when we go to the Gutzwiller wave function with pure density correlations. In this case, all exchange terms in (2.23) are neglected. Then, even the ground state is modified since the atomic spin triplet with $S^z = 0$ moves up in energy into the range of the atomic spin singlets. Again, the magnetisation curve shifts to much smaller interaction strengths. Both results indicate that itinerant ferromagnetism is strongly influenced by the atomic multiplet spectra.

In figure 9.2(left/a), we chose the particle density per band to be $n = 0.29$, right at the maximum of the density of state curve, compare figure 9.1. For this case, there are finite

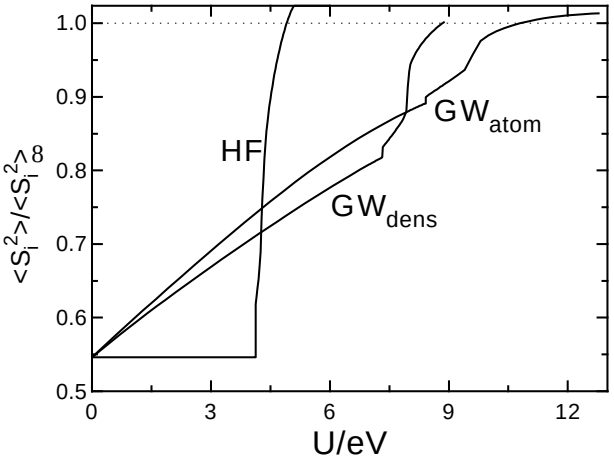

Figure 9.3: Size of the local spin $\langle(\hat{\vec{S}}_i)^2\rangle$ as a function of the interaction strength for $J = 0.2U$ and band filling $n = 0.35$ for the Hartree–Fock theory (HF) and the Gutzwiller wave functions ($\mathrm{GW_{dens}}$, $\mathrm{GW_{atom}}$).

slopes of the $M(U)$ curves at U_F, and a 'Stoner criterion' for the onset of ferromagnetism applies. In figure 9.2(left/b), we chose the particle density per band as $n = 0.35$. As seen from figure 9.1, the density of states at the Fermi energy $D_0(E_{\mathrm{F},\uparrow}) + D_0(E_{\mathrm{F},\downarrow})$ first *increases* as a function of the magnetisation density. Therefore, a discontinuous transition thus occurs from the paramagnet to the ferromagnet.

In the case of pure density correlations, a second jump in the $M(U)$ curve is observed that is absent in the other two curves. As discussed in reference [123], this jump is related to another feature of the density of states. In the Hartree–Fock theory, this feature is too weak to be of any significance in comparison to the interaction energy. When the full atomic correlations are taken into account, this first-order jump at a finite magnetisation density disappears due to the enhanced flexibility of the variational wave function. Nevertheless, in this range of a strongly varying magnetisation density, we find rapid variations of the various double occupancies, similar to the behaviour near the Brinkman–Rice transition for $n = 0.5$ in section 9.3.

Another remarkable difference between the Hartree–Fock and the Gutzwiller method lies in the approach to ferromagnetic saturation. In the Hartree–Fock theory, the magnetisation saturates at U values about 20% to 40% above the onset of ferromagnetism at U_F^HF. In contrast, in the variational approach saturation is reached at about twice the onset value, $U_\mathrm{sat} \lesssim 2U_\mathrm{F}$. However, even when the minority spin occupancies are zero and $\langle\hat{S}_z^\mathrm{at}\rangle$ is constant, the majority spin occupancies $s_\uparrow$ and $d_t^{\uparrow\uparrow}$ vary with U since the limit of zero empty sites is reached only for $U \to \infty$.

In figure 9.2(right), we display the J-U phase diagram for both fillings. It shows that the Hartree–Fock theory always predicts a ferromagnetic instability. In contrast, the correlated electron approach strongly supports the idea that a substantial on-site Hund's rule exchange is required for the occurrence of ferromagnetism at realistic interaction strengths. For the case $n = 0.29$, the differences between the phase diagrams for the two correlated electron wave functions are minor. Due to the large density of states at the Fermi energy, the critical interaction strengths for the ferromagnetic transition are comparably small, and the densities for the double occupancies in both correlated wave functions do not differ much. For the larger band filling $n = 0.35$, i.e., away from the peak in the density of state, the values for U_F are considerably larger and, in the atomic correlation case, the Gutzwiller wave functions can generate local spin triplets more easily while keeping the global paramagnetic phase.

The magnitude of the local spin as a function of U is shown in figure 9.3. For $U \to \infty$, each site is either singly occupied with probability $2 - 4n$ or doubly occupied (spin $S = 1$)

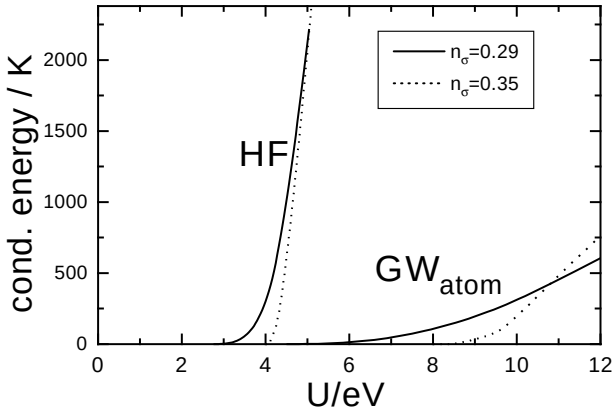

Figure 9.4: Condensation energy as a function of U for $J = 0.2U$ for the Hartree–Fock theory (HF) and the Gutzwiller wave function ($\mathrm{GW_{atom}}$) for $n = 0.29$ (full lines) and $n = 0.35$ (dashed lines).

with probability $4n - 1$. Hence,

$$\langle(\vec{S}_i)^2\rangle_\infty = (3/4)(2 - 4n) + 2(4n - 1) = 5n - 1/2 \; . \tag{9.11}$$

For the correlated wave functions, this limit is reached from *above* since, for $U < \infty$, charge fluctuations first increase the number of spin-one sites at the expense of spin-1/2 sites, which turn into empty sites. A further decrease of U will also activate the singlet double occupancies and higher multiple occupancies. Thus, the local spin eventually reduces below $\langle(\vec{S}_i)^2\rangle_\infty$. On the contrary, the Hartree–Fock theory does not give the proper large-U limit for the local spin. Instead, the Hartree–Fock limit is given by

$$\langle(\vec{S}_i)^2\rangle_\infty^{\mathrm{HF}} = n(3 + 2n) \; . \tag{9.12}$$

The change of $\langle(\vec{S}_i)^2\rangle$ at U_F is only a minor effect within the correlated electron approach. In particular, this holds true for the case of atomic correlations, where about 90% of the local spin saturation value is already reached in the paramagnetic state. Again, the Hartree–Fock results are completely different. There, the local spin sharply increases as a function of the interaction strength since the absence of correlations fixes

$$\langle(\vec{S}_i)^2\rangle^{\mathrm{HF}}(U < U_\mathrm{F}^{\mathrm{HF}}) = \langle(\vec{S}_i)^2\rangle(U = 0). \tag{9.13}$$

Finally, in figure 9.4, we display the energy differences between the paramagnetic and ferromagnetic ground states as a function of the interaction strength for $J = 0.1U$. For the correlated electron case, this quantity is of the order of the Curie temperature, which is in the range of $100\,\mathrm{K} - 1000\,\mathrm{K}$ in real materials. On the other hand, the Hartree–Fock theory yields small condensation energies only in the range of $U \approx 4\,\mathrm{eV}$; for larger U, the condensation energy is of order U. Including the correlation effects, we have relatively small condensation energies even for interaction values as large as twice the bandwidth ($U \approx 10\,\mathrm{eV}$).

9.1.4 Spin-wave Excitations

As discussed in the previous section, the stability of a ferromagnetic solution is drastically overestimated in a Hartree-Fock treatment since only the Stoner parameter $I = (U + J)/2$ governs the magnetic behaviour in that approach. The paramagnet becomes unstable as soon as the Stoner-criterion

$$I\, D_0(E_\mathrm{F}) > 1 \tag{9.14}$$

is fulfilled, where $D_0(E_\mathrm{F})$ is the density of states at the Fermi level. This means that a ferromagnetic transition occurs for any value of the local exchange constant J. This is in striking

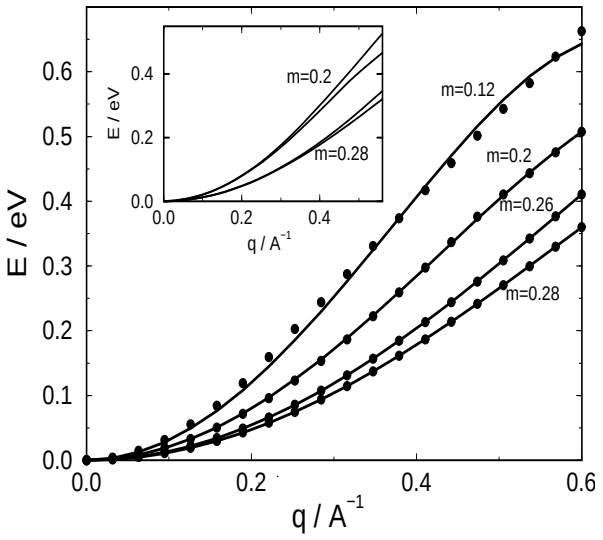

Figure 9.5: Variational spin-wave dispersion in x direction, $E^{\mathrm{var}}((q,0,0))$, for a generic two-band model with $n = 0.29$, $J = 0.2U$, and the values $U/\mathrm{eV} = 7.8$, 10, 12, 13.6 correspond to magnetisations $m = 0.12$, 0.20, 0.26, 0.28. The lattice constant is $a = 2.5\,\text{Å}$. Inset: $E^{\mathrm{var}}((q,0,0))$ and $E^{\mathrm{var}}((q/\sqrt{2},q/\sqrt{2},0))$ for $m = 0.2$ and $m = 0.28$, respectively. The spin-wave dispersion is almost isotropic for strong ferromagnets.

contrast to our Gutzwiller variational approach, where a sizeable Hund's-rule coupling J is crucial for the formation of ferromagnetic order. Thus, for small values of J, the Hartree-Fock theory leads to qualitatively incorrect results. These significant differences complicate a comparison between the variational spin-wave approach, introduced in section 8.1, and the random-phase approximation because the latter is based on a Hartree-Fock description of the ground state. For the same set of parameters J and U, the underlying ground states are completely different and, therefore, a comparison of the spin-wave properties is not meaningful. It thus appears more reasonable to consider the results of both methods for the same magnetisation m, and not for the same parameters J and U.

In figure 9.5, the variational spin-wave dispersion in x-direction is shown for four different magnetisations. Here, we used the same tight-binding parameters as in our analysis of the ground state in the previous section. The average electron density per orbital and spin direction in the paramagnet is $n = 0.29$. We keep the ratio $J/U = 0.2$ fixed and consider different values $U/\mathrm{eV} = 7.8$, 10, 12, 13.6, which correspond to a magnetisation per band of $m = 0.12$, 0.20, 0.26, 0.28. The last value belongs to the almost fully polarised ferromagnet ($m \approx n$). As can be seen from figure 9.5, the spin-wave dispersion drastically depends on the magnetisation. The data can be fitted very well to

$$E^{\mathrm{var}}((q_x,0,0)) = Dq_x^2(1+\beta q_x^2) + \mathcal{O}(q_x^6)\,, \tag{9.15}$$

in qualitative agreement with experiments on iron-group metals. In the case of a strong ferromagnet, we obtain $D = 1.4\,\mathrm{eV\AA}^2$ and $D = 1.2\,\mathrm{eV\AA}^2$ for $m = 0.26$ and $m = 0.28$, respectively. This is the right order of magnitude in nickel, where $D = 0.43\,\mathrm{eV\AA}^2$ was observed experimentally [215]. The inset of figure 9.5 shows that the spin-wave dispersion is almost isotropic, which also agrees with experimental observations. In our variational many-body approach, the spin-wave stiffness *decreases* as a function of U. This does not come as a surprise because the effective coupling between the sites decreases when the electron hopping between the sites becomes less effective.

In figure 9.6, the results for the spin-wave dispersion in the RPA are shown for three different values of U. In contrast to our variational approach, the RPA predicts a *negative* slope of the dispersion for non-saturated ferromagnetism, $M < n$. Note that for $U = 5.2\,\mathrm{eV}$ the system has just attained the fully polarised state, see figure 9.2(left). However, even

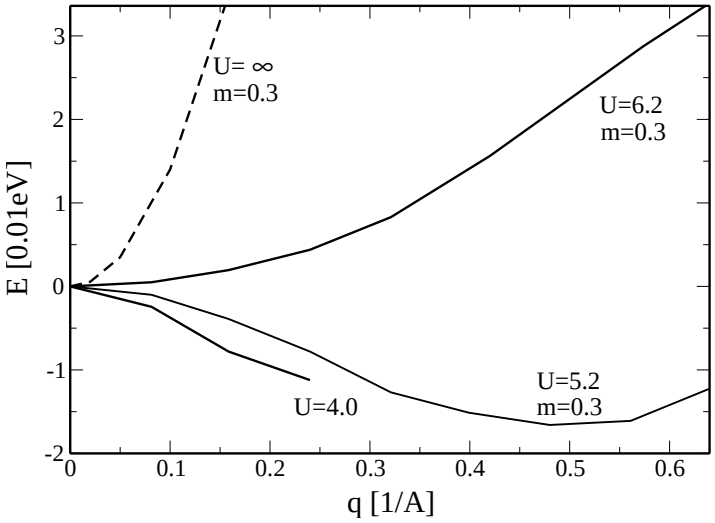

Figure 9.6: RPA spin-wave dispersion in x direction, $E^{\mathrm{RPA}}((q,0,0))$, for a generic two-band model with $n = 0.29$ and $J = 0.2U$. The value $U = 4.0\,\mathrm{eV}$ corresponds to $m < n$ in Hartree-Fock theory whereas $U = 5.2\,\mathrm{eV}$ and $U = 6.2\,\mathrm{eV}$ correspond to the fully polarised Hartree-Fock ground state. Also shown is the spin-wave dispersion for $U = \infty$. The lattice constant is $a = 2.5\,\text{Å}$.

in this case, a well-defined RPA spin-wave excitation does not yet exist. It requires a further increase of U until the fully polarised collinear Hartree-Fock ground state appears to be stable. Since the RPA probes the 'local' stability of a mean-field state, it is conceivable that another ferromagnetic Hartree-Fock state with some spiral order has a lower energy than the collinear state. However, ferromagnetic phases with spiral order are not generic for transition metals. We argue that this prediction of exotic ferromagnetic spin structures is an artefact of the Hartree-Fock approach.

In the case of a stable collinear ferromagnetic Hartree-Fock ground state, the RPA spin-wave stiffness *increases* as a function of U, again in contrast to our variational approach. For all generic cases, $D^{\mathrm{RPA}}(U \to \infty) \geq D^{\mathrm{var}}(U \to \infty)$ holds in the limit of infinite coupling. In our case, $D^{\mathrm{RPA}}(U \to \infty) = 1.4\,\mathrm{eV\text{Å}}^2$, as compared to $D^{\mathrm{var}}(U \to \infty) = 0.4\,\mathrm{eV\text{Å}}^2$. The variational and RPA results differ significantly in the strong-coupling limit, too. Nevertheless, there are some intermediate coupling strengths where the variational and the RPA spin-wave stiffness agree. Such accidental agreements may also occur when RPA results are successfully compared to experimental data as, e.g., in reference [216].

9.2 Orbital Order in a Spinless Two-Band Model

The investigation of orbital degrees of freedom has become an important field in theoretical solid-state physics over the past two decades. There are a number of materials that are believed to show phase transitions with orbital order parameters. Among them, the perovskite manganites, e.g., $\mathrm{La}_{1-x}\mathrm{Sr}_x\mathrm{MnO}_3$, have attracted particular interest because of the colossal magnetoresistance behaviour, which is observed in these materials. In theoretical studies on manganites, one often neglects the almost localised Mn $t_{2\mathrm{g}}$ orbitals, and investigates solely the electronic properties of a system with two e_{g} orbitals per lattice site. In order to study the ferromagnetic phase of such a model, Takahashi and Shiba [217] further neglected the spin-degrees of freedom because the Hund's rule coupling was assumed to align the spins in the two e_{g} orbitals.

The mean-field study in [217] found a surprisingly large number of stable orbitally ordered phases for the spinless e_{g} model. However, as we have seen in the previous section, mean-field approximations overestimate the stability of ordered phases in correlated-electron systems. Therefore, in this section, we investigate the emergence of orbital order in the two-orbital Hubbard model without spin-degrees of freedom by means of our Gutzwiller theory.

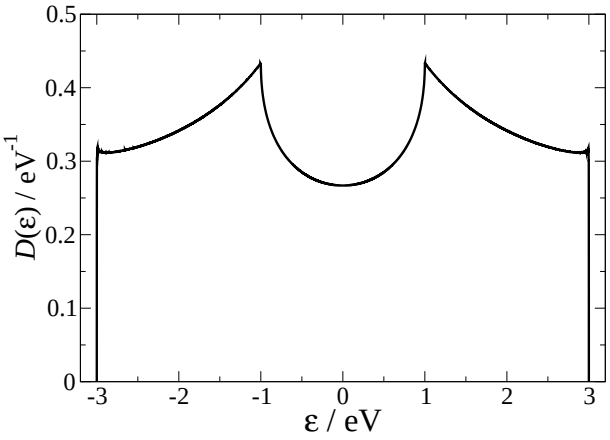

Figure 9.7: Density of states of the model system (9.16)

9.2.1 Model System and Types of Order Parameters

Without the spin-degrees of freedom, our two-orbital model reduces to

$$\hat{H}_{2\mathrm{b}} = \hat{H}_0 + \hat{H}_I \,, \tag{9.16a}$$

$$\hat{H}_0 \equiv \sum_{i,j} \sum_{b,b'=1}^{2} t_{i,j}^{b,b'} \hat{c}_{i,b}^{\dagger} \hat{c}_{j,b'} \,, \tag{9.16b}$$

$$\hat{H}_U \equiv U \sum_{i} \hat{n}_{i,1} \hat{n}_{i,2} \,. \tag{9.16c}$$

The Hamiltonian (9.16) is formally equivalent to the one-band Hubbard model (2.20) if the indices b, b' are regarded as spins. However, the tight-binding parameters in (9.16b) would be unusual for a genuine one-band model since they contain inter-orbital hopping terms. The Hubbard parameter U in (9.16c) is given as $U = U' - J$, where U' and J are the Coulomb and the exchange interaction in the original two-band Hamiltonian (2.23).

In line with reference [217], we restrict our investigation to systems with only nearest-neighbour hopping and choose $t_{dd\sigma} = 1\,\mathrm{eV}$, $t_{dd\delta} = 0\,\mathrm{eV}$. Additional hopping terms would only destabilise the orbital order we are interested in. For the e_g-orbitals $|z_1\rangle \equiv |x^2 - y^2\rangle$, $|z_2\rangle \equiv |3z^2 - r^2\rangle$, the one-particle Hamiltonian in momentum space becomes

$$\hat{H}_0 = \sum_{\mathbf{k}} \sum_{b,b'} \varepsilon^z_{\boldsymbol{k};b,b'} \hat{c}^{\dagger}_{\boldsymbol{k};z,b} \hat{c}_{\boldsymbol{k};z,b'} \,, \tag{9.17}$$

with

$$\varepsilon^z_{\boldsymbol{k};1,1} = \big(\cos(k_x) + \cos(k_y) + 4\cos(k_z)\big)/2 \,,$$

$$\varepsilon^z_{\boldsymbol{k};2,2} = 3\big(\cos(k_x) + \cos(k_y)\big)/2 \,, \tag{9.18a}$$

$$\varepsilon^z_{\boldsymbol{k};1,2} = -\sqrt{3}\big(\cos(k_x) - \cos(k_y)\big)/2 = \varepsilon^z_{\boldsymbol{k};2,1} \,. \tag{9.18b}$$

The $\mathbf{k}$-integrated density of states $D_0(\varepsilon)$ that results from this band structure is shown in figure 9.7.

For our investigation of orbital order, we need to introduce two more basis representations of the orbital space,

$$|x_1\rangle \equiv \frac{1}{\sqrt{2}}\big(|z_1\rangle + |z_2\rangle\big) \,, \tag{9.19a}$$

$$|x_2\rangle \equiv \frac{1}{\sqrt{2}}\big(|z_1\rangle - |z_2\rangle\big) \,, \tag{9.19b}$$

and

$$|y_1\rangle \equiv \frac{1}{\sqrt{2}}\big(|z_1\rangle + \mathrm{i}|z_2\rangle\big)\,, \tag{9.20a}$$

$$|y_2\rangle \equiv \frac{1}{\sqrt{2}}\big(|z_1\rangle - \mathrm{i}|z_2\rangle\big)\,. \tag{9.20b}$$

The dispersion relations in momentum space for the 'x'- and the 'y'-basis become

$$\varepsilon^x_{\boldsymbol{k};1,1} = \big((2-\sqrt{3})\cos(k_x) + (2+\sqrt{3})\cos(k_y) + 2\cos(k_z)\big)/2\,, \tag{9.21a}$$

$$\varepsilon^x_{\boldsymbol{k};2,2} = \big((2+\sqrt{3})\cos(k_x) + (2-\sqrt{3})\cos(k_y) + 2\cos(k_z)\big)/2, \tag{9.21b}$$

$$\varepsilon^x_{\boldsymbol{k};1,2} = \cos(k_x) + \cos(k_y) - 2\cos(k_z))/2 = \varepsilon^x_{\boldsymbol{k};2,1}\,, \tag{9.21c}$$

$$\varepsilon^y_{\boldsymbol{k};1,1} = \cos(k_x) + \cos(k_y) + \cos(k_z) = \varepsilon^y_{\boldsymbol{k};2,2}\,, \tag{9.21d}$$

$$\varepsilon^y_{\boldsymbol{k};1,2} = \big((1+\sqrt{3}\mathrm{i})\cos(k_x) + (1-\sqrt{3}\mathrm{i})\cos(k_y) - 2\cos(k_z)\big)/2\,, \tag{9.21e}$$

$$\varepsilon^y_{\boldsymbol{k};2,1} = \Big(\varepsilon^y_{\boldsymbol{k};1,2}\Big)^*\,. \tag{9.21f}$$

The interaction term (9.16c) has the same form for all three basis representations $\xi = x, y, z$.

We describe orbital order in our model system (9.16) through the order parameters

$$\tau_{i,\xi} \equiv \big(\langle\hat{n}_{i,\xi_1}\rangle - \langle\hat{n}_{i,\xi_2}\rangle\big)/2\,, \tag{9.22a}$$

$$\hat{n}_{i,\xi_b} \equiv \hat{c}^\dagger_{i,\xi_b}\hat{c}_{i,\xi_b}\,, \tag{9.22b}$$

for each of the three representations ξ. Using the Pauli matrices $\tilde{1}, \tilde{\tau}^x, \tilde{\tau}^y, \tilde{\tau}^z$, the order parameter can also be written as (compare reference [217])

$$\tau_{i,\xi} = \frac{1}{2}\sum_{b,b'}\big\langle \hat{c}^\dagger_{i,z_b}(\tilde{\tau}^\xi)_{b,b'}\hat{c}_{i,z_{b'}}\big\rangle\,. \tag{9.23}$$

Besides the orbital character of the order parameter, we need to specify its lattice-site dependence. Following reference [217] we consider orders of the form

$$\tau_{i,\xi} = \tau_{\xi,0}\exp(\mathrm{i}\mathbf{Q}\mathbf{R}_i) \tag{9.24}$$

with commensurate vectors $\mathbf{Q}$ that belong to the Γ point ($\mathbf{Q} = (0,0,0)$), the R point ($\mathbf{Q} = (\pi,\pi,\pi)$), the X point ($\mathbf{Q} = (0,0,\pi)$), and the M point ($\mathbf{Q} = (\pi,\pi,0)$). The real parameter $\tau_{\xi,0}$ in (9.24) is independent of the lattice site vector $\mathbf{R}_i$ and assumed to be positive. Note that, for vectors $\mathbf{Q} \neq (0,0,0)$, equation (9.24) divides the lattice into an 'A'-lattice with a majority ξ_1 occupation ($\tau_{i,\xi} > 0$), and a 'B'-lattice with a majority ξ_2 occupation ($\tau_{i,\xi} < 0$).

9.2.2 Evaluation of the Energy Functionals

For the investigation of the Hamiltonian (9.16), we work with the local correlation operator

$$\hat{P}_i = \sum_I \lambda_{i,I}\hat{m}_{i,I} \tag{9.25}$$

where, as usual, $\hat{m}_I = |I\rangle\langle I|$ projects onto the four local configuration states $|I\rangle$, i.e., the empty state $|\emptyset\rangle$, the doubly-occupied state $|d\rangle$ and the two single electron states $|\xi_1\rangle, |\xi_2\rangle$. Note that $|\xi_1\rangle$ and $|\xi_2\rangle$ depend on the orbital representation ξ whereas the states $|\emptyset\rangle$ and $|d\rangle$ are invariant

under the orbital transformations (9.19) and (9.20). For the variational parameters $\lambda_{i;I}$, we make an Ansatz that is consistent with the spatial symmetry of the order parameter,

$$\begin{aligned} \lambda_{i;\emptyset} &= \lambda_{\emptyset}\,, && (9.26a)\\ \lambda_{i;d} &= \lambda_{d}\,, && (9.26b)\\ \lambda_{i;\xi_1} &= \lambda_s + \delta\lambda_s \exp\left(\mathrm{i}\mathbf{Q}\mathbf{R}_i\right), && (9.26c)\\ \lambda_{i;\xi_2} &= \lambda_s - \delta\lambda_s \exp\left(\mathrm{i}\mathbf{Q}\mathbf{R}_i\right), && (9.26d) \end{aligned}$$

where the parameters $\lambda_\emptyset$, λ_d, λ_s, $\delta\lambda_s$ are independent of the lattice site vector $\mathbf{R}_i$.

We only consider single-particle wave functions $|\Psi_0\rangle$ for which the local density matrix $\tilde{C}^0$ is diagonal with respect to b, b',

$$C^0_{i;\xi_b,\xi_{b'}} \equiv \left\langle \hat{c}^\dagger_{i,\xi_b} \hat{c}_{i,\xi_{b'}} \right\rangle_{\Psi_0} \equiv n^0_{i,\xi_b} \delta_{b,b'}\,. \tag{9.27}$$

Finite non-diagonal elements in $\tilde{C}^0$ could only appear if we were mixing different order parameters.

With the expectation values $m_{i;I} \equiv \lambda^2_{i;I} \langle \hat{m}_{i;I} \rangle_{\Psi_0}$, the constraints (5.48) can be readily solved by expressing all local occupancies in terms of the average numbers of doubly-occupied sites $m_{i;d}$,

$$\begin{aligned} m_{i;\emptyset} &= 1 - n^0_{i,\xi_1} - n^0_{i,\xi_2} + m_{i;d}\,, && (9.28a)\\ m_{i;\xi_b} &= n^0_{i,\xi_b} - m_{i;d}\,. && (9.28b) \end{aligned}$$

Apart from the still unspecified single-particle wave function $|\Psi_0\rangle$ and the corresponding local density matrices $\tilde{C}^0_i$, the probabilities $m_{i;d}$ are the only remaining variational parameters. We skip the explicit declaration of the orbital representation ξ for the rest of this section and write b instead of ξ_b in all indices.

With our general results, as derived in chapter 5, the expectation value of the single-particle Hamiltonian (9.16b) becomes

$$E_0 = \langle \hat{H}_0 \rangle_{\Psi_\mathrm{G}} = \sum_{i,j} \sum_{b,b'} \sqrt{q_{i,b} q_{j,b'}}\, t^{b,b'}_{i,j} \left\langle \hat{c}^\dagger_{i,b} \hat{c}_{j,b'} \right\rangle_{\Psi_0} \equiv \langle \hat{H}'_0 \rangle_{\Psi_0} \tag{9.29}$$

with the renormalisation factors

$$q_{i,b} = \frac{1}{n^0_{i,b}(1 - n^0_{i,b})} \left(\sqrt{m_{i;\emptyset} m_{i;b}} + \sqrt{m_{i;\bar{b}} m_{i;d}} \right)^2 , \tag{9.30}$$

and $\bar{b}$ is defined via $\bar{1} \equiv 2$ and $\bar{2} \equiv 1$.

The lattice symmetry of the order parameter leads to further simplifications. We introduce the majority and the minority orbital density

$$n^0_\pm \equiv n^0 \pm \tau_0 \tag{9.31}$$

such that

$$n^0_{i,1} = n^0_\pm\,,\ n^0_{i,2} = n^0_\mp\,. \tag{9.32}$$

The upper and lower signs in (9.32), and in corresponding equations below, belong to lattice sites $i \in A$ and $i \in B$, respectively. For the other local expectation values, we find

$$\begin{aligned} m_{i;d} &= m_d\,, && (9.33a)\\ m_{i;1} &\equiv m_\pm = n^0_\pm - m_d\,, && (9.33b)\\ m_{i;2} &\equiv m_\mp = n^0_\mp - m_d\,, && (9.33c)\\ m_{i;\emptyset} &= 1 - 2n^0 + m_d\,. && (9.33d) \end{aligned}$$

A similar notation is introduced for the q-factors

$$q_{i,1} \equiv q_{\pm} \quad , \quad q_{i,2} \equiv q_{\mp} \; , \tag{9.34}$$

where

$$q_{\pm} \equiv \frac{1}{n^0_{\pm}(1-n^0_{\pm})} \left(\sqrt{m_{\emptyset} m_{\pm}} + \sqrt{m_{\mp} m_d}\right)^2 \; . \tag{9.35}$$

The expectation value (9.29) splits into four components

$$E_0 = q_+ E^{++} + q_- E^{--} + \sqrt{q_+ q_-}(E^{+-} + E^{-+}) \; , \tag{9.36}$$

which belong to the four different hopping channels between majority ('+') and minority ('−') states. In momentum space, the one-particle expectation values in (9.36) can be written as

$$\begin{aligned} E^{\omega\omega'} &= \frac{1}{4} \sum_{\mathbf{k}} \sum_{b,b'} \varepsilon^z_{\mathbf{k};b,b'} \Big(M^1_{b,b'} \langle \hat{c}^\dagger_{\mathbf{k};z,b} \hat{c}_{\mathbf{k};z,b'} \rangle_{\Psi_0} + \omega M^2_{b,b'} \langle \hat{c}^\dagger_{\mathbf{k}+\mathbf{Q};z,b} \hat{c}_{\mathbf{k};z,b'} \rangle_{\Psi_0} \\ &\quad + \omega' M^3_{b,b'} \langle \hat{c}^\dagger_{\mathbf{k};z,b} \hat{c}_{\mathbf{k}+\mathbf{Q};z,b'} \rangle_{\Psi_0} + \omega\omega' M^4_{b,b'} \langle \hat{c}^\dagger_{\mathbf{k}+\mathbf{Q};z,b} \hat{c}_{\mathbf{k}+\mathbf{Q},z,b'} \rangle_{\Psi_0} \Big) \end{aligned} \tag{9.37}$$

where ω, ω' represent the + or − signs, and the coefficients $M^\gamma_{b,b'}$ are given as the elements of the matrices

$$\begin{aligned} \tilde{M}^1 &= \begin{pmatrix} 1 & 1 \\ 1 & 1 \end{pmatrix} \quad , \quad \tilde{M}^2 = \begin{pmatrix} 1 & 1 \\ -1 & -1 \end{pmatrix} \; , \\ \tilde{M}^3 &= \begin{pmatrix} 1 & -1 \\ 1 & -1 \end{pmatrix} \quad , \quad \tilde{M}^4 = \begin{pmatrix} 1 & -1 \\ -1 & 1 \end{pmatrix} \; . \end{aligned} \tag{9.38}$$

For the evaluation of the expectation values in (9.37), we determine the single-particle wave function $|\Psi_0\rangle$. As shown in section (5.3), $|\Psi_0\rangle$ is given as the ground state of the effective single-particle Hamiltonian

$$\hat{H}^{\rm eff}_0 = \hat{H}'_0 - \eta \sum_i \exp\left(\mathrm{i}\mathbf{Q}\mathbf{R}_i\right)(\hat{n}_{i,1} - \hat{n}_{i,2}) \, , \tag{9.39}$$

where $\hat{H}'_0$ was introduced in (9.29) and the term proportional to the variational parameter η allows the order parameter τ_0 to be varied.

Here, we only aim to investigate the stability of the orbitally unordered state. Therefore, we just need to analyse the energy expression (9.36) for small values of the order parameter τ_0. An expansion of the q-factors (9.35) up to second order in τ_0,

$$q_{\pm} \approx \tilde{q}_0 \pm \tilde{q}_1 \tau_0 + \tilde{q}_2 \tau_0^2 \; , \tag{9.40}$$

yields

$$\sqrt{q_+ q_-} \approx \tilde{q}_0 + \left(\tilde{q}_2 - \frac{\tilde{q}_1^2}{2\tilde{q}_0}\right) \tau_0^2 \, . \tag{9.41}$$

Note that the coefficients $\tilde{q}_\gamma$ are still functions of n^0 and m_d. To leading order in τ_0, the effective Hamiltonian (9.39) becomes

$$\hat{H}^{\rm eff}_0 = \tilde{q}_0 \sum_{\mathbf{k}} \sum_{b,b'} \varepsilon^z_{\mathbf{k};b,b'} \hat{c}^\dagger_{\mathbf{k};z,b} \hat{c}_{\mathbf{k};z,b'} - \eta \sum_{\mathbf{k}} \left(\hat{c}^\dagger_{\mathbf{k};z,1} \hat{c}_{\mathbf{k}+\mathbf{Q};z,1} - \hat{c}^\dagger_{\mathbf{k};z,2} \hat{c}_{\mathbf{k}+\mathbf{Q};z,2} \right) \tag{9.42}$$

because we can set $q_{i,b} = \tilde{q}_0$ in $\hat{H}_0'$, equation (9.29). The single-particle Hamiltonian (9.42) is easily diagonalised numerically. This diagonalisation provides the coefficients in the quadratic expansion of (9.37) ,

$$E^{\pm\pm} = E_0 + E_2\tau_0^2 \,, \tag{9.43a}$$
$$E^{\pm\mp} = E_0' + E_2'\tau_0^2 \,, \tag{9.43b}$$

and, consequently, of the variational ground-state energy

$$E_{\mathrm{var}} = \tilde{q}_0 E_0^{\mathrm{tot}} + \left(\tilde{q}_0 E_2^{\mathrm{tot}} + \tilde{q}_2 E_0^{\mathrm{tot}} - E_0' \frac{\tilde{q}_1^2}{\tilde{q}_0} \right) \tau_0^2 + U m_d \,. \tag{9.44}$$

Here, we introduced

$$E_\gamma^{\mathrm{tot}} \equiv 2(E_\gamma + E_\gamma') \tag{9.45}$$

for $\gamma = 0$ or 2. The minimisation of E_{var} with respect to m_d can be carried out for $\tau_0 = 0$,

$$E_0^{\mathrm{tot}} \left. \frac{\partial \tilde{q}_0}{\partial m_d} \right|_{m_d = \bar{m}_d} + U = 0 \,, \tag{9.46}$$

which determines the optimum number $\bar{m}_d$ of doubly-occupied sites as a function of U and n^0. This allows us to express the variational energy solely in terms of τ_0,

$$E_{\mathrm{var}} = \tilde{q}_0 E_0^{\mathrm{tot}} + c_{\tau_0} \tau_0^2 \,. \tag{9.47}$$

A negative sign of the coefficient

$$c_{\tau_0} = \tilde{q}_0 E_2^{\mathrm{tot}} + \tilde{q}_2 E_0^{\mathrm{tot}} - E_0' \frac{\tilde{q}_1^2}{\tilde{q}_0} = c_{\tau_0}(U, n^0) \tag{9.48}$$

in (9.48) indicates the instability of the unordered state. Note that a positive c_{τ_0} does not necessarily prove the stability of the unordered state because it does not exclude first-order transitions.

In Hartree-Fock theory, a quadratic expansion of the ground-state energy leads to

$$E_{\mathrm{var}}^{\mathrm{HF}} = E_0^{\mathrm{tot}} + (E_2^{\mathrm{tot}} - U)\tau_0^2 \,, \tag{9.49}$$

and the critical interaction strength in this approach is therefore given as

$$U_{\mathrm{C}}^{\mathrm{HF}} = E_2^{\mathrm{tot}} \,. \tag{9.50}$$

9.2.3 Results

In figures 9.8, we show the critical interaction strength (9.50) in Hartree-Fock theory as a function of density for the various types of orbital order introduced at the beginning of this section. Our data agree with those reported in reference [217]. Note that in Hartree-Fock theory, the critical interaction strength is finite for all densities $n^0 > 0$ and diverges only in the limit $n^0 \to 0$.

The phases in figure 9.8(left) are not stable within our correlated Gutzwiller approach for all densities and interaction parameters. This holds in particular for the order parameter τ_R^y, which has surprisingly small critical values $U_{\mathrm{C}}^{\mathrm{HF}}$ around quarter filling $2n^0 \approx 0.5$.

For the four surviving phases in figure 9.8(right), we show the ratio $U_{\mathrm{C}}^{\mathrm{GW}}/U_{\mathrm{C}}^{\mathrm{HF}}$ of the critical parameters in Gutzwiller and Hartree-Fock theory as a function of density in figure 9.9. Apparently, there is only a narrow window of densities around half filling $2n^0 \approx 1$ where orbital

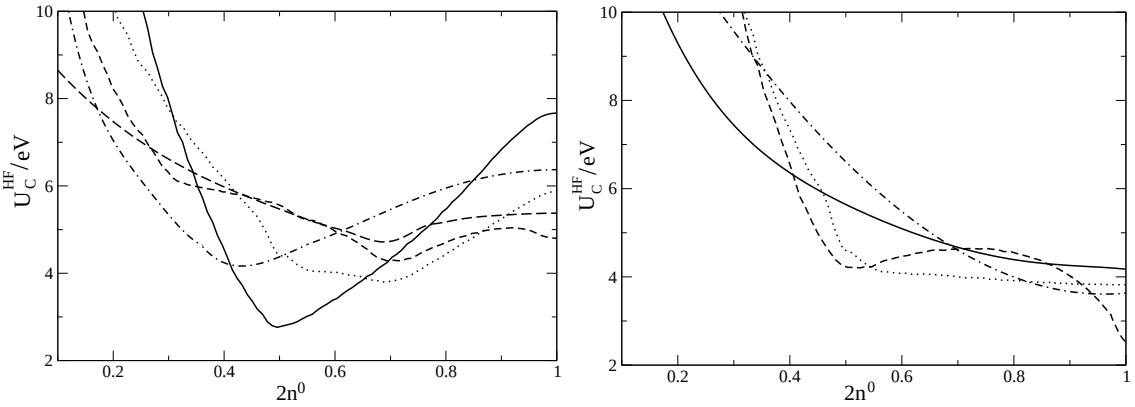

Figure 9.8: Critical interaction strength in Hartree-Fock theory. Left: orders τ_R^y (full line), τ_M^z (dashed), $\tau_\Gamma^{z(x)}$ (long-dashed), τ_M^y (dotted), and τ_X^x (dash-dotted), which are not stable within the Gutzwiller theory. Right: orders $\tau_{\Gamma(X)}^y$ (full line), $\tau_R^{z(x)}$ (dashed), τ_M^x (dotted), and τ_X^z (dash-dotted).

order occurs in the Gutzwiller theory. This is in sharp contrast to the Hartree-Fock findings in figure 9.8(right). For three of the phases, the orbital order may disappear again if U exceeds some second critical value $\tilde{U}_{\mathrm{C}}^{\mathrm{GW}} > U_{\mathrm{C}}^{\mathrm{GW}}$. This behaviour is also different from the Hartree-Fock theory in which the orbital order is stable for all $U > U_{\mathrm{C}}^{\mathrm{HF}}$. Mathematically, the appearance of the second critical parameter $\tilde{U}_{\mathrm{C}}^{\mathrm{GW}}$ is due to the fact that $\tilde{q}_2$ in (9.40) has a minimum as a function of m_d. Hence, the coefficient c_{τ_0} may have one or two roots as a function of U, depending on the other parameters in (9.48). The appearance of the second transition is therefore a genuine many-particle effect. Only one of the four orders, τ_M^x, is unstable in the limit $U \to \infty$ for all densities. For the three other orders, we find critical densities n_{c}^0 with a stable order for all $n^0 > n_{\mathrm{c}}^0$ in the limit $U \to \infty$. The values of n_{c}^0 are displayed by arrows in figure 9.9.

The failure of Hartree-Fock theory to describe the orbitally ordered phases of the two-band model is not surprising. It is well known, for example, that Hartree-Fock theory also grossly overestimates the stability of ferromagnetic ground states in a one-band Hubbard model [218] or in two-band models, as we have seen in section 9.1.3.

9.3 Metal to Insulator Transitions in a Degenerate Two-Band Model

As shown by Brinkman and Rice [102], and recapitulated in section 5.4, the Gutzwiller theory for a one-band model at half filling exhibits a metal to insulator transition at finite values U_{C} of the interaction parameter U. Obviously, one expects that similar transitions occur at integer fillings of multi-band models. In the following, we summarise the results for the metal-insulator transition in the model with two degenerate e_{g} orbitals per site that was introduced in section (9.1).

For multi-band systems with $2N$ spin-orbitals per site, the Brinkman–Rice transition occurs at integer numbers, i.e., for $1 \leq 2n \leq 2N$ of electrons per atom. For densities $n = 1/4$ or $n = 3/4$, the transition in the two-band model is continuous like the Brinkman-Rice transition in the one-band case, see reference [122]. Therefore, we focus on the case $n = 2$, where, in general, the transition is *discontinuous* in the bandwidth reduction factor q. This means that a jump occurs at the Brinkman–Rice transition from a finite value q_{BR} in the metallic phase

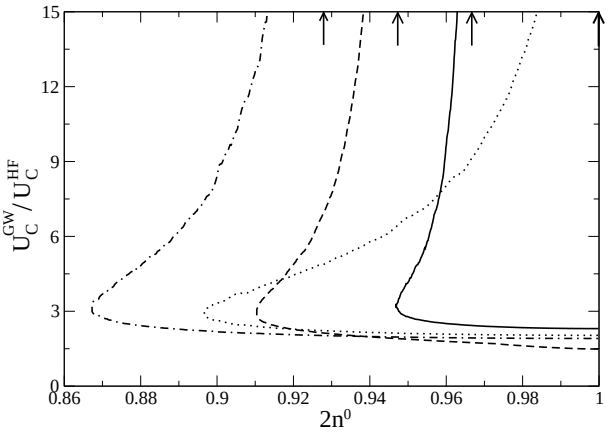

Figure 9.9: Critical interaction strength in Gutzwiller theory for the orders $\tau^y_{\Gamma(X)}$ (full line), $\tau^{z(x)}_R$ (dashed), τ^x_M (dotted), and τ^z_X (dash-dotted). The arrows indicate the critical densities $2n^0_c$ for $U \to \infty$.

to $q = 0$ in the insulating phase.

In figure 9.10(left), the q values are shown as a function of U for various J/U ratios. The singular case $J = 0$ ($U = U'$) differs from the generic situation both qualitatively and quantitatively. For models with $2N$ spin-orbitals per site and a purely Hubbard-type local interaction, $\hat{H}_{\rm I} = U \sum_{\sigma,\sigma'} \hat{n}_\sigma \hat{n}_{\sigma'}$, the critical interaction is given as [119]

$$U_C = \frac{\sqrt{n(1-n+1/(2N))} + \sqrt{(n+1/(2N))(1-n)}}{(1-n)n} |\varepsilon_0| \,,$$

where ε_0 is the uncorrelated ground-state energy per lattice site. Note, however, that the Brinkman–Rice transition is continuous *only* at this point, and values of J/U as small as 10^{-2} produce finite jumps of a significant size. A (realistic) value of $U' = 0.8U$ ($J = 0.1U$) is enough to reduce the critical interaction strength $U_{\rm BR}$ for the Brinkman–Rice transition by a factor of two.

The reason for this behaviour is readily understood. All atomic two-electron states are degenerate in energy only for $U' = U$ ($J = 0$). Thus, all double occupancies have equal weight near the Brinkman–Rice transition, both in the metallic and insulating phase. Any finite J value will remove the degeneracies and re-establish the generic case.

As seen from figure 9.10(left), the critical interaction strength $U_{\rm BR}$ and the size of the q-factor strongly depend on the size of the Hund's-rule coupling J/U. In figure 9.10(right), we display the behaviour of $q_{\rm BR}$ as a function of U'/U at the corresponding critical interaction strengths $U_{\rm BR}$. For the Gutzwiller wave function with atomic correlations ($\mathrm{GW_{atom}}$), a maximum of $q^{\rm max}_{\rm BR} \approx 0.4$ for $U' < U$ occurs near $U'/U = 0.9$ ($J/U = 0.05$). A shallow minimum of $q^{\rm min}_{\rm BR} \approx 0.1$ is seen near $U'/U \approx 0.14$ ($J/U = 0.43$). On the contrary, the same curve for the Gutzwiller wave function with pure density correlations ($\mathrm{GW_{dens}}$) increases monotonically as a function of J/U towards $q^{\rm dens}_{\rm BR} \approx 0.6$ at $U'/U = 0$.

In the range $0 \leq U'/U < 1$, we always find $q^{\rm dens}_{\rm BR} > q_{\rm BR}$. Moreover, we have $U_{\rm BR} > U^{\rm dens}_{\rm BR}$, see figure 9.10(left). As expected, the metallic state is stabilised by the introduction of the full atomic correlations. Nevertheless, the two values for the Brinkman–Rice transition are fairly close to each other, $U_{\rm BR} \gtrsim U^{\rm dens}_{\rm BR}$. Therefore, it is interesting to plot the value of the q factor for the case of atomic correlations at $U = U^{\rm dens}_{\rm BR}$. It is very similar to the $q_{\rm BR}$ curve for pure density correlations (see figure 9.10(right)). This shows that the q factor sharply –yet continuously– drops as a function of U in the region $U^{\rm dens}_{\rm BR} \leq U < U_{\rm BR}$ before it jumps from $q_{\rm BR}$ to zero at the Brinkman–Rice transition.

In figure 9.11, we display the paramagnetic (U, U') phase diagram at half band filling. It is seen that the additional atomic correlations ($\mathrm{GW_{atom}}$) further stabilise the metallic phase for all $U > U'$ ($J > 0$), as compared to the result of the density correlations. The figure

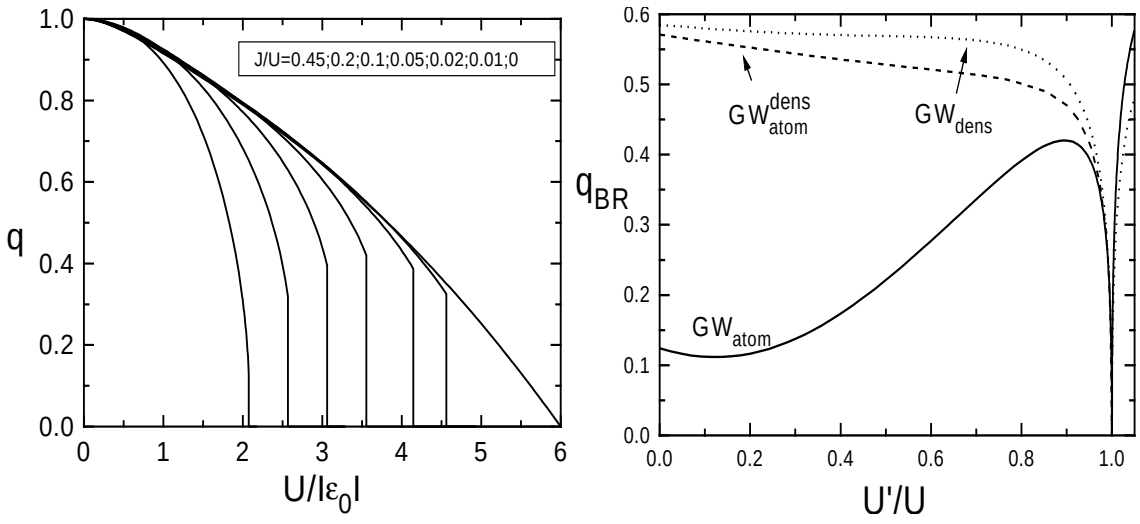

Figure 9.10: Left: Bandwidth renormalisation factor q at half band filling as a function of U for various values of J ($J = (U - U')/2$). Right: Bandwidth renormalisation factor at the Brinkman–Rice transition $U = U_{\mathrm{BR}}$ as a function of U'/U for the Gutzwiller wave function with atomic correlations (full line) and pure density correlations (dotted line). Also shown is the value of the q factor for $\mathrm{GW}_{\mathrm{atom}}$ at $U = U_{\mathrm{BR}}^{\mathrm{dens}}$ (dashed line).

also shows the gain in the variational energy when we use the Gutzwiller wave functions with full atomic correlations instead of pure density correlations. The gain is shown for fixed value $U = U_{\mathrm{BR}}^{\mathrm{dens}}$ as a function of U'/U. It is quite considerable, of the order of 0.1 eV, for realistic values of $J/U \approx 0.1$.

In the unphysical regime $J < 0$ ($U' > U$), the metal is *less* stable in the presence of full atomic correlations. Note that in this parameter range the insulating ground state is different for the two variational wave functions: a unique atomic ${}^1A_1$ state with energy $U - |J|$ versus two degenerate $|\uparrow\downarrow, 0\rangle$ and $|0, \uparrow\downarrow\rangle$ states of energy U for pure density correlations. As a consequence, the violation of the atomic symmetry in this limit leads to a qualitatively different result for pure density correlations.

Apparently, the exchange interactions in multi-band systems have a profound influence on the qualitative nature of Mott metal-insulator transitions. In the Gutzwiller theory, these transitions are, in general, of first order in the hopping renormalisation factor q. Whether or not these findings are an artefact of our approach or generic for multi-band systems is still not clear; so far, the results of the Dynamical-Mean-Field-Theory are inconclusive. In reference [219], our results were qualitatively reproduced within a 'linearised DMFT calculation'. In contrast, a study based on the 'numerical renormalisation group' found discontinuities only for models with density-density type exchange interactions, see reference [220].

9.4 Orbital Selective Mott Transitions and Local Hybridisation

Metal-insulator transitions in Hubbard models with different densities of states have attracted a lot of interest in recent years [221–228]. A dispute arose over the question whether or not the transition occurs at different interaction strengths for the wide and the narrow band. A transition with different critical interaction parameters is usually denoted as an 'orbital selective Mott transition' (OSMT). Apparently, a consensus has now been reached that such an OSMT can occur in Hubbard models with different bandwidths, subject to the bandwidth ratio α of the narrow and the wide band and the value of the local exchange interaction J.

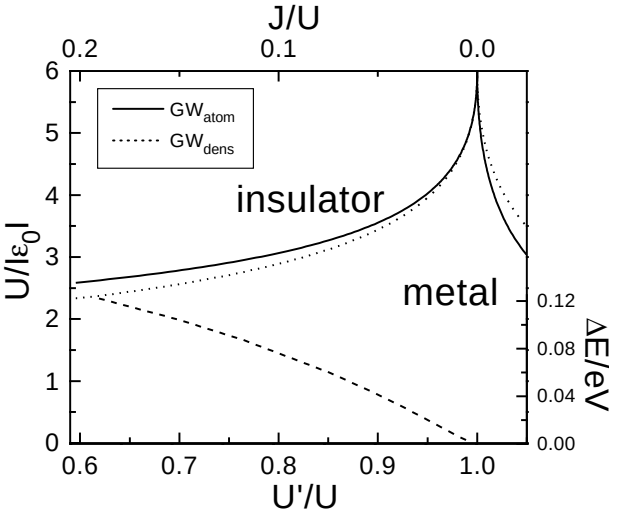

Figure 9.11: Phase diagram and critical interaction strength for the Brinkman–Rice transition in Gutzwiller wave functions with atomic ($\mathrm{GW_{atom}}$) and pure density ($\mathrm{GW_{dens}}$) correlations as a function of U'/U (left Y-axis). The dashed curve shows the energy gain for atomic correlations against pure density correlations at $U = U_{\mathrm{BR}}^{\mathrm{dens}}$ (right Y-axis).

In most of the previous calculations on OSMTs, the Dynamical-Mean-Field-Theory was employed. The OSMT in a two-band Hubbard model was first investigated by means of the Gutzwiller theory in reference [228]. In that work, the authors found an OSMT both for vanishing ($J = 0$) as well as for finite ($J \neq 0$) local exchange interaction. For $J = 0$, the critical band-width ratio was found to be $\alpha_c = 0.2$. The Gutzwiller results in [228] were in good agreement with data from DMFT and a slave-spin approach proposed in reference [226].

In this section, we analyse the OSMT in a two-band model in more detail. In particular, we permit a finite expectation value $\Delta_0 = \langle \hat{c}_{i,1}^\dagger \hat{c}_{i,2} \rangle$ for the local hybridisation, which can change the nature of the OSMT. Such a hybridisation could be finite spontaneously, solely due to the Coulomb interaction, or due to a finite hybridisation term in the Hamiltonian. We will investigate both possibilities.

9.4.1 Model Hamiltonian and Gutzwiller Wave Function

We investigate our generic two-band Hubbard model with the local Hamiltonian (2.23) and the single-particle Hamiltonian

$$\hat{H}_0 = \sum_{i,j;b,s} t_{i,j}^b \hat{c}_{i,(b,s)}^\dagger \hat{c}_{j,(b,s)} \ , \tag{9.51}$$

where we assume that the hopping amplitudes

$$t_{i,j}^b = \alpha_b t_{i,j} \tag{9.52}$$

depend on the orbital index b only via overall bandwidth factors α_b. This leads to an orbital-dependent renormalisation

$$D_b(\varepsilon) = \frac{1}{\alpha_b} D_0 \left(\frac{\varepsilon}{\alpha_b} \right) \tag{9.53}$$

of the bare density of states

$$D_0(\varepsilon) = \frac{1}{L} \sum_{\boldsymbol{k}} \delta(\varepsilon - \varepsilon_{\boldsymbol{k}}) \ , \tag{9.54}$$

where $\varepsilon_{\boldsymbol{k}}$ is the Fourier transform of $t_{i,j}$. In this section, only symmetric densities of states will be considered $D(-\varepsilon) = D(\varepsilon)$. As in section 9.2, we will also consider the corresponding spinless model, which has been introduced in equations (9.16).

We work with a real variational-parameter matrix $\lambda_{\Gamma,\Gamma'}$ and, since there is no spin order, we assume that only states with the same quantum number S_z lead to finite non-diagonal elements. Due to these symmetries, the local correlation operator contains up to five variational parameters for the spinless model and up to 26 for the full two-band model.

Throughout this section we will investigate the half-filled case of our model systems and allow for a finite local hybridisation

$$\Delta_0 = \langle \hat{c}^\dagger_{i,(1,s)} \hat{c}_{i,(2,s} \rangle_{\Psi_0}. \tag{9.55}$$

With respect to the operators $\hat{c}^\dagger$ and $\hat{c}$, the local density matrix is therefore non-diagonal. As shown in our derivation of expectation values in section 5.2, it is more convenient to work with creation and annihilation operators

$$\hat{h}^{(\dagger)}_{i,(1,s)} = \frac{1}{\sqrt{2}} \left(\hat{c}^{(\dagger)}_{i,(1,s)} + \hat{c}^{(\dagger)}_{i,(2,s)} \right) , \tag{9.56a}$$

$$\hat{h}^{(\dagger)}_{i,(2,s)} = \frac{1}{\sqrt{2}} \left(\hat{c}^{(\dagger)}_{i,(1,s)} - \hat{c}^{(\dagger)}_{i,(2,s)} \right) \tag{9.56b}$$

that have a diagonal local density matrix,

$$n^{(h)}_b = \langle \hat{h}^\dagger_{i,(b,s)} \hat{h}_{i,(b',s)} \rangle_{\Psi_0} = \delta_{b,b'} \Big(\frac{1}{2} \pm \Delta_0 \Big). \tag{9.57}$$

With respect to these operators, the single-particle Hamiltonian $\hat{H}_0$ reads

$$\hat{H}_0 = \sum_{i,j;b,b';s} \tilde{t}^{b,b'}_{i,j} \hat{h}^\dagger_{i,(b,s)} \hat{h}_{j,(b',s)} , \tag{9.58}$$

where

$$\tilde{t}^{b,b'}_{i,j} = \frac{t_{i,j}}{2} \big(\delta_{b,b'} + \Delta\alpha(1 - \delta_{b,b'}) \big) . \tag{9.59}$$

Both atomic Hamiltonians (2.23) and (9.16c) keep their form under a transformation from the $\hat{c}$-basis to the $\hat{h}$-basis.

9.4.2 Orbital-Selective Mott Transition in an asymmetric Two-Band Hubbard Model

First, we consider the metal-insulator transition in the asymmetric two-band Hubbard model without local hybridisation. For our numerical calculations, we use a semi-elliptic density of states

$$D^{\mathrm{s}}_0(\varepsilon) \equiv \frac{2}{\pi} \sqrt{1 - \varepsilon^2} , \tag{9.60}$$

where we have defined the energy unit as $D = 1$, half of the bare bandwidth. For our analytical considerations, we do not need to specify the bare density of states (9.60). It turns out that $D(\varepsilon)$ enters the results only through the integral

$$\varepsilon_0 = \int_{-\infty}^{0} \mathrm{d}\varepsilon D(\varepsilon)\varepsilon \quad \left(= -\frac{2}{3\pi} \text{ for } D(\varepsilon) = D^{\mathrm{s}}_0(\varepsilon) \right) , \tag{9.61}$$

and through its value $D(0)$ at the Fermi level. When we set $\alpha_1 = 1$ and introduce the bandwidth ratio $\alpha \equiv \alpha_1/\alpha_2 \leq 1$, the expectation value for the one-particle Hamiltonian (9.51) is given by

$$\langle \hat{H}_0 \rangle_{\Psi_{\mathrm{G}}} = (q_1^2 + q_2^2 \alpha)\varepsilon_0 . \tag{9.62}$$

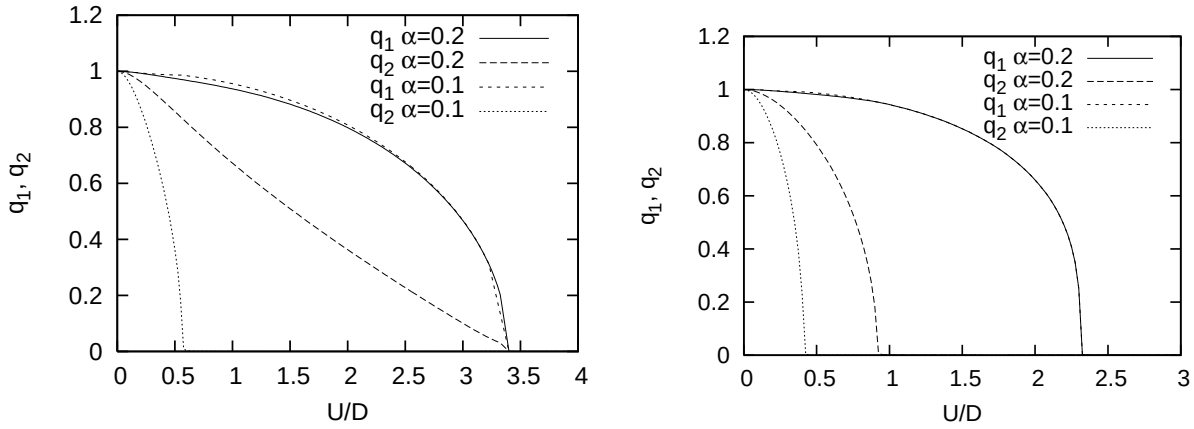

Figure 9.12: Renormlisation factors q_b for $\Delta = 0$, and bandwidth ratios $\alpha = 0.2$, $\alpha = 0.1$; Left: $J = 0$; Right: $J = 0.1$.

Without hybridisation, the variational ground-state energy has to be minimised only with respect to the variational parameters $\lambda_{\Gamma,\Gamma'}$. In figure 9.12(left), we show the resulting renormalisation factors q_b as a function of U for $J = 0$ and two different bandwidth ratios α. As already observed in reference [228], it depends on the value of α whether or not there is an orbital selective Mott transition. For $J = 0$, the critical ratio is $\alpha_c = 0.2$, i.e., the renormalisation factors q_1, q_2 vanish at two different critical values $U_{c2} < U_{c1}$ if $\alpha < \alpha_c$. By switching on J, the critical ratio α_c becomes larger and the Mott transitions take place at smaller values of U; see figure 9.12(right). These findings are in good agreement with the results of Dynamical-Mean-Field-Theory; for a comparison, see reference [228].

For $J = 0$, we can gain more insight into the nature of the different Mott transitions in our model by some analytical calculations. First, we consider the case $\alpha > \alpha_c$. If we approach the Mott transition from below, we can neglect the variational parameters for empty and fourfold occupied sites. Due to the high symmetry of the model for $J = 0$, the ground-state energy is then a function of only three variational parameters, d, ϕ, and, θ,

$$E = 2\varepsilon_0 d\,(1-2d)\,f\,(\phi,\theta) + (1+d)\,U\ , \tag{9.63}$$

where

$$\begin{aligned} f\,(\phi,\theta) &= 4\alpha_1 \left(\sin(\phi)\sin(\theta) + \sqrt{2}\cos(\phi)\cos(\theta)\right)^2 \\ &\quad +4\alpha_2 \left(\cos(\phi)\sin(\theta) + \sqrt{2}\sin(\phi)\cos(\theta)\right)^2 . \end{aligned} \tag{9.64}$$

Here, $\tan(\phi)^2$ gives the ratio of the probabilities to find a singly-occupied site with an electron in the wide and in the narrow orbital. The ratio of the probabilities for doubly-occupied sites with two electrons in the same and in different orbitals is parametrised by $\tan(\theta)^2$. The variational parameter d gives the total probability for single occupation. At the Mott transition, where $d \to 0$, the two angles ϕ, θ can be calculated analytically

$$\theta_0 \equiv \theta(d\to 0) = \frac{1}{2}\arccos\left(\frac{-17+2\alpha-17\alpha^2}{3\,(1-34\alpha+\alpha^2)}\right)\ , \tag{9.65a}$$

$$\phi_0 \equiv \phi(d\to 0) = \frac{1}{2}\arctan\left(\frac{(1+\alpha)2\sqrt{2}\sin 2\theta_0}{(1-\alpha)(1+\cos 2\theta_0)}\right). \tag{9.65b}$$

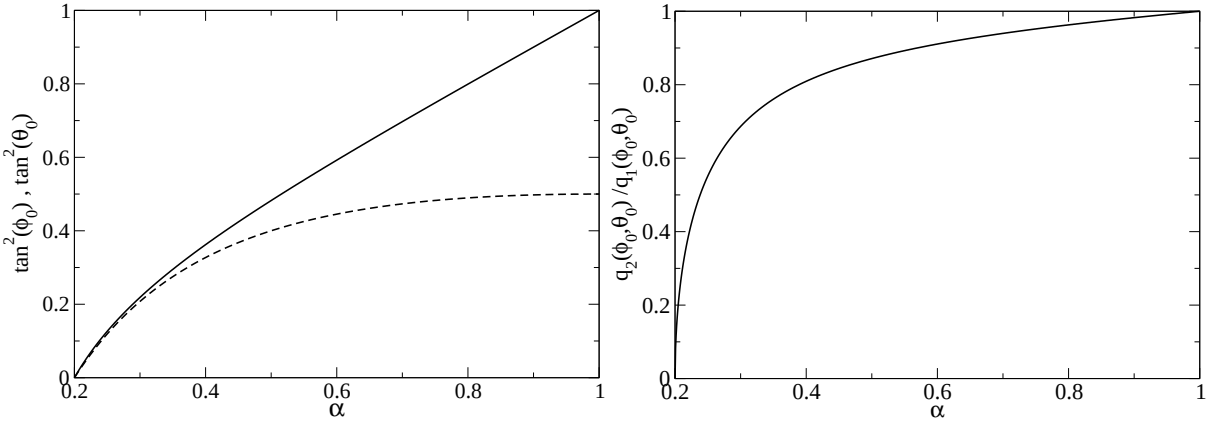

Figure 9.13: Left: $\tan(\phi_0)^2$ (full line) and $\tan(\theta_0)^2$ (dashed) at the Mott transition as a function of bandwidth ratio α; Right: Ratio of renormalisation factors q_2/q_1 at the Mott transition as a function of α.

Both values, $\tan(\phi_0)^2$, and $\tan(\theta_0)^2$ are shown as functions of α in figure 9.13(left).

As expected, the weight of local states with no electron in the narrow band vanishes for $\alpha \to \alpha_c$. The renormalisation factors q_b both vanish proportional to a square-root, $q_b \sim \sqrt{U_c - U}$, when U approaches U_c from below. The ratio q_2/q_1 is finite for $U \to U_c$ and goes to zero proportional to $\sqrt{\alpha - \alpha_c}$, see figure 9.13 (right). Finally, the critical interaction strength $U_{c2} = U_{c1}$ is given by

$$U_{c1} = 2|\varepsilon_0| f(\phi_0, \theta_0) \qquad (\alpha > \alpha_c) \ . \tag{9.66}$$

Next, we consider the case $\alpha < \alpha_c$. For interaction parameters $U_{c2} < U < U_{c1}$, the electrons in the narrow band are localised and the wide band can be treated as an effective one-band model. This leads us to the critical interaction parameter

$$U_{c1} = 2|\varepsilon_0| f(0,0) = 16|\varepsilon_0| \qquad (\alpha < \alpha_c) \tag{9.67}$$

for the Brinkman-Rice transition of the wide band. Starting from the Brinkman-Rice solution for $U < U_{c1}$, we can expand the variational energy to leading (i.e., second) order with respect to the three parameters $\{v_i\} = \{\phi, \theta, m_\emptyset\}$,

$$E = E_0 + \sum_{i,j=1}^{3} v_i \tilde{E}_{i,j} v_j \, . \tag{9.68}$$

The localisation of the narrow band becomes unstable when the matrix $\tilde{E}$ has negative eigenvalues for physical parameters $v_i > 0$. This evaluation yields the following expression for the narrow-band critical interaction strength

$$U_{c2} = 16|\varepsilon_0| \frac{\alpha}{1 - 4\alpha} \qquad (\alpha < \alpha_c). \tag{9.69}$$

The resulting phase diagram for all $0 \le \alpha \le 1$ is shown in figure 9.14.

9.4.3 Spinless Two-Band Model with Spontaneous Hybridisation

As the simplest example for a model with different densities of states, we investigate the spinless two-band model. In the half-filled case and without spontaneous hybridisation ($\Delta_0 = 0$), the

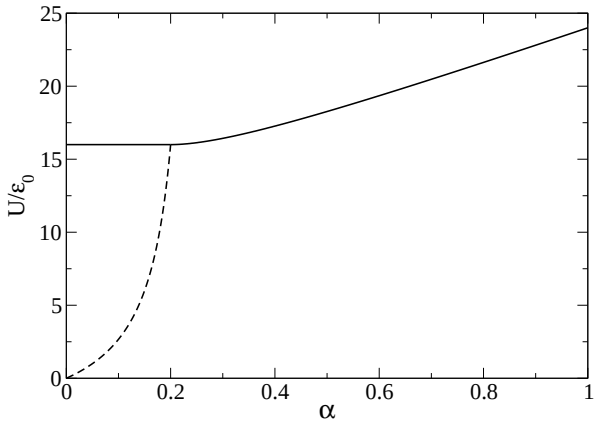

Figure 9.14: Critical interaction parameters U_{c1} (full line) and U_{c2} (dashed) as a function of α (see eqs. (9.66), (9.67), (9.69)).

constraints (5.47) can be solved analytically for this model, see section 5.4.1. The variational energy is then solely a function of λ_d,

$$E_{\text{var}} = 4\lambda_d^2 \left(1 - \frac{\lambda_d^2}{2}\right) \varepsilon_0 + \frac{U}{4}\lambda_d^2 \,. \tag{9.70}$$

The energy (9.70) can be minimised analytically. As a result, we find again the Brinkman-Rice solution

$$q_{\text{BR}} = 1 - \left(\frac{U}{U_c}\right)^2 , \tag{9.71a}$$

$$d_{\text{BR}} = \frac{1}{4}\left(1 - \frac{U}{U_c}\right) \tag{9.71b}$$

for the renormalisation factor $q = \delta_{b,b'} q_{b,b'}$ and the expectation value of the double occupancy $d = \lambda_d^2/4$. The Brinkman-Rice metal-insulator transition occurs at the critical value $U = U_c \equiv 16|\varepsilon_0|$, see section 5.4.1.

We now investigate the stability of the solution against a spontaneous hybridisation of the two bands. For the renormalisation factors α_b, we set $\alpha_1 + \alpha_2 = 2$, i.e., the difference of the bandwidths is parametrised by $\Delta\alpha \equiv \alpha_1 - \alpha_2$. Starting from the analytic solution for vanishing hybridisation, we can calculate the variational ground-state energy to leading order in Δ_0,

$$E_{\Delta_0} = E_{\text{BR}} + C(U, \Delta\alpha)\Delta_0^2 \,. \tag{9.72}$$

A spontaneous hybridisation will appear if the coefficient C in (9.72) is negative. The analytical evaluation leads to the Stoner-type instability criterion

$$\frac{f(\Delta\alpha)}{U_c D(0)} < \frac{U/U_c\,(2 + U/U_c)}{2\,(1 + U/U_c)^2} \equiv g\,(U/U_c)\,, \tag{9.73}$$

where

$$f(\Delta\alpha) \equiv \frac{\Delta\alpha}{2\text{arcsinh}\left(\Delta\alpha/\sqrt{4 - \Delta\alpha^2}\right)}. \tag{9.74}$$

In figure 9.15, the function $f(\Delta\alpha)$ and the right hand side of equation (9.73) are shown as a function of $\Delta\alpha$ and U, respectively. As can be seen from this figure, the function $f(\Delta\alpha)$ and therefore the left hand side of (9.73) approach zero for $\Delta\alpha \to 2$. On the other hand, the right hand side of (9.73) is positive for all $U > 0$. This means that for arbitrary values of U there exists a critical bandwidth difference $\Delta\alpha_c$ with $\Delta_0 > 0$ for $\alpha > \alpha_c$. Figure 9.16 (left)

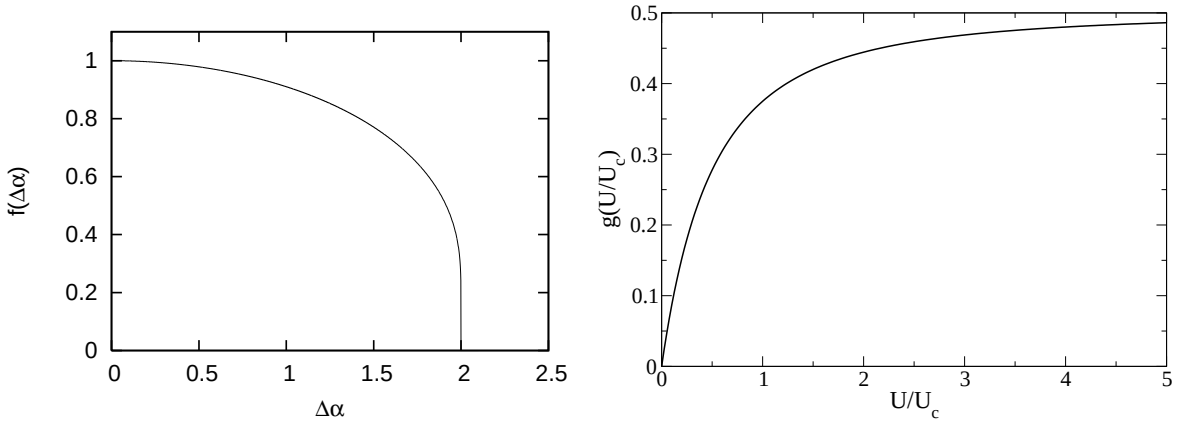

Figure 9.15: Left: $f\,(\Delta\alpha)$, equation (9.74); Right: $g(U/U_\mathrm{c})$, equation (9.73)

shows the phase diagram for ground states with and without finite hybridisation for different values of the density of states $D(0)$ at the Fermi level. Whether or not there is a transition in the large U limit for all values of $\Delta\alpha$ depends on the value of $D(0)$. This is illustrated in figure 9.16 (right), where the critical difference $\Delta\alpha_\mathrm{c}$ for the transition is shown as a function of $D(0)$ in the limit $U \to \infty$. Note that a spontaneous hybridisation has already been observed in a Falicov-Kimball model within a mean-field approximation [229]. This is in agreement with our results in the limit $\Delta\alpha \to 2$.

Our analytical results on the spinless two-band Hubbard model show that a difference in the bandwidth increases the tendency of the system to exhibit spontaneous hybridisation between the narrow band and the wide band. Mathematically, the reason for this is quite simple. Both the expectation value of the one-particle energy $\langle\hat{H}_0\rangle$ and the Coulomb interaction $\langle\hat{H}_\mathrm{loc}\rangle$ are changing quadratically in Δ_0. However, in the limit $\Delta\alpha \to 0$ the energy gain from $\langle\hat{H}_\mathrm{loc}\rangle$ always exceeds the decrease in energy from $\langle\hat{H}_0\rangle$. At first glance, one might think that the same behaviour should be observed in the OSMT phase of the two-band model with the only difference that it is not the bare, but the effective width of the narrow band that vanishes. As we will discuss in the next section, however, this hypothesis turns out to be incorrect.

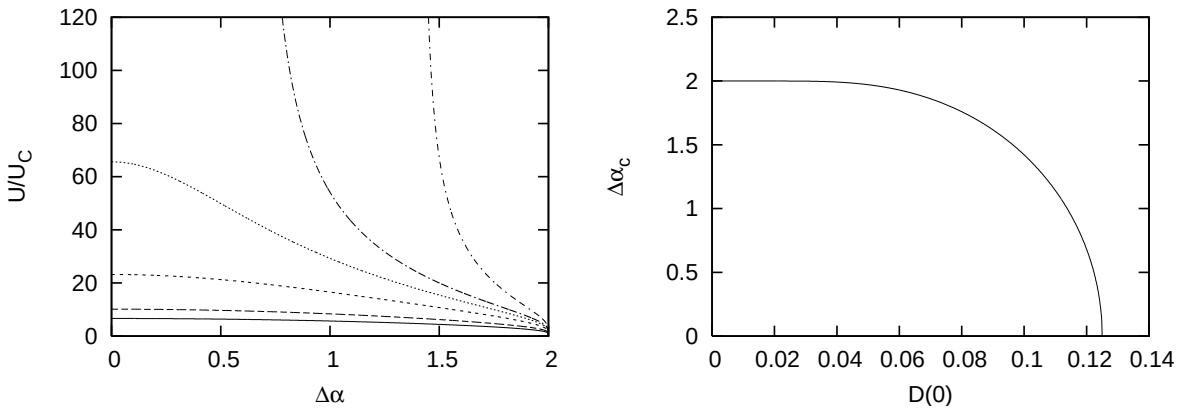

Figure 9.16: Left: phase diagram of the spinless two-band Hubbard model for different densities of states at the Fermi level $D(0) = 0.25, 0.2, 0.15, 0.13, 0.125, 0.1$ (from the bottom to the top of the figure) Right: critical difference $\Delta\alpha_\mathrm{c}$ in the limit $U \to \infty$ as a function of $D(0)$.

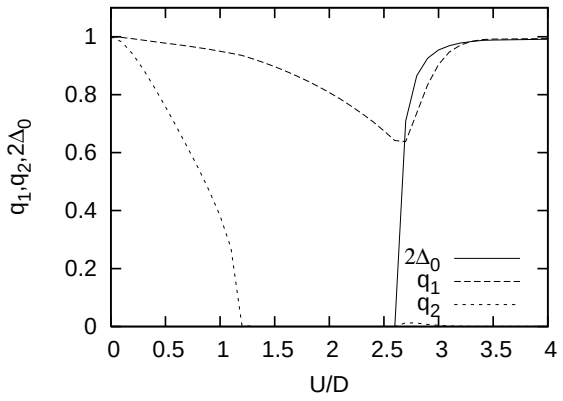

Figure 9.17: Renormalisation factors q_1, q_2 and hybridisation $2\Delta_0$ for $J = 0$ and $\alpha = 0.15$.

9.4.4 Spontaneous Hybridisation in the Two-Band Model

We present numerical results for the two-band model with a finite local hybridisation (9.55). As shown in the previous section, a vanishing width of the narrow band can be the driving force for a spontaneous local hybridisation of the wide band and the narrow band. In our two-band model, however, the vanishing of the effective bandwidth for $q_2 \to 0$ does not have the same effect. This can be seen in figure 9.17, where we show the results for the renormalisation factors q_1, q_2 and the hybridisation Δ_0. Unlike in the spinless model, there is not necessarily a finite hybridisation when the effective narrow bandwidth goes to zero for $U \to U_{c2}$. The reason for this differing behaviour is an additional contribution to the one-particle energy of the full two-band model. To leading order in Δ_0, there is a third term from the expansion of the narrow-band renormalisation factor

$$q_2 \approx q_2(\Delta_0 = 0) + c\Delta_0^2 \,. \tag{9.75}$$

The coefficient c is negative and, multiplied with the negative bare one-particle energy of the narrow band, it leads to an increase of the total energy. This contribution to the energy overcompensates the negative term from the Coulomb interaction.

A finite hybridisation Δ_0 sets in at larger values of U when the system is already in the OSMT phase, see figure 9.17. Numerically, it seems as if Δ_0 approaches its maximum value $\Delta_0^{\max} = 1/2$ only in the limit $U \to \infty$.

In all systems with finite values of J that we investigated, we did not find a solution with a spontaneous hybridisation. It is not excluded, though, that, for values of J smaller than some critical parameter J_c there is a solution with a finite hybridisation. However, it is difficult to determine this small parameter J_c numerically.

9.4.5 Orbital-Selective Mott Transition in a Two-Band Model with Finite Hybridisation

The assumption that there is no hybridisation between the two degenerate bands in the Hamiltonian of our model is quite artificial. In this section, we will therefore investigate how the OSMT is affected if we add a hybridisation term of the form

$$\hat{H}_{\text{hyb}} = -\tilde{\eta} \sum_{i,s} \hat{c}^\dagger_{i,(1,)} \hat{c}_{i,(2,s)} + \text{h.c.} \tag{9.76}$$

to our Hamiltonian (2.23).

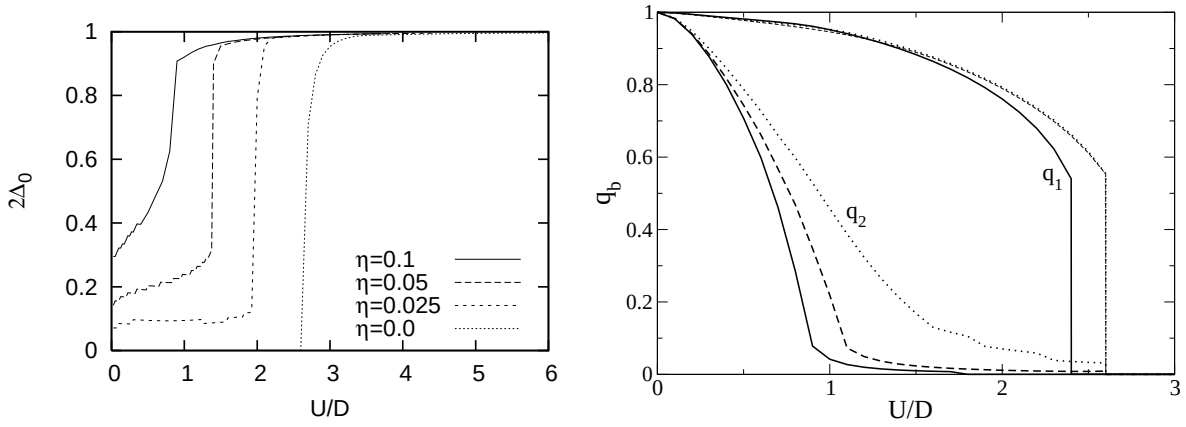

Figure 9.18: Left: expectation value $2\Delta_0$ as a function of U for several values of $\tilde{\eta}$; Right: Renormalisation factors q_1, q_2 for $\alpha = 0.15$ and $\tilde{\eta} = 0.025D$, $J = 0.05U$ (full line), $\tilde{\eta} = 0.025D$, $J = 0.025U$ (dashed), $\tilde{\eta} = 0.05D$, $J = 0.025U$ (dotted).

For $J = 0$, we find that the OSMT phase is destroyed for any finite value of $\tilde{\eta}$. This is illustrated in figure 9.18 (left) where we show the expectation value Δ_0 as a function of U for several values of $\tilde{\eta}$.

For finite J, the behaviour of our model is more ambiguous. As we have seen before, a finite J stabilises the OSMT phase whereas a finite $\tilde{\eta}$ tends to destroy it. Therefore, it depends on the ratio of both quantities whether or not an OSMT is found. Figure 9.18 (right) shows the renormalisation factors q_b for different values of J and $\tilde{\eta}$. For $J = 0.025U$ and $\tilde{\eta} = 0.05D$, the OSMT is completely suppressed. This is still the case for the smaller value $\tilde{\eta} = 0.025D$, although the narrow band factor q_2 is already quite small in the region of U parameters where it would be zero for $\tilde{\eta} = 0$. Finally, for larger values $J = 0.05U$ an OSMT phase is restored for interaction parameters $U > U_{c2}$ where U_{c2} is larger then the corresponding value for $\tilde{\eta} = 0$.

In summary, our numerical calculations show that appearance and disappearance of an OSMT results from a subtle interplay of the local exchange interaction J and the local hybridisation $\tilde{\eta}$.

Chapter 10

Materials

In this final chapter, we report on two materials, which we have investigated with our Gutzwiller variational theory. Results for the quasi-particle bands and the magnetic properties of fcc nickel are presented in section 10.1. In section 10.2, we investigate the electronic properties and, in particular, the Fermi-surface topology of Na_xCoO_2.

10.1 Magnetic and Electronic Properties of Nickel

In this section, we address ferromagnetic nickel as the prototype of band ferromagnetic materials. On the experimental side, one of the reasons why nickel has been in the focus of interest, much more than iron or cobalt, is the relative ease to grow large single crystals. Consequently, a lot of experimental investigations have been carried out on nickel in order to determine its magnetic properties and electronic structure. For a review, we refer to references [230–233].

10.1.1 The Nickel Problem

On the theoretical side, of all the iron group magnetic metals, nickel is the most celebrated case of discrepancies between Spin Density-Functional Theory (SDFT) predictions and experimental results. Early on, de-Haas–van-Alphen data indicated the presence of only one hole ellipsoid in the Fermi surface of the minority spin bands, located around the X-point of the Brillouin zone [234]. In contrast, energy band calculations using SDFT predict two hole ellipsoids around the X-point, the X_5-state of pure $d(t_{2g})$ orbital character, and the X_2-state of pure $d(e_g)$ orbital character. Concomitantly, neutron scattering experiments [235] revealed that the orbital character of the nickel magnetic moment exhibits less e_g admixture than predicted by energy-band calculations.

Measurements by angle-resolved photoemission-spectroscopy (ARPES) confirmed the de-Haas-van-Alphen results: the minority X_2-state of pure $d(e_g)$ orbital character was found to lie slightly below the Fermi level. Furthermore, the photoemission data differ considerably from SDFT over the whole range of occupied $3d$ bands. Most importantly, the width of the occupied part of the $3d$ bands is approximately $W = 3.3\,\mathrm{eV}$ [236, 237], whereas SDFT gives $W_{\mathrm{SDFT}} = 4.5\,\mathrm{eV}$, or larger [238]. ARPES studies also reveal big discrepancies between SDFT and experiment in the exchange splittings of majority and minority spin bands near the Fermi energy. The SDFT results give a rather isotropic exchange splitting of about 650 meV to 750 meV, whereas photoemission data show small and highly anisotropic exchange splittings between 160 meV for pure $3d(e_g)$-states such as X_2 and 330 meV for pure $3d(t_{2g})$-states such as S_3 near the X-point.

Another discrepancy concerns the position of the $L_{2'}$-state. Experimentally, it is found approximately 1.0 eV below the Fermi energy E_{F} whereas the SDFT puts it to about 0.3 eV below E_{F}. This state is special as it represents the most binding, pure $4p$-state. An incorrect $4p$-level implies that DFT slightly underestimates the partial density of the $4p$ electrons and, thus, the $3d$-hole density. This appears to be a general problem of the underlying DFT calculation. The same problem appears for $4d$ transition metals of bcc structure: the position of the purely $5p$-state $N_{2'}$ also appears shifted by about 0.7 eV to lower energies as compared to the DFT results, see reference [239] .

Lastly, the size and the direction of the magnetic moment pose a big problem to SDFT. Early experiments using ferromagnetic electron resonance and the Einstein–de-Haas effect have produced the values $g = 2.183$ and $g' = 1.835$, which result in an orbital moment of $\mu_{\mathrm{orb}} = 0.0507\mu_{\mathrm{B}}$ per atom for nickel [230]. In general, the values of the orbital part of the magnetic moments in band ferromagnets are not very well reproduced in SDFT. Iron and cobalt show large deviations [240], even in relativistic SDFT calculations [241]. Moreover, the magneto-crystalline anisotropy energies are not correct, i.e., they come with the wrong sign in SDFT. As shown by Aubert and Gersdorf [242, 243], the value of the dominant anisotropy constant is $K_1 = -8.8\,\mu$eV, i.e., the (111) direction is the easy axis in nickel. For a (001) magnetic moment, the energy is higher with an energy difference $E_{\mathrm{aniso}} \equiv E_{111} - E_{001} \approx -3\,\mu$eV per atom. In contrast, it is $E_{\mathrm{aniso}} > 0$ in SDFT calculations, e.g., by Daalderop [241] so that $K_1 > 0$. The SDFT results for cobalt and iron are equally disappointing. At low temperatures, the complex behaviour of the magnetic anisotropy as a function of temperature and the magnetic field was interpreted by Gersdorf [242] to be caused by a shift of the electronic state (001) $X_{2\downarrow}$ to about 3 meV *above* the Fermi energy. The famous second hole ellipsoid around the $X_{2\downarrow}$ indeed exists [242] as long as the magnetic moment has an angle of less than 18 degrees with the (001) direction. However, the states (100) $X_{2\downarrow}$ and (010) $X_{2\downarrow}$ remain below E_{F}, about 33 meV [242].

All these discrepancies could not be overcome by SDFT modifications such as the GGA variants [244, 245]. Apparently, a substantial improvement of SDFT results for nickel along these lines is presently not within reach. Recent correlated electron theories remove the SDFT shortcomings only partially. For example, with LDA+U-type calculations it seems to be possible to adjust to experiment the orbital moment, the magnetic anisotropy, and the Fermi-surface topology [246, 247]; however, other quantities, especially the entire quasi-particle band structure, remain elusive within these theories.

10.1.2 Model and Wave-Function Specifications

In order to apply the Gutzwiller theory, the parameters of a proper multi-band Hubbard Hamiltonian need to be specified; these are the hopping amplitudes, the local potential terms, the local spin-orbit coupling, and the local Coulomb interaction parameters, see also appendix G.1. In addition, we have to specify the class of Gutzwiller wave functions that we use for our investigation.

Electron-Transfer Amplitudes and Local Potential Terms

For nickel, we consider a minimal model that includes only those bands that are partly filled within a paramagnetic LDA calculation. Therefore, our multi-band Hubbard Hamiltonian $\hat{H}_{\mathrm{H}}$ comprises of 18 spin orbitals, namely $3d$, $4s$, and $4p$. The non-magnetic local-density approximation to DFT provides the LDA band structure $E^{\mathrm{LDA}}_{\boldsymbol{k},\gamma}$. We represent the bare energy-band matrix elements $\varepsilon^{0}_{\boldsymbol{k};\sigma,\sigma'}$ in the kinetic energy operator $\hat{H}_0$ in terms of real electron-transfer integrals $t^{\sigma,\sigma'}(\boldsymbol{r})$ in the two-centre approximation [214], which range up to third nearest

$N_{\boldsymbol{r}}$	$ss\sigma$	$sp\sigma$	$sd\sigma$	$pp\sigma$	$pp\pi$
1	−1.0292	1.2047	−0.5933	1.2144	−0.5284
2	−0.1039	0.2234	−0.1089	0.5989	−0.2205
3	−0.0050	−0.0223	−0.0223	0.0137	0.0076
	$pd\sigma$	$pd\pi$	$dd\sigma$	$dd\pi$	$dd\delta$
1	−0.6960	0.2300	−0.4780	0.3150	−0.0481
2	−0.2092	0.0524	−0.0848	0.0336	−0.0007
3	−0.0439	−0.0023	−0.0245	−0.0011	0.0024

Table 10.1: Electron-transfer parameters $t^{\sigma,\sigma'}(\boldsymbol{r})$ to $N_{\boldsymbol{r}}$-th neighbours (all energies in eV).

neighbours, $N_{\boldsymbol{r}} \leq 3$. These parameters and the local potential terms ε_σ are chosen in such a way that our tight-binding fit reproduces the LDA band structure. In this fit, we include information on the symmetry of the single-particle states, see e.g., reference [248]. For the optimal choice, the $\boldsymbol{k}$-averaged root-mean-square deviation between our tight-binding fit and the LDA band structure up to 2 eV above the Fermi energy is 15 meV for the $3d$ bands and for the $4sp$ bands. Our values of the electron-transfer parameters are summarised in Table 10.1.

For the on-site parameters, we find for both spin species

$$\begin{aligned}
\varepsilon_{4s,4s} &\equiv \varepsilon_s &&= 5.6022\,\text{eV}\,, \\
\varepsilon^{\text{LDA}}_{4p,4p} &\equiv \varepsilon^{\text{LDA}}_p &&= 8.5335\,\text{eV}\,, \\
\varepsilon_{4p,4p} &\equiv \varepsilon^{\text{shift}}_p &&= 7.7835\,\text{eV}\,, \\
\varepsilon_{3d(t_{2g}),3d(t_{2g})} &\equiv \varepsilon_{t_{2g}} &&= -0.0290\,\text{eV}\,, \\
\varepsilon_{3d(e_g),3d(e_g)} &\equiv \varepsilon_{e_g} &&= 0.0436\,\text{eV}\,,
\end{aligned} \tag{10.1}$$

where $\varepsilon^{\text{LDA}}_p$ is the result from the fit to LDA and $\varepsilon^{\text{shift}}_p$ is used in practical calculations for a better agreement between our Gutzwiller theory and ARPES experiments for nickel, see below. For the total crystal-field splitting, we find $\varepsilon_{\text{cf}} = \varepsilon_{t_{2g}} - \varepsilon_{e_g} = -0.0726\,\text{eV}$.

The energetically highest-lying state of pure d character is X_5 (purely t_{2g}), 0.18 eV above the Fermi energy. The state X_2 (purely e_g) lies 0.025 eV above E_{F}. The width of the $3d$ bands can be estimated from $E(X_5) - E(X_1) = 4.45\,\text{eV}$ (X_1 is predominantly of $d(e_g)$ character), or from $E(X_5) - E(L_1) = 4.63\,\text{eV}$ (L_1 is predominantly $d(t_{2g})$).

Next, we address the $L_{2'}$-state. Experiment locates this state at about 1.0 eV below E_{F}. The SDFT calculations for ferromagnetic nickel as well as our Gutzwiller theory find the $L_{2'}$-state about 0.3 eV below the Fermi energy when we use the LDA $4p$ orbital energy $\varepsilon^{\text{LDA}}_p = 8.5335\,\text{eV}$. Therefore, we shift the $4p$ orbital energy by 0.75 eV to $\varepsilon^{\text{shift}}_p = 7.7835\,\text{eV}$, and find the $L_{2'}$-state 0.97 eV below E_{F}. In the following, we present results that use $\varepsilon^{\text{shift}}_p = 7.7835\,\text{eV}$. This choice enhances the $4p$ partial density by approximately 0.1 electron and, correspondingly, enhances the $3d$ hole charge by the same amount so that we work with $n_d = 8.78$. The remaining 1.22 valence electrons are about evenly split between the $4s$ level and the three $4p$ levels.

Local Hamiltonian

As described above, the paramagnetic LDA calculation provides a first single-particle contribution to the local Hamiltonian,

$$\hat{H}^{\text{onsite}}_{\text{loc}} = \sum_{i,\sigma} \varepsilon_\sigma \hat{c}^\dagger_{i,\sigma} \hat{c}_{i,\sigma} \tag{10.2}$$

with $|\sigma\rangle = |4s, 4p, 3d\rangle \otimes |\uparrow, \downarrow\rangle$. In addition to these single-particle contributions, we include the spin-orbit interaction for the $3d$ electrons only, $|\sigma\rangle = |3d\rangle \otimes |\uparrow, \downarrow\rangle$. Hereby, we restrict ourselves to the dominant, purely atomic contributions of the form

$$\hat{H}^{\mathrm{so}}_{\mathrm{loc}} = \sum_{i,\sigma,\sigma'} \frac{\zeta}{2} \langle \sigma | \hat{l}_x \tilde{\sigma}_x + \hat{l}_y \tilde{\sigma}_y + \hat{l}_z \tilde{\sigma}_z | \sigma' \rangle \hat{c}^\dagger_{i,\sigma} \hat{c}_{i,\sigma'} \ . \tag{10.3}$$

Here, ζ is the strength of the spin-orbit coupling, $\tilde{\sigma}_{x,y,z}$ are the three Pauli matrices, and $\hat{l}_{x,y,z}$ are the Cartesian components of the vector operator for the angular momentum. For the spin-orbit coupling constant, we choose $\zeta = 0.080\,\mathrm{eV}$ as in references [249, 250].

The second part of the local interaction is the two-particle Coulomb interaction $\hat{H}_{\mathrm{I}}$ in (2.15). The intra-atomic interactions in the $4s$ and $4p$ shell are rather weak when compared to the broad $4sp$ energy bands. Thus, we expect only small correlation effects in these bands. We also neglect correlations between $4sp$ electrons and $3d$ electrons beyond those contained in the LDA band structure. This is a more serious approximation as we neglect magnetic polarisation effects on the $4sp$ bands and thus may underestimate the $4sp$ contribution to the magnetic moment. Under these assumptions, the spin-orbit sum in the interaction part of (2.15) runs over the $3d$ orbitals only. The local Hamiltonian is then given by

$$\hat{H}_{\mathrm{loc}} = \hat{H}_{\mathrm{I}} + \hat{H}^{\mathrm{onsite}}_{\mathrm{loc}} + \hat{H}^{\mathrm{so}}_{\mathrm{loc}} \ . \tag{10.4}$$

For the d-orbitals, we introduce a basis $\left|\Gamma^{3d}\right\rangle$ of eigenstates of $\hat{H}_{\mathrm{I}}$,

$$\hat{H}_{\mathrm{I}} |\Gamma^{3d}\rangle = E_{\Gamma^{3d}} |\Gamma^{3d}\rangle \ . \tag{10.5}$$

The atomic states $|\Gamma\rangle$ that we will use in our definition of the Guzwiller correlation operator, can be written as product states,

$$|\Gamma\rangle = |\Gamma^{3d}\rangle |\Gamma^{4s}\rangle |\Gamma^{4p}\rangle \ . \tag{10.6}$$

Since, in our Gutzwiller theory, we only correlate the $3d$ states $|\Gamma^{3d}\rangle$, the variational parameters $\lambda_{\Gamma,\Gamma'}$ are independent of the $4sp$ configuration $|\Gamma^{4s}\rangle|\Gamma^{4p}\rangle$. This leads to a numerically tractable problem if the number of non-diagonal elements in $\lambda_{\Gamma,\Gamma'}$ does not significantly exceed the number of diagonal elements.

Naturally, we should not completely ignore the Coulomb interaction of the $4sp$ electrons. In this case, a big charge flow from the $3d$ to the $4sp$ bands and unphysically small occupations of the $3d$ shell would result. One way to overcome the charge flow problem, is to introduce a chemical potential that keeps the $3d$ partial charge fixed during the calculations, $n_d = 8.78$; see [251] for an alternate method, which gives essentially the same results.

The Gutzwiller theory produces an optimum magnetic (spin-only) moment, which is too large by about 10%. It should be mentioned that the SDFT results show a similarly large overshooting of the magnetic moment. To best compare with experiment, we thus carry out calculations at fixed magnetic moment for the total energy, with either the spin-only moment fixed to the (spin-only) experimental value of $\mu_{\mathrm{spin}} = 0.55\mu_{\mathrm{B}}$, or with the total magnetic moment fixed to the full experimental moment of $\mu = 0.606\mu_{\mathrm{B}}$ when the spin-orbit coupling is included.

Parameters for the Coulomb Interaction

It remains to determine the Coulomb interaction parameters $U^{\sigma_1,\sigma_2,\sigma_3,\sigma_4}$ in (2.15). In the spherical-atom approximation, there are only three independent interaction parameters, for

example the three Racah parameters A, B, and C; see appendix C. The spherical-atom approximation is excellent in cubic systems. In principle, the Coulomb interaction among $3d(t_{2g})$ electrons may differ from the Coulomb interaction among $3d(e_g)$ electrons because the radial parts of their orbital wave functions could be different. Measurements of d-d transitions of magnetic impurities with cubic site symmetry in non-magnetic oxide hosts show that these differences are marginal. The d^3 multiplets ^3H and ^3P, which are accidentally degenerate in spherical-atom approximation, split by cubic two-particle corrections but not by the crystal field. However, they are found to be degenerate within the experimental resolution of some meV [92]. In test calculations, we have used different A parameters for $d(t_{2g})$ electrons and $d(e_g)$ electrons but we have not found any features in our quasi-particle energies, which would indicate a failure of the spherical-atom approximation.

The Racah parameters B and C are related to the Slater integrals F_2 and F_4. They determine the splitting of the multiplets of a specific $3d^n$ configuration. They can be determined experimentally from d-d transition spectra for magnetic impurity ions in non-magnetic insulating hosts. Typical values for all kinds of transition metal ions are tabulated in [92]. It is found experimentally that the ratio C/B varies smoothly between 4 and 5; $C/B = 4$ is obtained theoretically when hydrogen $3d$ wave functions are used. Experimentally, the values for B and C for Ni^{2+} and Ni^{3+} ions are known [92]. When we linearly extrapolate these values to a neutral atom we find our values for nickel as $B = 0.09\,\mathrm{eV}$ and $C = 0.40\,\mathrm{eV}$ so that we employ a ratio $C/B = 4.4$. The values for B and C are close to the 'bare' atomic values, i.e., the screening appears to be of little importance to B and C. For a fixed ratio C/B, we may replace the two interaction parameters B and C by a single effective parameter J, as is quite often done in the LDA+U literature. This exchange coupling J is related to B and C by

$$\frac{B}{2} + \frac{C}{5} = \frac{J}{7}\,. \tag{10.7}$$

For our nickel values for B and C, we find $J = 0.88\,\mathrm{eV}$, a value very similar to the ones used by Anisimov et al. [252] and others.

The Racah parameter A (basically the U parameter of the Hubbard model) determines the separation of the various d^n multiplets. The 'bare' values, as calculated, e.g., from atomic wave functions are of the order of 25 eV, as discussed already in Herring's book on magnetism [253] and confirmed recently in [254]. There is a technique to extract U parameters using 'constraint' density-functional theory and supercell geometries. It has been found that for minimum-basis models the U-values are smallest. For example, in the case of the cuprates, values $U \leq 2\,\mathrm{eV}$ were found for a single-band Hubbard model whereas a three-band model including the oxygen $2p$ states employs $U_{dd} \approx 8\,\mathrm{eV}$ [255]. Similar results have been found in the case of $BaBiO_3$ [256]. For $3d$ band models, values of $U = 4 \ldots 6\,\mathrm{eV}$ have been reported [252]. For the $4s$-$4p$-$3d$ multi-band case of nickel, no such calculations are available but values $U \approx 10\,\mathrm{eV}$ appear to be reasonable. We choose A in such a way that our Gutzwiller theory reproduces the experimental $3d$ band width. For our 18 orbital basis, we find $A = 9\,\mathrm{eV}$ to reproduce best the quasi-particle $3d$ band width $W = 3.3\,\mathrm{eV}$; a value of $A = 12\,\mathrm{eV}$ leads to $W = 3.0\,\mathrm{eV}$. If we worked with a model of only ten $3d$ spin orbitals, the corresponding band-width reduction is achieved for $A \approx 4\,\mathrm{eV}$.

Gutzwiller Wave Functions

For a multi-band model with ten correlated spin orbitals, it is impossible to evaluate the entire variational space defined by our general class of Gutzwiller wave functions (4.25). For example, if we work with a symmetric variational-parameter matrix and assume that all elements $\lambda_{\Gamma,\Gamma'}$

can be finite for states $|\Gamma\rangle$, $|\Gamma'\rangle$ with the same particle number, we find

$$N_{\mathrm{vp}} = \frac{1}{2}\sum_{n=0}^{10}\binom{10}{n}^2 = 92378 \tag{10.8}$$

as the total number of variational parameters. Even with our efficient minimisation algorithm, described in appendix H, the treatment of such a large number of variational parameters is infeasible.

Fortunately, for physical reasons, it is not necessary to exploit the entire space of parameters $\lambda_{\Gamma,\Gamma'}$. Depending on the particle number, there will be many states $|\Gamma\rangle$, which give no contribution to the variational energy since their probability to be occupied is almost zero. For example, in case of nickel with approximately 8.8 d-electrons per atom, all states $|\Gamma\rangle$ with particle numbers $|\Gamma| < 7$ give only a small contribution and the corresponding non-diagonal elements of the variational-parameter matrix can surely be neglected.

For those states $|\Gamma\rangle$ that mostly determine the variational energy, the matrix $\lambda_{\Gamma,\Gamma'}$ has to obey the symmetries of the lattice. In nickel, with its cubic site symmetry, it seems reasonable to couple all states $|\Gamma\rangle$, $|\Gamma'\rangle$ that belong to the same representation of the point symmetry group. In this way, however, we would violate the spherical approximation, which is used in our construction of the atomic Hamiltonian. In order to be consistent, we thus allow a coupling only for those states $|\Gamma\rangle$, $|\Gamma'\rangle$ that belong to the same degenerate spherical multiplet. If we allow a coupling of all states $|\Gamma\rangle$, $|\Gamma'\rangle$ belonging to the same cubic representation, certain results can change significantly, e.g., those for the exchange splitting. In this case, if we want to reproduce the experimental data, we have to go beyond the spherical approximation also in our construction of the atomic Hamiltonian. Since it is not clear, how the ten Coulomb parameters in cubic symmetry can be found from first principles, they would have to be determined by means of an unsatisfactory fitting procedure. Therefore, we find it more reasonable to work with a consistent spherical approximation both for the Hamiltonian and the variational-parameter matrix.

Apart from the variational-parameter matrix $\lambda_{\Gamma,\Gamma'}$ we have to specify the single-particle wave function $|\Psi_0\rangle$. As shown in section 5.3, it is given as the ground state of an effective single-particle Hamiltonian, see equation (5.97). This Hamiltonian contains Lagrange parameters $\eta_{\sigma,\sigma'}$, which have to be varied in order to minimise the ground-state energy. For symmetry reasons, not all of the $10^2 = 100$ parameters $\eta_{\sigma,\sigma'}$ can be finite. In the presence of spin-orbit coupling, the number n_{ie} of finite parameters depends on the magnetic moment direction; we find $n_{\mathrm{ie}} = 22$ for $\vec{\mu}||[111]$ and $n_{\mathrm{ie}} = 18$ for $\vec{\mu}||[001]$.

Numerically, a minimisation with respect to all n_{ie} parameters $\eta_{\sigma,\sigma'}$ is quite costly because each variation involves many momentum-space integrations. At present, we therefore work with a simplified effective Hamiltonian that contains effective parameters only for all physically relevant one-particle terms. An algorithm that allows to minimise the energy with respect to all n_{ie} parameters is described in appendix H.2.

In cubic symmetry, there exist only four independent matrix elements of the local (d-electron) density matrix. The trace of the matrix is fixed by the total d-electron number. The three remaining matrix elements are governed by parameters $\eta^d_{\sigma,\sigma'}$, which are given by the orbital-dependent exchange fields $\Delta_{t_{2\mathrm{g}}}$, $\Delta_{e_{\mathrm{g}}}$, and the effective crystal-field splitting $\varepsilon^{\mathrm{eff}}_{\mathrm{CF}}$. The non-cubic symmetry resulting from the addition of the spin-orbit coupling adds many more formally independent $\eta^d_{\sigma,\sigma'}$ terms. Both for $\vec{\mu}||[001]$ (tetragonal symmetry) and for $\vec{\mu}||[111]$ (trigonal symmetry) there are two more exchange-fields and two more crystal-field splittings. All these eight terms are included in our simplified effective Hamiltonian $\hat{\tilde{H}}^{\mathrm{eff}}_0$.

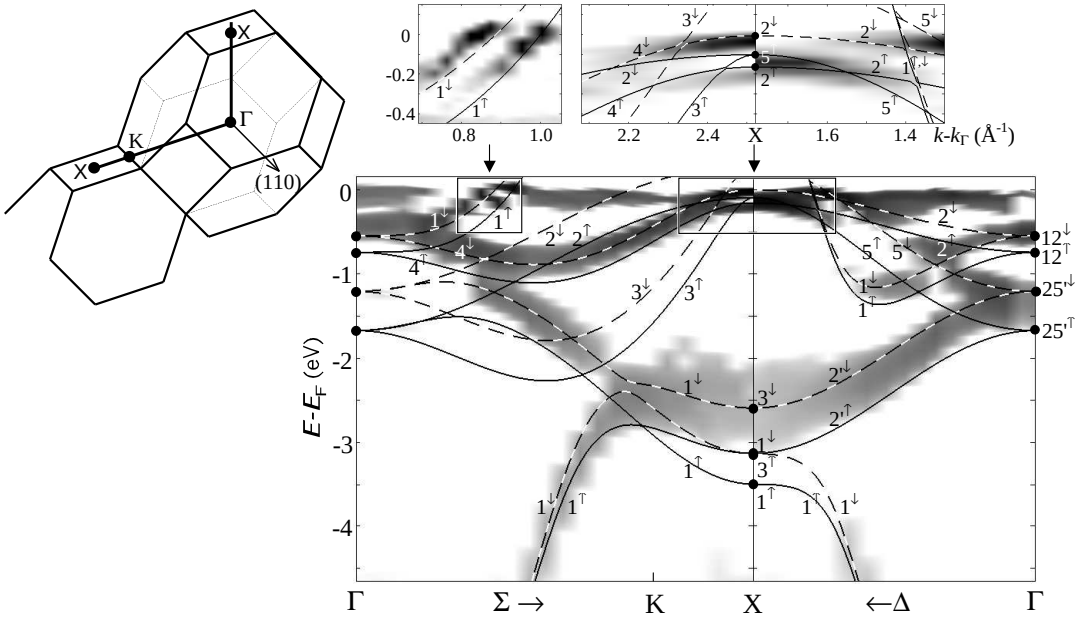

Figure 10.1: Grey-scale plot of the negative second derivative of the ARPES intensity for nickel with respect to energy, $-d^2I/dE^2$, on a logarithmic scale (insets: linear scale) for the ΓKX and ΓX directions of the BZ. The dispersionless structure at E_F is due to a residual Fermi edge resulting from indirect transitions. Some bands (Δ_2, X_1, Σ_2, Σ_3, Σ_1 towards Γ) are not seen due to unfavourable matrix elements, depending on geometry and chosen final state. Theoretical curves are the results of the Gutzwiller theory, see also table 10.2.

10.1.3 Quasi-Particle Band Structure

We consider separately the results of our theory for a model with and without spin-orbit coupling. For gross features, such as the quasi-particle band structure, the spin-orbit coupling is only a small perturbation and can, in principle, be neglected.

We find the best agreement [138, 257] with the experimental occupied $3d$ band width $W_{3d} = 3.3\,\mathrm{eV}$ for a value $A = 9\,\mathrm{eV}$, see table 10.2 and figure 10.1. Then, the condensation energy, i.e., the energy gain for the ferromagnetic phase as compared to the paramagnetic one, is $E_\mathrm{cond} \approx 40\,\mathrm{meV} = 0.8 k_\mathrm{B} T_\mathrm{C}$ ($T_\mathrm{C} = 630\,\mathrm{K}$ is the Curie temperature). This value of A is larger than in other multi-band studies on transition metals, see, e.g., references [258, 259]. In [258], only $3d$ bands were incorporated. If we eliminate in our calculations the rather large $4sp$-$3d$ hybridisations we also find that values of $A = 2\,\mathrm{eV} \ldots 3\,\mathrm{eV}$ give ferromagnetic solutions with $E_\mathrm{cond} = 40\,\mathrm{meV}$ and $W_{3d} \approx 3\,\mathrm{eV}$. The results of [259], where the $4sp$ bands have also been included, are at variance with our findings.

In the Gutzwiller calculation, the energy of the state $X_{2\downarrow}$ is pinned slightly below the Fermi energy, in agreement with experiment. This is an essential improvement over LSDA calculations, which predict a second hole pocket at the X point. Even a drastic change in the Racah parameter A to values $8\,\mathrm{eV} \leq A \leq 12\,\mathrm{eV}$ does not change much the basic features of the Gutzwiller quasi-particle band structure. The pinning of $X_{2\downarrow}$ is caused by the small variational parameter $\Delta(e_g)$, which in turn leads to a large fraction of t_{2g} holes in the minority spin bands, produced by a relatively large $\Delta(t_{2g})$. Due to the large nearest-neighbour hopping between t_{2g} orbitals, it is energetically favourable to generate as many t_{2g} holes in the minority spin bands as possible.

As mentioned before, there is a significant discrepancy between the experimental and the

Sym.	Ch.	Experiment	Gutzwiller	LSDA
$\langle\Gamma_1\rangle$	S	8.90±0.30	8.86	8.96[−0.11]
$\langle\Gamma_{25'}\rangle$	T	1.30±0.06	1.44[0.46]	1.99[0.43]
$\langle\Gamma_{12}\rangle$	E	0.48±0.08	0.65[0.195]	0.86[0.41]
$\langle X_1\rangle$	sE	3.30±0.20	3.31[0.36]	4.37[0.20]
$\langle X_3\rangle$	T	2.63±0.10	2.86[0.54]	3.82[0.37]
$X_{2\uparrow}$	E	0.21±0.03	0.165	0.35
$X_{2\downarrow}$	E	0.04±0.03	0.01	−0.09
$X_{5\uparrow}$	T	0.15±0.03	0.10	0.23
$\Delta_{e_g}(X_2)$	E	0.17±0.05	0.155	0.44
$\Delta_{t_{2g}}(X_5)$	T	0.33±0.04	0.38	0.56
$\langle K_2\rangle$	spTe	2.48±0.06	2.59[0.50]	3.37[0.32]
$\langle K_4\rangle$	pE	0.47±0.03	0.51[0.185]	0.70[0.41]
$\langle L_1\rangle$	sT	3.66±0.10	3.51[0.515]	4.56[0.23]
$\langle L_3\rangle$	tE	1.43±0.07	1.51[0.34]	2.02[0.40]
$L_{3\uparrow}$	Te	0.18±0.03	0.215[0.30]	0.38[0.50]
$\langle L_{2'}\rangle$	P	1.00±0.20	0.97[0.0]	0.24[−0.12]
$\langle W_1\rangle$	sE	0.65±0.10	0.69[0.30]	0.94[0.39]
$W_{1'\uparrow}$	T	0.15±0.10	0.11[0.52]	0.23[0.56]
$\langle\Lambda_{3;1/3}\rangle$	ptE	0.57[0.16±0.02]	0.67[0.32]	0.90[0.42]
$\langle\Lambda_{3;1/2}\rangle$	ptE	0.50[0.21±0.02]	0.55[0.37]	0.76[0.44]
$\langle\Lambda_{3;2/3}\rangle$	pTE	0.35[0.25±0.02]	0.33[0.41]	0.49[0.48]

Table 10.2: Binding energies in eV with respect to the Fermi energy E_F. $\langle\ldots\rangle$ indicates the spin average, error bars in the experiments without spin resolution are given as ±. Theoretical data show the spin average and the exchange splittings in square brackets. The second column denote the dominant orbital character of the states. The spin-polarised data $\langle\Lambda_{3;f}\rangle$ were taken at fractions f of the ΓL distance, with the emphasis on the analysis of the exchange splittings. For all calculations, a spin moment of $\mu = 0.55\mu_\mathrm{B}$ was used. The Gutzwiller calculations were carried out for $A = 9\,\mathrm{eV}$, $n_d = 8.78$.

LSDA value for the energy of the $4p$-type $L_{2'}$ state. Its theoretical value $E_\mathrm{LSDA}(L_{2'}) = -0.24\,\mathrm{eV}$, is much higher than in experiment, $E(L_{2'}) = -1.0\,\mathrm{eV}$, see table 10.2, column LSDA. The position of the $L_{2'}$ state in the Gutzwiller theory differs from LSDA only if we allow for a charge flow from $4p$ to 3d orbitals. For this, we have to include the interaction between the 3d and the $4sp$ orbitals. At least on a mean-field level, which should be sufficient, the inclusion of such additional interaction terms poses no serious problem. However, it brings up additional correlation parameters, which eventually would have to be chosen such that the theoretical and the experimental position of the $L_{2'}$ state agree. Physically such a fitting procedure therefore leads to the same result as if we shift the bare $L_{2'}$-energy by hand. This is what we did in our Gutzwiller calculations.

A lowering of the bare $4p$ level ε_p by 0.75 eV considerably improves the agreement with experiment, especially for all states near the Fermi energy and thus also for the values of the exchange splittings. The ARPES data reveal $\Delta_{e_g}(X_2) = 170 \pm 50\,\mathrm{meV}$ for the pure $d(e_g)$ state X_2, and $\Delta_{e_g}(X_5) = 330 \pm 40\,\mathrm{meV}$ [236] for the pure $d(t_{2g})$ state X_5, which agrees well with the Gutzwiller data. Lowering the $4p$ level leads to a charge flow of about 0.1 electrons from $3d$ to $4p$. The extra 0.1 d-hole charge fully contributes to the magnetic moment, and the exchange splittings are reduced accordingly. This would also be true for any LSDA calculation when the $4p/3d$ charge ratio was improved. Note that the Gutzwiller exchange splittings increase as a function of the binding energy by about 50%, as can be seen, e.g., from the values of the pure t_{2g} states X_5, $\Gamma_{25'}$, and X_3. In contrast, they decrease in the LSDA because of the bigger orbital basis used there.

Our method allows us to analyse how the individual multiplets contribute to the $3d$ charge and to the magnetic moment. Only the $3d8$, $3d9$ and $3d10$ configurations are important, which is sufficient to permit the itinerancy of the $3d$ electrons ($q_\sigma \approx 0.7$). Approximately 60% of the moment arises from the four inequivalent $d9$ multiplets, which, in the hole picture, are single-

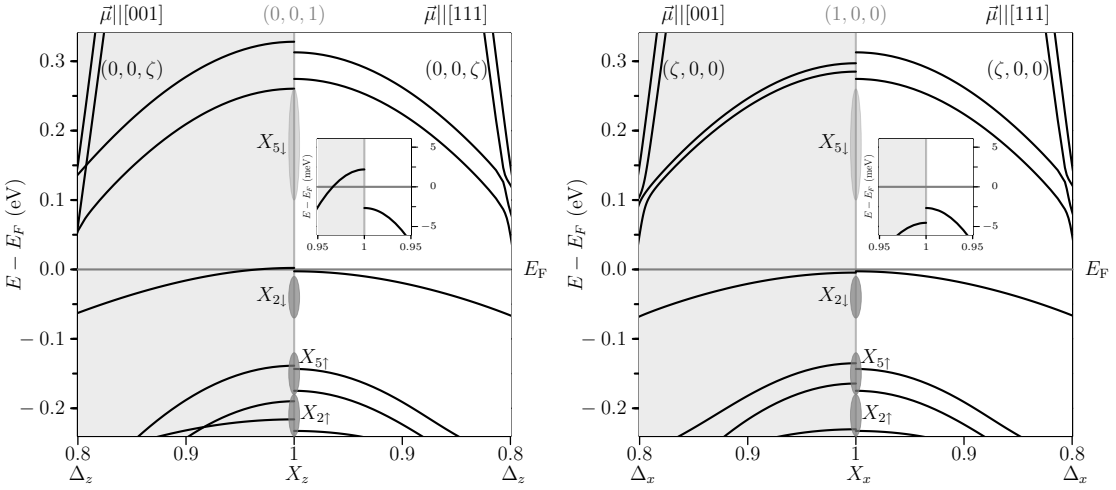

Figure 10.2: Quasi-particle band structure along the Δ-line around the X_z-point (left figure) and the X_x-point (right figure) of the Brillouin zone for magnetic-moment directions $\vec{\mu} \parallel [001]$ and $\vec{\mu} \parallel [001]$. The inset shows an enlarged view of the band structure around the Fermi energy, which displays the additional hole ellipsoid for $\vec{\mu} \parallel [001]$ more clearly. Note that the $X_{2\downarrow}$-band is below the Fermi energy for both magnetic-moment directions.

particle states. The eight $S_z = \pm 1$ components of the $d8$ triplets contribute approximately 40% – the occupation of the low-lying triplet states is increased as compared to the competing singlet states, in accordance with Hund's first rule. The enhanced triplet occupancies are already present in the paramagnetic case, and lead to local spin-expectation values $\langle \vec{S}_i^{\,2} \rangle$, which are significantly larger than in the independent-particle limit. We interpret these as preformed local moments.

10.1.4 Magnetic anisotropy and Gersdorf effect

The numerical minimisation is much more time consuming for a system with spin-orbit coupling than without. First, spin-orbit coupling requires the momentum-space integration to be extended from 1/48th to the full Brillouin zone. Furthermore, the small values of the 'Magnetic Anisotropy Energy' (MAE) necessitate a much finer mesh for the momentum-space integration. Second, the energy needs to be minimised with respect to nine external variational parameters in $\hat{\tilde{H}}_0^{\mathrm{eff}}$. Altogether, the minimisation of the total energy is approximately 10^4 times more time consuming for a system with spin-orbit coupling than in the absence of $\hat{H}_{\mathrm{SO}}$.

We carried out the minimisation of the variational energy with respect to the 'inner' parameters $\lambda_{\Gamma,\Gamma'}$ and the 'outer' parameters for both magnetic moment directions $\vec{\mu}||[111]$ and $\vec{\mu}||[001]$. The optimum value of the effective spin-orbit coupling is $\zeta_{\mathrm{eff}} \approx 68\,\mathrm{meV}$ in both cases, about 15% smaller than the bare value $\zeta = 80\,\mathrm{meV}$. There seems to be no simple rule that determines the relative size of ζ and ζ_{eff}. For example, for iron we found an effective spin-orbit coupling considerably larger than the corresponding bare value.

In figure 10.2, we show the quasi-particle band structure that arises from our calculation around the X-points $X_z \equiv (001)$ and $X_x \equiv (100)$. When the magnetic moment is along the easy axis, the band structure around both X-points coincides and the minority state $X_{2\downarrow}$ is below the Fermi energy. Note that in the presence of spin-orbit coupling the spin label in $X_{2\downarrow}$ is not well defined but merely refers to the main spin-component of this state. For a magnetic

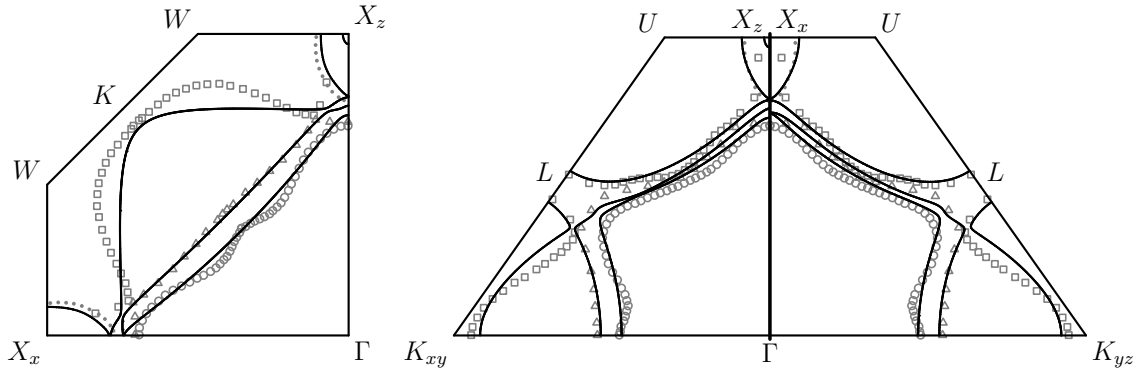

Figure 10.3: Fermi-surface cuts with various planes in the Brillouin zone. Lines: Gutzwiller theory including spin-orbit coupling; Squares and triangles: experimental data reported in Ref. [260]; Dots: experimental data of Tsui [234].

moment along the [001]-direction, however, the two states $X_{2\downarrow}$ have different energies. The $X_{2\downarrow}$ state at X_x remains below the Fermi level, whereas the corresponding state at X_z creates a new hole pocket around this X-point. This is the scenario proposed by Gersdorf [243].

In our calculations for nickel, the MAE is $E_{\mathrm{MAE}} \approx 3.5\,\mu\mathrm{eV/atom}$, quite close to the experimental value $E_{\mathrm{exp}} \approx 3.0\,\mu\mathrm{eV/atom}$. Note that the MAE has to be calculated quite carefully within the Gutzwiller approach. In particular, one has to keep in mind that any approximation on the parameters $\lambda_{\Gamma,\Gamma'}$ that reduces the variational flexibility may lead to a grossly overestimated MAE. This is a serious problem, in particular, in the case of iron [100]. For nickel, however, a mixing of states $|\Gamma\rangle, |\Gamma'\rangle$ has little effect on the variational energy, and even a diagonal variational parameter matrix $\lambda_{\Gamma,\Gamma'} \sim \delta_{\Gamma,\Gamma'}$ would lead to reasonable results, i.e., $E_{\mathrm{MAE}} \approx 10\,\mu\mathrm{eV}$ per atom. The absolute value of the MAE mildly depends on the parameters for the spin-orbit coupling ζ and the Racah-C, e.g., an increase of ζ by 50% doubles the MAE. However, the sign of the MAE is a robust result of our calculation.

In figure 10.3, we show Fermi-surface cuts that we find within our Gutzwiller theory. The experimental values are taken from dHvA experiments by Tsui [234] and by Stark as reported in references [260]. The agreement is quite satisfactory along high-symmetry lines, whereas there are significant discrepancies away from them. We do believe that the wiggles, which appear in the experimental data, are, in fact, spurious and we propose to redo these measurements. Instead of constructing the Fermi surface from those raw data, as it was done in Ref. [260], we suggest a direct comparison of the experimental dHvA-signal with our corresponding theoretical data.

10.1.5 Kinks in the Quasi-Particle Dispersion

The accuracy of our theoretical results allows to determine subtle deviations of the measured quasi-particle band energies from the expected Fermi-liquid behaviour [261]. As shown in figure 10.3, a band crosses the Fermi energy on the high-symmetry line that connects the K and the Γ point in the Brillouin zone. The energies of this band, as calculated in the Gutzwiller theory and measured in ARPES experiments, are displayed in figure 10.4(left). There is a clear deviation between theory and experiment with pronounced kinks in the energy regions $\omega \approx 30\,\mathrm{meV}$ and $\omega \approx 250\,\mathrm{meV}$, see figure 10.4(right), where the difference between the theoretical and the experimental energies is displayed as circles. Note that a very similar kink behaviour has been observed for the quasi-particle bands of iron [262].

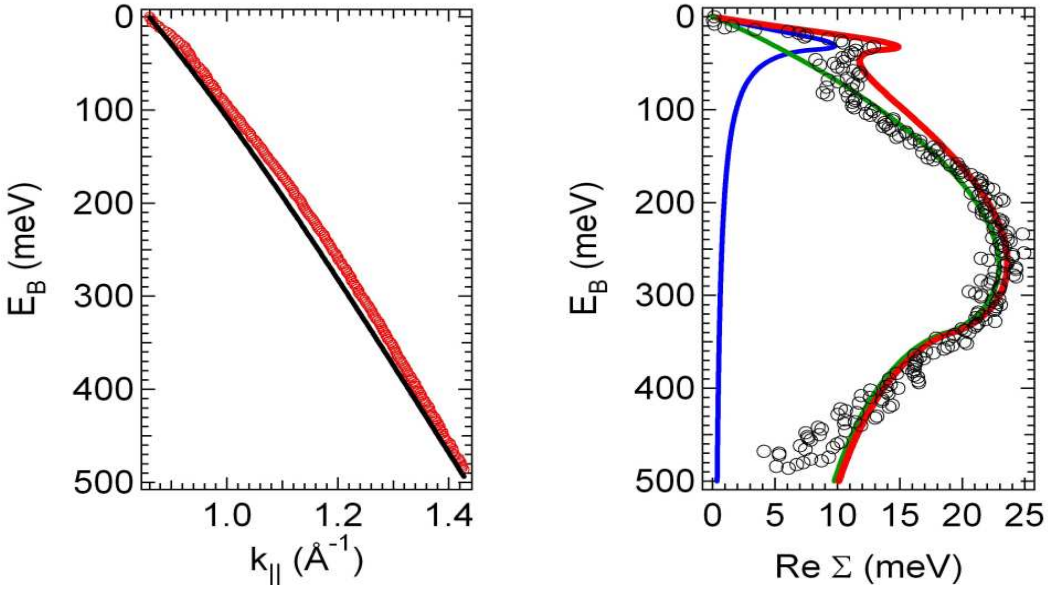

Figure 10.4: Left: ARPES band data (thick line) and Gutzwiller dispersion (thin line) on the high-symmetry line connecting the K and the Γ point. Right: Difference between the energies in the left figure (circles); real parts of $\Sigma_{\mathrm{ph}}(\omega)$ and Σ_{mag} and the sum of both (from left to right in the energy region $\omega < 200\,\mathrm{meV}$) calculated with the Ansatz (10.9).

From a theoretical point of view, the kinks in the quasi-particle dispersion must be due to a self-energy term $\tilde{\Sigma}(\omega)$ in addition to the one covered by our Fermi-liquid description, see equation (7.11). Note that, for our phenomenological considerations in this section, we neglect the momentum-vector dependence and the matrix structure of the self-energy in multi-band systems. The results in figure 10.4(right) indicate that the real part of $\tilde{\Sigma}(\omega)$ is only a small perturbation to the leading Fermi-liquid term $\sim \Sigma^{\mathrm{R}}\omega$ since, otherwise, it would change the quasi-particle dispersion more drastically. Therefore, the difference between the theoretical and the experimental energies, as displayed in figure 10.4(right), gives the real part of the 'renormalised' self-energy $\Sigma(\omega) = z\tilde{\Sigma}(\omega)$. Here, $z = (1 - \Sigma^{\mathrm{R}})^{-1} \approx 0.7$ is the quasi-particle renormalisation. Since $\Sigma(\omega)$ and $\tilde{\Sigma}(\omega)$ differ only by a constant factor, we can address the 'renormalised' self-energy $\Sigma(\omega)$ instead of $\tilde{\Sigma}(\omega)$ in the following considerations.

The ARPES experiment also allows the imaginary part of the self-energy to be determined from the width of the momentum distribution curves (MDC). Through this procedure one finds values of $\mathrm{Im}\Sigma(\omega)$, which are displayed as circles in figure 10.5. Here, an asymmetric Lorentz function has been used for the fitting of the MDC peaks.

The feature in the self-energy around 30 meV is well known in metals and generally believed to be due to electron-phonon coupling [263]. A possible explanation of the second structure around 250 meV could be the coupling of electrons to magnons. The energy scale of magnons in nickel is known from inelastic neutron scattering, which yields values of up to 250 meV [215]. Such an interpretation is in line with quite a number of theoretical works, e.g., on cuprates, in which the emergence of kinks has also been attributed to the coupling of quasi-particles and bosonic (antiferromagnetic) spin excitations, see, e.g., references [264–266].

One can investigate the scenario of a coupling between quasi-particles and bosonic degrees of freedom more quantitatively by means of the phenomenological Ansatz

$$\mathrm{Im}\Sigma_{\mathrm{ph/mag}}(\omega) = \lambda_{\mathrm{ph/mag}} \int_0^{\omega} \rho_{\mathrm{ph/mag}}(\omega')\Theta(\bar{\omega}_{\mathrm{ph/mag}} - \omega')\mathrm{d}\omega' \tag{10.9}$$

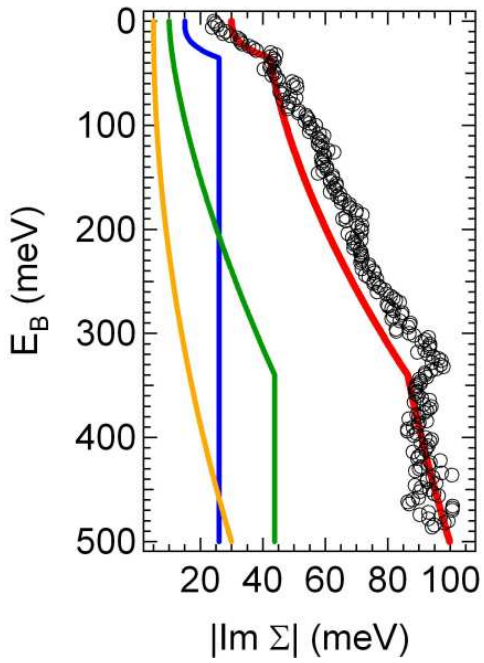

Figure 10.5: Circles: The imaginary part of the renormalised self-energy extracted from the width of the momentum distribution curves. Lines: The imaginary part of the renormalised self-energies calculated with the Ansatz (10.9); The lines show (in the energy region $\omega < 200\,\mathrm{meV}$ from left to right): i) $\Sigma^{\mathrm{I}}\omega^2$, ii) $\mathrm{Im}\Sigma_{\mathrm{mag}}(\omega)$, iii) $\mathrm{Im}\Sigma_{\mathrm{ph}}(\omega)$, and iv) the sum of the first three terms.

for the phonon ($\Sigma_{\mathrm{ph}}(\omega)$) and the magnon ($\Sigma_{\mathrm{mag}}(\omega)$) contribution to the self-energy. Here, $\rho_{\mathrm{ph}} \sim \omega^2$ and $\rho_{\mathrm{mag}} \sim \sqrt{\omega}$ are the densities of states for bosons and magnons. The cut-offs $\bar{\omega}_{\mathrm{ph/mag}}$ and the coupling parameters $\lambda_{\mathrm{ph/mag}}$ are fitted in order to reproduce the imaginary part of the self-energy extracted from the experiment. Note that the real part can be calculated from (10.9) by means of a Kramers-Kronig transformation. In both figures 10.4(right) and 10.5, the results of this fit procedure are displayed as lines. Obviously, both the real and the imaginary part of the self-energy are very well reproduced by the simple Ansatz (10.9). The fit parameters that were used in figures 10.4(right) and 10.5m are $\bar{\omega}_{\mathrm{mag}} = 340\,\mathrm{meV}$, $\bar{\omega}_{\mathrm{ph}} = 35\,\mathrm{meV}$, $\lambda_{\mathrm{ph}} = 0.3$, and $\lambda_{\mathrm{ph}} = 0.15$. Note that, in the imaginary part, one also has to include the normal term $\Sigma^{\mathrm{I}}\omega^2$ from Fermi-liquid theory where Σ^{I} serves as an additional fit parameter.

Although our phenomenological Ansatz supports the idea that the kinks observed in nickel result from a coupling of quasi-particles to bosonic degrees of freedom, such an approach falls short of a genuine microscopic theory. At the moment, however, there is not even a reliable theory that correctly describes the magnon excitations in nickel. Therefore, it is unlikely that a microscopic theory will be developed in the foreseeable future, which yields a indisputable explanation of the kinks observed in nickel. As an alternative scenario, it was shown in reference [267] that kinks can also appear in many-particle systems solely due to the frequency dependence of the local self-energy within the Dynamical-Mean-Field-Theory. It is difficult to assess, however, whether or not the findings in [267] are relevant for the physical properties of nickel.

In summary, we have resolved the long-standing problem to explain theoretically the electronic and magnetic properties of elementary fcc nickel. Our results for the quasi-particle bands are in very good agreement with ARPES experiments and we find the experimental Fermi-surface topology. The accuracy of our results allows the detection of additional terms in the self-energy, which lead to kinks in the quasi-particle dispersion. Furthermore, we explain the subtle effects that the spin-orbit coupling has in nickel. Our theory yields the correct magnetic anisotropy energy and we confirm the Gersdorf scenario: The Fermi-surface topology changes around the X-point (001) when the magnetic moment direction is rotated from $\vec{\mu}||[111]$ to $\vec{\mu}||[001]$ by an external magnetic field.

10.2 Fermi Surface of Na_xCoO_2

The intercalated layer compound Na_xCoO_2 has been studied intensively in recent years since, as a function of sodium doping x, it exhibits a few remarkable properties, see below. LDA calculations indicate that the bands of this system around the Fermi level predominantly belong to the Cobalt t_{2g} orbitals. The e_g bands are found approx. 1.5 eV above the Fermi energy and may therefore be neglected in Hubbard-model studies. Due to the layered structure, the three t_{2g} orbitals split into an a_g and the doubly degenerate $e_{g'}$ orbitals. The Na doping x leads to a band filling of d^{5+x} for the six partially filled t_{2g} spin-orbital states.

For $x \approx 0.60 - 0.75$, one finds an unusually large thermopower [268] in Na_xCoO_2. Around the doping $x \approx 0.3$, a transition to a superconducting state is observed below a temperature $T_S \approx 4.5\,K$ [269, 270]. The systems exhibits an unusual metal-insulator transition for $x = 0.5$, which is suspected to be caused by a charge-density wave [271, 272]. The magnetic susceptibility differs qualitatively for dopings $x > 0.5$ and $x < 0.5$: for $x < 0.5$ one finds a paramagnetic metal [271] while for $x > 0.5$ the susceptibility shows a Curie-Weiss behaviour [273, 274].

The results of ARPES experiments on Na_xCoO_2 cannot be properly explained by means of LDA-calculations. As usual in transition-metal compounds, there is a significant renormalisation, $z_{exp} \approx 0.6$, of the d-bands compared to the LDA band structure. In addition, the LDA fails to explain the observed Fermi-surface topology for a Na doping of $x \approx 0.3$. In LDA calculations, the Fermi surface consists of a large hole pocket around the Γ-point and six small pockets near the K-point [275]. The pockets near the K-point, however, have not been observed experimentally [276, 277].

The significant band-width renormalisation indicates that the local Coulomb interaction of electrons in the Cobalt t_{2g} orbitals has to be treated by more reliable many-particle theories than LDA in order to understand the electronic properties of Na_xCoO_2. We give a brief review of previous many-particle studies on Na_xCoO_2 in section 10.2.1. The results for the Fermi-surface topology in those earlier works, however, have not been conclusive. As we will show in section 10.2.3, where we present our own findings, the Fermi-surface topology quite sensitively depends on the choice of the model parameters that are used in a correlated electron approach. This may partly explain the problems to obtain a consistent theoretical picture of the quasi-particle energies and the Fermi-surface topology in Na_xCoO_2.

10.2.1 Tight-Binding Hamiltonian

Tight-binding fits to the LDA band structure of Na_xCoO_2 have been proposed by several groups for their respective many-particle investigations [278–286]. Although the resulting tight-binding band structures are overall quite similar they deviate with respect to some seemingly irrelevant properties. As will be shown below, those subtle differences can lead to qualitatively different results if many-particle correlation effects are properly taken into account.

In figure 10.6, we show two different tight-binding band structures along high-symmetry lines, which have been investigated in references [278, 279, 283–285]. We denote the corresponding single-particle Hamiltonians as $\hat{H}_{0;I}$ [285] and $\hat{H}_{0;Z}$ [279]. The Fermi energy $E_F = 0$ in figure 10.6 corresponds to a Na doping of $x \approx 0.3$, i.e., the total band filling is 5.3.

The main differences between the two band structures in figure 10.6 are found on the line connecting the M and the K point at energies $\omega \approx -1.2\,eV$. Near the Fermi energy both band structures look very similar. Note that the band that crosses the Fermi energy twice between the K and the Γ-point is responsible for the controversial hole pockets, which are not observed in experiments.

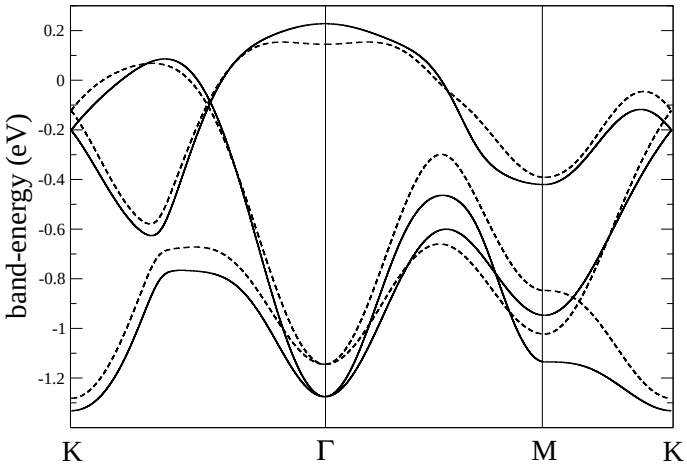

Figure 10.6: Band structures along high-symmetry lines for the tight-binding Hamiltonians $\hat{H}_{0;\mathrm{I}}$ [285] (solid line) and $\hat{H}_{0;\mathrm{Z}}$ [279] (dashed line).

It turns out that the splitting $\Delta = \varepsilon_{a_\mathrm{g}} - \varepsilon_{e'_\mathrm{g}}$ between a_g and $e_{\mathrm{g}'}$ orbitals is a decisive quantity, which very much determines the physics of the system in many-particle theories. Its value is still a controversial issue. In the Hamiltonians $\hat{H}_{0;\mathrm{I}}$ and $\hat{H}_{0;\mathrm{Z}}$, it is $\Delta = -132\,\mathrm{meV}$ and $\Delta = -10\,\mathrm{meV}$, respectively. A positive value of $\Delta = 350\,\mathrm{meV}$ has been found in quantum-chemical calculations [281, 286]. This value, however, seems to be in disagreement with all LDA results. In reference [287], it is shown that Δ, to a certain extend, depends on the Na doping of x. In the interesting region $x \approx 0.3$, a value of $\Delta \approx -100\,\mathrm{meV}$ is reported in that work, which is close to the one used in the tight-binding Hamiltonian $\hat{H}_{0;\mathrm{I}}$.

10.2.2 Previous Results of Many-Particle Theory Approaches

The local Hamiltonian $\hat{H}_\mathrm{I}^{3\mathrm{b}}$ in the three-band Hubbard model, which describes the $t_{2\mathrm{g}}$ orbitals, can be derived from equation (C.3) by keeping just the $t_{2\mathrm{g}}$ terms,

$$\begin{aligned}\hat{H}_\mathrm{I}^{3\mathrm{b}} &= U\sum_t \hat{n}_{t,\uparrow}\hat{n}_{t,\downarrow} + \frac{U'}{2}\sum_{t(\neq)t';s,s'} \hat{n}_{t,s}\hat{n}_{t',s'} - \frac{J}{2}\sum_{t(\neq)t';s} \hat{n}_{t,s}\hat{n}_{t',s} \\ &\quad + \frac{J}{2}\sum_{t(\neq)t';s} \hat{c}^\dagger_{t,s}\hat{c}^\dagger_{t',\bar{s}}\hat{c}_{t,\bar{s}}\hat{c}_{t',s} + \frac{J}{2}\sum_{t(\neq)t'} \left(\hat{c}^\dagger_{t,\uparrow}\hat{c}^\dagger_{t,\downarrow}\hat{c}_{t',\downarrow}\hat{c}_{t',\uparrow} + \hat{c}^\dagger_{t',\uparrow}\hat{c}^\dagger_{t',\downarrow}\hat{c}_{t,\downarrow}\hat{c}_{t,\uparrow}\right) .\end{aligned} \tag{10.10}$$

In the following, we assume that the spherical symmetry holds for the Coulomb parameters U, U', and J, i.e., we have

$$U = A + 4B + 3C\,, \tag{10.11a}$$
$$U' = A - 2B + C\,, \tag{10.11b}$$
$$J = 3B + C\,. \tag{10.11c}$$

In this case, the parameters obey the same relation, $U - U' = 2J$, as the e_g orbitals and only two of the three parameters are independent.

For the tight-binding Hamiltonian $\hat{H}_{0;\mathrm{Z}}$, a Gutzwiller theory calculation has been carried out for $J = 0$, $U = \infty$ [279]. The resulting band structures and the Fermi surfaces are shown for three different band fillings in figure 10.7. The most interesting feature in that figure is the vanishing of the hole pockets near the K-point for the doping $x = 0.3$, in agreement with the experimental data. Assuming an infinite Hubbard-U parameter, however, is certainly not realistic for $\mathrm{Na}_x\mathrm{CoO}_2$. In fact, the renormalisation of the bands in figure 10.7 is significantly larger, $z \approx 0.3$, than the one found in ARPES experiments, $z_\mathrm{exp} \approx 0.6$.

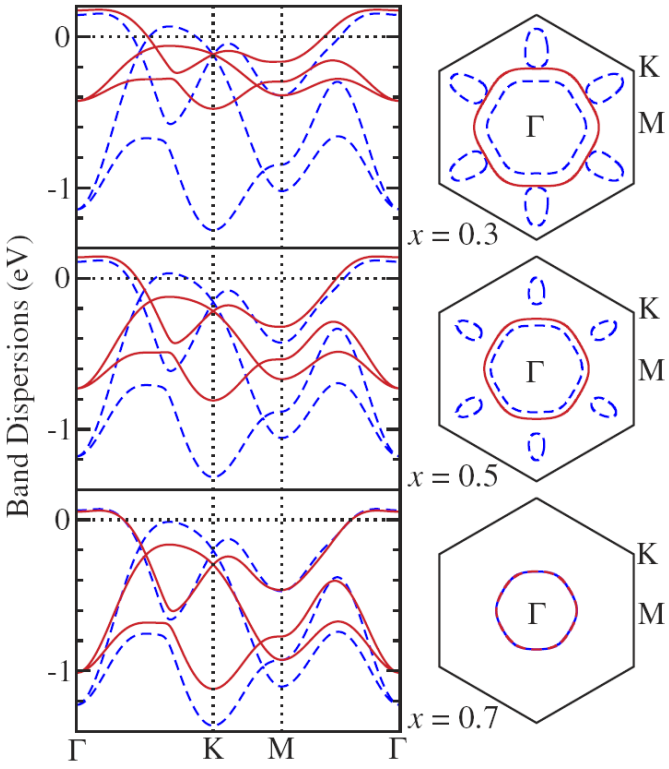

Figure 10.7: Left: Band dipersions for $\hat{H}_{0;\mathrm{Z}}$ and Na doping x=0.3, x=0.5, x=0.7; bare bands (solid lines), Gutzwiller theory with $J = 0$, $U = \infty$ (dashed lines). Right: Corresponding Fermi surfaces. All figures are taken from reference [279].

For the Hamiltonian $\hat{H}_{0;\mathrm{I}}$, DMFT calculations lead to very different results. Both, in a 'Quantum-Monte-Carlo' (QMC) [278] and an 'exact diagonalisation' (ED) treatment [283] of the DMFT equations, the disputed hole pockets were found to be even slightly enlarged compared to the underlying LDA calculation. In contrast, for the Hamiltonian $\hat{H}_{0;\mathrm{Z}}$, a QMC-DMFT study [284] confirms the findings in reference [279] qualitatively: the hole pockets vanish for values of $U > 6\,\mathrm{eV}$ in that DMFT approach. The authors of reference [284] further found that increasing the Δ-parameter from $\Delta = -10\,\mathrm{eV}$ in $\hat{H}_{0;\mathrm{Z}}$ to positive values of approx. 40-90 eV significantly decreases the critical interaction strength of U for which the hole pockets disappear. These findings have been qualitatively reproduced in an ED-DMFT study [285].

The previous DMFT results indicate that the properties of the three-band models that are used for the investigation of $\mathrm{Na}_x\mathrm{CoO}_2$ depend sensitively on the input parameters. Such DMFT calculations for a three-band model are numerically quite demanding. In contrast, studies with the Gutzwiller theory are simple and allow to study such systems for a large number of correlation parameters and with a high precision. Therefore, we present our own Gutzwiller results for the Fermi surface topology of both Hamiltonians $\hat{H}_{0;\mathrm{Z}}$ and $\hat{H}_{0;\mathrm{I}}$ in the following chapter. A more detailed investigation of quasi-particle dispersions, orbital densities, and spin-orbit coupling effects will be published elsewhere [288].

Note that results of a self-consistent Gutzwiller+LDA calculation for $\mathrm{Na}_x\mathrm{CoO}_2$ have been presented in reference [289]. In that work, however, the authors did not study a fixed and well defined multi-band Hubbard Hamiltonian and it is therefore difficult to compare our, or the DMFT findings, to their results.

10.2.3 Gutzwiller-Theory Results

The eigenstates $|\Gamma\rangle$ of the $t_{2\mathrm{g}}$ Hamiltonian (10.10) all belong to different representations of the cubic symmetry group [92]. Therefore, it is justified to work with a diagonal variational-parameter matrix $\lambda_{\Gamma,\Gamma'} \sim \delta_{\Gamma,\Gamma'}$ in the Gutzwiller correlation operator (4.25b).

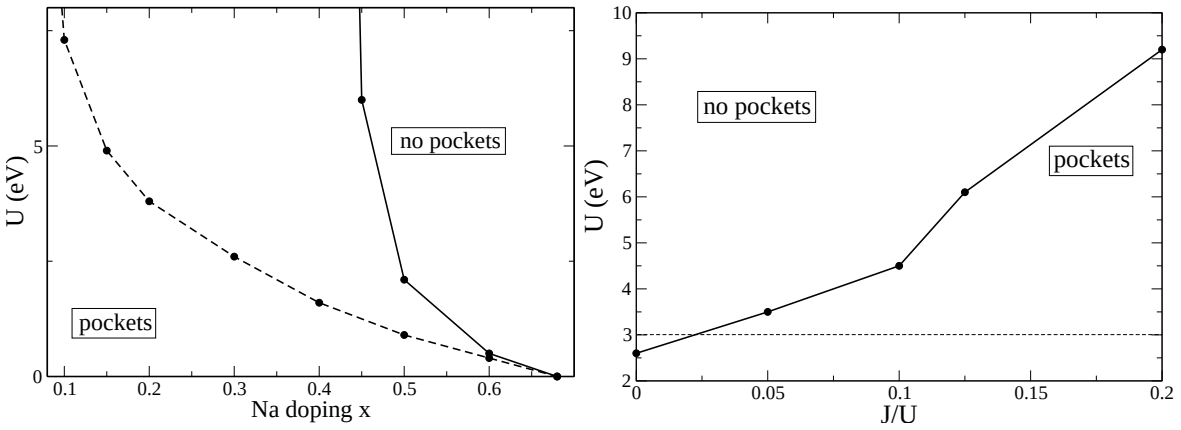

Figure 10.8: Left: Phases with and without hole pockets for $J = 0$ as a function of U and x and tight-binding Hamiltonians $\hat{H}_{0;\mathrm{I}}$ (solid line) and $\hat{H}_{0;\mathrm{Z}}$ (dashed line). Right: Phasediagram for $\hat{H}_{0;\mathrm{Z}}$, $x = 0.3$ as a function of U and J.

The only free parameter $\eta_{\sigma,\sigma}$ in the single-particle Hamiltonian (5.96) describes the effective splitting Δ^{eff} of a_{g} and $e_{\mathrm{g}'}$ orbitals. This parameter has a leading influence on the quasi-particle band structure and the Fermi-surface topology and has to be determined by a minimisation of the variational ground-state energy.

For the tight-binding Hamiltonian $\hat{H}_{0;\mathrm{I}}$, our calculations confirm the findings in [278, 283]: the LDA hole pockets near the K-points do not disappear for finite values of the correlation parameters U and J and a Na doping of $x = 0.3$. This can be seen, e.g., in figure 10.8(left), which shows the phases with and without hole pockets for $J = 0$ as a function of U and x. The hole pockets vanish for the Hamiltonian $\hat{H}_{0;\mathrm{I}}$ (solid line) only for a doping of $x > 0.44$. The second curve (dashed line) shows the same phase diagram for the tight-binding Hamiltonian $\hat{H}_{0;\mathrm{Z}}$. Here, the pockets vanish in a much larger region of doping values x and Coulomb-interactions U. There is a transition, in particular, for a doping of $x \approx 0.3$. For this doping, $x \approx 0.3$, figure 10.8(right) shows the phase diagram as a function of U and J. As can be seen from this figure, a finite value of J shifts the transition to significantly larger values of U.

Unfortunately, phase diagrams, as those shown in figures 10.8, are presently not available from DMFT calculations. We can only compare the critical interaction strengths U_{C} for the Hamiltonian $\hat{H}_{0;\mathrm{Z}}$ and $x = 0.3$. In our approach, this value is $U_{\mathrm{C}} \approx 2.6\,\mathrm{eV}$, while it is reported as $U_{\mathrm{C}} \approx 6\,\mathrm{eV}$ in reference [284]. The reason for this discrepancy is presently unclear.

One should keep in mind that both approaches, the DMFT and the Gutzwiller theory, are derived in the limit of infinite spatial dimensions. It is therefore questionable whether they are able to capture correctly the physics of an effectively two-dimensional system. This is in doubt, in particular, when the physical properties of the models that are used to describe that two-dimensional system depends sensitively on the input parameters.

Chapter 11

Conclusions

In this work, we have given a thorough introduction to the Gutzwiller variational theory and all methods that are closely related to it. We summarise our main results in the first part of this final chapter, and close this work with a brief outlook, which discusses some of the problems that we intend to address in the near future.

11.1 Summary

Gutzwiller wave functions provide an approximate description of many-particle ground states for realistic multi-band Hubbard models (chapter 4). An exact analytic evaluation of these wave functions succeeds in the limit of infinite spatial dimensions (chapter 5). We use the resulting variational energy functional to calculate approximately the ground-state properties of correlated electron systems in finite dimensions ('Gutzwiller theory'). On top of the Gutzwiller description of the ground state, we describe the elementary single-particle excitations as Landau-Gutzwiller quasi-particles within a Fermi-liquid theory (chapter 7). Such calculations yield quasi-particle dispersions, that can be compared to photoemission (ARPES) experiments. The time-dependent Gutzwiller theory (chapter 8) allows us to calculate two-particle Green's functions, e.g., the magnetic susceptibility, which is measured in magnetic neutron scattering experiments.

Due to a proper treatment of the local Coulomb interaction in the Gutzwiller theory, this approach is evidently superior to effective single-particle approaches. This has been demonstrated in various parts of this work, e.g., in our studies on two-band models (chapter 9). For the investigation of realistic correlated electron models, which describe, e.g., transition metals and their compounds, most of the established methods of many-particle theory cannot be successfully implemented. Therefore, the Gutzwiller theory is a significant improvement of our theoretical 'tool box' for such realistic models. This holds true for the calculation of ground-state properties, quasi-particle excitations, and two-particle response functions.

At present, it is impossible to assess the reliability of the Gutzwiller-theory results for three-dimensional systems in any rigorous way. Therefore, only a comparison to experiments will give us more insight into the merits and shortcomings of the Gutzwiller variational approach. Our results for the electronic and magnetic properties of nickel (chapter 10) are quite encouraging in this regard. We have been able to resolve all basic problems of the DFT calculations on nickel, in particular those that arise from the spin-orbit coupling.

Despite the considerable length of this work, some interesting aspects and developments in the context of the Gutzwiller variational theory could not be fully treated. For example, we have left out entirely a description of the numerical methods, which were used to evaluate Gutzwiller wave functions on finite lattices ('variational quantum Monte-Carlo'). We tried our

best, however, to give proper references to all relevant work not covered by this presentation.

11.2 Outlook

The numerical algorithm for the minimisation of the Gutzwiller energy functional, which we have used to investigate nickel, can be applied to quite a number of systems with partially filled $3d$-shells. In order to gain more insight into the reliability of our approach, we find it most important to start with a thorough investigation of other $3d$-transition metals. These systems are presently not in the focus of solid-state theory. However, they are much better studied experimentally than various transition-metal compounds that have received more attention in recent years.

A future project will be the investigation of lanthanides and actinides. Their partially filled f-shells require some further development of the minimisation algorithm in order to cope with the large number of local multiplets. However, we do not think that such improvements will be a major obstacle for the investigation of f-electron systems within the Gutzwiller theory.

Studies of the time-dependent Gutzwiller theory for multi-band models are already under way. As a first step, we presently are developing an algorithm that allows us to calculate the magnetic susceptibility of the ferromagnetic two-band model that has been introduced in section 9.1. In the long term, we aim to calculate two-particle response functions for realistic multi-band models that describe transition metals and their compounds.

The Gutzwiller theory, as we have presented it in this work, is based on the investigation of multi-band Hubbard models. These models are derived from an ab-initio calculation and they remain fixed during the minimisation of the Gutzwiller energy functional. Such an approach may fail if the correlated Gutzwiller ground state differs significantly from the corresponding ab-initio ground state. For example, in iron, the exchange splitting is approximately 1.5 eV and, therefore, the ferromagnetic and the paramagnetic ground states are very different. Hence, working with a static Hubbard model that is derived from a paramagnetic ab-initio calculation may be insufficient in such cases. As a way out of this dilemma, one can try to use a self-consistent Gutzwiller-DFT scheme as was introduced in references [290, 291]. Future studies will show how numerically demanding such self-consistent calculations are and whether or not they lead to significant changes in results.

It is well known that the Gutzwiller theory for the two-dimensional t-J model yields a superconducting ground state [27]. If applied to the two-dimensional Hubbard model, however, the Gutzwiller theory shows no superconductivity, even in the large-U limit. To resolve this seeming contradiction, one has to include non-local terms in the Gutzwiller correlation operator. The evaluation of expectation values requires a perturbative expansion of expectation values with respect to those additional terms. We are planning to perform such calculations in order to investigate the superconducting instabilities in a two-dimensional Hubbard model.

Appendix A

Wick's Theorem

In several sections of this work, we use a simplified version of Wick's theorem, which, in its general form, is an essential part of diagrammatic perturbation theory for many-particle systems; see, e.g., reference [183]. Here, we only need the time-independent version of this theorem, which states that, for a one-particle product state

$$|\Psi_0\rangle = \prod_{\gamma(\text{occ.})} \hat{h}^\dagger_\gamma |0\rangle \ , \tag{A.1}$$

the expectation value of a many-particle operator is given by the determinant

$$\left\langle \hat{c}^\dagger_{\sigma_1} \hat{c}^\dagger_{\sigma_2} \dots \hat{c}^\dagger_{\sigma_n} \hat{c}_{\sigma'_n} \dots \hat{c}_{\sigma'_2} \hat{c}_{\sigma'_1} \right\rangle_{\Psi_0} = |\Omega| \ , \tag{A.2}$$

with the matrix

$$\Omega = \begin{pmatrix} C^0_{\sigma_1,\sigma'_1} & C^0_{\sigma_1,\sigma'_2} & \dots & C^0_{\sigma_1,\sigma'_n} \\ C^0_{\sigma_2,\sigma'_1} & C^0_{\sigma_2,\sigma'_2} & \dots & C^0_{\sigma_2,\sigma'_n} \\ \dots & \dots & \dots & \dots \\ C^0_{\sigma_n,\sigma'_1} & C^0_{\sigma_n,\sigma'_2} & \dots & C^0_{\sigma_n,\sigma'_n} \end{pmatrix} . \tag{A.3}$$

Here, the matrix elements are

$$C^0_{\sigma,\sigma'} = \left\langle \hat{c}^\dagger_\sigma \hat{c}_{\sigma'} \right\rangle_{\Psi_0} = \sum_{\gamma(\text{occ.})} u^*_{\gamma,\sigma} u_{\gamma,\sigma'} \ , \tag{A.4}$$

where the unitary matrix $u_{\gamma,\sigma}$ connects the two one-particle basis sets $|\sigma\rangle$ and $|\gamma\rangle$ and the corresponding creation operators

$$\hat{h}^\dagger_\gamma = \sum_\sigma u_{\gamma,\sigma} \hat{c}^\dagger_\sigma \ , \tag{A.5a}$$

$$\hat{c}^\dagger_\sigma = \sum_\gamma u^*_{\gamma,\sigma} \hat{h}^\dagger_\gamma \ . \tag{A.5b}$$

For the proof of equation (A.2), we apply the transformation (A.5) to the left hand side of (A.2),

$$(A.2) = \sum_{\substack{\gamma_1,\dots,\gamma_n \\ \gamma'_1,\dots,\gamma'_n}} u^*_{\gamma_1\sigma_1} \dots u^*_{\gamma_n\sigma_n} u_{\gamma'_n\sigma'_n} \dots u_{\gamma'_1\sigma'_1} \left\langle \hat{h}^\dagger_{\gamma_1} \dots \hat{h}^\dagger_{\gamma_n} \hat{h}_{\gamma'_n} \dots \hat{h}_{\gamma'_1} \right\rangle_{\Psi_0} . \tag{A.6}$$

The expectation value in (A.6) is finite only if the sets $Y \equiv \{\gamma_1, \dots, \gamma_n\}$ and $Y' \equiv \{\gamma'_1, \dots, \gamma'_n\}$ coincide and all $\gamma_i \in Y$ belong to the occupied states in (A.1). Then, for each set Y there

are $n!$ contributions from the sum over Y', given by the $n!$ permutations $\mathrm{P}(\{1\dots n\})$ of the index set $\{1\dots n\}$. The expectation value in (A.1) is $\mathrm{sign}(P) = \pm 1$ depending whether the permutation $\mathrm{P}(\{1\dots n\})$ is odd or even. Hence, we find

$$(A.2) = \sum_{\gamma_1,\dots,\gamma_n(\mathrm{occ.})} \sum_{\mathrm{P}(\{1\dots n\})} \mathrm{sign}(P) u^*_{\gamma_1\sigma_1} u_{\gamma_1\sigma_{\mathrm{P}(1)}} \dots u^*_{\gamma_n\sigma_n} u_{\gamma_n\sigma_{\mathrm{P}(n)}} \tag{A.7a}$$

$$= \sum_{\mathrm{P}(\{1\dots n\})} \mathrm{sign}(P) C^0_{\sigma_1,\sigma_{\mathrm{P}(1)}} \dots C^0_{\sigma_N,\sigma_{\mathrm{P}(n)}} \, . \tag{A.7b}$$

which is just the Leibniz representation of the determinant (A.1).

A similar, but somewhat more general expectation value is

$$m^0_{I,I'} \equiv \left\langle \left(|I\rangle\langle I'| \right) \right\rangle_{\Psi_0} , \tag{A.8}$$

with the configuration transition operator

$$|I\rangle\langle I'| = \prod_{\sigma\in I} \hat{c}^\dagger_\sigma \prod_{\sigma'\in I'} \hat{c}_{\sigma'} \prod_{\sigma''\in J} (1 - \hat{n}_{\sigma''}) \, . \tag{A.9}$$

and $J \equiv (1\dots N)\backslash(I\cup I')$. The evaluation of $m^0_{I,I'}$ goes along the same lines as for (A.2). One finds

$$m^0_{I,I'} = \begin{vmatrix} \Omega^{I,I'} & -\Omega^{I,J} \\ \Omega^{J,I'} & \bar{\Omega}^{J,J} \end{vmatrix} \tag{A.10}$$

with the matrices $\Omega_{I,I'} = \Omega$ as already defined in (A.3) if we take $(\sigma_1,\dots,\sigma_N) = I$ and $(\sigma'_1,\dots,\sigma'_N) = I'$. The matrices $\Omega_{I,J}$ and $\Omega_{J,I'}$ are defined accordingly. Finally, the matrix $\bar{\Omega}^{J,J}$ in (A.10) is given as

$$\bar{\Omega}_{J,J} \equiv \begin{pmatrix} 1 - C^0_{\sigma_1,\sigma_1} & -C^0_{\sigma_1,\sigma_2} & \dots & -C^0_{\sigma_1,\sigma_{|J|}} \\ -C^0_{\sigma_2,\sigma_1} & 1 - C^0_{\sigma_2,\sigma_2} & \dots & -C^0_{\sigma_2,\sigma_{|J|}} \\ \dots & \dots & \dots & \dots \\ -C^0_{\sigma_{|J|},\sigma_1} & -C^0_{\sigma_{|J|},\sigma_2} & \dots & 1 - C^0_{\sigma_{|J|},\sigma_{|J|}} \end{pmatrix} , \tag{A.11}$$

where $\sigma_i \in J$.

In systems with superconducting order parameters, one faces a situation where, instead of equation (A.5), a Bogoliubov transformation [183, 193],

$$\hat{c}^\dagger_\sigma = \sum_\gamma \left(u^*_{\gamma,\sigma} \hat{h}^\dagger_\gamma + v_{\gamma,\sigma} \hat{h}_\gamma \right) , \tag{A.12a}$$

$$\hat{h}^\dagger_\gamma = \sum_\sigma \left(u_{\gamma,\sigma} \hat{c}^\dagger_\sigma + v_{\gamma,\sigma} \hat{c}_\sigma \right) , \tag{A.12b}$$

relates the operators $\hat{h}^\dagger_\gamma$ and $\hat{c}^\dagger_\sigma$. Note that in order to maintain the fermionic character of the operators $\hat{h}^{(\dagger)}_\gamma$ we have to demand that

$$\tilde{1} = \tilde{U}^\dagger\tilde{U} - \tilde{U}^\dagger\tilde{U} \, , \tag{A.13a}$$

$$0 = \tilde{U}^\dagger\tilde{V} - \tilde{V}\tilde{U}^\dagger \, , \tag{A.13b}$$

where $\tilde{U}$ and $\tilde{V}$ are the matrices with the elements $u_{\gamma,\sigma}$ and $v_{\gamma,\sigma}$, respectively.

For a single-particle product state

$$|\Psi_0\rangle = \prod_{\gamma(\mathrm{occ.})} \hat{h}^\dagger_\gamma |0\rangle \, , \tag{A.14}$$

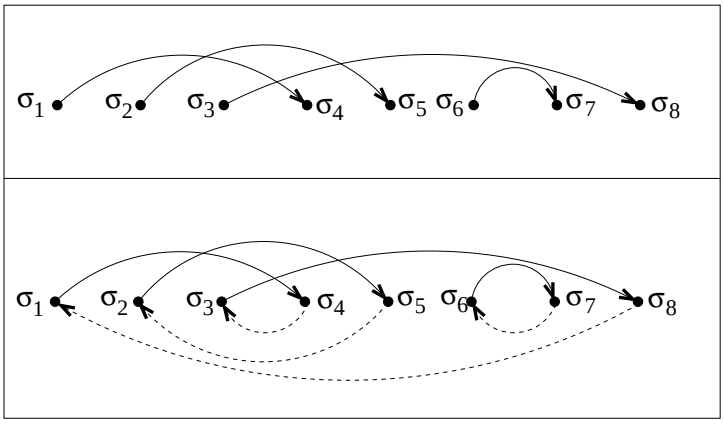

Figure A.1: Illustration of the diagrammatic rules for the evaluation of an expectation value (A.17); for details, see text.

equations (A.12) lead again to a factorisation of expectation values similar to the one in (A.7). As the main difference, it arises that we have to take into account the normal contractions

$$C^0_{\sigma,\sigma'} = \langle \hat{c}^\dagger_\sigma \hat{c}_{\sigma'} \rangle_{\Psi_0} = \sum_{\gamma(\text{occ.})} |u_{\gamma,\sigma}|^2 + \sum_{\gamma(\text{unocc.})} |v_{\gamma,\sigma}|^2 \,, \tag{A.15}$$

as well as the anomalous ones,

$$\Delta_{\sigma,\sigma'} = \langle \hat{c}^\dagger_\sigma \hat{c}^\dagger_{\sigma'} \rangle_{\Psi_0} = \sum_{\gamma(\text{occ.})} u^*_{\gamma,\sigma} v_{\gamma,\sigma'} + \sum_{\gamma(\text{unocc.})} v_{\gamma,\sigma} u^*_{\gamma,\sigma'} \,, \tag{A.16a}$$

$$\Delta^*_{\sigma,\sigma'} = \langle \hat{c}_{\sigma'} \hat{c}_\sigma \rangle_{\Psi_0} = \sum_{\gamma(\text{occ.})} v_{\gamma,\sigma} u^*_{\gamma,\sigma'} + \sum_{\gamma(\text{unocc.})} v^*_{\gamma,\sigma} u_{\gamma,\sigma'} \,. \tag{A.16b}$$

Unfortunately, in this case one cannot write the expectation values of many-particle operators as simple determinants. However, if we evaluate the general expectation value

$$\langle \hat{a}_{\sigma_1} \hat{a}_{\sigma_1} \dots \hat{a}_{\sigma_{(2n)}} \rangle \tag{A.17}$$

with Wick's theorem all contributions can be described and determined diagrammatically. The $2n$ operators $\hat{a}_{\sigma_i}$ in (A.17) may be creation as well as annhiliation operators. The diagrams, which describe all contributions to (A.17) can be determined by the following rules:

i) Draw $2n$ points for the operators $\hat{a}_{\sigma_i}$, see figure A.1.

ii) Find all $N_d = (2n-1)!!$ topologically different ways ('diagrams') to connect each point σ_i to another one σ_j (with $j > i$) via a line with an arrow from left to right. The value D^m of each diagram (with $m = 1, \dots, N_d$) is given by the product over all lines where a line represents an expectation value $\langle \hat{a}_{\sigma_i} \hat{a}_{\sigma_j} \rangle_{\Psi_0}$. For example, the contribution of the diagram in figure A.1 (top part) is

$$\langle \hat{a}_{\sigma_1} \hat{a}_{\sigma_4} \rangle_{\Psi_0} \langle \hat{a}_{\sigma_2} \hat{a}_{\sigma_5} \rangle_{\Psi_0} \langle \hat{a}_{\sigma_3} \hat{a}_{\sigma_8} \rangle_{\Psi_0} \langle \hat{a}_{\sigma_6} \hat{a}_{\sigma_7} \rangle_{\Psi_0} \,. \tag{A.18}$$

iii) Connect each site with an incoming line (e.g., σ_i) to its nearest available neighbour to the left with an outgoing line (e.g., σ_j with $j < i$). Here, 'availability' means that the site σ_j is not already connected to another site σ'_i that is closer to σ_j than σ_i. For example, in figure A.1 (bottom part) the site σ_3 is not available for site σ_5 since it is already connected to σ_4.

iv) Count the number $n_{\mathrm{c}}(m)$ of connected sub-diagrams in D^m. Then, the sign of a diagram is given as $(-1)^n(-1)^{n_{\mathrm{c}}(m)}$. For example, in figure A.1 there are three connected sub-diagrams containing the sites $(\sigma_1, \sigma_3, \sigma_4, \sigma_8)$, (σ_2, σ_5), and (σ_6, σ_7), respectively. Therefore, the sign of this diagram is $(-1)^4(-1)^3 = -1$.

v) Carry out the sum

$$(A.17) = (-1)^n \sum_m^{N_d} D^m (-1)^{n_{\mathrm{c}}(m)} \ . \tag{A.19}$$

Appendix B

Two-Site Hubbard Model

B.1 Exact Solution

In this appendix, we determine the eigenstates and energies of the two-site Hubbard model

$$\hat{H}_{\mathrm{ts}} = t \sum_{s} \left(\hat{c}^{\dagger}_{1,s} \hat{c}_{2,s} + \hat{c}^{\dagger}_{2,s} \hat{c}_{1,s} \right) + U \sum_{i=1}^{2} \hat{n}_{i,\uparrow} \hat{n}_{i,\downarrow} = \hat{H}_0 + \hat{H}_{\mathrm{I}} \, . \tag{B.1}$$

For all particle numbers $N \neq 2$, the solution is quite simple since all eigenstates are simple Slater determinants. The eight states with single or triple particle occupation are given by

$$|1, s, \pm\rangle = \frac{1}{\sqrt{2}} \left(\hat{c}^{\dagger}_{1,s} \pm \hat{c}^{\dagger}_{2,s} \right) |0\rangle \tag{B.2a}$$

$$|3, s, \pm\rangle = \frac{1}{\sqrt{2}} \left(\hat{c}_{1,s} \pm \hat{c}_{2,s} \right) |4\rangle \tag{B.2b}$$

where $|0\rangle$ and $|4\rangle = \prod_{i,s} \hat{c}^{\dagger}_{i,s} |0\rangle$ are the states with $N = 0$ and $N = 4$ particles, respectively. The energies of these states are

$$E_0 = 0 \, , \tag{B.3}$$

$$E_{1,s,\pm} = \pm t \, , \tag{B.4}$$

$$E_{3,s,\pm} = U \mp t \, , \tag{B.5}$$

$$E_{4,\pm} = 2U \, . \tag{B.6}$$

Now we consider the slightly more involved $N = 2$ eigenstates. Since $\hat{H}_{\mathrm{ts}}$ commutes with the total-spin operator $\hat{\boldsymbol{S}}^2$, its eigenvectors have a defined spin S. This determines already the three degenerate triplet states

$$|2, \mathrm{t}, 1\rangle = \hat{c}^{\dagger}_{1,\uparrow} \hat{c}^{\dagger}_{2,\uparrow} |0\rangle \, , \tag{B.7a}$$

$$|2, \mathrm{t}, 0\rangle = \frac{1}{\sqrt{2}} \left(\hat{c}^{\dagger}_{1,\uparrow} \hat{c}^{\dagger}_{2,\downarrow} + \hat{c}^{\dagger}_{1,\downarrow} \hat{c}^{\dagger}_{2,\uparrow} \right) |0\rangle \, , \tag{B.7b}$$

$$|2, \mathrm{t}, -1\rangle = \hat{c}^{\dagger}_{1,\downarrow} \hat{c}^{\dagger}_{2,\downarrow} |0\rangle \tag{B.7c}$$

with the energy $E_{2,\mathrm{t}} = 0$. The Hamiltonian and $\hat{\boldsymbol{S}}^2$ both commute with the 'parity operator' $\hat{T}_{\mathrm{par}}$ which, by definition, exchanges the site indices $i = 1, 2$. Therefore, the remaining three eigenstates of $\hat{H}_{\mathrm{ts}}$ can be chosen as eigenstates of $\hat{T}_{\mathrm{par}}$ with eigenvalues $t_{\mathrm{par}} = \pm 1$. The singlet state with $t_{\mathrm{par}} = -1$ is

$$|2, \mathrm{s}, -1\rangle = \frac{1}{\sqrt{2}} \left(\hat{c}^{\dagger}_{1,\uparrow} \hat{c}^{\dagger}_{1,\downarrow} - \hat{c}^{\dagger}_{2,\uparrow} \hat{c}^{\dagger}_{2,\downarrow} \right) |0\rangle \, . \tag{B.8}$$

It has the energy

$$E_{2,\mathrm{s},-1} = \langle 2,\mathrm{s},1|\, \hat{H}_{\mathrm{ts}}\, |2,\mathrm{s},1\rangle = U\ . \tag{B.9}$$

For the two remaining states,

$$|2,\mathrm{s},1\rangle_1 \;=\; \frac{1}{\sqrt{2}}\left(\hat{c}^\dagger_{1,\uparrow}\hat{c}^\dagger_{2,\downarrow} - \hat{c}^\dagger_{1,\downarrow}\hat{c}^\dagger_{2,\uparrow}\right)|0\rangle\ , \tag{B.10a}$$

$$|2,\mathrm{s},1\rangle_2 \;=\; \frac{1}{\sqrt{2}}\left(\hat{c}^\dagger_{1,\uparrow}\hat{c}^\dagger_{1,\downarrow} + \hat{c}^\dagger_{2,\uparrow}\hat{c}^\dagger_{2,\downarrow}\right)|0\rangle\ , \tag{B.10b}$$

with $t_{\mathrm{par}} = 1$ we have to diagonalise the Hamiltonian in their subspace. This leads to the Hamilton matrix

$$\tilde{H} = {}_i\langle 2,\mathrm{s},1|\hat{H}_{\mathrm{ts}}|2,\mathrm{s},1\rangle_j = \begin{pmatrix} 0 & 2t \\ 2t & U \end{pmatrix}\ . \tag{B.11}$$

with the eigenvalues

$$E^{\pm}_{2,\mathrm{s},1} = \frac{1}{2}\left(U \pm \sqrt{U^2 - 16t^2}\right) \tag{B.12a}$$

and eigenvectors

$$|\Psi_\pm\rangle = \cos(\phi_\pm)\,|2,\mathrm{s},1\rangle_1 + \sin(\phi_\pm)\,|2,\mathrm{s},1\rangle_2\ . \tag{B.12b}$$

Here, the angles $\phi_\pm$ are defined as

$$\tan\phi_\pm = \frac{U \pm \sqrt{U^2 + 16t^2}}{4t}\ . \tag{B.12c}$$

For $U > 0$, the ground state is $|\Psi_-\rangle$, which, in the strong coupling limit $U \gg t$, has the form

$$|\Psi_-\rangle \overset{U\gg t}{\to} |2,\mathrm{s},1\rangle_1 \tag{B.13a}$$

and the energy

$$E^{-}_{2,\mathrm{s},1} = \frac{1}{2}\left(U - \sqrt{U^2 + 16t^2}\right) \overset{U\gg t}{\to} -\frac{4t^2}{U}\ . \tag{B.13b}$$

B.2 Density-Matrix Functional Theory

As an example, we study the two-site Hubbard model within the framework of the exact density-matrix functional theory. As shown in section 3.2.5, the ground-state energy of a lattice model is a functional of the ground-state density matrix. When we employ all symmetries of the ground state, the density matrix has only two independent entries, namely

$$n \equiv \left\langle \hat{c}^\dagger_{b,s}\hat{c}_{b,s}\right\rangle_{\Psi_-} \tag{B.14}$$

and

$$T \equiv \left\langle \hat{c}^\dagger_{1,s}\hat{c}_{2,s}\right\rangle_{\Psi_-} = \left\langle \hat{c}^\dagger_{2,s}\hat{c}_{1,s}\right\rangle_{\Psi_-} = \cos(\phi_-)\sin(\phi_-)\ . \tag{B.15}$$

With a fixed particle density, $n = 1/2$, the only element of the density matrix that varies as a function of t/U is the hopping expectation value T. Hence, there is a universal functional $E_{\mathrm{I}}(T) = W(T)$ for the interaction energy, which, for fixed U, only depends on T. In order to set up this functional, we introduce a fictitious hopping parameter

$$\tilde{t}(U,T) = \frac{UT}{\sqrt{1-4T^2}}\ , \tag{B.16}$$

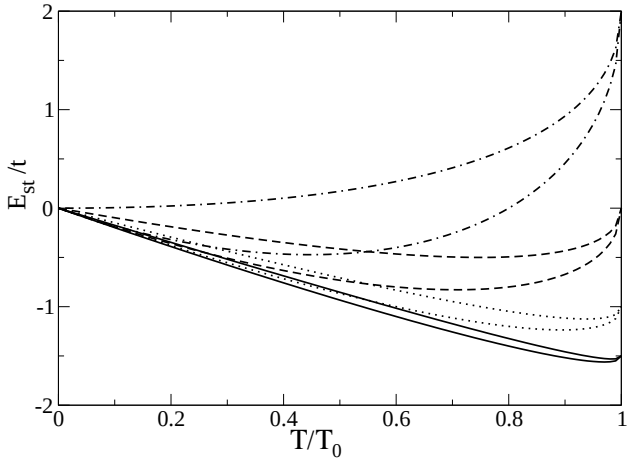

Figure B.1: The exact and the Gutzwiller approximation energy functional $E_{\rm ts}(T)$ for the two-site Hubbard model. The parameters are $U/t = 1$ (solid line), $U/t = 2$ (dotted line), $U/t = 4$ (dashed line), $U/t = 4$ (dotted-dashed line). The exact energy is always below the energy of the Gutzwiller approximation.

which, if we set $t = \tilde{t}(U,T)$ in (B.12c), solves equation (B.15). By replacing t we can write the expectation value of the double-occupancy operator

$$d(T) \equiv \langle \hat{n}_{b\uparrow}\hat{n}_{b\downarrow}\rangle_{\Psi_-} = \frac{1}{2}\sin^2(\phi_-) \tag{B.17}$$

as

$$d(T) = \frac{1}{4}\left(1 - \sqrt{1-(T/T_0)^2}\right) . \tag{B.18}$$

Here, $T_0 = \pm 1/2$ is the expectation value (B.15) for $U = 0$. As expected from our findings in section 3.2.5, the Coulomb-interaction is a universal functional of the density matrix

$$E_{\rm I}(T) = U d(T) , \tag{B.19}$$

i.e., it does not depend on the 'physical' hopping-parameter t in the Hamiltonian (B.1). The total energy functional has the form

$$E_{\rm ts}(T) = -4tT + 2U d(T) . \tag{B.20}$$

It yields, through its minimum, the exact ground-state energy (B.13b). In figure B.1, the energy functional $E_{\rm ts}(T)$ is displayed for various values of t/U. For comparison, the figure also contains the corresponding energy functional in the Gutzwiller approximation; see appendix G.2.

Appendix C

Atomic Hamiltonian for d-Orbitals in a Cubic Environment

We give the explicit form of the atomic Hamiltonian for a system of five d-orbitals in a cubic environment. All details of the derivation can be found in reference [92].

The d-orbitals in an atom are five degenerate states with angular momentum $l = 2$. In polar coordinates r, ϕ, θ, they have the form

$$\varphi_m(r, \phi, \theta) = R(r) Y_{2,m}(\phi, \theta) \tag{C.1}$$

with some radial function $R(r)$ and the 'spherical harmonics' $Y_{lm}(\phi, \theta)$ [2]. The five-fold degeneracy is a consequence of the rotational invariance of the atomic system. In a cubic environment, the eigenstates of the system belong to a representation of the cubic point-symmetry group. It turns out [92] that the five-fold degenerate d-orbitals split into three degenerate $t_{2\mathrm{g}}$ orbitals

$$\varphi_\xi(r, \phi, \theta) = \frac{\mathrm{i}}{\sqrt{2}} R_{t_{2\mathrm{g}}}(r) \left[Y_{2,1}(\phi, \theta) + Y_{2,-1}(\phi, \theta) \right] \sim yz \,, \tag{C.2a}$$

$$\varphi_\eta(r, \phi, \theta) = -\frac{1}{\sqrt{2}} R_{t_{2\mathrm{g}}}(r) \left[Y_{2,1}(\phi, \theta) - Y_{2,-1}(\phi, \theta) \right] \sim xz \,, \tag{C.2b}$$

$$\varphi_\zeta(r, \phi, \theta) = -\frac{\mathrm{i}}{\sqrt{2}} R_{t_{2\mathrm{g}}}(r) \left[Y_{2,2}(\phi, \theta) - Y_{2,-2}(\phi, \theta) \right] \sim xy \,, \tag{C.2c}$$

and two degenerate e_g orbitals

$$\varphi_u(r, \phi, \theta)) = R_{e_\mathrm{g}}(r) Y_{2,0}(\phi, \theta) \sim (3z^2 - r^2) \,, \tag{C.2d}$$

$$\varphi_v(r, \phi, \theta)) = \frac{1}{\sqrt{2}} R_{e_\mathrm{g}} \left[Y_{2,2}(\phi, \theta) + Y_{2,-2}(\phi, \theta) \right] \sim (x^2 - y^2) \,. \tag{C.2e}$$

Here, we introduced the Cartesian coordinates x, y, z, which represent the three C_4 symmetry axes [292] of the system. The angular dependence of the five real wave functions (C.2) is illustrated in the polar coordinate plot in figure C.1.

In order to set up the atomic Hamiltonian in second quantisation, we have to calculate the Coulomb matrix elements (2.3d) where the indices $\sigma_i = (b, s)$ combine the five orbital states b and the two spin states s. A lengthy analysis, see reference [92], yields the following

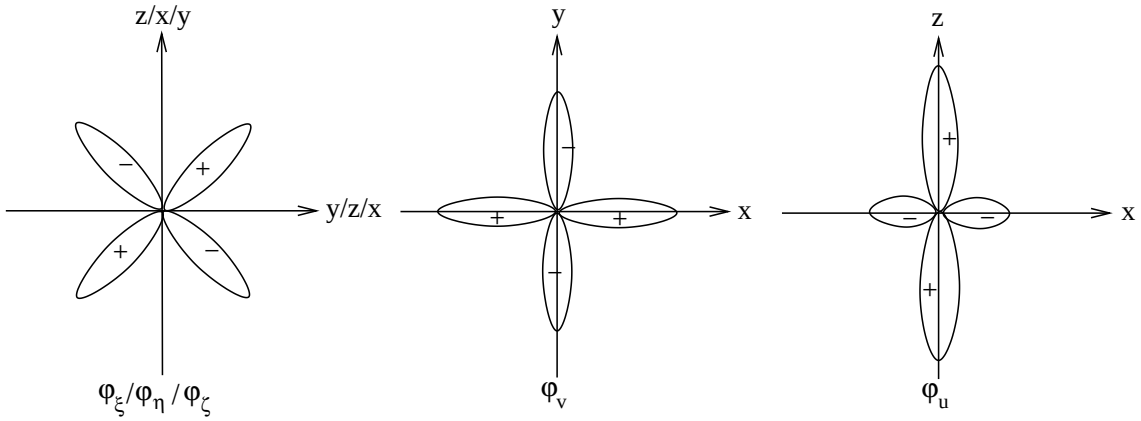

Figure C.1: A polar coordinate plot of the t_{2g} and e_g orbitals.

Hamiltonian

$$\begin{aligned}\hat{H}_I^{\mathrm{d}} &= \frac{1}{2}\sum_{b,s} U(b,b)\hat{n}_{b,s}\hat{n}_{b,\bar{s}} + \frac{1}{2}\sum_{\substack{b(\neq)b'\\ s,s'}} (U(b,b') - \delta_{s,s'}J(b,b'))\hat{n}_{b,s}\hat{n}_{b',s'} \\ &+\frac{1}{2}\sum_{b(\neq)b'} J(b,b')\left[\left(\hat{c}^\dagger_{b,\uparrow}\hat{c}^\dagger_{b,\downarrow}\hat{c}_{b',\downarrow}\hat{c}_{b',\uparrow} + \mathrm{h.c.}\right) + \sum_s \hat{c}^\dagger_{b,s}\hat{c}^\dagger_{b',\bar{s}}\hat{c}_{b,\bar{s}}\hat{c}_{b',s}\right] \\ &+ \sum_{\substack{t,e(\neq)e'\\ s,s'}} (T(t;e,e') - \delta_{s,s'}A(t;e,e'))\hat{n}_{t,s}\hat{c}^\dagger_{e,s'}\hat{c}_{e',s'} \\ &+ \sum_{t,e(\neq)e'} A(t;e,e')\left[\left(\hat{c}^\dagger_{t,\uparrow}\hat{c}^\dagger_{t,\downarrow}\hat{c}_{e,\downarrow}\hat{c}_{e',\uparrow} + \mathrm{h.c.}\right) + \sum_s \hat{c}^\dagger_{t,s}\hat{c}^\dagger_{e,\bar{s}}\hat{c}_{t,\bar{s}}\hat{c}_{e',s}\right] \\ &+ \sum_{\substack{t(\neq)t'(\neq)t'',e\\ s,s'}} S(t,t';t'',e)\left(\hat{c}^\dagger_{t,s}\hat{c}^\dagger_{t',s'}\hat{c}_{t'',s'}\hat{c}_{e,s} + \mathrm{h.c.}\right)\ .\end{aligned} \tag{C.3}$$

Here, the sums over b, (t,t',t''), and (e,e') include either all orbitals, the t_{2g} orbitals, or the e_g orbitals, respectively. Furthermore, we use the convention $\bar{\uparrow}=\downarrow$, $\bar{\downarrow}=\uparrow$. A symmetry analysis of the integrals (2.3d) reveals that, only ten of the coefficients $U(b,b')$, $J(b,b')$, $T(t;e,e')$, $T(t;e,e')$ and $S(t,t';t'',e)$ in (C.3), are independent. There are five 'diagonal' Coulomb integrals,

$$U(u,v), U(\zeta,\zeta), U(\xi,\eta), U(\zeta,u), U(\zeta,v) \tag{C.4a}$$

with

$$U(b,b') \equiv \int \mathrm{d}^3r \int \mathrm{d}^3r' |\varphi_b(\boldsymbol{r})|^2 \frac{e^2}{|\boldsymbol{r}-\boldsymbol{r}'|} |\varphi_{b'}(\boldsymbol{r}')|^2\ , \tag{C.4b}$$

and four 'exchange' integrals

$$J(u,v), J(\xi,\eta), J(\zeta,u), J(\zeta,v) \tag{C.4c}$$

with

$$J(b,b') \equiv \int \mathrm{d}^3r \int \mathrm{d}^3r' \varphi^*_b(\boldsymbol{r})\varphi^*_{b'}(\boldsymbol{r}') \frac{e^2}{|\boldsymbol{r}-\boldsymbol{r}'|} |\varphi_b(\boldsymbol{r}')\varphi_{b'}(\boldsymbol{r})\ . \tag{C.4d}$$

The last independent parameter is

$$S(\eta,\xi;\zeta,u) \equiv \int \mathrm{d}^3r \int \mathrm{d}^3r' \varphi^*_\eta(\boldsymbol{r})\varphi^*_\xi(\boldsymbol{r}') \frac{e^2}{|\boldsymbol{r}-\boldsymbol{r}'|} |\varphi_\zeta(\boldsymbol{r}')\varphi_u(\boldsymbol{r})\ . \tag{C.4e}$$

All other (finite) parameters in (C.3) are determined by the ten independent parameters through

$$\begin{aligned}
U(u,u) &= U(v,v) = U(u,v) + 2J(u,v)\ , && \text{(C.5a)}\\
U(\xi,u) &= U(\eta,u) = (U(\zeta,u) + 3U(\zeta,v))/4\ , && \text{(C.5b)}\\
U(\xi,v) &= U(\eta,v) = (3U(\zeta,u) + U(\zeta,v))/4\ , && \text{(C.5c)}\\
J(\xi,u) &= J(\eta,u) = (J(\zeta,u) + 3J(\zeta,v))/4\ , && \text{(C.5d)}\\
J(\xi,v) &= J(\eta,v) = (3J(\zeta,u) + J(\zeta,v))/4\ , && \text{(C.5e)}\\
T(\eta;u,v) &= \sqrt{3}(U(\zeta,u) - U(\zeta,v))/4 = -T(\xi;u,v)\ , && \text{(C.5f)}\\
A(\eta;u,v) &= \sqrt{3}(J(\zeta,u) - J(\zeta,v))/4 = -A(\xi;u,v)\ , && \text{(C.5g)}\\
S(\xi,\eta;\zeta,u) &= S(\eta,\xi;\zeta,u)\ , && \text{(C.5h)}\\
S(\zeta,\xi;\eta,u) &= -2S(\eta,\xi;\zeta,u)\ , && \text{(C.5i)}\\
S(\xi,\eta;\zeta,v) &= -\sqrt{3}S(\eta,\xi;\zeta,u)\ , && \text{(C.5j)}\\
S(\eta,\xi;\zeta,v) &= \sqrt{3}S(\eta,\xi;\zeta,u)\ . && \text{(C.5k)}
\end{aligned}$$

If we assume, as a further approximation, that the radial wave functions coincide, i.e.,

$$R_{t_{2g}}(r) = R_{e_g}(r) = R(r) \tag{C.6}$$

we only have three independent parameters. One may choose them as the three Racah parameters

$$\begin{aligned}
A &= F^0 - \frac{1}{9}F^4\ , && \text{(C.7a)}\\
B &= \frac{1}{49}(F^2 - \frac{5}{9}F^4)\ , && \text{(C.7b)}\\
C &= \frac{5}{63}F^4\ , && \text{(C.7c)}
\end{aligned}$$

which are defined through the 'Slater-Condon parameters'

$$F^k = \int_0^\infty \mathrm{d}r_1 r_1^2 \int_0^\infty \mathrm{d}r_2 r_2^2 R^2(r_1) R^2(r_2) \frac{r_<^k}{r_>^{k+1}}\ . \tag{C.8}$$

Here, $r_<$ and $r_>$ are the smaller and bigger of the two radii r_1 and r_2, respectively. The ten independent cubic parameters (C.4) can, in this case, be derived from the Racah-parameters as follows

$$\begin{aligned}
U(u,v) &= A - 4B + C\ , && \text{(C.9a)}\\
J(u,v) &= 4B + C\ , && \text{(C.9b)}\\
U(\zeta,\zeta) &= A + 4B + 3C\ , && \text{(C.9c)}\\
U(\xi,\eta) &= A - 2B + C\ , && \text{(C.9d)}\\
J(\xi,\eta) &= 3B + C\ , && \text{(C.9e)}\\
U(\zeta,u) &= A - 4B + C\ , && \text{(C.9f)}\\
U(\zeta,v) &= A + 4B + C\ , && \text{(C.9g)}\\
J(\zeta,u) &= 4B + C\ , && \text{(C.9h)}\\
J(\zeta,v) &= C\ , && \text{(C.9i)}\\
S(\eta,\xi;\zeta,u) &= -\sqrt{3}B\ . && \text{(C.9j)}
\end{aligned}$$

Appendix D

Equivalence of Gutzwiller Wave Functions

As a supplement to section 4.2, we prove that, for a single-band Hubbard model, the two spaces of variational wave functions defined by

$$|\Psi_{\mathrm{G}}\rangle = \prod_i \hat{P}_i \, |\Psi_0\rangle = \prod_{i,I} \lambda_{i;I}^{\hat{m}_{i;I}} \, |\Psi_0\rangle \tag{D.1}$$

and

$$\left|\Psi'_{\mathrm{G}}\right\rangle = \prod_i \hat{P}'_i \left|\Psi'_0\right\rangle = \prod_i g^{\hat{d}_i} \left|\Psi'_0\right\rangle \tag{D.2}$$

are equivalent. We start from the operator indentities

$$\hat{m}_{i;\emptyset} = 1 - \hat{n}_{i,\uparrow} - \hat{n}_{i,\downarrow} + \hat{d}_i \, , \tag{D.3a}$$

$$\hat{m}_{i;s} = \hat{n}_{i,s} - \hat{d}_i \, , \tag{D.3b}$$

in order to write the local correlation operator $\hat{P}_i$ in (D.1) as

$$\hat{P}_i = \left(\frac{\lambda_{i;\emptyset}\lambda_{i;d}}{\lambda_{i;\uparrow}\lambda_{i;\downarrow}}\right)^{\hat{d}_i} \lambda_{i;\emptyset} \left(\frac{\lambda_{i;\uparrow}}{\lambda_{i;\emptyset}}\right)^{\hat{n}_{i,\uparrow}} \left(\frac{\lambda_{i;\downarrow}}{\lambda_{i;\emptyset}}\right)^{\hat{n}_{i,\downarrow}} \, . \tag{D.4}$$

By choosing $g_i = (\lambda_{i;\emptyset}\lambda_{i;d})/(\lambda_{i;\uparrow}\lambda_{i;\downarrow})$ the wave function (D.1) can be written as

$$|\Psi_{\mathrm{G}}\rangle = \prod_i \hat{P}'_i \, |\Phi_0\rangle \tag{D.5}$$

with

$$|\Phi_0\rangle = \prod_i \lambda_{i;\emptyset} \left(\frac{\lambda_{i;\uparrow}}{\lambda_{i;\emptyset}}\right)^{\hat{n}_{i,\uparrow}} \left(\frac{\lambda_{i;\downarrow}}{\lambda_{i;\emptyset}}\right)^{\hat{n}_{i,\downarrow}} \left|\Psi_0\right\rangle \, . \tag{D.6}$$

A comparison of (D.5) with (D.2) reveals that, in order to prove the equivalence of (D.1) and (D.2), we just have to show that (D.6) is a single-particle product state.

Let

$$|\Psi_0\rangle = \prod_{\gamma=1}^{N} \hat{h}_\gamma^\dagger \, |0\rangle \tag{D.7}$$

be a single-particle product state with creation operators

$$\hat{h}_\gamma^\dagger = \sum_i u_{\gamma,i} \hat{c}_i^\dagger \, , \tag{D.8}$$

where $u_{\gamma,i}$ is some unitary matrix. We want to show that

$$|\Phi_0\rangle = \prod_i \eta_i^{\hat{n}_i} \prod_{\gamma=1}^{N} \hat{h}_\gamma^\dagger |0\rangle = \prod_{\gamma=1}^{N} \hat{f}_\gamma^\dagger |0\rangle \tag{D.9}$$

with

$$\hat{f}_\gamma^\dagger \equiv \sum_i \tilde{u}_{\gamma,i} \hat{c}_i^\dagger \tag{D.10}$$

and

$$\tilde{u}_{\gamma,i} \equiv \eta_i u_{\gamma,i} \tag{D.11}$$

is also a single-particle product state for arbitrary parameters η_i. Note that the operators (D.10) are no proper fermionic creation operators since the matrix $\tilde{u}_{\gamma,i}$ is not necessarily unitary. However, we can use, for example, the Gram-Schmidt procedure to generate coefficients $\alpha_{\gamma,\gamma'}$ such that

$$\hat{g}_\gamma^\dagger = \sum_{\gamma'=1}^{\gamma} \alpha_{\gamma,\gamma'} \hat{f}_{\gamma'}^\dagger \tag{D.12}$$

is a proper set of fermionic creation operators. With these new operators, we can write the state (D.9) as

$$\prod_{\gamma=1}^{N} \hat{f}_\gamma^\dagger |0\rangle = C^{-1} \prod_{\gamma=1}^{N} \hat{g}_\gamma^\dagger |0\rangle \ , \tag{D.13}$$

where

$$C \equiv \prod_{\gamma=1}^{N} \alpha_{\gamma,\gamma} \tag{D.14}$$

is an irrelevant renormalisation constant. With equation (D.13), we have succeeded to show that (D.9) and (D.6) are single-particle product states and, therefore, the two spaces of variational wave functions (D.1) and (D.2) coincide.

Appendix E

Symmetry Considerations

E.1 Elements of the Variational-Parameter Matrix

The Gutzwiller correlation operator (4.25b) contains the matrix of variational parameters $\lambda_{\Gamma,\Gamma'} = \lambda_{i;\Gamma,\Gamma'}$ for each lattice site i. Here, we address the question what symmetries these parameters have to obey in order not to violate the symmetry of the system.

Any point-symmetry operation ξ on a lattice site i, described by an operator $\hat{S}_{i,\xi}$, should leave the Gutzwiller wave function invariant,

$$\hat{S}_{i,\xi} \left|\Psi_{\mathrm{G}}\right\rangle = \left|\Psi_{\mathrm{G}}\right\rangle \ , \tag{E.1}$$

apart from an irrelevant phase factor, which is skipped in equation (E.1). We assume that, by construction, the single-particle state $|\Psi_0\rangle$ in (4.25a) has the correct symmetry, i.e., we have

$$\hat{S}_{i,\xi} \left|\Psi_0\right\rangle = \left|\Psi_0\right\rangle \tag{E.2}$$

for all ξ. Both equations (E.1) and (E.2) together lead to the condition

$$\left[\hat{S}_{i,\xi}, \hat{P}_{\mathrm{G}}\right] = 0 \Leftrightarrow \left[\hat{S}_{i,\xi}, \hat{P}_i\right] = 0 \ . \tag{E.3}$$

Usually one chooses the local states $|\Gamma\rangle$ as the eigenstates of some auxiliary local Hamiltonian that has the correct site symmetry. In this way, the basis states $|\Gamma\rangle$ automatically belong to a certain irreducible representation R of the symmetry group, i.e., they are in a certain subspace $\mathcal{H}^{R,i}$ and transform like

$$\hat{S}_{i,\xi} \left|\Gamma\right\rangle = \sum_{\Gamma' \in \mathcal{H}^{R,i}} D^R_{\Gamma,\Gamma'}(\xi) \left|\Gamma'\right\rangle \ . \tag{E.4}$$

Here, the elements of the matrices $\tilde{D}^R(\xi)$ obey the orthogonality theorem [292]

$$\sum_{\xi} \left(D^R_{\Gamma_1,\Gamma_2}(\xi)\right)^* D^{R'}_{\Gamma_3,\Gamma_4}(\xi) \sim \delta_{R,R'} \delta_{\Gamma_1,\Gamma_3} \delta_{\Gamma_2,\Gamma_4} \tag{E.5}$$

The explicit form of the correlation operator (4.25b) and equation (E.4) together yield the condition

$$\left[\tilde{\lambda}, \tilde{D}(\xi)\right] = 0 \ , \tag{E.6}$$

which the variational-parameter matrix $\lambda_{\Gamma,\Gamma}$ has to meet in order to ensure the correct symmetry of the Gutzwiller wave function. The elements of the matrix $\tilde{D}(\xi)$ in (E.6) are either zero or given as $D_{\Gamma,\Gamma}(\xi) = D^R_{\Gamma,\Gamma'}(\xi)$ for states $|\Gamma\rangle$, $|\Gamma\rangle'$ that belong to the same irreducible subspace $\mathcal{H}^{R,i}$.

E.2 Diagonal Local Matrices

We skip the constant lattice site index in this section. There are three purely local matrices that enter the Gutzwiller energy functional : (i) the uncorrelated local density matrix $C^0_{\sigma,\sigma'}$ (equation (5.35)), (ii) the renormalisation matrix $q_\sigma^{\sigma'}$ (equation (5.80a)) and (iii) the constraint matrix $\mathrm{C}_{\sigma,\sigma'}$ defined by the on the r.h.s. of equation (5.47b).

First, we show that $\tilde{C}^0$ is diagonal if all orbitals $|\sigma\rangle$ belong to an irreducible representation R of the point-symmetry group and each representation appears only once. This condition excludes, e.g., lattice sites with two s-orbitals. With equation (E.2) and the unitarity $\hat{S}_\xi^+ \hat{S}_\xi = 1$ of the symmetry operators $\hat{S}_\xi^+$, we find

$$C^0_{\sigma,\sigma'} = \langle \Psi_0 | \hat{c}^\dagger_\sigma \hat{c}_{\sigma'} | \Psi_0 \rangle \tag{E.7a}$$

$$= \langle \Psi_0 | \hat{S}_\xi \hat{c}^\dagger_\sigma \hat{S}_\xi^+ \hat{S}_\xi \hat{c}_{\sigma'} \hat{S}_\xi^+ | \Psi_0 \rangle \; . \tag{E.7b}$$

The transformation

$$\hat{S}_\xi \hat{c}^\dagger_\sigma \hat{S}_\xi^+ = \sum_{\sigma'} D^R_{\sigma,\sigma'}(\xi) \hat{c}^\dagger_{\sigma'} \tag{E.8}$$

of the fermionic operators yields

$$C^0_{\sigma_1,\sigma_2} = \sum_{\sigma_1',\sigma_2'} \left(D^R_{\sigma_1,\sigma_1'}(\xi) \right)^* D^R_{\sigma_2,\sigma_2'}(\xi) C^0_{\sigma_1',\sigma_2'} \; . \tag{E.9}$$

By carrying out the sum over ξ in (E.9) the orthogonality theorem (E.5) leads to the expected result

$$C^0_{\sigma,\sigma'} \sim \delta_{\sigma,\sigma'} \; . \tag{E.10}$$

For a basis $|\sigma\rangle$ with a diagonal local density matrix, we find

$$q_\sigma^{\sigma'} \sim \langle \Psi_0 | \hat{P}^\dagger \hat{c}^\dagger_\sigma \hat{P} \hat{c}_{\sigma'} | \Psi_0 \rangle \; , \tag{E.11a}$$

$$\mathrm{C}_{\sigma,\sigma'} = \langle \Psi_0 | \hat{P}^\dagger \hat{P} \hat{c}^\dagger_\sigma \hat{c}_{\sigma'} | \Psi_0 \rangle \tag{E.11b}$$

for the renormalisation matrix and the constraint matrix. Since $\hat{P}$ commutes with all operators $\hat{S}_\xi$ we can use exactly the same arguments as for $C^0_{\sigma,\sigma'}$ to show that $q_\sigma^{\sigma'}$ and $\mathrm{C}_{\sigma,\sigma'}$ are diagonal for all orbitals $|\sigma\rangle$, $|\sigma\rangle$ that belong to different irreducible representations. The same applies to the correlated local density matrix (5.70).

E.3 Global Spin Symmetry

The variational spin-wave dispersion (8.72) is gapless only if the Gutzwiller wave function $|\Psi_\mathrm{G}\rangle$ is an eigenstate of the global spin operator $\hat{\boldsymbol{S}}^2$ and its z-component $\hat{S}_z$, see equations (8.74)-(8.77). This symmetry is not fulfilled for an arbitrary choice of the variational parameters $\lambda_{\Gamma,\Gamma'}$ in (4.25b). In this appendix, we introduce two ways to implement the correct spin symmetry. Without loss of generality, we consider a diagonal variational-parameter matrix $\lambda_{\Gamma,\Gamma'} = \delta_{\Gamma,\Gamma'}\lambda_\Gamma$, with unspecified multiplet states $|\Gamma\rangle$.

The first way to guarantee the global spin symmetry starts from the observation that the single-particle product state $|\Psi_0\rangle$ in (4.25a) can readily be chosen as an eigenstate both of $\hat{S}^z$ and $\hat{\boldsymbol{S}}^2$. Recall that any wave function of the form

$$|\Psi_0\rangle = \prod_\gamma \hat{c}^\dagger_{\gamma,\uparrow} \hat{c}^\dagger_{\gamma,\downarrow} \prod_{\gamma'} \hat{c}^\dagger_{\gamma',\uparrow} |0\rangle \tag{E.12}$$

is an eigenstate of $\hat{\boldsymbol{S}}^2$ and $\hat{S}^z$ with eigenvalues S_z and $S_z(S_z+1)$, respectively. Here, the states $|\gamma'\rangle$ belong to an arbitrary basis of spatial single-particle wave functions.

With a single-particle wave function of the form (E.12), $|\Psi_\mathrm{G}\rangle$ is an eigenstate of $\hat{S}^z$ with the same eigenvalue S_z if the states $|\Gamma\rangle$ are chosen as eigenstates of the local spin operator $\hat{S}_{i,z}$ in z-direction. Then, we ensure the correct spin-symmetry if $|\Psi_\mathrm{G}\rangle$ is an eigenstate of

$$\hat{S}^+\hat{S}^- = \hat{\boldsymbol{S}}^2 + \hat{S}^z - (\hat{S}^z)^2 \,. \tag{E.13}$$

This is equivalent to

$$\left\langle \hat{S}^+\hat{S}^- \right\rangle_{\Psi_\mathrm{G}} = 2S_z \tag{E.14}$$

since we may assume that the spin in $|\Psi_\mathrm{G}\rangle$ has a maximal component in z-direction. The left-hand-side of equation (E.14),

$$\left\langle \hat{S}^+\hat{S}^- \right\rangle_{\Psi_\mathrm{G}} = \sum_{i,j,b,b'} \left\langle \Psi_\mathrm{G} \middle| \hat{c}^\dagger_{i,b,\uparrow}\hat{c}_{i,b,\downarrow}\hat{c}^\dagger_{j,b',\downarrow}\hat{c}_{j,b',\uparrow} \middle| \Psi_\mathrm{G} \right\rangle \tag{E.15}$$

can be evaluated in the limit of infinite spatial dimensions, see reference [151]. This equation constitutes *one* additional condition for the variational parameters λ_Γ that need to be met to ensure the correct spin symmetry. However, this condition is not very useful because it contains non-local expectation values, which makes its implementation into a numerical minimisation scheme quite difficult. Therefore, we propose a second, more feasible strategy on how the correct spin symmetry can be established.

We will show that

$$\hat{S}^+\hat{S}^- \,|\Psi_\mathrm{G}\rangle = \big(S(S+1) - S_z(S_z-1)\big)\,|\Psi_\mathrm{G}\rangle = 2S_z\,|\Psi_\mathrm{G}\rangle \tag{E.16}$$

is fulfilled if the following conditions are met:

i) Each state $|\Gamma\rangle_i$ belongs to a well defined spin-multiplet, $|\Gamma\rangle_i \in \tilde{M}_{i,D}$, where the set

$$\tilde{M}_D \equiv \left\{ |\Gamma_D^{S_z}\rangle_i \right\} \tag{E.17}$$

contains states $|\Gamma_D^{S_z}\rangle_i$ with a total spin S_D and a z-component $-S_D \le S_z \le S_D$.

ii) The variational parameters $\lambda_\Gamma = \lambda_D$ are the same for all states that belong to the same spin-multiplet.

To prove equation (E.16), we first note that the projector on the multiplet $\tilde{M}_{i,D}$,

$$\hat{\mathcal{P}}_{i,D} \equiv \sum_{S_z=-S_D}^{S_D} |\Gamma_D^{S_z}\rangle_i \,{}_i\langle\Gamma_D^{S_z}| \,, \tag{E.18}$$

commutes with all spin operators, i.e., we have

$$[\hat{\mathcal{P}}_{i,D}, \hat{S}_j^{+/-}] = 0 \tag{E.19}$$

for all i, j. From this equation, we conclude that

$$[\hat{S}^{+/-}, \hat{P}_\mathrm{G}] = 0 \,, \tag{E.20}$$

since we can write the local correlation operator (4.25b) as

$$\hat{P}_i = \sum_D \lambda_D \hat{\mathcal{P}}_{i,D} \,. \tag{E.21}$$

This leads us directly to the proof of equation (E.16)

$$\hat{S}^+\hat{S}^-|\Psi_{\mathrm{G}}\rangle = \hat{P}_{\mathrm{G}}\hat{S}^+\hat{S}^-\,|\Psi_0\rangle = (S_z(S_z+1) - S_z(S_z-1))\hat{P}_{\mathrm{G}}\,|\Psi_0\rangle \tag{E.22a}$$

$$= 2S_z|\Psi_{\mathrm{G}}\rangle\,. \tag{E.22b}$$

Note that condition ii) reduces the number of variational-parameters significantly because all parameters λ_Γ for states $|\Gamma\rangle$ that belong to the same spin multiplet are now determined by just one parameter λ_D. However, this restriction still allows different occupations of the several z-components because occupation expectation values

$$m_\Gamma = \lambda_{\Gamma_S} m_\Gamma^0 \tag{E.23}$$

also depend on the single-particle state $|\Psi_0\rangle$. An implementation of the additional constraints into the minimisation algorithm, which we describe in appendix H, is straightforward.

Appendix F

Systems with Superconductivity

In this appendix, we summarise the main results for Gutzwiller wave functions with a superconducting order parameter in the limit of infinite spatial dimensions. In order to describe superconductivity, we work with single-particle wave functions $|\Psi_0\rangle$ in the Gutzwiller Ansatz that have finite pairing amplitudes

$$\Delta_{i,j}^{0;\sigma,\sigma'} \equiv \langle \hat{c}_{i,\sigma}^{\dagger} \hat{c}_{j,\sigma'}^{\dagger} \rangle_{\Psi_0} = \left(\langle \hat{c}_{j,\sigma'} \hat{c}_{i,\sigma} \rangle_{\Psi_0} \right)^* . \tag{F.1}$$

Technically, the main problem for the diagrammatic evaluation in infinite dimensions arises from the local ('anomalous') pairing amplitudes $\Delta_{i,i}^{0;\sigma,\sigma'}$ while the non-local amplitudes, in principle, can be evaluated like hopping operators in section 5.2. In order to deal with normal and anomalous terms of the local density matrix on an equal footing, we introduce the tensor $\tilde{C}_i^0$ with the elements

$$C_{i;\sigma,\sigma'}^{0;\alpha,\alpha'} \equiv \langle \hat{c}_{i,\sigma}^{\alpha} \hat{c}_{i,\sigma'}^{\alpha'} \rangle_{\Psi_0} , \tag{F.2}$$

which generalises the local density matrix, equation (5.35). Here, the superscripts $\alpha, \alpha' = +/-$ were introduced in order to distinguish creation and annihilation operators,

$$\hat{c}^{+} \equiv \hat{c}^{\dagger} \ , \ \hat{c}^{-} \equiv \hat{c} . \tag{F.3}$$

Mathematically, these superscripts are interpreted as numbers, e.g., for $\alpha = -$ we have

$$\hat{c}^{\alpha} \equiv \hat{c} \ , \ \hat{c}^{-\alpha} \equiv \hat{c}^{\dagger} . \tag{F.4}$$

As we will see below, the anomalous local amplitudes force us to work with a local correlation operator

$$\hat{P} = \sum_{\Gamma,\Gamma'} \lambda_{\Gamma,\Gamma'} |\Gamma\rangle \langle \Gamma'| , \tag{F.5}$$

in which $\lambda_{\Gamma,\Gamma'}$ is finite not only for states with equal particle number, $\Delta N_{\Gamma,\Gamma'} \equiv |\Gamma| - |\Gamma'| = 0$, but also for those states with an even (and finite) difference $\Delta N_{\Gamma,\Gamma'}$. For example, the proper local correlation operator for the single-band Hubbard model with a finite local amplitude

$$\Delta_0 \equiv C_{\uparrow,\downarrow}^{0;+,+} \tag{F.6}$$

turns out to be

$$\hat{P} = \lambda_d \hat{m}_d + \sum_s \lambda_s \hat{m}_s + \lambda_\emptyset \hat{m}_\emptyset + \left(\lambda_B \hat{c}_{\uparrow}^{\dagger} \hat{c}_{\downarrow}^{\dagger} + \text{h.c.} \right) . \tag{F.7}$$

Note that we frequently drop lattice site indices in formulae for local quantities.

F.1 Diagrammatics and Local Constraints

In order to evaluate a general expectation value of the form (5.18), we may use again Wick's theorem, which also applies to systems with finite pairing amplitudes, see appendix A. This leads us to the diagrammatic evaluation, which we introduced in section 5.1.2, with the only difference that lattice sites are now also connected by lines that are ingoing or outgoing on both sides. Such lines represent the anomalous contractions, equation (F.1), in addition to the normal contractions, equation (5.20). All other diagrammatic rules remain unchanged, in particular the scaling of diagrams with the spatial dimension D, see section 5.1.1

For the evaluation of the expectation values (5.38) in infinite dimension, we expand $\hat{P}_m^\dagger \hat{P}_m$ in terms of Hartree-Fock operators

$$\left[\hat{P}^\dagger \hat{P}\right]^{\mathrm{HF}} = \sum_{\substack{I_1,I_2 \\ (|I_1|+|I_2|\geq 2)}} x_{I_1,I_2}\left(\hat{C}_{I_1}^\dagger \hat{C}_{I_2} - \left[\hat{C}_{I_1}^\dagger \hat{C}_{I_2}\right]^{\mathrm{HF}}\right), \tag{F.8}$$

in the same way as in equation (5.40a). Note that the definition (F.8) generalises equation (5.40b) because, here, the particle numbers $|I_i|$ need not to be the same and, accordingly, we have to work with the condition $|I_1| + |I_2| \geq 2$ instead of $|I_i| \geq 1$ in (5.40b). All other definitions in connection with the Hartree-Fock operators, i.e., equations (5.41), remain unchanged.

For example, in the case of the single-band correlation operator (F.7), one has to expand

$$\hat{P}^2 = (\lambda_d^2 + |\lambda_B|^2)\hat{m}_d + \sum_s \lambda_s^2 \hat{m}_s + (\lambda_\emptyset^2 + |\lambda_B|^2)\hat{m}_\emptyset + (\lambda_\emptyset + \lambda_d)(\lambda_B \hat{c}_\uparrow^\dagger \hat{c}_\downarrow^\dagger + \text{h.c.}) \tag{F.9a}$$

$$= \left(\lambda_d^2 - \sum_s \lambda_s^2 + \lambda_\emptyset^2 + 2|\lambda_B|^2\right)\hat{c}_\uparrow^\dagger \hat{c}_\downarrow^\dagger \hat{c}_\downarrow \hat{c}_\uparrow \tag{F.9b}$$

$$+ \sum_s (\lambda_s^2 - \lambda_\emptyset^2 - |\lambda_B|^2)\hat{c}_s^\dagger \hat{c}_s + (\lambda_\emptyset + \lambda_d)(\lambda_B \hat{c}_\uparrow^\dagger \hat{c}_\downarrow^\dagger + \text{h.c.}) + \lambda_\emptyset^2$$

in terms of the Hartree-Fock operators

$$\left[\hat{c}_\uparrow^\dagger \hat{c}_\downarrow^\dagger \hat{c}_\downarrow \hat{c}_\uparrow\right]^{\mathrm{HF}} = \sum_s \hat{c}_s^\dagger \hat{c}_s \langle \hat{c}_{\bar{s}}^\dagger \hat{c}_{\bar{s}} \rangle_{\Psi_0} + \hat{c}_\uparrow^\dagger \hat{c}_\downarrow^\dagger \langle \hat{c}_\downarrow \hat{c}_\uparrow \rangle_{\Psi_0} + \hat{c}_\downarrow \hat{c}_\uparrow \langle \hat{c}_\uparrow^\dagger \hat{c}_\downarrow^\dagger \rangle_{\Psi_0} \tag{F.10a}$$

$$- \langle \hat{c}_\uparrow^\dagger \hat{c}_\uparrow \rangle_{\Psi_0} \langle \hat{c}_\downarrow^\dagger \hat{c}_\downarrow \rangle_{\Psi_0} ,$$

$$\left[\hat{c}_s^\alpha \hat{c}_{s'}^{\alpha'}\right]^{\mathrm{HF}} = \langle \hat{c}_s^\alpha \hat{c}_{s'}^{\alpha'} \rangle_{\Psi_0} , \tag{F.10b}$$

to set up $[\hat{P}^2]^{\mathrm{HF}}$.

By construction, the terms $\sim x_{I_1,I_2}$ in the expansion (F.8) generate diagrams with exactly $|I_1|$ ($|I_2|$) lines leaving (entering) a site. For the expansion in infinite dimensions, we demand that all inner vertices have at least four incoming or outcoming lines, i.e., the coefficients x_{I_1,I_2} have to fulfil

$$x_{m;\emptyset,\emptyset} = 1 , \tag{F.11a}$$

$$x_{m;I_1,I_2} = 0 , \tag{F.11b}$$

for all I_i with $|I_1|+|I_2| = 2$. By definition of the Gutzwiller correlation operator (F.5), $|I_1|-|I_2|$ is an even number and the case $|I_1| + |I_2| = 1$ with a single line entering a vertex is therefore excluded. Relations (F.11) are equivalent to the local conditions

$$1 = \langle \hat{P}^\dagger \hat{P} \rangle_{\Psi_0} , \tag{F.12a}$$

$$\langle \hat{c}_\sigma^\alpha \hat{c}_{\sigma'}^{\alpha'} \rangle_{\Psi_0} = \langle \hat{c}_\sigma^\alpha \hat{c}_{\sigma'}^{\alpha'} \hat{P}^\dagger \hat{P} \rangle_{\Psi_0} , \tag{F.12b}$$

which, using equation (F.2), can be written explicitly as

$$1 = \sum_{I_1,I_2} \overline{\lambda}_{I_1,I_2} m^0_{I_1,I_2} \,, \tag{F.13a}$$

$$C^{0;\alpha,\alpha'}_{\sigma,\sigma'} = \sum_{I_1,I_2,I_3} \langle I_1|\hat{c}^{\alpha}_{\sigma}\hat{c}^{\alpha'}_{\sigma'}|I_3\rangle \overline{\lambda}_{I_3,I_2} m^0_{I_1,I_2} \,. \tag{F.13b}$$

Here, the coefficients $\overline{\lambda}_{I_1,I_2}$ are defined in equations (5.39) and the expectation values $m^0_{I_1,I_2}$ can be evaluated with Wicks's theorem. Note that we find equivalent sets of constraints if we move the operators $\hat{P}^\dagger\hat{P}$ relative to $\hat{c}^{\alpha}_{\sigma}$ or $\hat{c}^{\alpha'}_{\sigma'}$ in (F.12).

For example, in case of the single-band model with the correlation operator (F.7) and the corresponding square (F.9a), the constraints are given by

$$1 = (\lambda_d^2 + |\lambda_B|^2) m_d^0 + \sum_s \lambda_s^2 m_s^0 + (\lambda_\emptyset^2 + |\lambda_B|^2) m_\emptyset^0 + (\lambda_\emptyset + \lambda_d)(\lambda_B \Delta_0 + \text{c.c.}) \,, \tag{F.14a}$$

$$n_s^0 = (\lambda_d^2 + |\lambda_B|^2) m_d^0 + \lambda_s^2 m_s^0 + (\lambda_\emptyset + \lambda_d)\lambda_B \Delta_0 \,, \tag{F.14b}$$

$$\Delta_0 = (\lambda_\emptyset^2 + |\lambda_B|^2) \Delta_0 + (\lambda_\emptyset + \lambda_d)\lambda_B^* m_d^0 \,, \tag{F.14c}$$

where we introduced

$$m^0_\emptyset = (1 - n^0_\uparrow)(1 - n^0_\downarrow) + |\Delta_0|^2 \,, \tag{F.15a}$$

$$m^0_s = n^0_s(1 - n^0_{\bar{s}}) - |\Delta_0|^2 \,, \tag{F.15b}$$

$$m^0_d = n^0_\uparrow n^0_\downarrow + |\Delta_0|^2 \,, \tag{F.15c}$$

and Δ_0 has been defined in equation (F.6).

F.2 Expectation Values

The evaluation of the local Hamiltonian $\hat{H}_{\text{loc}}$ in equations (5.62)-(5.66) remains basically unchanged for systems with superconducting pairing. One just has to keep in mind that expectation values such as $m^0_{I_1,I_4}$ in equation (5.66) or $m^{0;\sigma'}_{I_1\setminus\sigma',I_4}$ in equation (5.81) are not given by equation (A.10), but they have to be determined by means of the diagrammatic rules described at the end of appendix A. For example,the expectation value for a local double-occupancy operator in the one-band model is given by

$$d = \langle \hat{d} \rangle_{\Psi_{\text{G}}} = (\lambda_d^2 + |\lambda_B|^2) m_d^0 \tag{F.16}$$

with m_d^0 introduced in (F.15c).

All other local expectation values are also given by their respective counterparts in section 5.2. In particular, the evaluation of the correlated local density matrix leads to equation (5.71) for the normal as well as for the anomalous parts of this matrix, i.e., we have

$$C^{\alpha,\alpha'}_{\sigma,\sigma'} \equiv \langle \hat{c}^{\alpha}_{\sigma}\hat{c}^{\alpha'}_{\sigma'} \rangle_{\Psi_{\text{G}}} = \sum_{I_1,\ldots,I_4} \lambda^*_{I_4,I_1} \lambda_{I_3,I_2} \langle I_4|\hat{c}^{\alpha}_{\sigma}\hat{c}^{\alpha'}_{\sigma'}|I_3\rangle m^0_{I_1,I_2} \,. \tag{F.17}$$

The main difference between wave functions with and without superconductivity arises for the expectation values $\langle \hat{c}^\dagger_{i,\sigma_1}\hat{c}_{j,\sigma_2} \rangle_{\Psi_{\text{G}}}$ of hopping operators since there are now four different possibilities for a single line connecting the sites i and j. We find

$$\begin{aligned} \left\langle \hat{c}^\dagger_{i,\sigma_1}\hat{c}_{j,\sigma_2} \right\rangle_{\Psi_{\text{G}}} = \sum_{\sigma_1',\sigma_2'} \Big[& q^{\sigma_1'}_{\sigma_1} \left(q^{\sigma_2'}_{\sigma_2}\right)^* \left\langle \hat{c}^\dagger_{i,\sigma_1'}\hat{c}_{j,\sigma_2'} \right\rangle_{\Psi_0} + \bar{q}^{\sigma_1'}_{\sigma_1} \left(q^{\sigma_2'}_{\sigma_2}\right)^* \left\langle \hat{c}_{i,\sigma_1'}\hat{c}_{j,\sigma_2'} \right\rangle_{\Psi_0} \\ & + q^{\sigma_1'}_{\sigma_1} \left(\bar{q}^{\sigma_2'}_{\sigma_2}\right)^* \left\langle \hat{c}^\dagger_{i,\sigma_1'}\hat{c}^\dagger_{j,\sigma_2'} \right\rangle_{\Psi_0} + \bar{q}^{\sigma_1'}_{\sigma_1} \left(\bar{q}^{\sigma_2'}_{\sigma_2}\right)^* \left\langle \hat{c}_{i,\sigma_1'}\hat{c}^\dagger_{j,\sigma_2'} \right\rangle_{\Psi_0} \Big] \,, \end{aligned} \tag{F.18}$$

as a generalisation of equation (5.78). The 'normal' elements $q_\sigma^{\sigma'}$ of the renormalisation matrix can be derived as in equations (5.79)-(5.81). For the anomalous elements $\bar{q}_\sigma^{\sigma'}$, we start from equation (5.79) and sum over all possibilities to take an *annihilation* operator $\hat{c}_{i,\sigma'}$ out of $|I_1\rangle\langle I_4|$ in order to create a line with another creation or annihilation operator on site j. There are three different contributions depending on whether the index σ' is an element of $I_1 \cap I_4$, $I_4 \backslash (I_1 \cap I_4)$, or $J = (1, \ldots, N) \backslash (I_1 \cup I_4)$. Altogether, this leads to

$$\bar{q}_\sigma^{\sigma'} = \sum_{I_1,\ldots,I_4} \lambda^*_{I_2,I_1} \lambda_{I_3,I_4} \langle I_2|\hat{c}_\sigma^\dagger|I_3\rangle \bar{H}^{\sigma'}_{I_1,I_4} \,, \tag{F.19}$$

where we introduced

$$\begin{aligned} \bar{H}^{\sigma'}_{I_1,I_4} \;\equiv\; & (1 - f_{\sigma',I_4}) \langle I_1|\hat{c}_{\sigma'}|I_1 \cup \sigma'\rangle m^0_{I_1\cup\sigma',I_4} \\ & + \langle I_4 \backslash \sigma'|\hat{c}_{\sigma'}|I_4\rangle \left(f_{\sigma',I_1} m^0_{I_1,I_4\backslash\sigma'} + (1 - f_{\sigma',I_1}) m^{0;\sigma'}_{I_1,I_4\backslash\sigma'} \right) \,. \end{aligned} \tag{F.20}$$

For example, in the case of the one-band model with the correlation operator (F.7), we find

$$\hat{P}^\dagger \hat{c}_s^\dagger \hat{P} = \lambda_d \lambda_{\bar{s}} \hat{c}_s^\dagger \hat{c}_{\bar{s}}^\dagger \hat{c}_{\bar{s}} + \lambda_\emptyset \lambda_s \hat{c}_s^\dagger \hat{c}_{\bar{s}} \hat{c}_{\bar{s}}^\dagger \pm \lambda_B^* (\lambda_{\bar{s}} \hat{c}_{\bar{s}} \hat{c}_s \hat{c}_s^\dagger + \lambda_{\bar{s}} \hat{c}_s^\dagger \hat{c}_{\bar{s}} \hat{c}_s) \,, \tag{F.21}$$

where the $+$ and $-$ sign apply to $s = \uparrow$ and $s = \downarrow$, respectively. An evaluation of (F.21) leads to a renormalisation matrix whose finite elements are

$$q_s^s = \lambda_d \lambda_{\bar{s}} n^0_{\bar{s}} + \lambda_\emptyset \lambda_s (1 - n^0_{\bar{s}}) + \lambda_B^* (\lambda_s + \lambda_{\bar{s}}) \Delta_0^* \,, \tag{F.22a}$$

$$\bar{q}_s^{\bar{s}} = \pm \left[(\lambda_d \lambda_{\bar{s}} - \lambda_\emptyset \lambda_s) \Delta_0 + \lambda_B^* (\lambda_{\bar{s}} (1 - n^0_s) - \lambda_s n^0_s) \right] \,. \tag{F.22b}$$

Note that the different signs in (F.22b) for spins $s = \uparrow, \downarrow$ are usually irrelevant since they are cancelled out in expectation values, e.g., for the hopping operator we find

$$\begin{aligned} \langle \hat{c}^\dagger_{i,s} \hat{c}_{j,s} \rangle_{\Psi_\mathrm{G}} \;=\; & |q_s^s|^2 \langle \hat{c}^\dagger_{i,\bar{s}} \hat{c}_{j,\bar{s}} \rangle_{\Psi_0} + |\bar{q}_s^{\bar{s}}|^2 \langle \hat{c}_{i,\bar{s}} \hat{c}^\dagger_{j,\bar{s}} \rangle_{\Psi_0} \\ & + \bar{q}_s^{\bar{s}} \left(q_s^s\right)^* \langle \hat{c}_{i,\bar{s}} \hat{c}_{j,s} \rangle_{\Psi_0} + q_s^s \left(\bar{q}_s^{\bar{s}}\right)^* \langle \hat{c}^\dagger_{i,s} \hat{c}^\dagger_{j,\bar{s}} \rangle_{\Psi_0} \,, \end{aligned} \tag{F.23}$$

as long as all expectation values with respect to $|\Psi_0\rangle$ have the correct spin symmetry.

F.3 Minimisation of the Ground-State Energy Functional

Summarising the results of section F.2 we set up the Gutzwiller energy functional and derive the effective single-particle Hamiltonian that describes quasi-particle excitations. We start with a derivation for general multi-band Hubbard models in section F.3.1. In section F.3.2, the results are specified for a single-band model.

F.3.1 Multi-Band Hubbard Models

The variational ground-state energy for systems with superconducting order is given by equation (5.87) with the modified single-particle energy functional

$$E_0(\{\tilde{\lambda}_i\}, \{\tilde{C}_i^0\}, |\Psi_0\rangle) = \sum_{i,j;\sigma,\sigma'} \sum_{\alpha,\alpha'=+,-} t_{i,j}^{\alpha,\alpha';\sigma,\sigma'} \langle \Psi_0 | \hat{c}^\alpha_{i,\sigma} \hat{c}^{\alpha'}_{j,\sigma'} | \Psi_0 \rangle \,. \tag{F.24}$$

Here, we introduced the effective hopping amplitudes

$$t_{i,j}^{+,-;\sigma,\sigma'} \equiv \frac{1}{2}\sum_{\tau\tau'}\left(\left(q_{i;\tau}^{\sigma}\right)^{*} q_{j;\tau'}^{\sigma'} t_{i,j}^{\tau\tau'} - \left(\bar{q}_{i;\tau}^{\sigma}\right)^{*} \bar{q}_{j;\tau'}^{\sigma'} t_{j,i}^{\tau',\tau}\right) , \tag{F.25a}$$

$$t_{i,j}^{-,+;\sigma,\sigma'} \equiv -\left(t_{i,j}^{+,-;\sigma,\sigma'}\right)^{*} , \tag{F.25b}$$

$$t_{i,j}^{+,+;\sigma,\sigma'} \equiv \frac{1}{2}\sum_{\tau\tau'}\left(\left(q_{i;\tau}^{\sigma}\right)^{*}\left(\bar{q}_{j;\tau'}^{\sigma'}\right)^{*} t_{i,j}^{\tau\tau'} - \left(\bar{q}_{i;\tau}^{\sigma}\right)^{*}\left(q_{j;\tau'}^{\sigma'}\right)^{*} t_{j,i}^{\tau',\tau}\right) , \tag{F.25c}$$

$$t_{i,j}^{-,-;\sigma,\sigma'} \equiv -\left(t_{i,j}^{+,+;\sigma,\sigma'}\right)^{*} . \tag{F.25d}$$

We assume, as we did in section 5.3, that the constraints (F.13) are satisfied explicitly, i.e., by a proper choice of the variational parameters $\lambda_{i;\Gamma,\Gamma'}$ with $|\Gamma| + |\Gamma'| \leq 2$. In this case, the energy is a functional of the remaining independent parameters $\lambda_{i;\Gamma,\Gamma'}^{\mathrm{i}}$, the local density matrices $\tilde{C}_i^0$, and the wave function $|\Psi_0\rangle$. We introduce Lagrange multipliers $\eta_{i;\sigma,\sigma'}^{\alpha,\alpha'}$ and E^{SP} for the density matrix equation (F.2) and the normalisation of $|\Psi_0\rangle$. Furthermore, we fix the avarage total particle number

$$N = Ln = \sum_{i,\sigma} C_{i;\sigma,\sigma}^{+,-}(\{\tilde{\lambda}_i^{\mathrm{i}}\}, \{\tilde{C}_i^0\}) \tag{F.26}$$

by means of the Lagrange multiplier E_{F}. Note that, unlike in section 5.3, the total particle numbers in $|\Psi_0\rangle$ and $|\Psi_{\mathrm{G}}\rangle$ do not coincide since the correlation operator (F.5) does not commute with the operator (5.75) for the local particle number.

With the Lagrange-parameter terms, we write the variational ground-state energy E_0^{var} as

$$E_0^{\mathrm{var}} = \underset{\{\tilde{\lambda}_i^{\mathrm{i}}\},\{\tilde{C}_i^0\},\{\tilde{\eta}_i\},|\Psi_0\rangle,E_{\mathrm{F}},E^{\mathrm{SP}}}{\mathrm{Minimum}} E_{\mathrm{c}}\left(\{\tilde{\lambda}_i^{\mathrm{i}}\}, \{\tilde{C}_i^0\}, \{\tilde{\eta}_i\}, |\Psi_0\rangle, E_{\mathrm{F}}, E^{\mathrm{SP}}\right) , \tag{F.27a}$$

$$\begin{aligned} E_{\mathrm{c}}(\ldots) = {} & E_{\mathrm{G}}\left(\{\tilde{\lambda}_i^{\mathrm{i}}\}, \{\tilde{C}_i^0\}, |\Psi_0\rangle\right) - E^{\mathrm{SP}}\left(\langle\Psi_0|\Psi_0\rangle - 1\right) \\ & + \sum_{i,\sigma,\sigma'}\sum_{\alpha,\alpha'}\left[\eta_{i;\sigma,\sigma'}^{\alpha,\alpha'}\left(C_{i;\sigma,\sigma'}^{0;\alpha,\alpha'} - \langle\Psi_0|\hat{c}_{i,\sigma}^{\alpha}\hat{c}_{i,\sigma'}^{\alpha'}|\Psi_0\rangle\right) + \mathrm{c.c.}\right] \\ & + E_{\mathrm{F}}\left(N - \sum_{i,\sigma} C_{i;\sigma,\sigma}^{+,-}\left(\{\tilde{\lambda}_i^{\mathrm{i}}\}, \{\tilde{C}_i^0\}\right)\right) . \end{aligned} \tag{F.27b}$$

The minimisation with respect to $|\Psi_0\rangle$ can be carried out explicitly and leads to the effective single-particle Schrödinger equation

$$\hat{H}_0^{\mathrm{eff}}|\Psi_0\rangle = E^{\mathrm{SP}}\left(\{\tilde{\lambda}_i^{\mathrm{i}}\}, \{\tilde{C}_i^0\}, \{\tilde{\eta}_i\}\right)|\Psi_0\rangle , \tag{F.28a}$$

$$\hat{H}_0^{\mathrm{eff}} \equiv \frac{1}{2}\sum_{i,\sigma;j,\sigma'}\sum_{\alpha,\alpha'}\left[\left(t_{i,j}^{\alpha,\alpha';\sigma,\sigma'} - 2\delta_{i,j}\eta_{i;\sigma,\sigma'}^{\alpha,\alpha'}\right)\hat{c}_{i,\sigma}^{\alpha}\hat{c}_{j,\sigma'}^{\alpha'} + \mathrm{h.c.}\right] \tag{F.28b}$$

$$= K_0 + \frac{1}{2}\sum_{i,\sigma;j,\sigma'}\sum_{\alpha,\alpha'}\left[\left[t_{i,j}^{\alpha,\alpha';\sigma,\sigma'} - \delta_{i,j}\left(\eta_{i;\sigma,\sigma'}^{\alpha,\alpha'} - \eta_{i;\sigma',\sigma}^{\alpha',\alpha}\right)\right]\hat{c}_{i,\sigma}^{\alpha}\hat{c}_{j,\sigma'}^{\alpha'} + \mathrm{h.c.}\right] ,$$

where

$$K_0 = -\sum_{i,\sigma}\left[\left(\eta_{i;\sigma,\sigma}^{+,-} + \eta_{i;\sigma,\sigma}^{-,+}\right) + \mathrm{c.c.}\right] . \tag{F.29}$$

The optimum wave function $|\Psi_0\rangle$ is assumed to be the ground state of the Hamiltonian (F.28c). In this way, $|\Psi_0\rangle$ becomes a function of $\{\tilde{\lambda}_i^{\mathrm{i}}\}, \{\tilde{C}_i^0\}, \{\tilde{\eta}_i\}$, and the remaining task is to find the

minimum

$$E_0^{\rm var} = \underset{\{\tilde\lambda_i^{\rm i}\},\{\tilde C_i^0\},\{\tilde\eta_i\},E_{\rm F}}{\rm Minimum} E_{\rm c}(\{\tilde\lambda_i^{\rm i}\},\{\tilde C_i^0\},\{\tilde\eta_i\},E_{\rm F})\ , \tag{F.30a}$$

$$\begin{aligned} E_{\rm c}(\ldots) &= E^{\rm SP}\left(\{\tilde\lambda_i^{\rm i}\},\{\tilde C_i^0\},\{\tilde\eta_i\}\right) + \sum_i E_{i;{\rm loc}}(\tilde\lambda_i^{\rm i},\tilde C_i^0) \\ &\quad + \sum_{i;\sigma,\sigma'}\left[\sum_{\alpha,\alpha'}\left(\eta_{i;\sigma,\sigma'}^{\alpha,\alpha'}C_{i;\sigma,\sigma'}^{\alpha,\alpha'}+{\rm c.c.}\right) - \delta_{\sigma,\sigma'}E_{\rm F}\left(C_{i;\sigma,\sigma}^{+,-}\left(\{\tilde\lambda_i^{\rm i}\},\{\tilde C_i^0\}\right)-n\right)\right]. \end{aligned} \tag{F.30b}$$

For a translationally invariant system, the single-particle Hamiltonian in the Bloch basis with wave vectors $\boldsymbol{k}$ has the form

$$\hat H_0^{\rm eff} = K_0 + \sum_{\boldsymbol{k};\sigma,\sigma'}\sum_{\alpha,\alpha'}\varepsilon_{\sigma,\sigma'}^{\alpha,\alpha'}(\boldsymbol{k})\hat c_{(\alpha\boldsymbol{k}),\sigma}^{\alpha}\hat c_{(-\alpha'\boldsymbol{k}),\sigma'}^{\alpha'}\ , \tag{F.31}$$

where the coefficients

$$\begin{aligned} \varepsilon_{\sigma,\sigma'}^{\alpha,\alpha'}(\boldsymbol{k}) &= \frac{1}{L}\sum_{i,j}e^{-{\rm i}\boldsymbol{k}(\boldsymbol{R}_j-\boldsymbol{R}_i)}\left(t_{i,j}^{\alpha,\alpha';\sigma,\sigma'} - \frac{1}{2}\delta_{i,j}\left(\eta_{\sigma,\sigma'}^{\alpha,\alpha'}-\eta_{\sigma',\sigma}^{\alpha',\alpha}+\left[\eta_{\sigma',\sigma}^{-\alpha',-\alpha}\right]^*-\left[\eta_{\sigma,\sigma'}^{-\alpha,-\alpha'}\right]^*\right)\right) \\ &= \frac{1}{2}\sum_{\tau\tau'}Q_{\tau\tau'}^{\alpha,\alpha';\sigma,\sigma'}\varepsilon_{\tau,\tau'}^0(\boldsymbol{k}) - \frac{1}{2}\left(\eta_{\sigma,\sigma'}^{\alpha,\alpha'}-\eta_{\sigma',\sigma}^{\alpha',\alpha}+\left[\eta_{\sigma'\sigma}^{-\alpha',-\alpha}\right]^*-\left[\eta_{\sigma,\sigma'}^{-\alpha,-\alpha'}\right]^*\right) \end{aligned} \tag{F.32}$$

are the elements of the matrices $\tilde\varepsilon_{\boldsymbol{k}}^{\alpha,\alpha'}$. In (F.32), we introduced the bare energy-band matrix

$$\varepsilon_{\sigma,\sigma'}^0(\boldsymbol{k}) \equiv \frac{1}{L}\sum_{i,j}t_{i,j}^{\sigma,\sigma'}e^{{\rm i}\boldsymbol{k}(\boldsymbol{R}_i-\boldsymbol{R}_j)}\ , \tag{F.33}$$

and the coefficients

$$Q_{\tau\tau'}^{+,-;\sigma,\sigma'} = (q_\tau^\sigma)^*\,q_{\tau'}^{\sigma'} - (\bar q_\tau^\sigma)^*\,\bar q_{\tau'}^{\sigma'}\ , \tag{F.34a}$$

$$Q_{\tau\tau'}^{-,+;\sigma,\sigma'} = -\left(Q_{\tau\tau'}^{+,-;\sigma,\sigma'}\right)^* \tag{F.34b}$$

$$Q_{\tau\tau'}^{+,+;\sigma,\sigma'} = (q_\tau^\sigma)^*\left(\bar q_{\tau'}^{\sigma'}\right)^* - (\bar q_\tau^\sigma)^*\left(q_{\tau'}^{\sigma'}\right)^*\ , \tag{F.34c}$$

$$Q_{\tau\tau'}^{-,-;\sigma,\sigma'} = -\left(Q_{\tau\tau'}^{+,+;\sigma,\sigma'}\right)^*\ . \tag{F.34d}$$

Let us regard the operators $\hat c_{\boldsymbol{k},\sigma}^{\alpha}$ as elements of vectors $\hat{\boldsymbol{c}}_{\boldsymbol{k}}^{\alpha}$. Then, the effective Hamiltonian $\hat H_0^{\rm eff}$ can be written in terms of matrix products,

$$\hat H_0^{\rm eff} = K_0 + \sum_{\boldsymbol{k}}\begin{pmatrix}\hat{\boldsymbol{c}}_{\boldsymbol{k}}^\dagger\\ \hat{\boldsymbol{c}}_{-\boldsymbol{k}}^-\end{pmatrix}^{\rm T}\begin{pmatrix}\tilde\varepsilon_{\boldsymbol{k}}^{+,-} & \tilde\varepsilon_{\boldsymbol{k}}^{+,+}\\ \tilde\varepsilon_{\boldsymbol{k}}^{-,-} & \tilde\varepsilon_{\boldsymbol{k}}^{-,+}\end{pmatrix}\begin{pmatrix}\hat{\boldsymbol{c}}_{\boldsymbol{k}}^-\\ \hat{\boldsymbol{c}}_{-\boldsymbol{k}}^\dagger\end{pmatrix}\ . \tag{F.35}$$

The matrix in (F.35) may be diagonalised by means of a Bogoliubov transformation

$$\begin{pmatrix}\hat{\boldsymbol{c}}_{\boldsymbol{k}}^-\\ \hat{\boldsymbol{c}}_{-\boldsymbol{k}}^\dagger\end{pmatrix} = \begin{pmatrix}\tilde u_{\boldsymbol{k}}^{-,-} & \tilde u_{\boldsymbol{k}}^{-,+}\\ \tilde u_{\boldsymbol{k}}^{+,-} & \tilde u_{\boldsymbol{k}}^{+,+}\end{pmatrix}\begin{pmatrix}\hat{\boldsymbol{h}}_{\boldsymbol{k}}^-\\ \hat{\boldsymbol{h}}_{-\boldsymbol{k}}^\dagger\end{pmatrix}\ , \tag{F.36}$$

where we introduced new fermionic operators $\hat{\boldsymbol{h}}_{\boldsymbol{k}}^{\alpha}$ and matrices $\tilde u_{\boldsymbol{k}}^{\alpha,\alpha'}$ with elements $\hat h_{\boldsymbol{k},\gamma}^{\alpha}$ and $u_{\sigma\gamma}^{\alpha,\alpha'}(\boldsymbol{k})$, respectively. For reasons of consistency, the matrices $\tilde u_{\boldsymbol{k}}^{\alpha,\alpha'}$ obey the symmetries

$$\tilde u_{-\boldsymbol{k}}^{+,+} = \left(\tilde u_{\boldsymbol{k}}^{-,-}\right)^*\ ,\quad \tilde u_{-\boldsymbol{k}}^{+,-} = \left(\tilde u_{\boldsymbol{k}}^{-,+}\right)^*\ . \tag{F.37}$$

The fermionic commutation rules of the new operators $\hat{\boldsymbol{h}}^{\alpha}_{\boldsymbol{k}}$ are ensured when the matrix in (F.36) is unitary. In (F.35)–(F.37) we have used the standard notations for the transposition $\tilde{M}^{\mathrm{T}}$, the complex conjugate $\tilde{M}^{*}$, and the Hermitian conjugate $\tilde{M}^{\dagger}$ of a matrix $\tilde{M}$.

After the diagonalisation, $\hat{H}_0^{\mathrm{eff}}$ becomes

$$\begin{aligned}\hat{H}_0^{\mathrm{eff}} &= K_0 + \frac{1}{2}\sum_{\boldsymbol{k}}\left(E_{\boldsymbol{k},\gamma}\hat{h}^{\dagger}_{\boldsymbol{k},\gamma}\hat{h}_{\boldsymbol{k},\gamma} - E_{\boldsymbol{k},\gamma}\hat{h}_{\boldsymbol{k},\gamma}\hat{h}^{\dagger}_{\boldsymbol{k},\gamma}\right)\\ &= K_0 + E_0 + \sum_{\boldsymbol{k}} E_{\boldsymbol{k},\gamma}\hat{h}^{\dagger}_{\boldsymbol{k},\gamma}\hat{h}_{\boldsymbol{k},\gamma}\;, \end{aligned} \tag{F.38}$$

where the real quantities $E_{\boldsymbol{k},\gamma} = \delta_{\gamma\gamma'}E_{\gamma\gamma'}(\boldsymbol{k})$ are the elements of the diagonal matrix

$$\tilde{E}_{\boldsymbol{k}} = 2\sum_{\alpha,\alpha'}\left(\tilde{u}^{(-\alpha)-}_{\boldsymbol{k}}\right)^{\dagger}\tilde{\varepsilon}^{\alpha,\alpha'}_{\boldsymbol{k}}\tilde{u}^{\alpha'-}_{\boldsymbol{k}}\;, \tag{F.39}$$

and

$$E_0 = -\frac{1}{2}\sum_{\boldsymbol{k}}\mathrm{Tr}\left(\tilde{E}_{\boldsymbol{k}}\right)\;. \tag{F.40}$$

For the derivation of equations (F.38)–(F.39), we have used the following symmetries of the matrices $\tilde{\varepsilon}^{\alpha,\alpha'}_{\boldsymbol{k}}$,

$$\tilde{\varepsilon}^{\alpha,\alpha'}_{-\boldsymbol{k}} = -\left(\tilde{\varepsilon}^{\alpha',\alpha}_{\boldsymbol{k}}\right)^{\mathrm{T}} = -\left(\tilde{\varepsilon}^{\alpha',\alpha}_{\boldsymbol{k}}\right)^{*} \qquad (\alpha \neq \alpha')\;, \tag{F.41a}$$

$$\tilde{\varepsilon}^{\alpha,\alpha}_{-\boldsymbol{k}} = -\left(\tilde{\varepsilon}^{\alpha,\alpha}_{\boldsymbol{k}}\right)^{\mathrm{T}} = -\left(\tilde{\varepsilon}^{\alpha',\alpha'}_{\boldsymbol{k}}\right)^{*} \qquad (\alpha \neq \alpha')\;. \tag{F.41b}$$

They follow from (F.32) and

$$\varepsilon^0_{\gamma',\gamma}(\boldsymbol{k}) = \left(\varepsilon^0_{\gamma,\gamma'}(\boldsymbol{k})\right)^{*} = \varepsilon^0_{\gamma,\gamma'}(-\boldsymbol{k})\;, \tag{F.42}$$

which results from the hermiticity of $\hat{H}_0$ and the fact that our electron-transfer amplitudes are real. Note that the matrices $\tilde{u}^{\alpha,\alpha'}_{\boldsymbol{k}}$, $\tilde{\varepsilon}^{\alpha,\alpha'}_{\boldsymbol{k}}$, the operators $\hat{h}^{\alpha}_{\boldsymbol{k},\gamma}$, and the energies $E_{\boldsymbol{k},\gamma}$ still depend on the parameters $\tilde{\lambda}^{\mathrm{i}}, \tilde{\eta}, \tilde{C}^0$. The Fermi gas ground state of (F.38) is given by

$$\left|\Psi_0\big(\tilde{\lambda}^{\mathrm{i}}, \tilde{\eta}, \tilde{C}^0\big)\right\rangle = \prod_{\boldsymbol{k},\gamma}{}' \hat{h}^{\dagger}_{\boldsymbol{k},\gamma}|\mathrm{vacuum}\rangle\;. \tag{F.43}$$

Here, the prime indicates that only those single-particle states with

$$E_{\boldsymbol{k},\gamma}\left(\tilde{\lambda}^{\mathrm{i}}, \tilde{\eta}, \tilde{C}^0\right) \leq E_{\mathrm{F}} \equiv 0 \tag{F.44}$$

are filled and

$$E^{\mathrm{SP}}\left(\tilde{\lambda}^{\mathrm{i}}, \tilde{\eta}, \tilde{C}^0\right) = K_0\left(\tilde{\eta}\right) + E_0\left(\tilde{\lambda}^{\mathrm{i}}, \tilde{\eta}, \tilde{C}^0\right) + \sum_{\boldsymbol{k},\gamma}{}' E_{\boldsymbol{k},\gamma}\left(\tilde{\lambda}^{\mathrm{i}}, \tilde{\eta}, \tilde{C}^0\right) \tag{F.45}$$

is the energy of the BCS-type ground state. In principle, the variational ground-state energy can now be calculated by a minimisation of the energy functional

$$\begin{aligned}E_{\mathrm{c}}(\tilde{\lambda}^{\mathrm{i}}, \tilde{C}^0, \tilde{\eta}, E_{\mathrm{F}}) &= E^{\mathrm{SP}}\left(\tilde{\lambda}^{\mathrm{i}}, \tilde{C}^0, \tilde{\eta}\right) + E^{\mathrm{at}}\left(\tilde{\lambda}^{\mathrm{i}}, \tilde{C}^0\right) + L\sum_{\sigma,\sigma'}\sum_{\alpha,\alpha'}\left(\eta^{\alpha,\alpha'}_{\sigma,\sigma'}C^{\alpha,\alpha'}_{\sigma,\sigma'} + \mathrm{c.c.}\right)\\ &\quad + LE_{\mathrm{F}}\Big(n - \sum_{\sigma} C^{+;-}_{\sigma,\sigma}\left(\tilde{\lambda}^{\mathrm{i}}, \tilde{C}^0\right)\Big)\end{aligned} \tag{F.46}$$

with respect to all parameters in $\tilde{\lambda}^{\mathrm{i}}, \tilde{C}^0, \tilde{\eta}, E_{\mathrm{F}}$.

F.3.2 Example: One-Band Hubbard Model

We introduced the correlation operator for a one-band model with a local order parameter Δ_0 in equation (F.7). It leads to the constraints (F.14), which can be used to express the three parameters $\lambda_\emptyset$, λ_s, λ_B in terms of the fourth parameter λ_d,

$$\begin{aligned} \lambda_1^2 &= 1 + x(m_d^0 - n_0) \,, \\ \lambda_\emptyset^2 &= \lambda_d^2 - x(1 - 2n_0) \,, \\ \lambda_B^2 &= 1 - \lambda_d^2 + x m_\emptyset^0 \,. \end{aligned} \tag{F.47}$$

Here, we introduced the abbreviation

$$x = \frac{B}{2A^2}\left(\sqrt{1 - \frac{4A^2C}{B^2}} - 1\right) \tag{F.48}$$

with

$$\begin{aligned} A &= \Delta_0^2 + (1 - 2n_0)m_\emptyset^0 \,, \\ B &= -4\lambda_d^2\Delta_0^2 m_\emptyset^0 + 2A(1 - \lambda_d^2)(1 - 2n_0) \,, \\ C &= (1 - \lambda_d^2)\left((1 - 2n_0)^2(1 - \lambda_d^2) - 4\Delta_0^2\lambda_d^2\right) \,. \end{aligned} \tag{F.49}$$

We work with a real pairing amplitude Δ_0 and assume that all quantities are spin-independent, i.e., it is $\lambda_1 \equiv \lambda_s$, $n_0 \equiv n_s^0$, and $m_1^0 \equiv m_s^0$.

The expectation value of the kinetic energy is given by

$$\sum_{i,j,s} t_{i,j}\langle \hat{c}_{i,s}^\dagger \hat{c}_{j,s}\rangle_{\mathrm{G}} = t_{i,j}\left(q^2\langle \hat{c}_{i,s}^\dagger \hat{c}_{j,s}\rangle_{\Psi_0} + \bar{q}^2\langle \hat{c}_{i,\bar{s}}\hat{c}_{j,\bar{s}}^\dagger\rangle_{\Psi_0}\right) \tag{F.50}$$

where we used

$$\sum_{i,j,s} t_{i,j}\langle \hat{c}_{i,s}^\dagger \hat{c}_{j,\bar{s}}^\dagger\rangle_{\Psi_0} = \sum_{i,j,s} t_{i,j}\langle \hat{c}_{i,s}\hat{c}_{j,\bar{s}}\rangle_{\Psi_0} = 0 \tag{F.51}$$

for real hopping parameters $t_{i,j}$. The renormalisation factors for normal and anomalous hopping, $q \equiv q_s^s$ and $\bar{q} \equiv |\bar{q}_s^{\bar{s}}|$, were introduced in equations (F.22).

The variational energy for the one-band Hubbard model then reads

$$E_{\mathrm{G}} = \langle \hat{H}\rangle_{\mathrm{G}} = Q\langle\Psi_0|\hat{H}_0|\Psi_0\rangle + Ud \equiv QE_0 + Ud \tag{F.52}$$

with the band-with renormalisation

$$Q \equiv q^2 - \bar{q}^2 \,, \tag{F.53}$$

and the double occupancy d given in equation (F.16). It has to be minimised with respect to λ_d and $|\Psi_0\rangle$ whereby the equations

$$\Delta_0 = \langle \hat{c}_{i,\uparrow}^\dagger \hat{c}_{i,\downarrow}^\dagger\rangle_{\Psi_0} \,, \tag{F.54a}$$

$$n_0 = \langle \hat{c}_{i,s}^\dagger \hat{c}_{i,s}\rangle_{\Psi_0} \,, \tag{F.54b}$$

and the normalisation of $|\Psi_0\rangle$ need to be obeyed. For this purpose, we introduce Lagrange parameters η_{n}, η_{s} and E^{SP}. Furthermore, we keep the average number of particles

$$\bar{n} = \frac{N}{L} \equiv n(\lambda_d, n_0, \Delta_0) = (2\lambda_1^2 m_1^0 + 2d) \,, \tag{F.55}$$

fixed by means of a Lagrange parameter E_{F}. The minimisation problem then becomes

$$\begin{aligned} E_0^{\mathrm{var}} &= \underset{\lambda_d,\eta_{\mathrm{n}},\eta_{\mathrm{s}},E_{\mathrm{F}},|\Psi_0\rangle}{\mathrm{Minimum}} \Big[E^{\mathrm{var}} - E^{\mathrm{SP}} \left(\langle\Psi_0|\Psi_0\rangle - 1\right) \\ &\quad + \eta_{\mathrm{s}} \sum_{i,\sigma} (\Delta_0 - \langle\Psi_0|\hat{c}^\dagger_{i,\uparrow}\hat{c}^\dagger_{i,\downarrow}|\Psi_0\rangle + \mathrm{c.c.}) \\ &\quad + \eta_{\mathrm{n}} \sum_{i,\sigma} (n_0 - \langle\Psi_0|\hat{c}^\dagger_{i,\sigma}\hat{c}_{i,\sigma}|\Psi_0\rangle) + E_{\mathrm{F}} L(\bar{n} - n(\lambda_d, n_0, \Delta_0)) \Big] \,. \end{aligned} \tag{F.56}$$

The minimisation with respect to $|\Psi_0\rangle$ can be carried out explicitly and leads to an effective Schrödinger equation in momentum space,

$$\hat{H}^{\mathrm{eff}}|\Psi_0\rangle = E^{\mathrm{SP}}|\Psi_0\rangle \,, \tag{F.57a}$$

$$\hat{H}^{\mathrm{eff}} = \sum_{\boldsymbol{k},\sigma} \varepsilon_{\boldsymbol{k}} \hat{c}^\dagger_{\boldsymbol{k},\sigma}\hat{c}_{\boldsymbol{k},\sigma} + \eta_{\mathrm{s}} \sum_{\boldsymbol{k}} (\hat{c}^\dagger_{\boldsymbol{k},\uparrow}\hat{c}^\dagger_{-\boldsymbol{k},\downarrow} + \mathrm{h.c.}) \tag{F.57b}$$

with

$$\varepsilon_{\boldsymbol{k}} = -\eta_{\mathrm{n}} + Q\varepsilon^0_{\boldsymbol{k}} \,, \tag{F.58a}$$

$$\varepsilon^0_{\boldsymbol{k}} = \frac{1}{L}\sum_{i,j} t_{i,j} e^{-\mathrm{i}k(i-j)} \,. \tag{F.58b}$$

The single-particle Schrödinger equation (F.57a) is readily solved,

$$\hat{H}^{\mathrm{eff}} = \sum_{\boldsymbol{k}} E_{\boldsymbol{k}} \left(\hat{h}^\dagger_{\boldsymbol{k},0}\hat{h}_{\boldsymbol{k},0} + \hat{h}^\dagger_{\boldsymbol{k},1}\hat{h}_{\boldsymbol{k},1} \right) + \mathrm{const.} \,, \tag{F.59}$$

by means of a Bogoliubov transformation

$$\hat{c}_{\boldsymbol{k},\uparrow} = u_{\boldsymbol{k}}\hat{h}_{\boldsymbol{k},0} + v_{\boldsymbol{k}}\hat{h}^\dagger_{-\boldsymbol{k},1} \,, \tag{F.60a}$$

$$\hat{c}^\dagger_{-\boldsymbol{k},\downarrow} = -v_{\boldsymbol{k}}\hat{h}_{\boldsymbol{k},0} + u_{\boldsymbol{k}}\hat{h}^\dagger_{-\boldsymbol{k},1} \,. \tag{F.60b}$$

Here, the real coefficients $u_{\boldsymbol{k}}$, $v_{\boldsymbol{k}}$ and the energies $E_{\boldsymbol{k}}$ are determined by the equations

$$E_{\boldsymbol{k}} = \varepsilon_{\boldsymbol{k}}(u^2_{\boldsymbol{k}} - v^2_{\boldsymbol{k}}) + 2\eta_{\mathrm{s}} u_{\boldsymbol{k}} v_{\boldsymbol{k}} \,, \tag{F.61a}$$

and

$$2\varepsilon_{\boldsymbol{k}} u_{\boldsymbol{k}} v_{\boldsymbol{k}} - \eta_{\mathrm{s}}(u^2_{\boldsymbol{k}} - v^2_{\boldsymbol{k}}) = 0 \quad , \quad u^2_{\boldsymbol{k}} + v^2_{\boldsymbol{k}} = 1 \,, \tag{F.61b}$$

which are solved by

$$E_{\boldsymbol{k}} = \mathrm{sign}(\varepsilon_{\boldsymbol{k}})\sqrt{\varepsilon^2_{\boldsymbol{k}} + \eta^2_{\mathrm{s}}} = \mathrm{sign}(\varepsilon^0_{\boldsymbol{k}})\sqrt{(Q\varepsilon^0_{\boldsymbol{k}} - \eta_{\mathrm{n}})^2 + \eta^2_{\mathrm{s}}} \,, \tag{F.62a}$$

$$u_{\boldsymbol{k}} = \frac{1}{\sqrt{2}}\sqrt{1 + \frac{\varepsilon_{\boldsymbol{k}}}{E_{\boldsymbol{k}}}} \,, \tag{F.62b}$$

$$v_{\boldsymbol{k}} = +\mathrm{sign}(\varepsilon_{\boldsymbol{k}}\eta_{\mathrm{s}})\frac{1}{\sqrt{2}}\sqrt{1 - \frac{\varepsilon_{\boldsymbol{k}}}{E_{\boldsymbol{k}}}} \,. \tag{F.62c}$$

The single-particle state $|\Psi_0\rangle$ has to be chosen as the ground state of (F.59)

$$|\Psi_0\rangle = \prod_{\boldsymbol{k}(E_{\boldsymbol{k}}<0)} h^\dagger_{\boldsymbol{k},0} h^\dagger_{\boldsymbol{k},1}|\mathrm{vac}\rangle \,. \tag{F.63}$$

In reference [138], it is shown that the eigenvalues (F.62a) in the effective Hamiltonian (F.59) can be interpreted as quasi-particle energies that might be measured in ARPES experiments. Therefore, the parameter η_{s} describes the superconducting gap and Q is a measure for the band-width renormalisation.

Appendix G

Connection with Constrained-Search Methods

The Gutzwiller theory, as derived in chapter 5, is based on the evaluation of multi-band Hubbard models. For the investigation of real materials, one has to connect this approach to an ab-initio method, e.g., the Density-Functional Theory. How this can be achieved is explained in section G.1. In section G.2, we discuss the connection between the Gutzwiller theory and the density-matrix functional theory, which was introduced in section 3.2.5.

G.1 Gutzwiller Theory and Density-Functional Theory

There are two ways to connect the Gutzwiller method to the density-functional theory. In our own numerical applications, see chapter 9, we have used the density-functional theory in order to set up a suitable multi-band Hubbard model to which we applied the Gutzwiller theory. How the relevant Hubbard model parameters can be extracted from ab-initio calculations will be briefly described in this section. Alternatively, one can try to implement the Gutzwiller energy functional into a modified density functional and solve the resulting equations self-consistently. We refer the reader to references [290, 291] where such methods have been proposed.

The Kohn-Sham equations (3.60) for a given material yield a band structure $E^{\mathrm{KS}}_{\boldsymbol{k},\gamma}$, which is hoped to cover correctly all contributions in the ab-initio Hamiltonian (2.3) except the local (atomic) Coulomb-interaction. In order to set up a Hubbard model, we needs to find a tight-binding Hamiltonian that reproduces the Kohn-Sham bands around the Fermi energy. To this end, we choose a large enough set of local orbitals with a hopping matrix $t^{\sigma,\sigma'}_{i,j}$ and local orbital potentials $\varepsilon_{i,\sigma}$, which are unspecified apart from constraints set by the symmetries of the lattice, see, e.g., reference [214] for cubic systems. The tight-binding fit yields a band structure $\tilde{E}_{\boldsymbol{k},\gamma}[\{t^{\sigma,\sigma'}_{i,j}\},\{\varepsilon_{i,\sigma}\}]$, which is still a function of $t^{\sigma,\sigma'}_{i,j}$ and $\varepsilon_{i,\sigma}$. The hopping parameters and the on-site energies can then be determined by minimising the cost function

$$Y[\{t^{\sigma,\sigma'}_{i,j}\},\{\varepsilon_{i,\sigma}\}] = \sum_{\boldsymbol{k},\gamma} \left(E^{\mathrm{KS}}_{\boldsymbol{k},\gamma} - \tilde{E}_{\boldsymbol{k},\gamma}[\{t^{\sigma,\sigma'}_{i,j}\},\{\varepsilon_{i,\sigma}\}]\right)^2 . \tag{G.1}$$

with respect to $t^{\sigma,\sigma'}_{i,j}$ and $\varepsilon_{i,\sigma}$. In practical applications, it is usually sufficient and more effective to include only a finite number of vectors $\boldsymbol{k}$ on high symmetry points in the sum (G.1). An alternative scheme to this tight-binding fit procedure is the downfolding method, see, e.g., [293] and references therein. If carried our with a sufficiently large orbital basis, both methods should lead to very similar tight-binding Hamiltonians.

Apart from technical details, it is clear how a tight-binding Hamiltonian can be extracted from the Kohn-Sham equations. The situation is very different for the local Coulomb interaction in (2.15). Obviously, the Coulomb parameters in the Hubbard model are not given by their bare values in (2.3d). Instead, they are effective parameters, which, to a certain extent, already contain screening effects, covered by the underlying density-functional calculation. Since the meaning of the Kohn-Sham equations for the physical many-particle system is basically unclear, it is also impossible to formulate a controlled way to extract local Coulomb parameters from such ab-initio calculations.

A frequently employed technique is the 'constrained LDA' method, which can give an estimate of a direct Hubbard U and an exchange parameter J. Due to the fundamental ambiguity of such procedures, however, we do not believe that the values extracted from such calculations should be taken too seriously. Therefore, for our own calculations, we found it inevitable to determine the Coulomb parameters by a mixture of symmetry arguments and a fitting to experimental data. In the case of transition metals, e.g., we work with a spherical approximation that leads to the three Racah parameters A, B, and C, see appendix C. The parameter A is then chosen in order to reproduce the experimental band width, while the parameters B and C follow from spectroscopy experiments of the corresponding transition-metal ions.

G.2 Gutzwiller Theory and Density-Matrix Functional Theory

In the second part of this appendix, we show that the Gutzwiller variational theory provides a feasible way to evaluate density-matrix functionals for multi-band Hubbard models. As argued in section 3.2.5, for a given Hubbard Hamiltonian

$$\hat{H}_{\mathrm{H}} = \sum_{i,j} \sum_{\sigma,\sigma'} t_{i,j}^{\sigma,\sigma'} + \sum_{i} \sum_{\Gamma} E_{\Gamma} \hat{m}_{i,\Gamma} \tag{G.2}$$

there exists a universal functional $E_{\mathrm{loc}}(\tilde{\rho})$ of the density matrix $\tilde{\rho}$ with the elements $\rho_{i,j}^{\sigma,\sigma'}$ such that the ground-state energy and the ground-state density matrix are obtained from the minimisation of

$$E[\tilde{\rho}] = \sum_{i,j} \sum_{\sigma,\sigma'} t_{i,j}^{\sigma,\sigma'} \rho_{i,j}^{\sigma,\sigma'} + E_{\mathrm{loc}}(\tilde{\rho}) \; . \tag{G.3}$$

The functional $E_{\mathrm{loc}}(\tilde{\rho})$ cannot be calculated exactly in most cases and, therefore, the theorem in itself is of limited use. The Gutzwiller theory, however, provides a feasible way to calculate $E_{\mathrm{loc}}(\tilde{\rho})$. In the Gutzwiller theory, the local interaction is a function of the independent variational parameters $\lambda^{\mathrm{i}}_{\Gamma,\Gamma'}$ and of the local uncorrelated density matrix, see equations 5.65 and (5.48). The same holds true for the correlated density matrix, which is given in equations (5.78) and (5.71) for $i \neq j$ and $i = j$, respectively. Therefore, the functional $E_{\mathrm{loc}}(\tilde{\rho})$ is given by a minimisation of E_{loc} with respect to $\lambda^{\mathrm{i}}_{\Gamma,\Gamma'}$ and $|\Psi_0\rangle$ where, as a constraint, the correlated density matrix $\tilde{\rho}$ is kept constant. In the future, we shall investigate the issue, whether or not the calculation of a functional $E_{\mathrm{loc}}(\tilde{\rho})$ can lead to an improved minimisation algorithm.

As a simple example, we consider the two-site Hubbard model, for which we can compare the local energy functional to the exact result as derived in appendix (B.2). We only consider the paramagnetic solution despite the fact that, as shown in section 5.4.2, it becomes unstable for $U > U_{\mathrm{C}}$. Like in the exact solution, we have to write the interaction energy as a function of the hopping expectation value T, equation (B.15). At half filling this expectation value in the Gutzwiller theory is given by

$$T = q(d) T_0 \tag{G.4}$$

with $q(d)$ defined in (5.112) and $T_0 = \pm 1/2$ where T_0 has the opposite sign of t. This equation yields the double occupancy

$$d(T) = \frac{1}{4}(1 - \sqrt{1 - T/T_0}) \tag{G.5}$$

and, hence, the energy functional reads

$$E_{\mathrm{G}}(T) = -4tT + 2Ud(T) \; . \tag{G.6}$$

Note that the functional $d(T)$ differs from the exact result (B.18) by the exponent of T/T_0. This difference in the exponent leads to qualitatively different results only in the large-U limit, i.e., for $T/T_0 \to 0$. It has been argued in references [85–88] that the functional (B.18) is also a good approximation for one-dimensional Hubbard models with an arbitrary number of lattice sites. The authors even suggested that it could be a good starting point for the investigation of two or three-dimensional Hubbard models, see [88].

The energy functional $E_{\mathrm{G}}(T)$ and the exact result (B.20) are displayed for several values of t in figure B.1. Not surprisingly, the functional agrees relatively well with the exact result for large t. For $t < U/8$, the Gutzwiller functional has its minimum at $T = 0$, which represents the spurious paramagnetic Brinkman-Rice state without double occupancies where all particles are localised ($q = 0$).

Appendix H

Numerical Minimisation of the Gutzwiller Energy Functional

The strategy for the minimisation of the Gutzwiller energy functional, which we introduced in section 5.3, was only useful for the determination of quasi-particle energies in section 7.3. For the actual numerical minimisation of the multi-band energy functional, one has to employ different strategies, which we discuss in this appendix.

The Gutzwiller energy functional, for a translationally invariant system, has the form

$$E_{\mathrm{G}}\big(\boldsymbol{v}, \tilde{C}^0, |\Psi_0\rangle\big) = L \sum_{\sigma_1,\sigma_2,\sigma_1',\sigma_2'} q_{\sigma_1}^{\sigma_1'} q_{\sigma_2}^{\sigma_2'} E_{\sigma_1,\sigma_2,\sigma_1',\sigma_2'} + L \sum_{Z,Z'} U_{Z,Z'} v_Z v_{Z'} \;, \tag{H.1}$$

where we used the abbreviation v_Z for the n_{v} variational parameters

$$v_Z = \frac{\lambda_{\Gamma,\Gamma'}}{\sqrt{m_\Gamma^0 m_{\Gamma'}^0}} \;, \tag{H.2}$$

which are considered as the elements of a vector $\boldsymbol{v}$. In our calculations on transition metals, we found the inner minimisation, as described in the following section, to be faster by orders of magnitude if we use the variational parameters (H.2) instead of $\lambda_{\Gamma,\Gamma'}$. So far, we have not found a satisfactory explanation for this numerical observation.

In equation (H.1), we introduced the tensor

$$E_{\sigma_1,\sigma_2,\sigma_1',\sigma_2'} \equiv \frac{1}{L} \sum_{\boldsymbol{k}} \varepsilon_{\boldsymbol{k};\sigma_1,\sigma_2} \big\langle \hat{c}^\dagger_{\boldsymbol{k},\sigma_1'} \hat{c}_{\boldsymbol{k},\sigma_2'} \big\rangle_{\Psi_0} \tag{H.3}$$

where $\varepsilon_{\boldsymbol{k};\sigma_1\sigma_2}$ is defined in equation (5.98b). The renormalisation matrix

$$q_\sigma^{\sigma'}(\boldsymbol{v}) = \sum_{Z,Z'} S_\sigma^{\sigma'}(Z,Z') v_Z v_{Z'} \tag{H.4}$$

is a function of the variational parameters v_Z and of the local non-interacting density matrix $\tilde{C}^0$; see equations (5.80) and (5.65), from which the explicit form of the coefficients $S_\sigma^{\sigma'}(Z,Z')$ and $U_{Z,Z'}$ can be derived. To keep notations simple in this appendix, we assume that all quantities are real. A generalisation of the algorithms for energy functionals that contain complex numbers is straightforward.

H.1 'Inner' Minimisation

We consider the energy functional

$$e_{\mathrm{G}}(\boldsymbol{v}) = \sum_{\sigma_1,\sigma_2,\sigma_1',\sigma_2'} q_{\sigma_1}^{\sigma_1'} \bar{q}_{\sigma_2}^{\sigma_2'} + \sum_{Z,Z'} U_{Z,Z'} v_Z v_{Z'} \,, \tag{H.5}$$

in which the single-particle state $|\Psi_0\rangle$ and, consequently, the local density matrix $\tilde{C}^0$ and the tensor (H.3) are fixed. In (H.5) we introduced

$$\bar{q}_{\sigma}^{\sigma'}(\boldsymbol{v}) \equiv \sum_{Z,Z'} \bar{S}_{\sigma}^{\sigma'}(Z,Z') v_Z v_{Z'} \tag{H.6}$$

with the coefficients

$$\bar{S}_{\sigma_1}^{\sigma_1'} \equiv \sum_{\sigma_2,\sigma_2'} E_{\sigma_1,\sigma_2,\sigma_1',\sigma_2'} S_{\sigma_2}^{\sigma_2'}(Z,Z') \,. \tag{H.7}$$

The variational parameters v_Z have to obey the constraints (5.48), which, for a fixed local density matrix, have the form

$$g_i(\boldsymbol{v}) = \sum_{Z,Z'} f_i(Z,Z') v_Z v_{Z'} = 0 \,. \tag{H.8}$$

An explicit expression of the coefficients $f_i(Z,Z')$ can be derived from equations (5.48). The n_{c} constraints (H.8) define a $(n_{\mathrm{v}} - n_{\mathrm{c}})$-dimensional manifold $\mathcal{M}_{\mathrm{c}}$ in the n_{v}-dimensional space $\mathcal{V}$ of variational parameters v_Z. In general, it is impossible to impose the constraints (H.8) analytically. Therefore, one needs to find an efficient numerical strategy to cope with them, see below.

The constraints (H.8), the local energy in (H.5), and the renormalisation matrices $\bar{q}_{\sigma}^{\sigma'}$ and $q_{\sigma}^{\sigma'}$ are all quadratic with respect to the variational parameters v_Z. Therefore, for a given vector $\boldsymbol{v} \in \mathcal{V}$, the gradients of all these quantities with respect to the parameters v_Z can be calculated quite easily. We denote the gradients of the constraints and of the energy as $\boldsymbol{F}^i(\boldsymbol{v})$ and $\boldsymbol{E}(\boldsymbol{v})$, respectively. Their elements are given by

$$F_Z^i(\boldsymbol{v}) \equiv \frac{\partial}{\partial v_Z} g_i(\boldsymbol{v}) \,, \tag{H.9}$$

and

$$E_Z(\boldsymbol{v}) \equiv \frac{\partial}{\partial v_Z} e_{\mathrm{G}}(\boldsymbol{v}) \,. \tag{H.10}$$

We aim at a minimisation of the energy (H.5) in the manifold $\mathcal{M}_{\mathrm{c}}$ defined by the constraints (H.8). To this end, we can always start our minimisation in the uncorrelated limit, i.e., at the point $\boldsymbol{v}_0$ (with $\lambda_{\Gamma,\Gamma'} = \delta_{\Gamma,\Gamma'}$) for which $\boldsymbol{v}_0 \in \mathcal{M}_{\mathrm{c}}$ is automatically fulfilled. Numerical strategies that try to move exactly along $\mathcal{M}_{\mathrm{c}}$ are quite cumbersome. Therefore, starting from a certain point $\boldsymbol{v}_0 \in \mathcal{M}_{\mathrm{c}}$, we allow the minimisation algorithm to violate the constraints by making 'short' steps to points $\boldsymbol{v}_1 \notin \mathcal{M}_{\mathrm{c}}$. To keep the violation of the constraints minimal, these steps have to take place in the subspace $\mathcal{M}_{\parallel}(\boldsymbol{v}_0)$ that is tangential to $\mathcal{M}_{\mathrm{c}}$ at the point $\boldsymbol{v}_0$. The direction of a step in $\mathcal{M}_{\parallel}(\boldsymbol{v}_0)$ is determined by the tangential component of the gradient $\boldsymbol{E}(\boldsymbol{v}_0)$ since it leads to a decrease of the energy.

In summary, and more precisely, the above ideas lead to the following algorithm for the 'inner' minimisation, i.e., the minimisation of (H.5) with respect to the parameters v_Z:

i) Find a point $\boldsymbol{v}_0$ in the variational parameter space $\mathcal{V}$ that obeys the constraints (H.8) (i.e, $\boldsymbol{v}_0 \in \mathcal{M}_{\rm c}$).

ii) Calculate the gradients $\boldsymbol{F}^i(\boldsymbol{v}_0)$ and $\boldsymbol{E}(\boldsymbol{v}_0)$.

iii) Determine the component $\boldsymbol{E}_\parallel(\boldsymbol{v}_0)$ of $\boldsymbol{E}(\boldsymbol{v}_0)$ in $\mathcal{M}_\parallel(\boldsymbol{v}_0)$ by the following procedure: The gradient $\boldsymbol{E}(\boldsymbol{v}_0)$ is written as

$$\boldsymbol{E}(\boldsymbol{v}_0) = \boldsymbol{E}_\parallel(\boldsymbol{v}_0) + \boldsymbol{E}_\perp(\boldsymbol{v}_0) \; , \tag{H.11}$$

where the tangential component $\boldsymbol{E}_\parallel(\boldsymbol{v}_0)$ is defined by

$$\boldsymbol{E}_\parallel(\boldsymbol{v}_0) \cdot \boldsymbol{F}^i(\boldsymbol{v}_0) = 0 \quad \forall i \; . \tag{H.12}$$

The perpendicular component can be expressed a linear combination

$$\boldsymbol{E}_\perp(\boldsymbol{v}_0) = \sum_{i=1}^{n_{\rm c}} \alpha_i \boldsymbol{F}^i(\boldsymbol{v}_0) \tag{H.13}$$

of the vectors $\boldsymbol{F}^i(\boldsymbol{v}_0)$. In order to determine the coefficients α_i, we multiply equation (H.11) with a vector $\boldsymbol{F}^j(\boldsymbol{v}_0)$ and use the expansion (H.13). This leads to

$$\boldsymbol{E}(\boldsymbol{v}_0) \cdot \boldsymbol{F}^j(\boldsymbol{v}_0) = \sum_i \boldsymbol{F}^i(\boldsymbol{v}_0) \cdot \boldsymbol{F}^j(\boldsymbol{v}_0) \alpha_i = \sum_i W_{j,i}(\boldsymbol{v}_0) \alpha_i \; , \tag{H.14}$$

where we used equation (H.12) and introduced the (symmetric) matrix $\tilde{W}(\boldsymbol{v})$ with the elements

$$W_{i,j}(\boldsymbol{v}) \equiv \boldsymbol{F}^i(\boldsymbol{v}) \cdot \boldsymbol{F}^j(\boldsymbol{v}) \; . \tag{H.15}$$

Now we are in the position to determine the coefficients α_i by an inversion of $\tilde{W}(\boldsymbol{v}_0)$, which yields

$$\alpha_i = \sum_j [\tilde{W}(\boldsymbol{v}_0)]^{-1}_{i,j} \left(\boldsymbol{E}(\boldsymbol{v}_0) \cdot \boldsymbol{F}^j(\boldsymbol{v}_0) \right) \; . \tag{H.16}$$

The inverse of the matrix $\tilde{W}(\boldsymbol{v}_0)$ is well defined as long as the vectors $\boldsymbol{F}^i(\boldsymbol{v}_0)$ are linearly independent. A linear dependency of these vectors can only arise if certain constraints (H.8) are redundant. In that case, the redundant constraints have to be eliminated right from the start. With the coefficients (H.16), we find

$$\boldsymbol{E}_\parallel(\boldsymbol{v}_0) = \boldsymbol{E}(\boldsymbol{v}_0) - \sum_i \alpha_i \boldsymbol{F}^i(\boldsymbol{v}_0) \; . \tag{H.17}$$

for the tangential component of $\boldsymbol{E}(\boldsymbol{v}_0)$.

iv) Make a 'proper' step in the direction of $-\boldsymbol{E}_\parallel(\boldsymbol{v}_0)$ to a new vector

$$\bar{\boldsymbol{v}}_1 = \boldsymbol{v}_0 - \beta \boldsymbol{E}_\parallel(\boldsymbol{v}_0) \; . \tag{H.18}$$

For the choice of the parameter β, various strategies are conceivable. Since the point $\bar{\boldsymbol{v}}_1$ is not in $\mathcal{M}_{\rm c}$, the energy gain is not necessarily a useful criterion and to determine it is also rather time consuming. Instead, we calculate

$$\Delta g(\bar{\boldsymbol{v}}_1) \equiv \sum_i [g_i(\bar{\boldsymbol{v}}_1)]^2 \geq 0 \tag{H.19}$$

as a measure for the violation of the constraints and choose the parameter β such that Δg does not exceed a certain critical value $\Delta g_{\rm c}$. This critical value can be automatically adjusted by the algorithm to ensure that, after returning to the hypersurface $\mathcal{M}_{\rm c}$, there is a sufficient energy gain.

v) In order to return to $\mathcal{M}_c$ from the point $\bar{\boldsymbol{v}}_1 \notin \mathcal{M}_c$, the following algorithm turned out to be useful: We seek a vector $\boldsymbol{v}_1$ that solves the constraint equations $g_i(\boldsymbol{v}_1) = 0$ and is as close as possible to $\bar{\boldsymbol{v}}_1$. To this end, we could calculate the gradients $\boldsymbol{F}^i(\bar{\boldsymbol{v}}_1)$ and try to solve the set of equations

$$g_i\left(\bar{\boldsymbol{v}}_1 + \sum_j \gamma_j \boldsymbol{F}^j(\bar{\boldsymbol{v}}_1)\right) = 0 \tag{H.20}$$

by a proper choice of the coefficients γ_j. Such an exact solution of equations (H.20), however, is quite time consuming. Therefore, we consider the linear set of equations

$$g_i(\bar{\boldsymbol{v}}_1) + \sum_j W_{i,j}(\bar{\boldsymbol{v}}_1)\gamma_j = 0 \;, \tag{H.21}$$

which results from an expansion of (H.20) to leading order in γ_j. Equations (H.21) can be readily solved by an inversion of the matrix $W_{i,j}(\bar{\boldsymbol{v}}_1)$,

$$\gamma_j = -\sum_i [W(\bar{\boldsymbol{v}}_1)]^{-1}_{j,i} g_i(\bar{\boldsymbol{v}}_1) \;, \tag{H.22}$$

which yields a new vector

$$\bar{\boldsymbol{v}}_1 \to \bar{\boldsymbol{v}}_1' = \bar{\boldsymbol{v}}_1 + \sum_j \gamma_j \boldsymbol{F}^j(\bar{\boldsymbol{v}}_1) \;. \tag{H.23}$$

This vector, in general, is not yet a solution of $g_i(\bar{\boldsymbol{v}}_1')$; however, it is usually closer to $\mathcal{M}_c$ than $\bar{\boldsymbol{v}}_1$ because $\Delta g(\bar{\boldsymbol{v}}_1') < \Delta g(\bar{\boldsymbol{v}}_1)$. By an iteration of equations (H.21)-(H.23) we eventually approach a vector $\boldsymbol{v}_1 \in \mathcal{M}_c$.

vi) If $e_G(\boldsymbol{v}_1) < e_G(\boldsymbol{v}_0)$ we restart the procedure at point ii) with $\boldsymbol{v}_0$ replaced by $\boldsymbol{v}_1$. In case that $e_G(\boldsymbol{v}_1) > e_G(\boldsymbol{v}_0)$, the critical value Δg_c has to be lowered and the algorithm continues with point iv). A useful measure for the convergence of the whole iteration is the norm of $\boldsymbol{E}_{\|}$. This number goes to zero near a minimum $\boldsymbol{v}_{\min}$ of the energy functional $e_G(\boldsymbol{v})$ for vectors $\boldsymbol{v} \in \mathcal{M}_c$.

H.2 'Outer' Minimisation

With the optimum variational parameters $\boldsymbol{v}_{\min}$ from the inner minimisation described in H.1, we find a new effective single-particle Hamiltonian $\hat{H}_0^{\text{eff}}$, equation (5.97). If we want to fix the local density matrix $C^0_{\sigma,\sigma'}$ at the value that was used during the previous inner minimisation, we have to adjust the Lagrange parameters $\eta_{\sigma,\sigma'}$ in $\hat{H}_0^{\text{eff}}$ accordingly. With the new ground state $|\Psi_0\rangle$ of $\hat{H}_0^{\text{eff}}$, we can start another run of the inner minimisation. Eventually, after a certain number of iterations one finds a constant solution, which yields the lowest energy for a fixed density matrix $C^0_{\sigma,\sigma'}$. To find the total minimum of the energy, one has to repeat this procedure for various values of $C^0_{\sigma,\sigma'}$. In this way, one determines the optimum local density matrix and the corresponding variational ground-state energy.

The minimisation strategy, which we just discussed, is obviously rather inefficient, since it takes a lot of time to determine the parameters $\eta_{\sigma,\sigma'}$ for a given local density matrix $C^0_{\sigma,\sigma'}$. A somewhat better approach results when we keep constant the set of Lagrange parameters $\eta_{\sigma,\sigma'}$ instead of $C^0_{\sigma,\sigma'}$ during the self-consistency cycle of the inner minimisation. However, this strategy also is only feasible for a small number of parameters $\eta_{\sigma,\sigma'}$. In the case that there are

many of such 'external' degrees of freedom in our variational problem, we have to employ a different algorithm, which will be discussed in the following.

In the variational ground state, the Lagrange parameters $\eta_{\sigma,\sigma'}$ are given by

$$\eta_{\sigma,\sigma'} = -\frac{\partial}{\partial C^0_{\sigma,\sigma'}} E_{\mathrm{G}}\big(\{\tilde{\lambda}^{\mathrm{i}}\}, \{\tilde{C}^0\}, |\Psi_0\rangle\big) \,, \tag{H.24}$$

which follows from the ground-state condition

$$\frac{\partial}{\partial C^0_{\sigma,\sigma'}} E_c(\ldots) = 0 \tag{H.25}$$

for the functional (5.94). It seems natural that equation (H.24) yields a reasonable guess for the parameters $\eta_{\sigma,\sigma'}$ even if the minimum of the energy functional has not yet been reached. This assumption leads us to the following algorithm for the outer minimisation:

i) Set $q^{\sigma'}_{\sigma} = \delta_{\sigma,\sigma'}$ and choose a reasonable set of Lagrange parameters $\eta^0_{\sigma,\sigma'}$, e.g., $\eta^0_{\sigma,\sigma'} = -\varepsilon_{\sigma,\sigma'}$ with the bare on-site energies $\varepsilon_{\sigma,\sigma'}$ in the local Hamiltonian (4.1).

ii) Find the ground state $|\Psi_0\rangle$ of the effective Hamiltonian $\hat{H}^{\mathrm{eff}}_0$ and determine $\tilde{C}^0$ and $E_{\sigma_1,\sigma_2,\sigma'_1,\sigma'_2}$.

iii) Carry out an internal minimisation as described in section H.1.

iv) A direct calculation of new parameters $\eta_{\sigma,\sigma'}$ with equation (H.24) is prevented by the fact that, in the energy functional $E_{\mathrm{G}}(\ldots)$, the constraints are already fulfilled explicitly. Therefore, we determine a new set of parameters $\eta^1_{\sigma,\sigma'}$ as follows:

   With the single-particle wave function $|\Psi_0\rangle$ fixed, the energy is a functional $E^{\mathrm{e}}(\boldsymbol{w})$ of the $(n_{\mathrm{v}} + n_{\mathrm{d}})$ parameters $C^0_{\sigma,\sigma'}$ and v_z, which are now considered as the elements w_y of a joint vector $\boldsymbol{w}$. Here, n_{d} is the number of finite elements in $C^0_{\sigma,\sigma'}$ and the components w_y of $\boldsymbol{w}$ with $1 \leq y \leq n_{\mathrm{d}}$ correspond to $C^0_{\sigma,\sigma'}$. The vector $\boldsymbol{w}$ that was found within the inner minimisation in iii) is denoted as $\boldsymbol{w}_0$. With respect to the enlarged parameter space of vectors $\boldsymbol{w}$, we define the gradients $\boldsymbol{E}(\boldsymbol{w})$ and $\boldsymbol{F}^i(\boldsymbol{w})$ of the energy and the constraints, respectively. In the same way as described in the previous section for the inner minimisation, we can determine the component $\boldsymbol{E}_{\|}(\boldsymbol{w}_0)$ of the energy gradient $\boldsymbol{E}(\boldsymbol{w}_0)$ that is tangential to the hypersurface defined by the constraints, see equations (H.11)-(H.17). The first n_{d} components of $\boldsymbol{E}_{\|}(\boldsymbol{w}_0)$ give us the derivatives of the energy with respect to $C^0_{\sigma,\sigma'}$ where the constraints are taken into account. Therefore, we choose

$$\eta^1_{\sigma,\sigma'} = -[\boldsymbol{E}_{\|}(\boldsymbol{w}_0)]_y \tag{H.26}$$

   with $1 \leq y \leq n_{\mathrm{d}}$ as a new set of Lagrange parameters, which are used for a next step of the iteration that starts at point ii). A local minimum of the energy is reached if we find $\eta^1_{\sigma,\sigma'} \approx \eta^0_{\sigma,\sigma'}$ in our iterative procedure.

The iterative procedure i)-iv) turns out to be very fast for systems that we have investigated so far and leads to sensible minima within approximately ten iterative cycles. It is therefore a very useful tool for the investigation of systems for which the large number of Lagrange parameters $\eta_{\sigma,\sigma'}$ prevents a scan of the entire variational space. Convergence problems with the iterative procedure might occur if there is more than one local minimum of the energy. In that case, the algorithm may have to be supported by a manual scan of the variational space in order to avoid oscillations between local minima.

Bibliography

[1] J. Solynom. *Fundamentals of the Physics of Solids, Volume 1.* Springer, Berlin, Heidelberg, New York, first edition, 2007.

[2] A. Messiah. *Quantum Mechanics, Volume 2.* North-Holland Publishing Company, Amsterdam, 1963.

[3] J. W. Negele and H. Orland. *Quantum Many-Particle Systems.* Addison-Wesley, New York, 1988.

[4] M. Born and J. R. Oppenheimer. *Ann. Phys.*, 84:457, 1927.

[5] J. M. Ziman. *Electrons and Phonons.* Clarendon Press, Oxford, 1962.

[6] P.-O. Löwdin. *J. Chem. Phys.*, 18:365, 1950.

[7] J. Hubbard. *Proc. R. Soc. A*, 276:238, 1963.

[8] J. Hubbard. *Proc. R. Soc. A*, 277:237, 1964.

[9] J. Hubbard. *Proc. R. Soc. A*, 281:401, 1964.

[10] F. H. L. Essler, H. Frahm, F. Göhmann, A. Klümper, and V. E. Korepin. *The One-Dimensional Hubbard Model.* Cambridge University Press, Cambridge, UK, 2005.

[11] A. Georges, G. Kotliar, W. Krauth, and M. J. Rozenberg. *Rev. Mod. Phys.*, 68:13, 1996.

[12] F. Gebhard. *The Mott Metal-Insulator Transition – Models and Methods.* Springer, Heidelberg, 1997.

[13] D. K. Campbell, J. T. Gammel, and E. Y. Loh. *Phys. Rev. B*, 38:12043, 1988.

[14] J. E. Hirsch. *Phys. Rev. B*, 40:2354, 1989.

[15] J. E. Hirsch. *Phys. Rev. B*, 40:9061, 1989.

[16] J. E. Hirsch. *Phys. Rev. B*, 42:771, 1990.

[17] D. Vollhardt, N. Blümer, K. Held, M. Kollar, J. Schlipf, and M. Ulmke. *Z. Phys. B*, 103:283, 1997.

[18] J. Wahle, N. Blümer, J. Schlipf, K. Held, and D. Vollhardt. *Phys. Rev. B*, 59:12749, 1998.

[19] A. Schiller, P. Kumar, R. Strack, and D. Vollhardt. *Phys. Rev. B*, 51:8337, 1995.

[20] W. Metzner. *Phys. Rev. B*, 43:8549, 1991.

[21] E. Kalinowski and F. Gebhard. *J. Low Temp. Phys.*, 76:979, 2002.

[22] M. P. Eastwood, F. Gebhard, E. Kalinowski, S. Nishimoto, and R. M. Noack. *Eur. Phys. J. B*, 35:155, 2003.

[23] N. Blümer and E. Kalinowski. *Phys. Rev. B*, 71:195102, 2005.

[24] N. Blümer and E. Kalinowski. *Physica B*, 359:648, 2005.

[25] A. B. Harris and R. V. Lange. *Phys. Rev.*, 157:295, 1967.

[26] J. E. Hirsch. *Phys. Rev. Lett*, 54:1317, 1985.

[27] C. Gros, R. Joynt, and T. M. Rice. *Phys. Rev. B*, 36:381, 1987.

[28] P. G. J. van Dongen. *Phys. Rev. B*, 49:7904, 1994.

[29] A. Paramekanti, M. Randeria, and N. Trivedi. *Phys. Rev. B*, 70:054504, 2004.

[30] G. D. Mahan. *Many Particle Physics*. Springer, Berlin, 2005.

[31] D. J. Thouless. *The Quantum Mechanics of Many-Body Systems*. Academic Press, New York, 1972.

[32] T. Koopmans. *Physica*, 1:104, 1933.

[33] H. J. Monkhorst. *Phys. Rev. B*, 20:1504, 1979.

[34] J. M. Luttinger. *Phys. Rev.*, 121:942, 1961.

[35] D. Pines and P. Nozières. *The Theory of Quantum Liquids*. Benjamin, New York, 1966.

[36] P. Nozières. *Theory of interacting Fermi-systems*. Addison-Wesley, Reading, 1997.

[37] A. W. Overhauser. *Phys. Rev. Lett*, 4:462, 1960.

[38] A. W. Overhauser. *Phys. Rev.*, 128:1437, 1962.

[39] A. Svane. *Phys. Rev. B*, 35:5496, 1987.

[40] L. H. Thomas. *Proc. Cambridge Phil. Soc.*, 23:542, 1927.

[41] E. Fermi. *Rend. Accad. Naz. Linzei*, 6:602, 1927.

[42] E. Fermi. *Z. Phys*, 48:73, 1928.

[43] P. A. M. Dirac. *Proc. Cambridge Phil. Soc.*, 26:376, 1930.

[44] C. F. Weizsäcker. *Z. Phys.*, 96:431, 1935.

[45] P. Hohenberg and W. Kohn. *Phys. Rev.*, 136:864, 1964.

[46] M. Levy. *Proc. Natl. Acad. Sci. USA*, 76:6062, 1979.

[47] K. Schönhammer, O. Gunnarsson, and R. M.Noack. *Phys. Rev. B*, 52:2504, 1995.

[48] W. Kohn and L. J. Sham. *Phys. Rev.*, 140:1133, 1965.

[49] R. O. Jones and O. Gunnarsson. *Rev. Mod. Phys.*, 61:689, 1989.

[50] R. M. Dreizler and E. K. U. Gross. *Density Functional Theory.* Springer, Berlin, 1990.

[51] H. Eschrig. *The Fundamentals of Density Functional Theory.* Teubner, Stuttgart, 1996.

[52] J. C. Slater. *Phys. Rev.*, 81:386, 1951.

[53] J. C. Slater. *The Self-Consistent Field for Molecules and Solids, Vol. IV.* McGraw-Hill, New York, 2007.

[54] L. Hedin and B. I. Lundquist. *J. Phys. C*, 4:2064, 1971.

[55] U. von Barth and L. Hedin. *J. Phys. C*, 5:1629, 1972.

[56] O. Gunnarsson and B. I. Lundquist. *Phys. Rev. B*, 13:4274, 1976.

[57] S. M. Dunaevskii. *Sov. Phys. Sol. State*, 20:1483, 1978.

[58] S. H. Vosko, L. Wilk, and M. Nusair. *Can. J. Phys.*, 58:1200, 1980.

[59] J. P. Perdew and A. Zunger. *Phys. Rev. B*, 23:5048, 1981.

[60] M. Levy. *Phys. Rev. A*, 26:1200, 1982.

[61] E. H. Lieb. *Int. J. Quant. Chem.*, 24:243, 1983.

[62] L. Hedin. *Phys. Rev.*, 139:A796, 1965.

[63] B. I. Lundquist. *Phys. Konsens. Mater*, 6:193, 1967.

[64] B. I. Lundquist. *Phys. Konsens. Mater*, 6:206, 1967.

[65] B. I. Lundquist. *Phys. Konsens. Mater*, 7:117, 1968.

[66] F. Aryasetiawan and O. Gunnarsson. *Rep. Prog. Phys.*, 61:237, 1998.

[67] T. L. Gilbert. *Phys. Rev. B*, 12:2111, 1975.

[68] S. Goedecker and C. J. Umrigar. *Phys. Rev. Lett*, 81:866, 1998.

[69] G. Csanyi and T. A. Arias. *Phys. Rev. B*, 61:7348, 2000.

[70] G. Csanyi, S. Goedecker, and T. A. Arias. *Phys. Rev. A*, 65:032510, 2002.

[71] M. A. Buijse and E. J. Baerends. *Mol. Phys.*, 100:2002, 401.

[72] K. Yasuda. *Phys. Rev. Lett*, 88:053001, 2002.

[73] J. Cioslowski, K. Pernal, and M. Buchowiecki. *J. Chem. Phys.*, 119:6443, 2003.

[74] C. Kollmar. *J. Chem. Phys.*, 121:11581, 2004.

[75] K. Pernal and J. Cioslowski. *J. Chem. Phys.*, 120:5987, 2004.

[76] O. Gritsenko, K. Pernal, and E. J. Baerends. *Phys. Rev. B*, 12:2111, 1975.

[77] P. Leiva and M. Piris. *J. Chem. Phys.*, 123:214102, 2005.

[78] J. Cioslowski and K. Pernal. *Phys. Rev. B*, 71:113103, 2005.

[79] N. N. Lathiotakis, N. Helbig, and E. K. U. Gross. *Phys. Rev. A*, 72:30501, 2005.

[80] C. Kollmar. *J. Chem. Phys.*, 125:084108, 2006.

[81] N. N. Lathiotakis, N. Helbig, and E. K. U. Gross. *Phys. Rev. B*, 75:195120, 2007.

[82] N. Helbig, N. N. Lathiotakis, M. Albrecht, and E. K. U. Gross. *Europhys. Lett.*, 77:67003, 2007.

[83] A. Schindlmayer and R. W. Godby. *Phys. Rev. B*, 51:10427, 1995.

[84] A. E. Carlsson. *Phys. Rev. B*, 56:12058, 1997.

[85] R. Lopez-Sandoval and G. M. Pastor. *Phys. Rev. B*, 61:1764, 2000.

[86] R. Lopez-Sandoval and G. M. Pastor. *Phys. Rev. B*, 66:155118, 2002.

[87] R. Lopez-Sandoval and G. M. Pastor. *Phys. Rev. B*, 67:35115, 2003.

[88] R. Lopez-Sandoval and G. M. Pastor. *Phys. Rev. B*, 69:085101, 2004.

[89] R. G. Henning and A. E. Carlsson. *Phys. Rev. B*, 63:115116, 2001.

[90] R. Requist and O. Pankratov. *Phys. Rev. B*, 77:235121, 2008.

[91] H. A. Bethe. *Proc. R. Soc. London*, 150:552, 1935.

[92] S. Sugano, Y. Tanabe, and H. Kamimura. *Multiplets of Transition-Metal Ions in Crystals*. Pure and Applied Physics 33, Academic Press, New York, 1970.

[93] E. Feenberg. *Theory of Quantum Liquids*. Academic Press, New York, 1969.

[94] B. E. Clements, E. Krotscheck, J. A. Smith, and C. E. Campbell. *Phys. Rev. B*, 47:5239, 1993.

[95] W. M. C. Foulkes, L. Mitas, R. J. Needs, and G. Rajagopal. *Rev. Mod. Phys.*, 73:33, 2001.

[96] M.C. Gutzwiller. *Phys. Rev. Lett*, 10:159, 1963.

[97] M.C. Gutzwiller. *Phys. Rev.*, 134:A923, 1964.

[98] M.C. Gutzwiller. *Phys. Rev.*, 137:A1726, 1965.

[99] J. Bünemann, W. Weber, and F. Gebhard. *Phys. Rev. B*, 57:6896, 1998.

[100] J. Bünemann, F. Gebhard, and W. Weber. In preparation, 2009.

[101] N. F. Mott. *Metal–Insulator Transitions*. Taylor and Francis, London, 1990.

[102] W. F. Brinkman and T. M. Rice. *Phys. Rev. B*, 2:4302, 1970.

[103] P. G. J. van Dongen, F. Gebhard, and D. Vollhardt. *Z. Phys. B*, 76:199, 1989.

[104] T. Ogawa, K. Kanda, and T. Matsubara. *Prog. Theor. Phys.*, 53:614, 1975.

[105] D. Vollhardt. *Rev. Mod. Phys.*, 56:99, 1984.

[106] F. Takano and M. Uchinami. *Prog. Theor. Phys.*, 53:1267, 1975.

[107] J. Florencio and K. A. Chao. *Phys. Rev. B*, 14:3121, 1976.

[108] C. M. Varma, W. Weber, and L. J. Randall. *Phys. Rev. B*, 33:1015, 1985.

[109] T. M. Rice and K. Ueda. *Phys. Rev. Lett*, 55:995, 1985.

[110] T. M. Rice and K. Ueda. *Phys. Rev. B*, 34:6420, 1986.

[111] B. H. Brandow. *Phys. Rev. B*, 33:1986, 215.

[112] P. Fazekas. *Solid State Commun.*, 60:431, 1986.

[113] V. Z. Vulovic and E. Abrahams. *Phys. Rev. B*, 36:2614, 1987.

[114] P. W. Anderson. *Phys. Rev.*, 124:41, 1961.

[115] K. A. Chao and M. C. Gutzwiller. *J. Appl. Phys.*, 42:1420, 1971.

[116] K. A. Chao. *Phys. Rev. B*, 4:4034, 1971.

[117] K. A. Chao. *Phys. Rev. B*, 8:1088, 1973.

[118] K. A. Chao. *J. Phys. C*, 7:127, 1974.

[119] J. P. Lu. *Phys. Rev. B*, 49:5687, 1994.

[120] J. P. Lu. *Mod. Phys. B*, 10:3717, 1996.

[121] T. Okabe. *J. Phys. Soc. Japan*, 65:1056, 1996.

[122] J. Bünemann and W. Weber. *Phys. Rev. B*, 55:4011, 1997.

[123] J. Bünemann and W. Weber. *Physica B*, 230:412, 1997.

[124] J. Bünemann. *Eur. Phys. J. B*, 4:29, 1998.

[125] G. Kotliar and A. 'E. Ruckenstein. *Phys. Rev. Lett*, 57:1362, 1986.

[126] W. Metzner and D. Vollhardt. *Phys. Rev. Lett.*, 59:121, 1987.

[127] W. Metzner and D. Vollhardt. *Phys. Rev. B*, 37:7382, 1988.

[128] F. Gebhard and D. Vollhardt. *Phys. Rev. Lett.*, 59:1472, 1987.

[129] F. Gebhard and D. Vollhardt. *Phys. Rev. B*, 38:6911, 1987.

[130] W. Metzner and D. Vollhardt. *Phys. Rev. Lett.*, 37:324, 1989.

[131] W. Metzner. *Z. Phys. B*, 77:253, 1989.

[132] M. Kollar and D. Vollhardt. *Phys. Rev. B*, 65:155121, 2002.

[133] F. Gebhard. *Phys. Rev. B*, 41:9452, 1990.

[134] P. Horsch and T. A. Kaplan. *J. Phys. C: Solid State Phys.*, 16:L1203, 1983.

[135] E. Koch, O. Gunnarsson, and R. M. Martin. *Phys. Rev. B*, 59:15632, 1999.

[136] B. Edegger, C. Gros, and V. N. Muthukumar. *Adv. Phys.*, 56:927, 2007.

[137] J. Bünemann, W. Weber, and F. Gebhard. *J. Phys. Cond. Matt*, 9:7343, 1997.

[138] J. Bünemann, F. Gebhard, and W. Weber. In A. Narlikar, editor, *Frontiers in Magnetic Materials*. Springer, Berlin, 2005.

[139] U. Brandt and C. Mielsch. *Z. Phys. B*, 75:1989, 365.

[140] U. Brandt and C. Mielsch. *Z. Phys. B*, 79:1990, 295.

[141] U. Brandt and C. Mielsch. *Z. Phys. B*, 82:1991, 37.

[142] E. Müller-Hartmann. *Z. Phys. B*, 74:507, 1989.

[143] E. Müller-Hartmann. *Z. Phys. B*, 76:211, 1989.

[144] D. Vollhardt. *Int. J. Mod. Phys. B*, 3:2189, 1989.

[145] D. Vollhardt. In V. J. Emery, editor, *Correlated Electron Systems, Vol 9*. World Scientific, Singapore, 1993.

[146] R. M. Noack and F. Gebhard. *Phys. Rev. Lett*, 82:1915, 1999.

[147] F. Gebhard, E. Jeckelmann, S. Mahlert, S. Nishimoto, and R. M. Noack. *Eur. Phys. J. B*, 36:491, 2003.

[148] B. Edegger, N. Fukushima, C. Gros, and V. N. Muthukumar. *Phys. Rev. B*, 72:134504, 2005.

[149] B. Edegger, C. Gros, V. N. Muthukumar, and P. W. Anderson. *Phys. Rev. Lett.*, 96:207002, 2006.

[150] B. Edegger, C. Gros, and V. N. Muthukumar. *Phys. Rev. B*, 74:165109, 2006.

[151] J. Bünemann. *J. Phys. Cond. Matt*, 13:5327, 2001.

[152] M. Dzierzawa, D.Baeriswyl, and M. diStasio. *Phys. Rev. B*, 51:1993, 1995.

[153] G. Stollhoff, , and P. Fulde. *J. Chem. Phys*, 73:4548, 1980.

[154] N. Fukushima, B. Edegger, V. N. Muthukumar, and C. Gros. *Phys. Rev. B*, 72:144505, 2005.

[155] W.-H. Ko, C. P. Nave, and P. A. Lee. *Phys. Rev. B*, 76:245113, 2007.

[156] N. Fukushima. *Phys. Rev. B*, 78:115105, 2008.

[157] R. E. Moritz. *Journal of the American Statistical Association*, 23:55, 1928.

[158] S. E. Barnes. *J. Phys. F*, 6:1375, 1976.

[159] S. E. Barnes. *J. Phys. F*, 6:2637, 1977.

[160] P. Coleman. *Phys. Rev. B*, 28:5255, 1983.

[161] P. Coleman. *Phys. Rev. B*, 29:3035, 1984.

[162] P. Coleman. *Phys. Rev. B*, 35:5072, 1987.

[163] N. Read and D. M. Newns. *J. Phys. C*, 16:3273, 1983.

[164] N. Read and D. M. Newns. *Adv. Phys.*, 36:799, 1987.

[165] N. E. Bickers. *Rev. Mod. Phys.*, 59:845, 1987.

[166] O. Gunnarsson and K. Schönhammer. *Phys. Rev. Lett*, 50:604, 1983.

[167] O. Gunnarsson and K. Schönhammer. *Phys. Rev. B*, 28:4315, 1983.

[168] F. Lechermann, A. Georges, G. Kotliar, and O. Parcollet. *Phys. Rev. B*, 76:155102, 2007.

[169] J. Hubbard. *Phys. Rev. Lett.*, 3:77, 1959.

[170] R. L. Stratonovich. *Sov. Phys. Dokl.*, 2:461, 1957.

[171] J. E. Hirsch. *Phys. Rev. B*, 28:4059, 1983.

[172] J. E. Hirsch. *Phys. Rev. B*, 31:4403, 1985.

[173] E. Y. Loh, J. E. Gubernatis, R. T. Scalettar, S. R. White, D. J. Scalapino, and R. L. Sugar. *Phys. Rev. B*, 41:9301, 1990.

[174] H. J. Schulz. *Phys. Rev. Lett.*, 65:2462, 1990.

[175] H. Hasegawa. *J. Phys. Soc. Japan*, 66:1391, 1997.

[176] R. Frésard and G. Kotliar. *Phys. Rev. B*, 56:12909, 1997.

[177] X. Dai, G. Kotliar, and Z. Fang. arxiv:cond-matt/0611075.

[178] J. Bünemann and F. Gebhard. *Phys. Rev. B*, 76:193104, 2007.

[179] E. Arrigoni and G. C. Strinati. *Phys. Rev. Lett.*, 71:3178, 1993.

[180] J. Bünemann, F. Gebhard, and R. Thul. *Phys. Rev. B*, 67:75103, 2003.

[181] F. Gebhard. *Phys. Rev. B*, 44:992, 1991.

[182] S. Hüfner. *Photoelectron Spectroscopy: Principles and Applications.* Springer, Berlin, 2007.

[183] A. L. Fetter and J. D. Walecka. *Quantum Theory of Many-Particle Systems.* Dover Publications, New York, 2003.

[184] J. M. Luttinger and J. C. Ward. *Phys. Rev.*, 118:1417, 1960.

[185] J. S. Langer. *Phys. Rev.*, 124:997, 1961.

[186] A. A. Abrikosov and I. M. Khalatnikov. *Rep. Prog. Phys.*, 22:329, 1959.

[187] A. J. Leggett. *Rev. Mod. Phys.*, 47:331, 1975.

[188] R. Kubo. *J. Phys. Soc. Japan*, 12:550, 1957.

[189] R. Kubo. *Lectures in Theoretical Physics.* Wiley-Interscience, New York, 1959.

[190] W. Marshall and S. W. Lovesey. *Theory of Thermal Neutron Scattering.* Oxford University Press, Oxford, 1971.

[191] J. Bünemann and F. Gebhard. *J. Phys. Cond. Matt.*, 13:9985, 2001.

[192] P. Ring and P. Schuck. *The Nuclear Many-Body Problem*. Springer-Verlag, New York, 1980.

[193] J.-P. Blaizot and G. Ripka. *Quantum Theory of Finite Systems*. MIT Press, Cambridge, MA, 1986.

[194] G. Seibold, E. Sigmund, and V. Hizhnyakov. *Phys. Rev. B*, 57:6937, 1998.

[195] G. Seibold and J. Lorenzana. *Phys. Rev. Lett.*, 86:2605, 2001.

[196] G. Seibold. *Phys. Rev. B*, 58:15520, 1998.

[197] G. Seibold, F. Becca, and J. Lorenzana. *Phys. Rev. B*, 67:085108, 2003.

[198] J. Lorenzana and G. Seibold. *Phys. Rev. Lett.*, 90:066404, 2003.

[199] G. Seibold and J. Lorenzana. *Phys. Rev. B*, 69:134513, 2004.

[200] G. Seibold, F. Becca, P. Rubin, and J. Lorenzana. *Phys. Rev. B*, 69:155113, 2004.

[201] J. Lorenzana, G. Seibold, and R. Coldea. *Phys. Rev. B*, 72:224511, 2005.

[202] G. Seibold and J. Lorenzana. *Phys. Rev. Lett.*, 94:107006, 2005.

[203] G. Seibold and J. Lorenzana. *Phys. Rev. B*, 73:144515, 2006.

[204] G. Seibold and J. Lorenzana. *Journal of Superconductivity and Novel Magnetism*, 20:619, 2007.

[205] G. Seibold, F. Becca, and J. Lorenzana. *Phys. Rev. Lett.*, 100:016405, 2008.

[206] G. Seibold, F. Becca, and J. Lorenzana. *Phys. Rev. B*, 78:045114, 2008.

[207] E. v. Oelsen, J. Bünemann, and G. Seibold. In preparation, 2009.

[208] A. Bijl. *Physica*, 8:655, 1940.

[209] R. P. Feynman. In C. J. Gorter, editor, *Progress in Low Temperature Physics*. North-Holland, Amsterdam, 1955.

[210] S. Stringari. *Phys. Rev. B*, 49:6710, 1994.

[211] R. D. Lowde and C. G. Windsor. *Adv. Phys.*, 19:813, 1970.

[212] G. Uhrig. *Phys. Rev. Lett.*, 77:3629, 1996.

[213] M. Ulmke. *Eur. Phys. J. B*, 1:301, 1998.

[214] J. C. Slater and G. F. Koster. *Phys. Rev.*, 94:1498, 1954.

[215] H. A. Mook and D. M. Paul. *Phys. Rev.Lett.*, 54:227, 1985.

[216] J. F. Cooke, J. W. Lynn, and H. L. Davis. *Phys. Rev. B*, 21:4118, 1980.

[217] A. Takahashi and H. Shiba. *J. Phys. Soc. Jpn*, 69:3328, 2000.

[218] P. Fazekas. *Lecture Notes on Electron Correlation and Magnetism*. World Scientific, Singapore, 1999.

[219] Y. Ōno, M. Potthoff, and R. Bulla. *Phys. Rev. B*, 67:035119, 2003.

[220] Th. Pruschke and R. Bulla. *Eur. Phys. J. B*, 44:217, 2005.

[221] A. Liebsch. *Europhys. Lett.*, 63:97, 2003.

[222] A. Liebsch. *Phys. Rev. Lett.*, 91:226401, 2003.

[223] A. Liebsch. *Phys. Rev. B*, 70:165103, 2004.

[224] A. Koga, N. Kawakami, T. Rice, and M. Sigrist. *Phys. Rev. Lett.*, 92:216402, 2004.

[225] A. Koga, N. Kawakami, T. Rice, and M. Sigrist. *Phys. Rev. B*, 72:045128, 2005.

[226] L. de Medici, A. Georges, and S. Biermann. *Phys. Rev. B*, 72:205124, 2005.

[227] R. Arita and K. Held. *Phys. Rev. B*, 72:201102, 2005.

[228] M. Ferrero, F. Becca, M. Fabrizio, and M. Capone. *Phys. Rev. B*, 72:205126, 2005.

[229] G. Czycholl. *Phys. Rev. B*, 59:2642, 1999.

[230] E. P. Wohlfarth. *Handbook of Magnetic Materials*. North Holland, Amsterdam, 1980.

[231] M. Donath. *Surf. Sci. Rep.*, 20:251, 1994.

[232] M. B. Stearns. In H. P .J. Wijn, editor, *Landolt–Börnstein New Series Group III*. Springer, Berlin, 19a edition, 1986.

[233] A. Goldmann, W. Gudat, and O. Rader. In A. Goldmann, editor, *Landolt–Börnstein New Series Group III*. Springer, Berlin, 23c2 edition, 1994.

[234] D. C. Tsui. *Phys. Rev.*, 164:669, 1967.

[235] H. A. Mook. *Phys. Rev.*, 148:495, 1966.

[236] D. E. Eastman, F. J. Himpsel, and J. A. Knapp. *Phys. Rev. Lett*, 40:1514, 1978.

[237] W. Eberhardt and E. W. Plummer. *Phys. Rev. B*, 21:3245, 1980.

[238] V. L. Moruzzi, J. F. Janak, and A. R. Williams. *Calculated Electronic Properties of Metals*. Pergamon Press, New York, 1978.

[239] G. W. Crabtree, D. H. Dye, D. P. Karim, D. D. Koelling, and J. B. Ketterson. *Phys. Rev. Lett*, 42:390, 1977.

[240] M. J. Singh, J. Callaway, and C. S. Wang. *Phys. Rev. B*, 14:1214, 1976.

[241] G. H. O. Daalderop, P. J. Kelly, and M. F. H. Schuursmans. *Phys. Rev. B*, 41:11919, 1990.

[242] R. Gersdorf and G. Aubert. *Physica B*, 95:135, 1978.

[243] R. Gersdorf and G. Aubert. *Phys. Rev. Lett.*, 40:344, 1978.

[244] J. P. Perdew and Y. Wang. *Phys. Rev. B*, 33:8800, 1986.

[245] A. D. Becke. *Phys. Rev. A*, 38:3098, 1988.

[246] I. Yang, S. Y. Savrasov, and G. Kotliar. *Phys. Rev. Lett.*, 87:216405, 2001.

[247] Y. Xie and J. A. Blackman. *Phys. Rev. Lett.*, 69:172407, 2004.

[248] W. Weber and L. F. Mattheiss. *Phys. Rev. B*, 25:2270, 1982.

[249] A. Abragam and B. Bleaney. *Electron paramagnetic resonance of transition ions*. Clarendon Press, Oxford, 1970.

[250] P. Bruno. Magnetismus von festkörpern und grenzflächen. In *IFF-Ferienkurs*. Forschungszentrum Jülich GmbH, Berlin, 1993.

[251] T. Ohm, S. Weiser, R. Umstätter, W. Weber, and J. Bünemann. *J. Low Temp. Phys.*, 126:1081, 2002.

[252] V. I. Anisimov, J. Zaanen, and O. K. Andersen. *Phys. Rev. B*, 44:943, 1990.

[253] C. Herring. In G. T. Rado and H. Suhl, editors, *Magnetism, Vol. IV*. Academic Press, New York, 1966.

[254] I. Schnell, G. Czycholl, and R. C. Albers. *Phys. Rev. B*, 68:245102, 2003.

[255] M. S. Hybertson, M. Schlüter, and N. E. Christensen. *Phys. Rev. B*, 39:9028, 1989.

[256] G. Vielsack and W. Weber. *Phys. Rev. B*, 54:6614, 1986.

[257] J. Bünemann, F. Gebhard, T. Ohm, R. Umstätter, S. Weiser, W. Weber, R. Claessen, D. Ehm, A. Harasawa, A. Kakizaki, A. Kimura, G. Nicolay, S. Shin, and V. N. Strocov. *Europhys. Lett.*, 61:667, 2003.

[258] M. B. Zölfl, Th. Pruschke, J. Keller, A. I. Poteryaev, I. A. Nekrasov, and V. I. Anisimov. *Phys. Rev. B*, 61:12810, 2000.

[259] M. I. Katsnelson A. I. Lichtenstein and G. Kotliar. *Phys. Rev. Lett.*, 87:67205, 2001.

[260] C.S. Wang and J. Callaway. *Phys. Rev. B*, 15:298, 1977.

[261] A. Hofman, X. Y. Cui, J. Schäfer, S. Meyer, P. Höpfner, M. Wisniewski, M. Paul, L. Patthey, E. Rotenberg, J. Bünemann, F. Gebhard, T. Ohm, W. Weber, and R. Claessen. submitted to PRL, 2009.

[262] J. Schäfer, D. Schrupp, E. Rotenberg, H. Koh, P. Blaha, and R. Claessen. *Phys. Rev. Lett.*, 92:097205, 2004.

[263] M. Higashiguchi, K. Shimada, K. Nishiura, X. Cui, H. Namatame, and M. Taniguchi. *Phys. Rev. B*, 72:214438, 2005.

[264] A. Macridin, M. Jarrell, T. Maier, and D. J. Scalapino. *Phys. Rev. Lett.*, 99:237001, 2007.

[265] F. Tan, Y. Wan, and Q.-H. Wang. *Phys. Rev. B*, 76:054505, 2007.

[266] Y. Kakehashi and P. Fulde. *J. Phys. Soc. Jpn.*, 74:2397, 2005.

[267] K. Byczuk, M. Kollar, K. Held, Y.-F. Yang, I. A. Nekrasov, Th. Pruschke, and D. Vollhardt. *Nature Physics*, 3:168, 2007.

[268] I. Terasaki, Y. Sasago, and K. Uchinokura. *Phys. Rev. B*, 56:R12685, 1997.

[269] K. Takada, H. Sakurai, E. Takayama-Muromachi, F. Izumi, R. Dilanian, and T. Sasaki. *Nature*, 422:53, 2003.

[270] R. E. Schaak, T. Klimczuk, M. L. Foo, and R. J. Cava. *Nature*, 424:527, 2003.

[271] M. L. Foo, Y. Wang, S. Watauchi, H. W. Zandbergen, T. He, R. J. Cava, and N. P. Ong. *Phys. Rev. Lett.*, 92:247001, 2004.

[272] N. L. Wang, D. Wu, G. Li, X. H. Chen, C. H. Wang, and X. G. Luo. *Phys. Rev. Lett.*, 93:147403, 2004.

[273] R. Ray, A. Ghoshray, K. Ghoshray, and S. Nakamura. *Phys. Rev. B*, 59:9454, 1999.

[274] Y. Wang, N. S. Rogado, R. J. Cava, and N. P. Ong. *Nature*, 423:425, 2003.

[275] D. J. Singh. *Phys. Rev. B*, 61:13397, 2000.

[276] M. Z. Hasan, Y.-D. Chuang, D. Qian, Y. W. Li, Y. Kong, A. Kuprin, A. V. Fedorov, R. Kimmerling, E. Rotenberg, K. Rossnagel, Z. Hussain, H. Koh, N. S. Rogado, M. L. Foo, and R. J. Cava. *Phys. Rev. Lett.*, 92:246402, 2004.

[277] H.-B. Yang, S.-C. Wang, A. K. P. Sekharan, H. Matsui, S. Souma, T. Sato, T. Takahashi, T. Takeuchi, J. C. Campuzano, R. Jin, B. C. Sales, D. Mandrus, Z. Wang, and H. Ding. *Phys. Rev. Lett.*, 92:246403, 2004.

[278] H. Ishida, M. D. Johannes, and A. Liebsch. *Phys. Rev. Lett.*, 94:196401, 2005.

[279] S. Zhou, M. Gao, H. Ding, P. A. Lee, and Z. Wang. *Phys. Rev. Lett.*, 94:206401, 2005.

[280] F. Lechermann, S. Biermann, and A. Georges. *Progr. Theor. Phys. Suppl.*, 160:233, 2005.

[281] S. Landron and M.-B. Lepetit. *Phys. Rev. B*, 74:184507, 2006.

[282] A. Bourgeois, A. A. Aligia, T. Kroll, and M. D. Núñez-Regueiro. *Phys. Rev. B*, 75:174518, 2007.

[283] C. A. Perroni, H. Ishida, and A. Liebsch. *Phys. Rev. B*, 75:045125, 2007.

[284] C. A. Marianetti, K. Haule, and O. Parcollet. *Phys. Rev. Lett.*, 99:246404, 2007.

[285] A. Liebsch and H. Ishida. *Eur. Phys. J. B*, 61:405, 2008.

[286] S. Landron and M.-B. Lepetit. *Phys. Rev. B*, 77:125106, 2008.

[287] D. Pillay, M. D. Johannes, I. I. Mazin, and O. K. Andersen. *Phys. Rev. B*, 78,:012501, 2008.

[288] T. Schickling, J. Bünemann, and F. Gebhard. in preparation.

[289] G. Wang, X. Dai, and Z. Fang. *Phys. Rev. Lett.*, 101:066403, 2008.

[290] K. M. Ho, J. Schmalian, and C. Z. Wang. *Phys. Rev. B*, 77:073101, 2008.

[291] X. Deng, X. Dai, and Z. Fang. *Europhys. Lett.*, 83:37008, 2008.

[292] M. Tinkham. *Group Theory and Quantum Mechanics*. Dover, New York, 1992.

[293] O. K. Andersen and T. Saha-Dasgupta. *Phys. Rev. B*, 62:R16219, 2000.

Acknowledgements

First, I would particularly like to thank my co-workers and mentors Florian Gebhard and Werner Weber for their great support over all these years of collaboration.

This work also would not have been possible without the contributions of a number of other people. I would like to express my gratitude to Ralf Claessen, Patrik Fazekas, Katalin Jávorne-Radnóczi, Torsten Ohm, David Rasch, Jörg Schäfer, Götz Seibold, Tobias Schickling, Vladimir Strocov, Rüdiger Thul, Rolf Umstätter, and Stefan Weiser.

Finally, for their proofreading of this work, or parts of it, my thanks go to Florian Gebhard, Reinhard Noack, Götz Seibold, Nelson Tum, and Werner Weber. Of course, any inaccuracies are to be borne by me alone.